Examining the effect of NOX2 NADPH oxidase inhibition on vascular repair and regeneration in insulin resistance

Dr. Noman Ali

Submitted in accordance with the requirements for the degree of Doctor of Philosophy

The University of Leeds

School of Medicine

2016

Intellectual Property and Publication Statements

The candidate confirms that the work submitted is his own, except where work which has formed part of jointly-authored publications has been included. The contribution of the candidate and the other authors to this work has been explicitly indicated below. The candidate confirms that appropriate credit has been given within the thesis where reference has been made to the work of others.

Ali, N., M.T. Kearney, and R.M. Cubbon, *The role of reactive oxygen species in insulin resistance–associated cardiovascular disease*. Diabetes Management, 2015. 5(3): p. 203-213.

Review article which forms part of Chapter 1 of my thesis. I drafted the manuscript which was then edited by my co-author.

Acknowledgements

The work presented here is my own, with the exception of certain experiments in which others' help has been explicitly acknowledged.

When I signed up to undertake a PhD I was warned that it would be challenging, and at times, frustrating. At the time I felt that I was well prepared but, being honest, I found the transition from the comforting familiarity of clinical medicine into the unfamiliar territory of basic science harder than I had anticipated. To have reached the point of being able to write up and submit a thesis is something that I am very proud of and something for which I owe a huge debt of gratitude to a great many people.

Firstly, I would like to pay tribute to my two supervisors, Dr Richard Cubbon and Professor Mark Kearney. Their guidance, encouragement and unwavering support has been instrumental in allowing me to get to this point. I would also like to thank the British Heart Foundation for their financial support.

I am grateful to all of my laboratory colleagues for their instruction, wisdom, and cooperation during these three years. Truly, I could not have wished for a friendlier or more helpful working environment. Space limitations mean I cannot mention all of the people I wish to thank by name, but I feel that the following are in need of specific recognition: Dr Nadira Yuldasheva for her tireless work and expertise in murine surgery, which played such a key role in shaping my project; Mrs Jessica Smith for her patience in teaching me so many laboratory techniques; and Dr Romana Mughal for her input with Western blotting.

A special mention must go to Drs Anshu Sengupta, Andy Walker, Peysh Patel, Amir Aziz, Ben Mercer, Marc Bailey, Katy Bridge, Kathryn Griffin, Kate Gatenby and John Dalton. Their company, and the laughter that they have provided, have made the last three years the most sociable of my career to date.

Finally, I have saved my biggest thank you for the people who are most important to me: My parents, without whose sacrifice I would have been unable to become a doctor; my sister Kiran for her love and advice; and most significantly, my wife Amarah and son Ibrahim for the joy that they have brought to my life.

Abstract

Diabetes mellitus (DM) is an established cause of increased mortality. Most deaths linked to DM are attributable to cardiovascular disease, and hyperglycaemia alone is not sufficient to explain the increased cardiovascular risk associated with DM. It is accepted that insulin resistance, the principal underlying cause of the most common form of DM, is independently linked to CVD. Prior research demonstrates insulin resistance is associated with excessive production of reactive oxygen species (ROS), in part via the enzyme NADPH oxidase 2 (NOX2). We hypothesised that reduction of NOX2-derived ROS represents a translationally promising strategy to improve the diminished vascular repair and regeneration observed in insulin resistance. This project explores the effect of NOX2 inhibition on angiogenesis and vascular repair in murine models of whole-body and endothelial-specific insulin resistance.

Mice with haploinsufficiency of the insulin receptor (IRKO), and those expressing a kinase dead human insulin receptor transgene in the endothelium (ESMIRO), were bred with NOX2 deficient mice. NOX2 knockdown was associated with significant improvement in vascular repair following arterial injury in ESMIRO mice. Subsequent work provided two potential explanations: improved endothelial cell migration, and an increased abundance of circulating progenitor cells. Pharmacological NOX2 inhibition partly recapitulated these findings *in vitro*, as treatment of insulin resistant human umbilical vein endothelial cells with the NOX2 inhibitor GP91-ds tat was associated with improved cell migration.

Whilst this project yielded a number of promising findings, it also highlighted pitfalls associated with manipulation of ROS. We corroborated two existing concerns relating to NOX2 inhibition: the potential to compromise immune function, and the risk of inciting a pro-inflammatory state. Although NOX2 remains a potentially suitable target for therapeutic intervention, greater understanding of NOX2 biology is required. We hope the work carried out in this project can be built upon to facilitate that understanding, ultimately generating novel therapeutic agents.

Contents

List of figures

Abbreviations

ACh	Acetylcholine
AcLDL	Acetylated low density lipoprotein
AGE	Advanced glycation end product
Akt	Protein kinase B
APC	Allophycocyanin
ApoE	Apolipoprotein E
AUC	Area under curve
BH_4	Tetrahydrobiopterin
BM	Bone marrow
Bp	Base pair
BSA	Bovine serum albumin
CAD	Coronary artery disease
CFU	Colony forming unit
CPC	Circulating progenitor cell
cGMP	Cyclic guanosine monophosphate
Ct	Cycle threshold
CV	Co-efficient of variation
CVD	Cardiovascular disease
C57BL/6	C57 black 6
DHE	Dihydroethidium

DiI	1,1’-dioctadecyl-3,3,3’3’-tetramethylindocarbocyanine perchlorate
DM	Diabetes Mellitus
DMEM	Dulbecco’s modified Eagle’s medium
DMSO	Dimethysulfoxide
DNA	Deoxyribonucleic acid
dNTP	Deoxynucleotide phosphate
EC	Endothelial cell
EDTA	Ethylenediaminetetraacetic acid
EdU	5-ethynyl-2’-deoxyuridine
EEPC	Early outgrowth endothelial progenitor cell
EGM	Endothelial growth medium
ELISA	Enzyme linked immunosorbent assay
eNOS	Endothelium derived nitric oxide synthase
EPC	Endothelial progenitor cell
EEPC	Early outgrowth endothelial progenitor cell
ESMIRO	Endothelium specific mutant insulin receptor over-expression
ET-1	Endothelin 1
FACS	Fluorescence activated cell sorting
Fc	Crystallisable fragment
FCS	Foetal calf serum
FFA	Free fatty acid

FITC	Fluorescein isothiocyanate
Flk1	Foetal liver kinase 1
FMD	Flow mediated dilatation
GLUT-4	Glucose transporter type 4
GTP	Guanosine triphosphate
GTT	Glucose tolerance testing
HBSS	Hank's balanced salt solution
HCl	Hydrochloric acid
hIR	Human insulin receptor
HUVEC	Human umbilical vein endothelial cell
H_2O_2	Hydrogen peroxide
IC	Isotype control
ICAM	Intracellular adhesion molecule
IHD	Ischaemic heart disease
IP	Intraperitoneal
IR	Insulin receptor
IRKO	Insulin receptor knockout
IRS-1	insulin receptor substrate 1
ITT	Insulin tolerance testing
IU	International unit
IVC	Inferior vena cava

KDR	Kinase domain receptor
LDL	Low density lipoprotein
LEPC	Late outgrowth endothelial progenitor cell
MAPK	Mitogen active protein kinase
MCP-1	Monocyte chemoattractant protein 1
MI	Myocardial infarction
mIR	Murine insulin receptor
mRNA	Messenger ribonucleic acid
mTORC2	Mammalian target of rapamycin complex 2
NADPH	Nicotinamide adenine dinucleotide phosphate
NaOH	Sodium hydroxide
NFκB	Nuclear factor kappa B
NO	Nitric oxide
NOS	Nitric oxide synthase
NOX	Nicotinamide adenine dinucleotide phosphate oxidase
O_2^-	Superoxide anion
OCT	Optimal cutting temperature compound
$ONOO^-$	Peroxynitrite
PBMC	Peripheral blood mononuclear cell
PCI	Percutaneous coronary intervention
PDGF	Platelet derived growth factor

PBS	Phosphate buffered solution
PCR	Polymerase chain reaction
PE	R-phycoerythrin
PEC	Pulmonary endothelial cell
PECAM-1	Platelet endothelial cell adhesion molecule 1
PI3K	Phosphatidyl inositol 3-kinase
PIP	Phosphatidyl inositol phosphate
PPAR	Peroxisome proliferator activated receptor
RNA	Ribonucleic acid
ROS	Reactive oxygen species
RPM	Revolutions per minute
Sca1	Stem-cell antigen 1
SEM	Standard error of mean
sGC	Soluble guanylyl cyclase
siRNA	Small interfering ribonucleic acid
SOD	Superoxide dismutase
T2DM	Type 2 diabetes
TAE	Tris-acetate-EDTA
Taq	Thermophillus aquaticus
TK	Tyrosine kinase
TNF-α	Tumour necrosis factor alpha

VCAM-1	Vascular cell adhesion molecule 1
VEGF	Vascular endothelial growth factor
VEGFR	Vascular endothelial growth factor receptor
VENIRKO	Vascular endothelial insulin receptor knockout
VSMC	Vascular smooth muscle cell
WT	Wild-type

Chapter 1**: Introduction**

Chapter 1 **Introduction**

Due to an alarming growth in prevalence, Diabetes Mellitus (DM) has attained the status of a global epidemic, with an estimated 382 million sufferers in the year 2013. Various factors, including the increasing prevalence of obesity and the ageing of the population, mean that this figure is forecast to continue its inexorable rise, with a current projection of 592 million by the year 2035 [1].

As well as being a cause of significant morbidity, DM is also an established cause of increased mortality and reduced life expectancy [2]. The Framingham Study [3] was one of the first to highlight the relationship between DM and an increased risk of cardiovascular disease (CVD), and it is now recognised that most deaths linked to DM are attributable to CVD. Whilst great advances have been made in CVD prevention amongst the general population, outcomes remain poor for patients with DM [4]. Sufferers of the disease are twice as likely as healthy individuals to experience complications of CVD such as myocardial infarction (MI) or stroke [5], and they tend to do so approximately 15 years prematurely [6].

Whilst DM is usually diagnosed on the basis of elevated blood glucose, hyperglycaemia alone is not sufficient to explain the increased cardiovascular (CV) risk associated with the disease [7]. Type 2 diabetes mellitus (T2DM), by far the predominant form of the disease, is preceded by a prolonged pre-diabetic stage, when in spite of subclinically abnormal blood glucose metabolism, CV risk is still significantly elevated [8]. This is thought to be due to an aggregation of cardiovascular risk factors, referred to as the metabolic syndrome, which may be underpinned by resistance to the vascular and metabolic effects of insulin.

Insulin resistance is implicated in both the initiation and progression of atherosclerosis, the key pathological process responsible for CVD. Whereas previously atherosclerosis was thought to result simply from lipid accumulation in arterial walls, it is now recognised as a much more complex and nuanced process, better characterised as a chronic inflammatory disease of blood vessels [9]. The earliest manifestation of atherosclerosis is endothelial dysfunction [10], and insulin resistance has been demonstrated to be instrumental in its development via disruption of endothelial nitric oxide (NO) production [11]. Insulin

resistance may also facilitate the progression of atherosclerosis by impairing endogenous vascular repair processes, which can retard atherogenesis and promote recovery of damaged endothelium in the context of vascular injury [12, 13].

One of the characteristics of insulin resistant states is excessive production of reactive oxygen species (ROS) [14], which has been demonstrated to be a key pathogenic process in endothelial dysfunction [15]. Recent work has also highlighted the critical role of ROS as signalling molecules in the process vascular repair [16]. ROS could therefore form a target for the prevention and treatment of insulin resistance-associated cardiovascular disease, a concept which forms the basis of this thesis.

1.1 Insulin signalling

Insulin is a peptide hormone whose amino acid sequence was first identified in 1952. Its structure comprises A & B peptide chains of 21 and 30 amino acids respectively, linked by disulphide bonds. Its synthesis takes place in the β cells situated within the pancreatic islets of Langerhans, and the first step is the formation of the precursor molecule preproinsulin. Removal of a signal peptide results in the formation of proinsulin, which is stored in secretory vesicles until enzymatic action facilitates a further cleavage into insulin and C peptide [17].

Insulin secretion via exocytosis into the circulation is triggered by multiple stimuli, the principal being elevated circulating concentrations of glucose. Exposure of the β cells to glucose results in intracellular glucose transport via GLUT1 and 2, leading to the generation of ATP. The increased intracellular ATP/ADP ratio causes closure of plasma membrane ATP-dependant K^+ channels and therefore membrane depolarisation. This depolarisation results in opening of voltage-gated Ca^{2+} channels, allowing an influx of calcium and thereby triggering insulin secretion [18].

1.1.1 Physiological insulin signalling

Insulin mediates its actions via binding to its cognate tyrosine kinase receptor (IR). The IR is a transmembrane structure which consists of two α and two β glycoprotein subunits linked together by disulphide bonds. Insulin binds to the receptor's extracellular α subunit, resulting in a conformational change which allows ATP to bind to the β subunit's intracellular domain [19]. The binding of ATP triggers receptor autophosphorylation, enabling the receptor's kinase activity toward intracellular protein substrates [20]. This results in tyrosine phosphorylation of various docking proteins, including the insulin receptor substrates (IRS) 1 and 2. Multiple downstream signalling cascades are subsequently activated, the principal two being the phosphoinositide 3-kinase (PI3K)/ Akt and mitogen-activated protein kinase (MAPK) pathways (figure 1).

PI3K/Akt pathway

Phosphorylated IRS binds and activates PI3K, which then generates phosphatidylinositol triphosphate (PIP_3). PIP_3 stimulates membrane localisation of phosphoinositide dependant

kinase-1 (PDK-1), which phosphorylates Akt at threonine 308, resulting in its partial activation. Completion of Akt activation is achieved by phosphorylation at serine 473, mediated by the mammalian target of rapamycin-2 complex (mTorc2). The resulting effects of this cascade depend on the tissue within which it takes place; in metabolic tissues, Akt activation promotes GLUT4 translocation to the cell membrane and intracellular glucose uptake. In vascular endothelial cells (ECs), a major effect is to activate the enzyme endothelial nitric oxide synthase (eNOS) which catalyses NO production [21].

MAPK pathway

The MAPK pathway is dependent on Ras interaction with the Src-homology domain 2 (SH2) of the Shc adaptor protein. Activation of this pathway is responsible for the mitogenic effects of insulin, such as vascular smooth muscle cell (VSMC) proliferation and migration, as well as production of the vasoconstrictor peptide endothelin 1 (ET-1) [22].

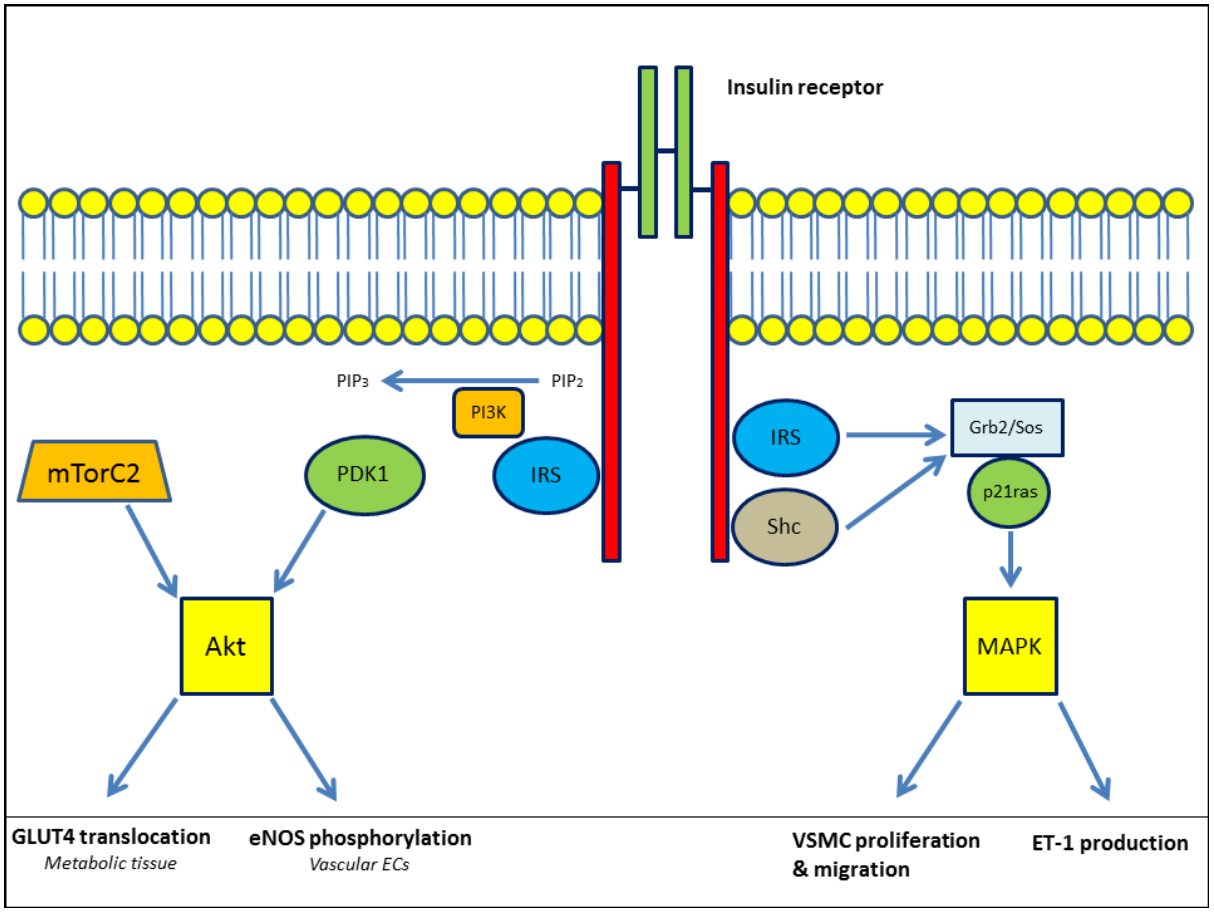

Figure 1. Insulin signalling cascade

Binding of insulin to its receptor triggers a series of intracellular signalling cascades resulting in activation of Akt and MAPK. The Akt pathway stimulates GLUT4 translocation in metabolic tissue and eNOS phosphorylation in vascular ECs, whilst the MAPK pathway mediates the mitogenic effects of insulin and the production of ET-1.

IRS: Insulin receptor substrate; PI3K: phosphoinositide 3-kinase; PDK1: phosphoinositide dependant kinase-1; mTorC2: mammalian target of rapamycin-2 complex; Grb2: growth factor receptor-bound protein 2; MAPK: mitogen-activated protein kinase; eNOS: endothelial nitric oxide synthase; EC: endothelial cell; VSMC: vascular smooth muscle cell; ET-1: endothelin 1. Adapted from Cubbon et al [21].

1.1.2 Insulin resistance

The term insulin resistance can denote an impairment of downstream signal transduction when insulin binds to its receptor, which culminates in reduced glucose uptake in metabolic tissues. However the deleterious effects of insulin resistance go beyond glucose homeostasis and also include dyslipidaemia, inflammation and a pro-thrombotic tendency [23]. A number of studies have demonstrated insulin resistance to be an independent risk factor for CVD [24, 25] and this has generated significant interest in elucidating the mechanisms by which it develops. The initiation and progression of insulin resistance is now understood to be a multi factorial phenomenon, with contributions from both genetic and modifiable environmental factors. The following section is a brief synopsis of a few of the putative contributory facets.

Naturally occurring mutations of the IR rare and usually result in a syndrome of extreme insulin resistance such as leprechaunism. Genomic analysis has demonstrated that mutations of the IR do not significantly contribute to the pathophysiology of T2DM or obesity [26]. Diminution of IR abundance would seem to be a more important contributing factor in the development of insulin resistance and has been noted in muscle and liver tissue from patients with T2DM as well as muscle and adipocyte tissue from obese subjects [26]. Murine models of reduced IR expression have proved useful in examining the sequelae of insulin resistance and will be discussed shortly.

Aberrances downstream from the IR are a recognised contributor to insulin resistance, an example being polymorphisms of IRS-1, a crucial mediating protein in the insulin signalling cascade. The most commonly occurring of these is G972R, which is found in Caucasian populations with a prevalence of 5.8%. Interestingly the prevalence amongst patients with T2DM is significantly higher, at 10.7% [27, 28]. Studies exploring the molecular effects of this sequence change in IRS-1 have demonstrated a defect in binding of the p85 subunit of PI3K to IRS-1 and a 36% decrease in IRS-1–associated PI3-kinase activity [29]. Polymorphisms have also been identified of PI3K, a common example of which involves the p85α subunit. The mutation has been identified in 31% of Caucasians in heterozygous form, and 2% in homozygous form where it results in a 32% decrease in insulin sensitivity in an intravenous glucose tolerance test [30].

Whilst genetic aberrations, such as those outlined above, can be important in the development of insulin resistance, there is little doubt that on a population level environmental factors such as obesity and ageing are the most significant contributors. Adipose tissue is understood to play an important role in the initiation of insulin resistance via alterations in levels of circulating free fatty acids (FFAs), promotion of inflammation and perturbation of the balance of adipokine secretion. Expansion of adipose tissue secondary to nutrient excess leads to increased levels of circulating free fatty acids (FFAs) which can directly impair insulin signalling. In human volunteers, intravenous infusion of a lipid emulsion causes a 10-fold rise in plasma FFAs, resulting in a 22% decrease in peripheral glucose uptake in the setting of hyperinsulinaemia [31]. The mechanism by which FFAs can impair insulin signalling remains incompletely understood, but members of the protein kinase C (PKC) family appear to play an important role by acting as lipid-sensing molecules which can then respond by using their kinase activity to alter cellular events [32]. Studies carried out in the 1980s demonstrated that activation of PKC using phorbol acetate could induce insulin resistance [33, 34]. Subsequent work in rodents found that elevated FFA levels via an infusion of intralipid/heparin was associated with activation of PKCθ as well as development of skeletal muscle insulin resistance [34]. Yu *et al* demonstrated PKCθ activation to be associated with impaired insulin signalling via decreased insulin-stimulated IRS-1 tyrosine phosphorylation [35]. More recent work has provided an explanation for this by highlighting the ability of PKCθ to phosphorylate IRS-1 on Ser 1101, blocking insulin-stimulated IRS-1 tyrosine phosphorylation [36] and therefore impeding downstream insulin signalling.

In addition to increasing FFA levels, expanded adipose tissue has a tendency to develop areas of micro-hypoxia and stress of the endoplasmic reticulum, resulting in inflammation and the release of cytokines such as TNFα [37, 38]. The release of inflammatory cytokines activate stress kinases, which also impair downstream signalling via the Akt pathway as a result of inhibitory phosphorylation of serine residues within IRS-1 [39, 40]. Adipose tissue can also influence insulin sensitivity via the secretion of its own endogenous cytokines, termed adipokines. In the setting of hypoxic adipose tissue, the balance of secreted adipokines is shifted in favour of those which promote insulin resistance rather than those which enhance insulin sensitivity [41].

The combination of inflammatory cytokines, activated macrophages and adipokines promotes ectopic accumulation of lipids in skeletal muscle [42] and of hepatic steatosis [43]. These effects contribute to insulin resistance within these tissues as well as release of further FFAs and cytokines to propagate the cycle.

Prolonged resistance to the effects of insulin results in compensatory hyperinsulinaemia in order to maintain glucose homeostasis. However, this attempt to overcome the effects of insulin resistance may further exacerbate the problem. Ueno *et al* observed impairment of signalling via the Akt pathway in liver and muscle tissue from healthy rats during extended hyperinsulinaemic-euglycaemic clamp studies [44]. In time, compensatory mechanisms become overwhelmed and hyperglycaemia manifests, heralding the onset of frank diabetes. Sustained hyperglycaemia itself can also promote progression of insulin resistance via generation of oxidative stress and advanced glycation end products (AGEs) [45, 46]. Both of these phenomena have been shown to impair insulin signalling via inhibitory phosphorylation of IRS-1 [47-49].

Studies published at the turn of the century identified a phenomenon termed 'pathway specific insulin resistance' whereby activation of the Akt pathway is impaired, whilst MAPK activity remains unaffected [50]. The net effect of this imbalance is to promote the mitogenic effects of insulin whilst hindering its ability to stimulate NO production. As well as classical insulin sensitive tissues such as muscle, this observation has also been noted in the vasculature [51], where the combination of VSMC proliferation and reduced NO bioavailability results in a pro-atherogenic state. Whilst the significance of this pathway specific model of insulin resistance in human disease remains unconfirmed, it does provide a link between the metabolic and vascular abnormalities noted in insulin resistant patients.

Murine models of insulin resistance

Examining the role of insulin resistance *per se* in human CVD is difficult due to the complex nature of measurement of insulin sensitivity by euglycaemic clamp techniques, as well as the confounding effect of other factors such as obesity, dyslipidaemia, hypertension and hyperglycaemia which often co-exist with insulin resistance. As such, murine models have also proven to be a very useful tool in exploring the impact of insulin resistance.

Mice with homozygous insufficiency of the IR have been demonstrated to have a lethal phenotype despite normal *in utero* development. The mice develop profound hyperglycaemia and diabetic ketoacidosis (DKA), resulting in death within 72 hours [52, 53]. However mice with haploinsufficiency for the IR (IRKO) are viable and have been extensively studied by our laboratory. IRKO mice have proven to be a good model of human metabolic syndrome due to a combination of preserved glucose regulation, post-prandial hyperinsulinaemia and hypertension [54]. Investigation into the downstream signalling defects in IRKO mice demonstrated normal vascular levels of eNOS mRNA but reduced insulin-induced eNOS phosphorylation relative to wild-type.

Murine models have also been used in order to isolate and examine the role of the endothelium in insulin resistance. The first murine model of endothelial-specific insulin resistance was VENIRKO, where Cre-lox recombination was used in order to knockout the insulin receptor in the endothelium [55]. As with IRKO counterparts, VENIRKO mice were found to have preserved glucose regulation. However in contrast to IRKO mice, VENIRKO mice display reduced levels of eNOS mRNA in aortic and cardiac tissue. Our group have developed and characterised an alternative transgenic murine model with endothelium-specific mutant dominant negative insulin receptor overexpression (ESMIRO). Whilst these mice behave similarly to IRKO mice with respect to preserved glucose regulation and diminished insulin-induced eNOS phosphorylation, they appear to have a milder phenotypic derangement than IRKO counterparts as evidenced by their normal blood pressure [56]. The effects of altered insulin signalling in murine models with respect to vascular function will be discussed in a later section.

1.2 Reactive oxygen species

The term reactive oxygen species (ROS) encompasses various molecules derived from the metabolism of oxygen which can be divided into free radicals (superoxide anion, peroxynitrite) and non-radicals (hydrogen peroxide, ozone). ROS have traditionally been seen as toxic byproducts of metabolism, a view first put forward by Denham Harman's 'free radical theory' in 1956 [57]. In the decades following this, ROS have been the subject of intense research and their accumulation has been implicated in the initiation and development of a range of cardiovascular diseases, including hypertension, hyperlipidaemia, ischaemic heart disease, congestive cardiac failure and diabetes mellitus [58]. However, in more recent years gathering evidence has shown that ROS have a role as intracellular signalling molecules. Signal transduction mediated by ROS, known as 'redox signalling', has been demonstrated to be crucial to numerous developmental and physiological processes [59].

1.2.1 Production and breakdown of ROS

ROS levels within cells are governed by the relative rates of their production and breakdown. The most significant producers of ROS are mitochondria and various enzyme groups including xanthine oxidase, lipoxygenase, uncoupled endothelial nitric oxide synthase (eNOS) and the NADPH oxidases (NOX). The lattermost of these is the principal source of ROS within the vasculature and will be discussed in more detail in the following section. Breakdown of ROS is also attributable to the actions of a selection of enzymes. Superoxide anion is dismuted into hydrogen peroxide and oxygen via the action of superoxide dismutase, whilst hydrogen peroxide breakdown into water and oxygen is facilitated by catalase, glutathione peroxidise and the thioredoxin enzyme system [60] (see figure 2).

In health, production and breakdown is balanced and a physiological level of ROS is therefore maintained. In situations where there is excessive production or insufficient breakdown of ROS, accumulation occurs and this is termed 'oxidative stress'. The excess ROS cause damage to cell constituents such as lipids, proteins, DNA and membranes due to free-radical mediated chain reactions [59].

Oxidative stress has been implicated in multiple forms of vascular disease and interestingly, NADPH oxidases have been demonstrated to be the predominant source of superoxide anion in patients with T2DM and advanced coronary artery disease [61] as well as those with metabolic syndrome [62] and obesity [63].

1.2.2 NADPH oxidases

In contrast to all other ROS producing enzymes, the NOXs produce ROS as their primary function, rather than as a by-product [64]. NOX2 is the prototypic NADPH oxidase, and was first discovered in phagocytes, where it aids in antimicrobial defence by producing a 'respiratory burst' of ROS to kill internalised bacteria [59]. Subsequent work found NOXs to also be present in non-phagocytic cells, leading to the discovery of a family of NOXs. We now recognise there to be 5 NOX homologues (NOX 1-5) and 2 dual oxidases (DUOX 1-2) [65].

Whilst all NOX isoforms produce ROS by transferring electrons from NADPH to molecular oxygen, each is unique with regard to tissue distribution and mechanism of activation. NOX 1, 2, 4 and 5 are most commonly expressed in vascular cells whilst the other homologues either have not been found, or are expressed at very low levels [66]. Interestingly, although NOX5 is expressed in human vasculature it has been found to be entirely absent in rodents [67].

NOX2

NOX2 is the most widely expressed NADPH isoform within the vasculature [66], and has also been identified in stem/progenitor cells [65]. Structurally it consists of a membrane spanning catalytic subunit termed gp91phox, which in order to function requires binding of the membrane bound p22phox subunit as well as further cytosolic components (p47phox, p67phox, p40phox and Rac) [15].

The requirement of binding of various cytosolic components in order to activate NOX2 means that multiple stimuli can trigger ROS production. The translocation and binding of p47phox to NOX2 is facilitated by phosphorylation, which can be triggered by vascular endothelial growth factor (VEGF), angiotensin 2, tumour necrosis factor α (TNFα) and oscillatory shear stress. Isoprenylation of Rac is also necessary for NOX2 activation and

this is triggered by cytokines, shear-stress and ischaemia-reperfusion [15]. Taking this into account, it can be seen why stimuli such as VEGF and ischaemia can result in ROS production. The predominant ROS produced by NOX2 is superoxide anion [68].

NOX1

NOX1 is most highly expressed in colon epithelium [68], but has also been found in ECs, smooth muscle cells (SMCs) and adventitial cells within the vasculature [66]. Similarities with NOX2 include structural homology (60% shared amino-acid identity), the fact that its primary product is superoxide anion, and its activity's dependence on binding with other subunits [68].

NOX4

In contrast to NOXs 1 and 2, NOX4 is constitutively active and does not require cytosolic activator subunits [15]. This suggests that ROS production by NOX4 is dependent on enzyme abundance and is thus regulated predominantly by level of expression [69]. A study performed by Craige *et al* [70] showed that endothelial NOX4 expression can be upregulated in response to hypoxia. A further difference between NOX4 and NOXs 1 and 2 is that NOX4 appears to generate predominantly hydrogen peroxide, rather than superoxide anion [69]. This notion is supported by studies which showed that peroxynitrite ($ONOO^-$) was not generated when NOX4 was overexpressed in the presence of NO [71, 72].

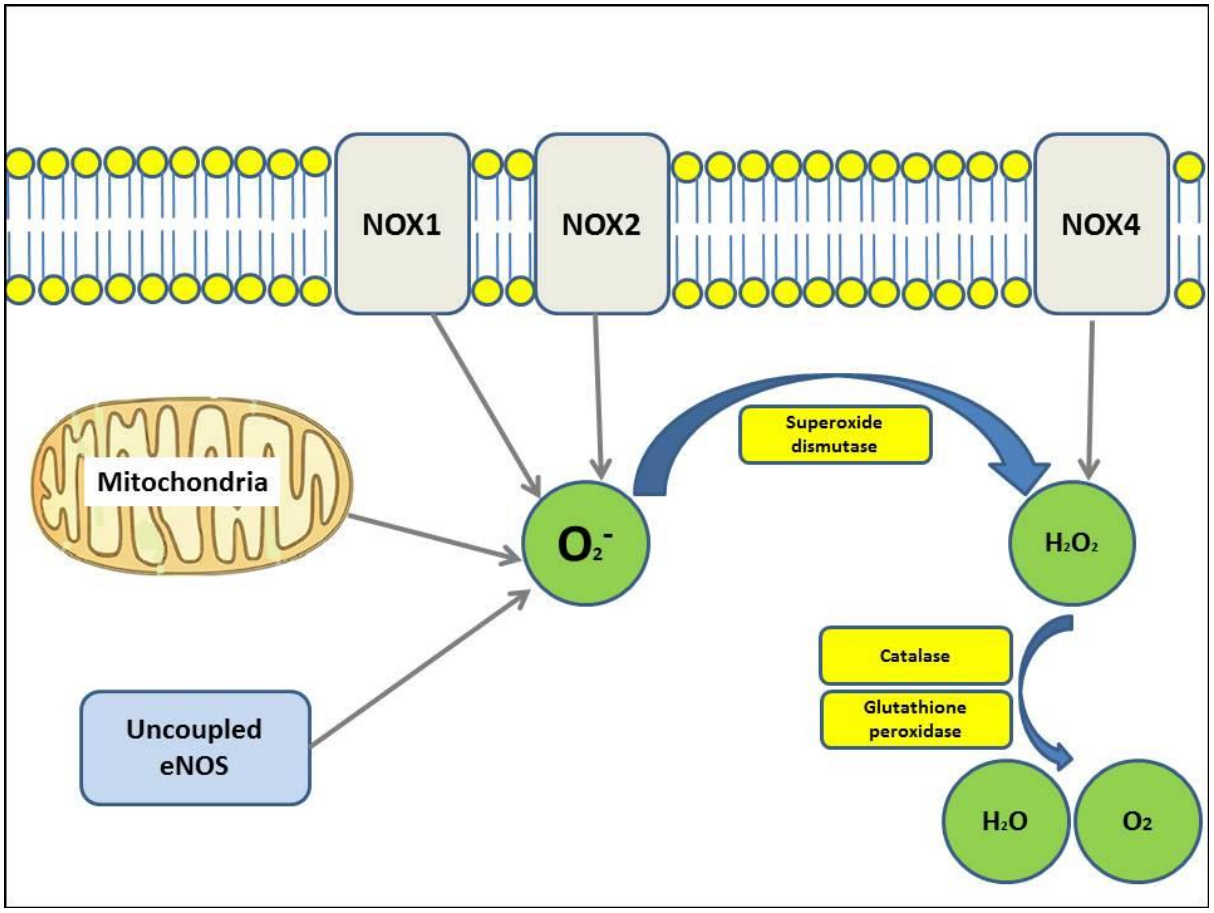

Figure 2. Production and breakdown of ROS

Membrane-bound NADPH oxidase enzymes (NOXs 1 and 2) as well as mitochondria and uncoupled eNOS are responsible for the majority of superoxide anion generation. Superoxide anion is dismuted to form hydrogen peroxide by the action of the enzyme superoxide dismutase. NADPH oxidase NOX4 also contributes to hydrogen peroxide generation, which is then itself broken down into water and oxygen by the actions of catalase or glutathione peroxidase. Taken with permission from Ali et al [73].

1.2.3 Redox signalling

Signal transduction by electron transfer, termed redox signalling, is an emerging area of investigation within cardiovascular research, and one in which ROS play the major role. In order to be able to function as signalling molecules, ROS need to demonstrate three specific characteristics [74]:

1. Reversibility of the signalling effect

2. Control of their concentration at the level of synthesis and removal

3. Existence of specific receptors

Superoxide anion and hydrogen peroxide are able to reversibly modify proteins in a manner which is comparable to the process of phosphorylation [75]. As discussed in the preceding section, their synthesis and removal are facilitated by groups of enzymes, thus allowing regulation of their concentration. Whilst they do not act on specific receptors to achieve their effect, specificity of action is achieved by two other mechanisms. Unlike other ROS, which are highly reactive and can irreversibly damage molecules, superoxide anion and hydrogen peroxide are relatively mild oxidants. This fact ensures that only certain molecules are susceptible to their modification, granting these ROS a degree of selectivity [74]. In addition, their specificity is aided by spatial regulation whereby these ROS are compartmentalised within cells. This is achieved by discrete localisation of NOX enzymes and the relative ubiquity of scavenging enzymes within the cytoplasm, which work to limit the escape and accumulation of ROS.

There are various proteins which form targets for redox regulation. The most widely studied of these are kinases, which can be regulated in a redox-sensitive manner, both directly and indirectly. Oxidation of protein tyrosine phosphatases (PTPs), which reverse the action of kinases, leads to their inhibition, thus providing indirect kinase regulation [76]. An important example of this in the context of angiogenesis is the relationship between the receptor tyrosine kinase VEGFR2 and the protein tyrosine phosphatases SHP-1, SHP-2 and low-molecular weight PTP (HCPTPA). As will be described later, signalling by VEGFR2 is crucial to angiogenesis and the aforementioned PTPs inducibly associate with it following VEGF binding [77], [78], [79]. These PTPs have an inhibitory effect on VEGFR2

autophosphorylation [80], [81] and therefore attenuate signal transduction. Thus VEGFR2-directed ROS production inactivates these PTPs in a positive feedback loop necessary for normal VEGF-induced angiogenesis.

With regard to direct redox-regulation of kinases, it is becoming apparent that oxidation by ROS can both activate and inactivate certain kinases (drawing another parallel between redox signalling and phosphorylation). This phenomenon is best recognised with Src tyrosine kinase; its activation by oxidation is well established [82], but recent work by Kemble *et al* [83] has found that oxidation can also result in formation of inactive dimers. Other redox sensitive kinases include receptor tyrosine kinases (e.g. insulin receptor, PDGF receptor) [84], AKT and MAP kinases [85], [86].

In addition to PTPs and kinases, transcription factors such as HIF-1, and proteinases such as matrix metalloproteinase (MMP), are also redox sensitive [74]. The importance of this to the processes of angiogenesis and vascular repair will be discussed later.

1.2.4 Oxidative stress and insulin resistance

A significant body of research has highlighted a link between oxidative stress and insulin resistance, and in 2006 Houstis *et al* demonstrated a causal relationship [87]. Whilst a number of putative mechanisms exist to explain how ROS may contribute to insulin resistance, the precise nature is likely to vary depending on the tissue in question [88]. This section will therefore focus on general principles based on our current understanding (See figure 3).

ROS can activate a specific group of MAPKs termed 'stress-activated protein kinases' (SAPKs), such as c-Jun N-terminal kinases (JNKs) and IκB kinase (IKK) [87], via two mechanisms; firstly, by inactivating molecules which would otherwise inhibit the SAPKs, such as MAPK phosphatases. Additionally, ROS are able to increase the expression of pro-inflammatory cytokines such as interleukin-6 (IL-6) and TNFα, which directly activate the MAPKs [89]. Once activated, these SAPKs induce phosphorylation of IRS-1 on serines 302, 307 and 612, which results in suppression of IRS-1 binding to the IR and PI3K as well as promoting IRS-1 breakdown [90]. This interference with the PI3K/Akt signalling cascade is a mechanism whereby ROS can contribute to the 'pathway-specific insulin resistance' discussed in section 1.1.2.

As well as inducing inhibitory phosphorylation of IRS-1 via activation of SAPKs, TNFα and IL-6 have been shown to exert a long term inhibitory effect on the gene transcription of IRS-1 and GLUT-4 [91]. Furthermore, it has been proposed that TNFα can interfere with IR function, as neutralisation of TNFα with a soluble TNF receptor-IgG fusion protein increases insulin-stimulated phosphorylation of the IR [40].

Interestingly, whilst the consensus of current understanding is of insulin resistance and oxidative stress being pathological phenomena closely intertwined with the development of CVD, there is some evidence which suggests that insulin resistance could in fact be a defence mechanism against nutrient excess [92]. Hoehn *et al* demonstrated that mitochondrial superoxide production is a common feature in various models of insulin resistance, and also that insulin resistance is rapidly reversible upon exposure to mitochondrial uncoupling agents. Furthermore, acute induction of mitochondrial superoxide production causes rapid attenuation of insulin action independent of the PI3K/Akt pathway. The group went on to demonstrate that mice over-expressing mitochondrial superoxide dismutase (MnSOD) are protected from high-fat diet (HFD) induced insulin resistance, and that $MnSOD^{+/-}$ mice become glucose intolerant on a standard chow diet. In their conclusion, the authors suggested that insulin resistance may be part of the antioxidant defence mechanism to protect cells from oxidative damage and therefore be an appropriate response to increased nutrient accumulation.

Whilst there are a number of proposed mechanisms which lead to the development of insulin resistance (some of which are outlined in section 1.1.2), oxidative stress appears to be one of the overarching phenomena that are implicated within these disparate pathological processes. Furthermore, as will be discussed in following sections, oxidative stress is also understood to be a critical link between established insulin resistance and the development of CVD.

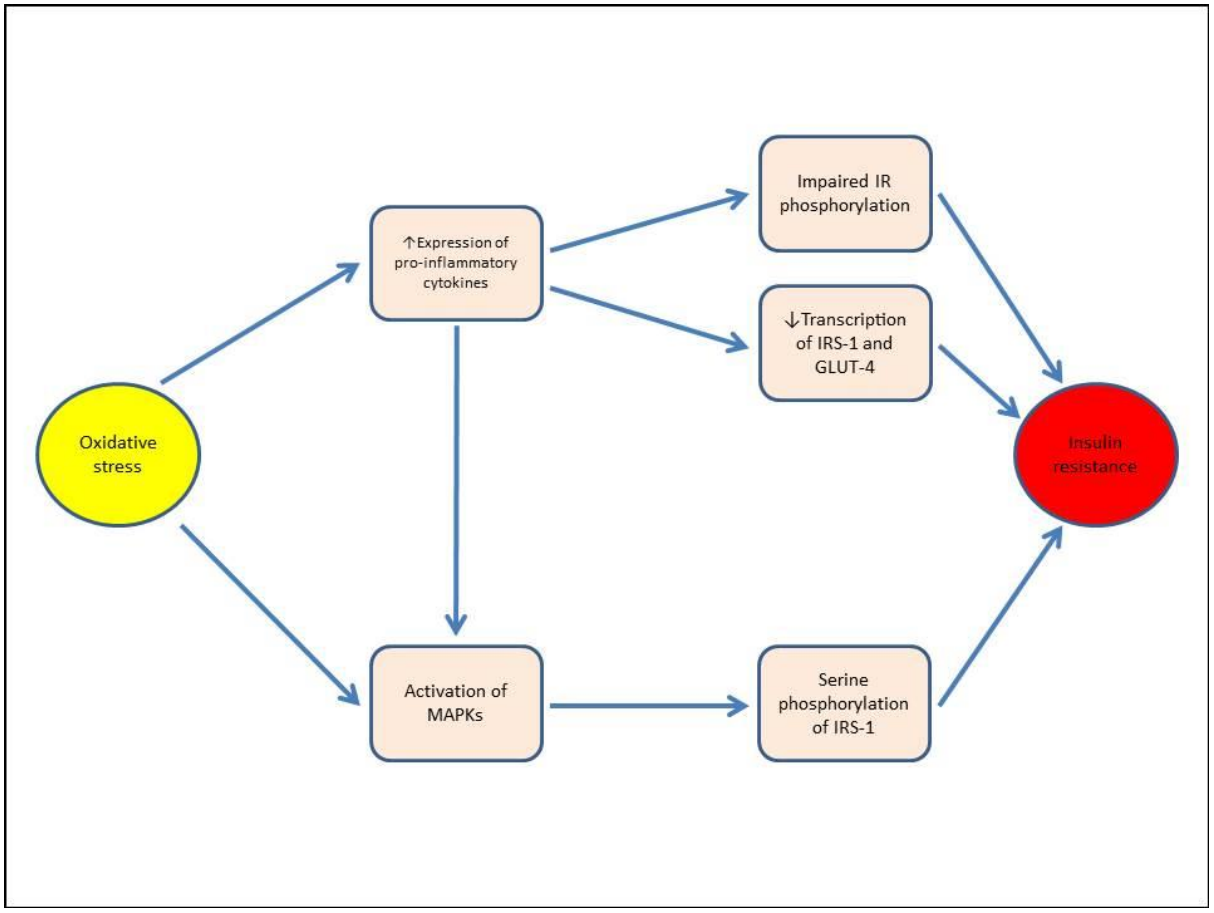

Figure 3. Oxidative stress and insulin resistance

Oxidative stress can induce increased expression of pro-inflammatory cytokines such as IL-6 and TNFα, which results in impaired IR phosphorylation and reduced transcription of IRS-1 and GLUT-4. In addition oxidative stress can activate stress-activated MAPKs such as JNKs and IKK which serve to phosphorylate IRS-1 on serines 302, 307 and 612, leading to impaired binding to the IR and PI3K. The net result of all of these actions contributes to the development of insulin resistance.

IL-6: interleukin-6; TNFα: tumour necrosis factor α; IR: insulin receptor; IRS-1: insulin receptor substrate-1; MAPK: mitogen activated protein kinase; JNK: c-Jun N-terminal kinases; IKK: IκB kinase; PI3K: phosphoinositide 3-kinase

1.3 Endothelial physiology and atherogenesis

1.3.1 Physiological role of the endothelium

The endothelium is a monocellular lining that covers the inner surface of the entire vascular system. Once thought of as an inert barrier with a purely protective function, our understanding has developed to the point where we now recognise the endothelium to be a complex and dynamic organ in its own right. Endothelial cells (ECs) have the capability to behave as both receptors and effectors, allowing them to sense different physical or chemical stimuli and then modify vessel function or release various substances in order to maintain physiological homeostasis [93]. One of the most important examples of this is the process of maintaining vascular tone. In order to achieve this, ECs produce and secrete a fine balance of substances that promote either vasoconstriction (ET-1, angiotensin 2 and various ROS) or vasodilation (NO, prostacyclin, hydrogen peroxide). By secretion of these mediators and others, the endothelium also plays an important role in platelet function, inflammation and coagulation.

1.3.2 Nitric oxide

Nitric oxide (NO) is one of the most important and widely studied mediators of vascular health. It is a biologically active, volatile gas which easily diffuses across plasma membranes due to its low molecular weight and lipophilicity [94]. NO is generated by the action of the enzyme nitric oxide synthase (NOS), of which there are three isoforms: endothelial (e)NOS, neuronal (n)NOS and inducible (i)NOS. All three isoforms share a dimeric structure, with a C-terminal reductase domain that binds nicotinamide adenine dinucleotide phosphate (NADPH) and an N-terminal oxygenase domain which binds L-arginine, tetrahydrobiopterin and a heme group [95]. Electron transfer from NADPH to the heme group leads to the reduction and activation of O_2, which facilitates hydroxylation of L-arginine to N-hydroxy-L-arginine. This is then oxidised to form NO and L-citrulline [96].

Whilst endothelial cells express both eNOS and iNOS, the predominant isoform found within the vasculature is eNOS. Of particular significance to its role within the cardiovascular system is the fact that both the expression and activity of eNOS can be regulated by specific stimuli; vascular endothelial growth factor (VEGF), shear stress and

insulin have all been shown to upregulate eNOS expression [97, 98], and can also trigger its activation via phosphorylation of serine 1177 [99]. This ability of eNOS expression and activation to change in response to pertinent stimuli is crucial in allowing the cardiovascular system to adapt and maintain homeostasis. Modulation of eNOS activity can also be achieved via phosphorylation of multiple other residues, and in response to elevated levels of intracellular calcium.

NO has a multitude of functions within the vasculature, the most studied of which is its role in maintaining vascular tone. This is achieved via mediation of vasodilation and has been demonstrated experimentally using levo-N-monomethyl arginine (L-NMMA), a specific inhibitor of NOS. Infusion of L-NMMA into rabbit models causes a marked increase in systolic blood pressure, whilst ex-vivo exposure of aortic rings to L-NMMA can reverse L-arginine mediated vasodilatation [100]. In human studies, infusion of L-NMMA into the brachial artery of healthy volunteers results in blunted flow-mediated vasodilation [101]. In order to exert its vasodilatory effect, NO crosses through ECs to reach VSMCs where activation of soluble guanylate cyclase results in production of cyclic guanosine monophosphate (cGMP). This sequence of events regulates cytoplasmic calcium concentrations, encouraging VSMC relaxation and therefore vasodilatation [102].

NO also has an important role in protecting against development and progression of atheroma. It has an anti-proliferative effect on VSMCs [103, 104], whilst also negatively regulating the expression of adhesion molecules such as P-selectin, vascular cell adhesion molecule-1 (VCAM-1) and intercellular adhesion molecule-1 (ICAM-1) on the surface of ECs [105]. Furthermore, an ability to interfere with leucocyte adhesion to ECs imbues NO with anti-inflammatory properties [106]. Taken together, these characteristics highlight NO to be an anti-atherogenic molecule, and its ability to inhibit platelet aggregation [107, 108] and thrombin-induced platelet adhesion to the vascular endothelium [109] means that it is also anti-thrombotic, reducing the risk of thrombus formation on vulnerable plaques. Given that the majority of CVD is atherosclerosis-mediated, the importance of NO to the maintenance of cardiovascular health can scarcely be overstated. The mechanism whereby insulin resistance can impair NO production has been discussed earlier, but NO bioavailability can also be reduced via sequestration by an excess of ROS and this will be discussed in section 1.3.4.

1.3.3 Endothelial dysfunction

Endothelial dysfunction can be defined as the pathological state resulting from an imbalance of vasodilating and vasoconstricting substances produced by or acting on ECs [110]. A hallmark of the condition is impairment of NO-mediated vasodilation due to either reduced production or increased breakdown/inactivation of NO.

Endothelial dysfunction is recognised as one of the initiating steps in the development of atherosclerosis [111]. Invasive assessment of endothelial function can be performed using acetylcholine (ACh), which induces endothelium-dependant dilation and smooth muscle-mediated constriction. In the coronary arteries of healthy individuals, the predominant response to ACh is endothelial-dependant dilation. However, when the endothelium is damaged the balance is shifted towards smooth muscle-mediated vasoconstriction. Comparison of coronary artery diameter before and after ACh infusion can thus be used to identify endothelial dysfunction. Non-invasive techniques to identify and quantify endothelial dysfunction have subsequently been developed, an example of which is ultrasound detected flow-mediated dilation (FMD) in the brachial artery in response to reactive hyperaemia. The increased blood flow and shear stress induced by the reactive hyperaemia stimulates NO release and FMD, which can be used as measure of vasomotor function [112].

Coronary angiography pre- and post-ACh infusion was used to provide the first human evidence of endothelial dysfunction in the presence of atherosclerosis, where paradoxical vasoconstriction was observed in the arteries of patients with both advanced and mild coronary artery disease (CAD) [113]. Ultrasonic detection of FMD has since been used to demonstrate endothelial dysfunction in the preclinical stage of atherosclerosis, prior to angiographic or ultrasonic evidence of atherosclerotic plaque, and it is now accepted that endothelial dysfunction is itself an independent predictor for the development of CVD [114].

1.3.4 Oxidative stress and endothelial dysfunction

At physiological levels, ROS play an important role in maintaining endothelial health. Hydrogen peroxide promotes calcium-dependant eNOS activity, allowing appropriate concentrations of NO to be produced [115]. However, when their concentration becomes

excessive, ROS can lead to a reduction in the bioavailability of NO, and so oxidative stress can promote endothelial dysfunction.

In conditions of oxidative stress, the excess of superoxide anion can sequester NO by reacting with it to form peroxynitrite ($ONOO^-$). Peroxynitrite can then oxidise the eNOS cofactor tetrahydrobiopterin (BH_4) to form the inactive molecule BH_2. This reaction leads to the uncoupling of eNOS, resulting in the production of further superoxide anion instead of NO, and thus propagating the cycle [116] (see figure 4).

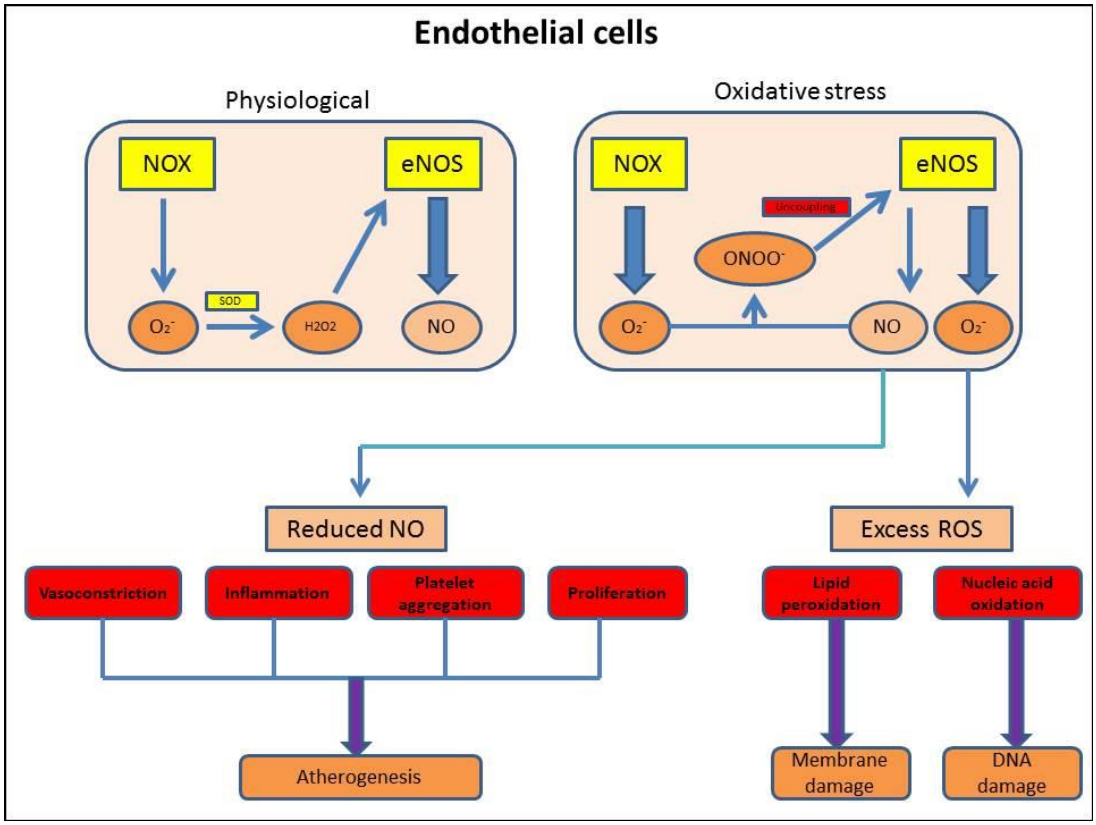

Figure 4. Oxidative stress and endothelial dysfunction

In health NADPH oxidase produces superoxide anion (O_2^-), which is dismuted into hydrogen peroxide (H_2O_2) by the action of superoxide dismutase (SOD). H_2O_2 can promote activation of eNOS, increasing nitric oxide (NO) bioavailability, which maintains endothelial function. In the setting of oxidative stress, excess production of O_2^- results in sequestration of NO via a reaction to produce peroxynitrite ($ONOO^-$). $ONOO^-$ oxidizes the eNOS cofactor BH_4, uncoupling eNOS to then produce further O_2^-. The reduction in NO bioavailability leads to impaired vasodilation as well as inflammation, platelet aggregation and cell proliferation, all of which are contributory factors to atherogenesis. The excess ROS can also react with cellular macromolecules such as lipids and nucleic acids resulting in damage to membranes and DNA. Taken with permission from Ali *et al* [73].

1.3.5 Atherosclerosis

Atherosclerosis is a disease whose insidious onset and progression belies the fact that it is thought to underpin up to half of all deaths in Western societies [117]. The enormous burden of morbidity and mortality resulting from atherosclerosis-related diseases mean that it has been an area of intense research for almost two centuries. In 1856 Rudolph Virchow challenged the contemporary dogma that atherosclerosis was purely a result of lipid accumulation within arterial walls, and hypothesised an important role for inflammatory changes in the development of the disease [118]. Over subsequent decades his theory has been expanded and refined to the point where we now appreciate atherosclerosis to be an inflammatory condition [10].

The earliest lesions associated with atherosclerosis can be identified in the first decade of life and are termed 'fatty streaks'. These tend to form preferentially at specific points within arteries such as bifurcations, or areas of curvature due to perturbations in blood flow dynamics. The turbulent flow in these areas generates shear stress that acts on the ECs and affects their morphology. Whereas in areas of laminar blood flow ECs are ellipsoid in shape and aligned in the direction of flow, in areas of disturbed flow the ECs have a polygonal shape and a disordered orientation [117]. These changes in the EC monolayer result in increased permeability to macromolecules such as low-density lipoprotein (LDL), allowing for the initiation of fatty streak formation. The abnormal shear stress also stimulates EC expression of cell surface molecules such as ICAM-1 [10], and release of mitogens such as platelet derived growth factor (PDGF)-B [119]. These modulate local immune response by encouraging recruitment of inflammatory cells, such as rolling and adhesion of monocytes. These monocytes can then migrate into the sub-endothelium where they can become activated and differentiate into macrophages [10]. Activated macrophages produce ROS which oxidise LDL to form oxidised LDL (ox-LDL), stimulating overlying ECs to produce pro-inflammatory molecules such as macrophage-colony stimulating factor (M-CSF) and monocyte chemoattractant protein (MCP), thus perpetuating the inflammatory infiltration cycle. Ox-LDL is also able to inhibit production of the anti-atherogenic molecule NO [117].

Macrophages within the fatty streak internalise and accumulate LDL, transforming into foam cells in a process mediated by cell-surface scavenger receptors. Expression of

scavenger receptors is regulated by cytokines such as TNFα and peroxisome proliferator-activated receptor-γ (PPAR γ), a transcription factor whose ligands include oxidized fatty acids [117]. Foam cells eventually undergo necrosis, releasing pro-inflammatory cytokines into the circulation. In conjunction with the cytokines and growth factors secreted by macrophages and T-cells, the effect is to stimulate migration and proliferation of SMCs as well as production of extra-cellular matrix. The resulting fibrosis allows a 'fibrous cap' to from, shielding the circulation from the thrombogenic core of the atherosclerotic lesion [117]. Whilst a plaque may remain stable for many years with a fibrous cap in place, a patient may experience symptoms based on the level of luminal obstruction caused by the lesion. If the vessel calibre is narrowed to the extent that adequate tissue perfusion during stress is impeded, conditions such as angina pectoris and intermittent claudication may develop.

The culminating event in the natural history of some atherosclerotic plaques is ulceration and rupture, triggering a sequence of events which result in thrombosis within the vessel. Pathological studies have shown that the likelihood of this cascade occurring is principally dependent upon the composition and vulnerability of the plaque, rather than degree of stenosis [117]. The main features thought to influence plaque vulnerability are the thickness of its fibrous cap, as well as the abundance of inflammatory cells within it, since macrophages produce various proteases that contribute to degradation of the cap. Additional factors which influence the stability of advanced lesions are intimal calcification and neovascularisation, which provides a route for inflammatory cells into the plaque [117]. Following rupture of the plaque, the thrombogenic core of the lesion is exposed to the platelets and coagulation factors within the circulation, resulting in thrombus formation, which can lead to acute vascular occlusion and downstream tissue infarction.

1.4 The role of ROS in insulin resistance-associated vascular disease

In order to dissect the role of ROS in the link between insulin resistance and vascular disease, our group has studied a number of murine models which aim to represent the pre-diabetic phenotype. In 2007 we published a study [120] demonstrating that IRKO mice displayed accelerated endothelial dysfunction relative to wild-type (WT) controls, in spite of preserved glucose regulation. The study also found that use of a SOD mimetic could restore endothelial function in IRKO mice, which were shown to generate greater quantities of ROS than WT counterparts. As well as the genetically induced insulin resistance examined in this study, there is also evidence to show that ROS have a role to play in the insulin resistance and endothelial dysfunction that is observed secondary to diet-induced obesity [121]. This paper demonstrated that middle-aged mice fed with a high fat diet (HFD) developed obesity, dyslipidaemia, hypertension, insulin resistance and endothelial dysfunction associated with increased NOX2 expression and ROS production. Inhibition of NOX2, either pharmacologically or genetically, reversed all of the HFD induced abnormalities except for hyperinsulinaemia. The conclusion from this study was that NOX2-derived ROS play a key role in damaging insulin signalling and endothelial function in dietary obesity after middle age.

Given the close relationship between insulin resistance and endothelial dysfunction, we have undertaken further work focussing on the effect of endothelial specific insulin resistance using ESMIRO mice. ESMIRO mice, which display normal glucose regulation, have impaired endothelial function associated with reduced NO bioavailability, which could be rescued *in vitro* with a SOD mimetic [56]. Furthermore, when ESMIRO mice were cross-bred with atherosclerosis-prone ApoE deficient mice, the resulting $ApoE^{-/-}$/ESMIRO mice exhibited accelerated atherosclerosis [13]. This finding has been independently corroborated by Rask-Madsen *et al,* who demonstrated that $ApoE^{-/-}$ mice with endothelial insulin receptor knockout had increased atherosclerosis relative to $ApoE^{-/-}$ mice [122].

In the aforementioned endothelium-specific insulin resistance studies performed by our group, the combination of elevated levels of ROS, and the ability of pharmacological superoxide diminution to reverse the observed endothelial dysfunction, implicates oxidative stress as an underlying mechanism. This suggests that NOX2, the primary

generator of superoxide anion within the vasculature, could form a target for reducing oxidative stress and the associated endothelial dysfunction in insulin resistance. To this end, our group has generated transgenic ESMIRO mice with global NOX2 knockout (ESMIRO/NOX2$^{y/-}$) and demonstrated that genetic NOX2 inhibition could reduce superoxide levels and improve vascular function [123]. These findings were replicated with use of either acute or chronic pharmacological inhibition using the NOX inhibitor GP91ds-tat. This study established NOX2 inhibition as a novel therapeutic target in insulin resistance-associated vascular dysfunction.

1.5 Vascular regeneration and repair

As discussed in section 1.3.5, the culminating event in atherosclerotic disease such as MI or stroke is the rupture of a plaque, triggering thrombus formation and acute vascular occlusion. Endogenous vascular repair mechanisms are responsible for re-endothelialisation of the blood vessels injured by the formation and rupture of plaques. Meanwhile, downstream tissues rendered ischaemic by vascular occlusion depend on the formation of neovessels for their reperfusion. There are three recognised forms of neovascularisation: angiogenesis, arteriogenesis and vasculogenesis.

1.5.1 Angiogenesis

Angiogenesis is the term given to the sprouting or intussusception of neovessels from pre-existing vasculature and is the predominant means of generating capillary beds in adulthood [124], as well as the key process involved in post-ischaemic neovascularisation [125]. The vascular endothelium is crucial to this process and ECs are required to proliferate, migrate and form capillary tubes [126]. This complex process is initiated by pro-angiogenic factors, with VEGF being the best recognised of these. Following exposure to VEGF, quiescent ECs form sprouts that comprise tip cells and stalk cells. The tip cells are positioned at the leading point of the sprouts and migrate along a VEGF gradient. The stalk cells proliferate behind the tip cells to form a column within which the capillary lumen forms [21]. Vessel loops are formed when tip cells anastomose with cells from neighbouring sprouts [126].

The initial hypothesis that insulin resistance can disturb angiogenesis came from extrapolation of data showing diminished vascular regeneration in a range of disorders underpinned by the phenomenon. Diabetes is known to impair collateral artery formation in the setting of coronary and peripheral arterial disease [127], and has been shown to be associated with impaired angiogenesis in chronic wounds [128]. Furthermore, obesity has been demonstrated to be associated with reduced angiogenesis following hind-limb ischaemia [129]. Following on from these and other similar studies, our group has provided direct evidence that insulin resistance *per se* can impede vascular regeneration, as IRKO mice were shown to display impaired post-ischaemic neovascularisation as well as *in vitro* indices of angiogenesis [130].

1.5.2 Vascular repair

Vascular repair is the process whereby injured, established conduit vessels are re-endothelialised in order to re-establish vessel integrity. There are currently two proposed mechanisms by which this occurs; proliferation and migration of ECs adjacent to the injured vessel segment which replace lost and damaged cells, and the recruitment of bone marrow derived progenitor cells which home to the site of injury and assist in repair by either direct incorporation or paracrine stimulation of resident ECs [131]. Debate is ongoing around the latter of these theories, and this will be discussed in more detail in section 1.5.3.

As well as impairing angiogenesis, insulin resistance has also been demonstrated to impede vascular repair, either in the context of diabetes, or in isolation. Diabetes has been shown to be associated with impaired coronary re-endothelialisation after percutaneous intervention [132], and further work on the IRKO mouse model by our group has demonstrated diminished femoral arterial repair following injury in the setting of insulin resistance [12].

1.5.3 Endothelial progenitor cells

Vasculogenesis, which is the *de novo* formation of blood vessels, was previously thought to be exclusively limited to embryonic development. However work done by Asahara *et al* [133] challenged this notion with the discovery of 'putative progenitor endothelial cells' in adults. The premise for this work was the hypothesis that peripheral blood contained stem cells which could differentiate into ECs. In order to examine this, the authors identified CD34 and VEGFR-2 as cell surface markers which are expressed by both ECs and haematopoietic stem cells (HSCs), but which are lost during maturation of the latter. Cells expressing either of these markers were isolated from human blood mononuclear cells by magnetic separation and were found to display an endothelial-like phenotype during *in vitro* culture-expansion, and augment angiogenesis when re-infused into mice with hind limb ischaemia.

This work has led to a great deal of subsequent research aimed at further characterising the nature of these cells, as well as their potential role in post-natal vasculogenesis. The cell surface selection markers used in the seminal Asahara *et al* paper have since been

extrapolated by other groups, with most studies using a combination of the haematopoietic cell markers CD133 and CD34, as well as the endothelial cell marker VEGFR-2. Cells which co-express these markers are identified by use of fluorescently labelled antibodies and flow cytometry and have been loosely termed 'endothelial progenitor cells' (EPCs) [134]. EPCs are postulated to be capable of contributing to vascular repair [135], and their abundance has been shown to independently predict future major cardiovascular events [136].

An alternative method for obtaining EPCs involves utilising cell culture techniques in order to manipulate circulating peripheral blood mononuclear cells (PBMCs), as originally demonstrated by Asahara *et al* [137]. These techniques have led to the discovery of two subsets of EPCs based on the duration of their culture in endothelial growth medium; 'early outgrowth EPCs' (EEPCs) following 4-7 days' culture, and 'late outgrowth EPCs' (LEPCs) following sustained culture over a period of weeks. These two groups of EPCs are disparate, both morphologically and functionally. EEPCs have a spindle-shaped appearance, similar to the cells seen by Asahara *et al* [133], have only a limited capacity for proliferation, and retain functional and surface marker characteristics of myeloid cells. *In vivo* studies have shown that EEPCs appear unable to incorporate directly into the endothelium but can augment angiogenesis and vascular repair in a paracrine fashion [138]. In contrast, LEPCs have an appearance akin to endothelial cells [137], are rapidly proliferative *in vitro* where they can form capillary-like structures [138], and display a true progenitor population hierarchy.

Further insights into EPC biology have been facilitated by the identification of murine equivalents of these cells. Murine EPCs are marked by co-expression of stem cell antigen 1 (Sca1) and VEGFR-2/Kinase insert domain receptor (KDR) [139]. Interestingly, whilst murine EEPCs have been consistently derived from blood as well as homogenised marrow and spleen tissue, sustained culture of murine LEPCs have proved to be much more challenging to establish [140].

The relationship between circulating EPCs and those derived by cell culture remains unclear. Whilst there have been *in vivo* studies to show that LEPCs are able to contribute directly to vascular regeneration [138], a study performed by Hagensen *et al* suggested that vascular repair following carotid artery wire injury is solely mediated by the migration

of ECs from adjacent healthy endothelium [141]. Nevertheless, whilst there remains significant debate regarding the existence and role of EPCs *in vivo*, there is a general acceptance that such cells represent a potential autologous cell-therapy to promote vascular repair and neovascularisation [135]. For the purpose of clarity, for the remainder of this thesis endothelial progenitor cells derived from cell culture techniques will be referred to as 'EPCs', whilst circulating progenitor cells will be referred to as 'CPCs', reflecting our ongoing uncertainty as to their role *in vivo*.

1.6 Redox signalling in angiogenesis and vascular repair

Having outlined the mechanisms involved in angiogenesis and vascular repair, the following section describes the role of ROS as signalling molecules within these pathways by highlighting a few key relationships (simplified schematic shown in figure 5).

1.6.1 ROS and VEGF

VEGF is the most widely studied pro-angiogenic factor and its signalling is achieved through interaction with three receptors; VEGFR1, VEGFR2 and VEGFR3 [142]. Its mitogenic and chemotactic effects in ECs are mediated principally through VEGFR2. Binding of VEGF to VEGFR2 promotes ROS production from two sources; firstly, by activation and translocation of Rac1 to the plasma membrane, thus completing the NOX2 NADPH oxidase complex. Secondly, it increases production of mitochondria derived ROS [143]. The resultant higher levels of ROS inactivate PTPs, removing their negative regulation of VEGFR2. This has the effect of enhancing VEGFR2 autophosphorylation, thereby activating downstream signalling pathways essential for EC proliferation and migration such as eNOS, MAPK and Akt [144].

Whilst VEGF can stimulate increased ROS production, the reverse is also true. ROS, produced either by NADPH oxidase or mitochondria, can induce the expression of redox-sensitive genes, such as VEGF, via induction of redox sensitive transcription factors including HIF-1 [144]. Thus a cyclical relationship exists between ROS and VEGF whereby increasing concentrations of one can promote production of the other.

It is important to note that whilst increasing ROS levels will increase VEGF-induced angiogenesis, this effect can be mitigated by VEGF-independent mechanisms above a certain ROS threshold. A study performed by Okuno *et al* [145] on the topic of pathological angiogenesis provided a novel explanation for the mechanism by which an excess of ROS could retard angiogenesis. The protein kinase ataxia telangiectasia mutated (ATM) is mutated in patients with the condition ataxia telangiectasia, which is characterised by blood vessel instability. The cited study found that inhibiting wild-type ATM in ECs led to an increased ROS level, thereby activating p38α which induces growth arrest and attenuates angiogenesis. Taking this into account, it appears that in the context of angiogenesis ROS

could be viewed as a double-edged sword depending on their prevailing level, and this is a theme which will be discussed later.

1.6.2 ROS and HIF-1

Hypoxia is a crucial stimulus for angiogenesis, and its effects are mediated by a group of 3 transcription factors called Hypoxia Inducible Factors (HIFs 1-3). ROS are involved in the regulation of HIF-1 levels by exerting a level of control on both its production and degradation [143]. ROS can increase HIF-1 production by activating the nuclear factor kappa-light-chain-enhancer of activated B cells (NF-kB) and PI3K/Akt/4E-BP1 pathways [146] and [147]. HIF degradation can also be suppressed by depletion of cellular ascorbate, which is a cofactor for prolyl hydroxylate proteins (PHDs). This inhibits HIFα hydroxylation, and therefore Von Hipel-Lindau (VHL) complex mediated ubiquitination of HIF [143].

1.6.3 ROS and CPCs

Current evidence suggests that CPCs are mobilised from the BM into peripheral blood in response to tissue injury or ischaemia [148], and then migrate to damaged endothelium. They may then contribute to neovascularisation or vascular repair by either differentiating into ECs or by secreting pro-angiogenic factors and cytokines [138].

Mobilisation

CPC mobilisation can be modulated by endogenous and pharmacological agents. Examples of endogenous cytokines which trigger CPC mobilisation include VEGF and stromal cell-derived factor 1 (SDF-1), both of which are produced by ischaemic tissues. Additionally, granulocyte monocyte colony-stimulating factor (GM-CSF), granulocyte colony-stimulating factor (G-CSF) and erythropoietin (EPO) have been found to be potent CPC mobilising agents. Pharmacological agents known to induce CPC mobilisation include statins and PPAR agonists [148].

The local bone marrow environment, termed the ‘stem-cell niche’, governs the maintenance and mobilisation of CPCs [148]. Cytokines which induce release of CPCs from BM interfere with the interactions between stem cells and BM stromal cells, allowing them to pass into the bloodstream. This process is mediated by proteinases such as elastase and MMPs [149]. MMP-9 cleaves membrane bound Kit ligand and releases soluble Kit ligand

(sKitL) which facilitates the mobilisation of CPCs from the stem cell niche [65]. Since MMP is a redox sensitive protein whose expression is upregulated by ROS, this imbues ROS with the ability promote CPC mobilisation.

Homing

Once released into the bloodstream, CPCs home to the area in need of neovascularisation or re-endothelialisation. This process appears to share common features with the homing of leucocytes to areas of inflammation and involves cytokines, adhesion molecules and proteases [150].

The cytokine SDF-1, noted earlier for its ability to trigger CPC mobilisation, is also involved in the recruitment of CPCs to target tissue. SDF-1 expression has been found to be up-regulated in ischaemia [151], and its over-expression has been shown to enhance stem cell homing and incorporation into ischaemic tissue [152]. A study by Urao *et al* [153] demonstrated the influence of ROS in this process. In a model of hind limb ischaemia, NOX2 knockout ($NOX2^{y/-}$) mice displayed impaired ischaemia-induced flow recovery and CPC mobilisation from BM. *In vitro* experiments showed progenitor cells from $NOX2^{y/-}$ BM to have impaired chemotaxis and invasion in response to SDF, associated with blunted SDF-1 mediated phosphorylation of Akt.

The homing capacity of CPCs also involves various adhesion molecules [150]. One of the crucial steps in the homing process is thought to be the rolling of the cells on the vascular endothelium, mediated by the selectin family of adhesion molecules. E-selectin is expressed exclusively on ECs, whilst P-selectin is expressed on both ECs and platelets [150]. NADPH oxidase-derived ROS have been found to be involved in the expression of both on the endothelial cell surface [154], [155] and [156]. Other adhesion molecules known to be of importance to EPC homing are ICAM-1 and VCAM-1, both of whose expression is known to be mediated by ROS [157].

1.6.4 ROS and Nitric Oxide

Nitric oxide is well established as being a critical molecule for maintenance of endothelial health, and it is also understood to be of importance in facilitating angiogenesis and vascular repair. Physiological concentrations of NO have been demonstrated to exert a direct effect on EC proliferation and survival [158], whilst CPC mobilisation also appears to be dependent upon NO [159]. Given these observations, it is perhaps unsurprising that eNOS deficient mice display impaired revascularisation [160].

As outlined in section 1.3.4, at physiological concentrations ROS (specifically hydrogen peroxide) activate eNOS, promoting production of NO. Conversely, at supra-physiological concentrations ROS can sequester NO resulting in the formation of $ONOO^-$, which ultimately causes uncoupling of eNOS.

Whilst the scavenging of NO in order to produce $ONOO^-$ clearly has detrimental effects on vascular function, it is important to note that $ONOO^-$ itself can be directly damaging. Ballinger *et al* demonstrated that mitochondrial protein synthesis is inhibited in a dose-dependent manner by $ONOO^-$, resulting in reduced cellular ATP levels and mitochondrial redox function [161]. In addition to direct cellular toxicity, $ONOO^-$ can also cause oxidative damage to cellular proteins and lipids [162].

1.6.5 ROS and ECs

ECs are instrumental in orchestrating the multiple events involved in angiogenesis and vascular repair. Peshavariya *et al* demonstrated that ROS play a role in regulating their proliferation and apoptosis [163]. This paper found that NOX4-derived hydrogen peroxide promotes EC proliferation via activation of ERK 1/2, whilst NOX2-derived ROS support cell survival by maintaining cytoskeletal integrity and preventing apoptosis.

EC migration is crucial to the process of vascular regeneration, and disruption of intercellular connections is required in order to facilitate this [164]. Vascular endothelial-(VE-) cadherin is the main adhesion component of these connections and is linked to the actin cytoskeleton by α and β catenins and p120. ROS-dependant phosphorylation is responsible for disassembly of the VE-cadherin-catenins complex and leads to EC junctional breakdown [143].

As well as assisting in breaking intercellular connections, ROS have a role in modulating the motility of migrating ECs. The process of actin network remodelling, which modulates cell shape and motility, is dependent on ROS for its regulation [165]. ECs also use ROS to direct their mobility by localising NADPH oxidase (and thus ROS production) to focal complexes in lamellipodia and membrane ruffles [166].

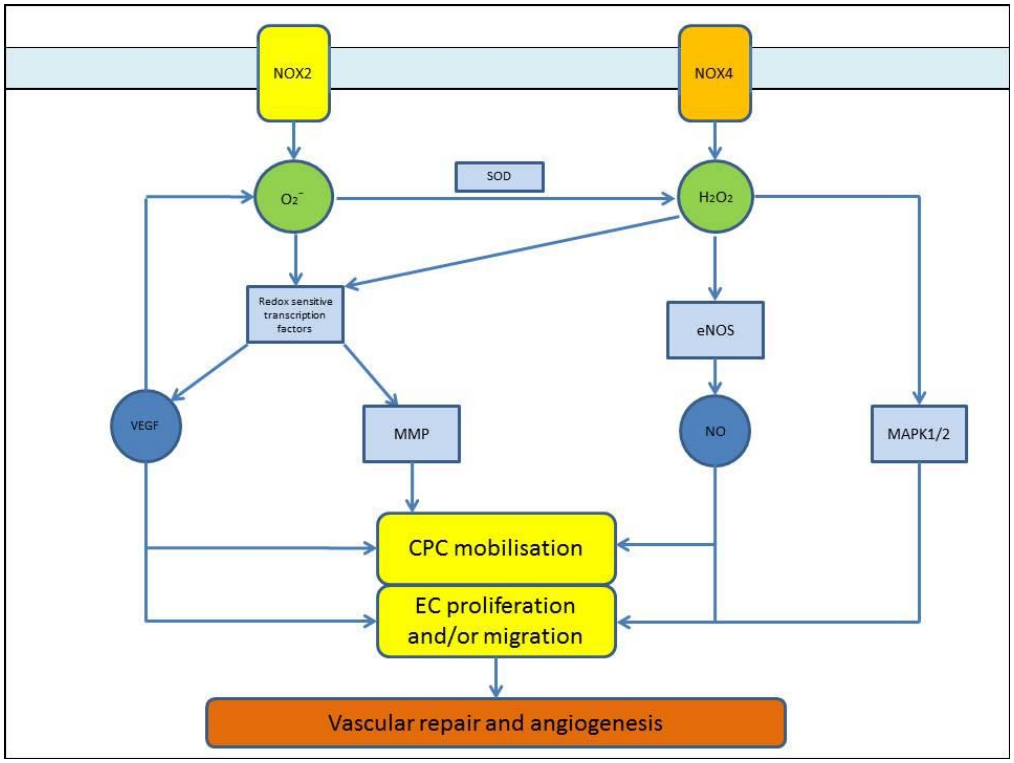

Figure 5. Redox signalling in angiogenesis and vascular repair

NOX2-derived superoxide anion (O2-) activates redox sensitive transcription factors, resulting in increased production of MMP and VEGF. MMP and VEGF are involved in CPC mobilisation, whilst VEGF is also important for EC proliferation/migration as well as stimulating further O2- production. Hydrogen peroxide (H2O2) is produced by NOX4 and via the action of superoxide dismutase (SOD) on O2-. H2O2 activates redox sensitive transcription factors as well as eNOS and MAPK1/2; eNOS produces NO which facilitates CPC mobilisation and EC migration, whilst MAPK1/2 are involved in EC proliferation and migration.

1.7 Manipulation of ROS in the context of angiogenesis and vascular repair

1.7.1 Angiogenesis

The preceding section of this chapter has explored the role of ROS on some of the individual components involved in the process of angiogenesis; numerous *in vivo* experiments have also been conducted which bring these together in order to provide a more holistic view. The research in this area has focussed mainly on angiogenesis in the setting of ischaemic revascularisation, tumour development and proliferative retinopathies.

Angiogenesis in ischaemic revascularisation

The term 'ischaemic revascularisation' refers to the process of collateral blood vessel formation which occurs following an MI, stroke or in the context of critical limb ischaemia in order to re-perfuse tissue which has been rendered ischaemic. The hindlimb ischaemia model, whereby femoral artery ligation is followed by assessment of ischaemia-mediated flow recovery, is a commonly used method to study this process and was used by Tojo *et al* [167] to investigate the role of NOX2 derived ROS on angiogenesis. The study found that NOX2 expression and ROS levels are increased in response to hindlimb ischaemia. Furthermore $NOX2^{y/-}$ mice were found to have impaired angiogenesis relative to WT controls. These findings were corroborated by Urao *et al* [153], who went on to show that the impaired angiogenesis seen in $NOX2^{y/-}$ mice could be ameliorated by the transplantation of WT BM. The conclusion from this study was that the effect of NOX2-derived ROS on angiogenesis is mediated via BM derived CPCs.

The same group then went on to investigate the role of endothelial-derived ROS in angiogenesis, looking specifically at H_2O_2 by using transgenic mice over-expressing endothelial catalase [168]. These transgenic mice were shown to have delayed blood flow recovery as well as reduced capillary formation and collateral remodelling in comparison to WT littermates. This led to the conclusion that endogenous EC-derived H_2O_2 is critical to post-ischaemic neovascularisation. These findings were in keeping with previous research done on endothelial-specific NOX4-derived ROS and angiogenesis. Craige *et al* [70] found

NOX4 to be expressed in response to hypoxia, both *in vitro* and *in vivo*, and that mice over-expressing NOX4 had augmented angiogenesis relative to WT following hindlimb ischaemia. Cultured ECs over-expressing NOX4 displayed increased eNOS expression and activity, leading to the conclusion that NOX4 promotes hypoxia-induced angiogenesis in an eNOS-dependant manner.

The previous study focussed on endothelial-specific NOX4, and research has also been done looking at the effect of global NOX4 knockout on angiogenesis. Schroder *et al* [69] found that $NOX4^{-/-}$ mice had attenuated angiogenesis relative to WT controls, and a link between NOX4 and eNOS expression was once again put forward. Zhang *et al* [169] found that myocardial angiogenesis is impaired in $NOX4^{-/-}$ mice compared to WT in the setting of pressure overload-induced cardiac hypertrophy, due to attenuation of HIF-1 activation, and therefore VEGF production.

This multitude of studies confirm the fact that ROS play an integral part in the process of angiogenesis, and that deletion of NADPH oxidases 2 or 4 in a physiological setting is detrimental. However, when considering human disease states and potential therapeutic strategies, manipulation of ROS levels in models better reflecting clinical disease is also important. To this end, studies have been performed assessing the impact of NADPH oxidase deletion on angiogenesis in situations of oxidative stress.

In 2006 Ebrahimian *et al* [170] published a paper exploring the effect of diabetes-induced oxidative stress on post-ischaemic angiogenesis. Using the previously described hindlimb ischaemia model, this study found type-1 diabetic mice to have impaired post-ischaemic neovascularisation relative to wild-type littermates. The study went on to show that reduction of ROS levels in the setting of diabetes, using $NOX2^{y/-}$ type-1 diabetic mice, could restore the angiogenic capacity back to WT levels. The finding that NOX2 deletion has a protective effect on angiogenesis in the context of oxidative stress has been corroborated by Haddad *et al* in two recent studies. In the first [171], the pathological state was exposure to cigarette smoke. WT and $NOX2^{y/-}$ mice were exposed to one cigarette twice a day for 14 days prior to unilateral femoral artery removal and their recovery from hindlimb ischaemia compared. The second study [172] used hypercholesterolaemia as the disease state, whereby wild-type and $NOX2^{y/-}$ mice were rendered hypercholesterolaemic by a 15 week high cholesterol diet, and once again compared with respect to their post-ischaemic

neovascularisation. In both studies NOX2 deletion, and the resultant reduction in ROS production, was shown to be beneficial to angiogenesis with the proposed mechanism being preservation of the VEGF/NO signalling pathway.

Tumour angiogenesis

Angiogenesis is crucial to tumour growth and development, reflected by the fact that it is recognised as one of the six hallmarks of cancer [173]. NOX1 derived ROS have been demonstrated to play a pivotal role in tumour angiogenesis [174], and Garrido-Urbani *et al* [175] went on to study the effect of NOX1 inhibition on tumour vasculogenesis. Using an *in vivo* matrigel angiogenesis assay, this study showed that $NOX1^{-/-}$ mice exhibit impaired angiogenesis and that tumour vascularisation is inhibited by genetic or pharmacological NOX1 inhibition. The authors' conclusion was that NOX1 is a mediator of tumour angiogenesis and exerts its effects via inhibition of the anti-angiogenic factor PPARα. Interestingly, the same study found genetic inhibition of NOX2 and NOX4 to have no effect on angiogenesis, which contrasts to the findings of previously mentioned studies in this chapter. This apparent contradiction is not yet fully understood, but may be a reflection of the mechanistic differences that exist between ischaemic revascularisation and tumour angiogenesis.

Angiogenesis in proliferative retinopathies

Pathological angiogenesis is a hallmark feature both diabetic retinopathy (DR) and retinopathy of prematurity (ROP). DR is the most common global cause of acquired blindness and has been divided into two stages: an early, non-proliferative stage and a later, proliferative stage. Oxidative stress has been recognised to play an important role in the development of the disease, and studies have shown that the retinas of diabetic rats have higher levels of NADPH oxidase and lower levels of SOD that those of their non-diabetic counterparts [176]. Increased NOX2 within retinal vessels has been correlated with increased VEGF expression and vascular permeability. Rojas *et al* found that deletion of NOX2 in either bone marrow or retina could attenuate the increased VEGF and ICAM-1 expression, as well as the leukostasis, seen in the retina of diabetic mice [177].

The role of ROS has also been examined in the pathogenesis of ROP. A study performed by Saito *et al* [178] reported that when rats with ROP were exposed to hyperoxia (28% O_2)

rather than room air (21% O_2) in phase 2 of ROP, there was increased activation of NOX2. Furthermore, it was reported that administration of the NADPH oxidase inhibitor apocynin reduced the intra-vitreous neovascularisation (INNV) area in these rats.

1.7.2 Vascular repair

As well as angiogenesis, there is also evidence to support a role for NADPH oxidase-derived ROS in the process of vascular repair. Schroder *et al* [16] found that re-endothelialisation of injured mouse carotid artery is enhanced by hypoxia and EPO, but that this effect is abrogated in $NOX2^{y/-}$ mice. Further data from this study went on to link this finding to a deficiency in hypoxia-induced CPC mobilisation in the $NOX2^{y/-}$ mice, which could be restored by the transplantation of WT BM. Data also exists which suggests a role for NOX1 in vascular repair, as shown by Lee *et al* [179]. In this study, $NOX1^{-/-}$ mice were found to have impaired neointimal formation following femoral artery wire injury when compared to WT controls. The authors' conclusion stated that NOX1 is critical to vascular repair due to its mediation of VSMC migration, proliferation, and extracellular matrix production.

1.8 ROS, other CVD risk factors and atherosclerosis

Beyond promoting endothelial dysfunction and impaired vascular regeneration, oxidative stress is also associated with risk factors for developing CVD (for a more detailed review, see Roberts *et al* [180]). A number of studies have demonstrated oxidative stress to be a contributory factor in the development of hypertension; in the context of angiotensin II-infused mice, NOX2 inhibition has been shown to normalise blood pressure [181] and conversely, endothelial-specific NOX2 overexpression to promote hypertension [182]. However, NOX2 may not mediate renin and endothelin-1 induced hypertension [183, 184]. Conversely, endothelial NOX4 overexpression has also been shown to reduce blood pressure due to the vasodilatory action of hydrogen peroxide [185]. Small-scale clinical trial data also illustrate the potential of broad-spectrum antioxidants to improve insulin sensitivity, adipokine profile, and indices of leukocyte-endothelial interaction over the short-term in overweight young adults [186]. However, as discussed in section 1.10, these promising findings have not translated into reductions in 'hard outcomes' in large clinical trials.

Whilst papers cited in this chapter have highlighted a role for ROS in atherogenesis in the context of insulin resistance, there is also recognition that oxidative stress can independently promote the development and progression of atherosclerosis. Evidence for this can be seen in a study published by Judkins *et al,* which demonstrated that atherosclerotic lesion area could be reduced by approximately 50% in high-fat-fed $ApoE^{-/-}$ mice via genetic inhibition of NOX2 [187]. More recently, an interesting paper has been published in which subclinical atherosclerosis was quantified in patients with chronic granulomatous disease (CGD), an immunodeficient state most often caused by defective gp91phox (NOX2). Despite a high prevalence of traditional cardiovascular risk factors, patients with CGD exhibited reduced carotid artery atherosclerosis relative to age-matched controls [188]. The findings of this study support a role for NOX2-derived ROS in the pathogenesis of atherosclerosis and although the mechanism was not explored in this paper, insights can be gained from previously published work. For example, oxidative stress is known to induce the expression of pro-inflammatory adhesion and chemotactic molecules such as vascular adhesion molecule 1 (VCAM-1) [189] and monocyte

chemoattractant protein 1 (MCP-1) [190], which in turn promote the recruitment and accumulation of inflammatory cells to atherosclerotic lesions [191, 192].

Whilst a protective effect of NOX2 inhibition on atherogenesis via diminution of pro-inflammatory mechanisms seems to be an intuitive explanation, it is important to note that this remains a contentious issue in the wider literature. Indeed, some other studies investigating the links between CGD, ROS, inflammation and atherosclerosis have published seemingly conflicting data. Firstly, Deffert *et al* [193] simulated CGD-associated hyperinflammation in mice with genetic inhibition of NOX2 via an intradermal injection of β –glycan. The study found that these mice suffered a massive and prolonged hyperinflammation, with lesions characterized by persistent neutrophilic infiltration, along with ulceration and necrosis. Further work in this study attributed this finding to increased macrophage secretion of interleukin 1β (IL-1β), interleukin 6 (IL-6) and TNF-α. A similar upregulation of pro-inflammatory cytokines was noted in a study examining the effect of NOX2 deficiency in atherosclerosis prone $ApoE^{-/-}$ mice with angiotensin 2-induced abdominal aortic aneurysms (AAA) [194]. This paper concluded that systemic NOX2 deficiency promotes AAA development due to enhanced macrophage secretion of not only 1L-1β, but also of MMP-9, which promotes tissue remodelling in AAA. Importantly, this study also suggested a trend towards increased atheroma burden in these mice, although this was not the principal focus of the manuscript. Although the validity of NOX2 as a therapeutic target in atherosclerosis remains unclear, it certainly warrants further investigation.

Excessive mitochondrial ROS production is also implicated in the development of cardiovascular disease, and a recent paper explored the role of mitochondria-derived ROS in the development of ischaemia-reperfusion injury [195]. Ischaemia-reperfusion injury is thought to be an important contributor to the damage caused by certain cardiovascular diseases, such as MI or stroke. This novel study identified the citric acid cycle intermediate succinate to be responsible for mitochondrial ROS production during reperfusion. The authors noted that during ischaemia, activity of the enzyme succinate dehydrogenase (SDH) is reversed which resulted in accumulation of succinate. Following reperfusion, the direction of SDH activity is normalised and the accumulated succinate is rapidly re-oxidised, driving extensive ROS production by reverse electron transport mitochondrial

complex 1. Significantly, pharmacological inhibition of succinate accumulation was demonstrated to ameliorate ischaemia-reperfusion injury in murine models of MI and stroke.

1.9 The 'redox window' hypothesis

The 'redox window' hypothesis was first put forward by Yun *el al* [196] when studying redox signalling in coronary collateral growth. It states that a hypothetical window exists in which "redox state not only permits, but also can amplify coronary collateral growth. A shift in the redox state to either to an overly reductive environment or an oxidative environment corrupts growth factor–initiated redox-dependent signalling."

The studies cited in the preceding sections serve to corroborate this theory. Reducing ROS levels below a certain threshold (into an "overly reductive environment") via deletion or inhibition of NADPH oxidase appears to be detrimental to vascular regeneration. However in situations of underlying oxidative stress, such as diabetes or hypercholesterolaemia, a reduction in ROS level has been shown to augment angiogenesis by shifting the redox state from an oxidative environment back into the hypothetical window. Furthermore, in situations where excessive and abnormal angiogenesis is pathological (tumours, retinopathies), reducing ROS levels via NADPH oxidase inhibition also appears to be beneficial in minimising disease progression (See figure 6). Support for this concept in human disease comes from the recent work of Ali *et al* [197], who showed that genetic variants associated with reduced expression of Gpx1 are associated with risk of arterial neointima formation. Surprisingly, they noted that beyond the somewhat predictable oxidative stress and enhanced atherosclerosis seen in Gpx1 knockout mice, glutathione accumulation resulted in simultaneous 'reductive stress', manifesting in the form of signalling dysregulation caused by inhibitory S-glutathionylation of the phosphatase SHP-2. This illustrates the complexity of redox imbalance in human disease, and supports the need for nuanced understanding of disease mechanisms in order to produce effective therapies.

Whilst the 'redox window hypothesis' was initially proposed in relation to angiogenesis, given that certain mechanistic overlaps and redox-sensitive mediators are shared, it would seem intuitive for the principle to be applicable to the process of vascular repair as well. The concept of improving angiogenesis and vascular repair in the setting of oxidative stress via reduction of ROS levels forms the premise of my project and will be expanded in section 2.

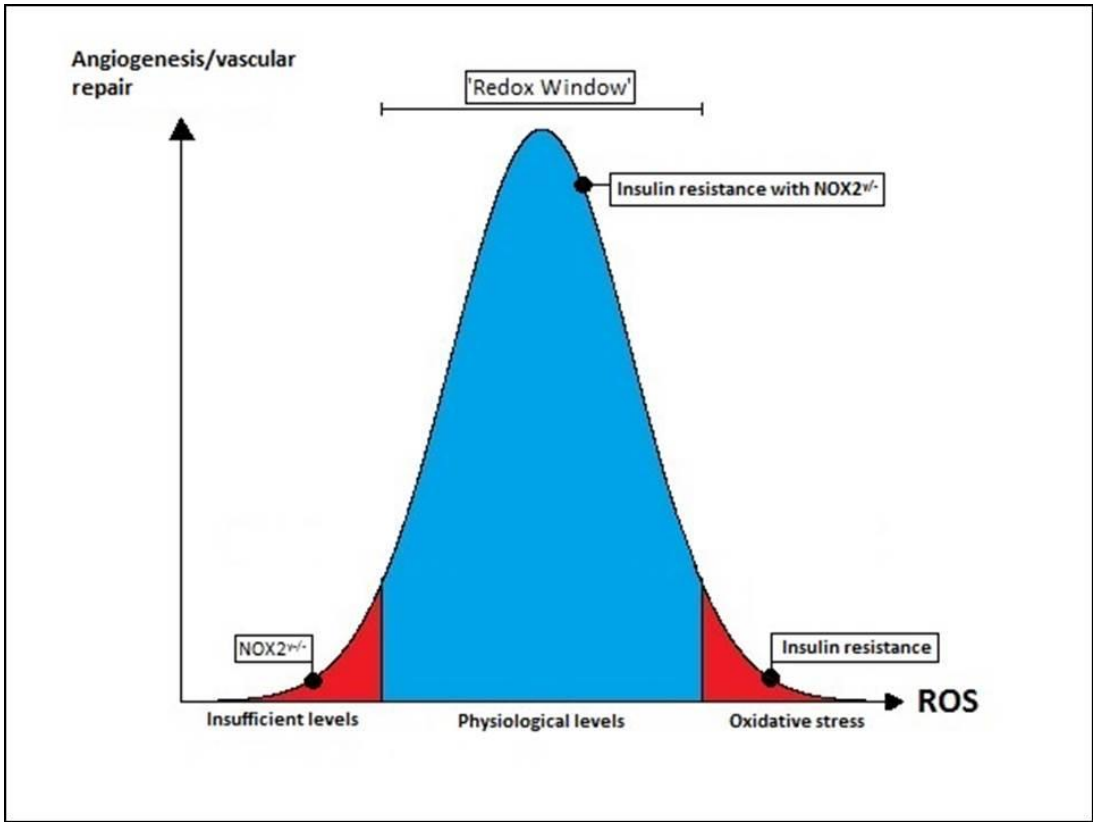

Figure 6. The 'redox window' hypothesis

NOX2 knockout results in impaired angiogenesis and vascular repair since insufficient levels of ROS are disruptive to redox signalling. However, when NOX2 is knocked down in the context of a disease process associated with oxidative stress, such as insulin resistance, angiogenesis and vascular repair can be augmented due to a shift into the optimal redox window. Taken with permission from Ali *et al* [116].

1.10 Clinical implications and the therapeutic application of anti-oxidants

Given the potential to prevent or treat a multitude of disease processes via manipulation of ROS levels, it is of no surprise that interest in the therapeutic application of anti-oxidants has been intense. However, clinical trials have thus far been disappointing. The initial strategy employed involved use of SOD-mimetics with the intention of restoring oxidative balance. Whilst this appeared to work well in laboratory studies, clinical translation was found to be poor [198]. Initial promise was also seen with the anti-oxidant vitamin E which was found to reduce the incidence of MI in two small trials [199, 200]. However further research provided evidence to the contrary with a number of larger trials showing vitamin E to be either non-beneficial [201-203] and indeed even harmful [204]. It must also be noted that there is currently no convincing published evidence that anti-oxidants can modulate pathological angiogenesis as seen in tumour development or proliferative retinopathies.

The presumed reasons for the unsatisfactory results seen so far with anti-oxidants are multiple [205]: firstly, when anti-oxidants such as vitamin E scavenge radicals they themselves become radicals with the associated deleterious effects. Secondly, as discussed in section 1.2.3, ROS production is specifically localised within cells and it is likely that the anti-oxidants aren't able to effectively reach the required sites. Finally, and most significantly, the anti-oxidant approaches described thus far were non-selective in their scavenging of ROS. Given the importance of physiological levels of ROS in redox signalling, the damage caused to homeostatic processes by a blanket reduction in their levels likely outweighs any potential benefit to the disease processes being targeted.

Based on the issues identified with non-selective ROS level reduction, research has turned to explore the concept of NADPH oxidase inhibitors [206]. This area shows a great deal of potential, but a number of challenges remain. The most widely studied NADPH oxidase inhibitors are apocynin and diphenyleneiodonium (DPI), and while they have been of great value in research, their lack of specificity for NADPH oxidase over other enzymes limits their potential in clinical practice.

Taking all of the above into account, the ideal solution appears to be a specific NOX1/2 inhibitor which is able to maintain ROS levels within the redox window, whereby vascular

regeneration is augmented but homeostatic functions are not compromised. Further research is required in order to better characterise specific NADPH oxidase isoforms and the extent of enzymatic blockade required to in order to achieve the desired lowering of ROS levels. The necessity for further investigation into this area forms the rationale for my project, where I intend to assess the effect of NOX2 inhibition on angiogenesis and vascular repair in the context of insulin resistance. Given the importance of the specificity of inhibition, two complementary approaches will be used in order to curtail NOX2 activity: genetic knockdown of the enzyme, and NOX2-specific pharmacological inhibition using the synthetic peptide GP91ds-tat. The aims and objectives for the project are discussed in detail in the following section.

Chapter 2: **Aims and Hypotheses**

Chapter 2 **Aims and Hypotheses**

The aim of this project was to explore the potential of manipulating ROS levels in order to enhance vascular repair and regeneration in the context of insulin resistance. The first part of the project focussed on murine models of insulin resistance, whilst the second part involved use of human umbilical vein endothelial cells (HUVECs)

2.1 Murine models of insulin resistance

IRKO and ESMIRO mice were bred with mice that have a genetic knockdown of the NOX2 enzyme (GP91phox$^{y/-}$) in order to produce double transgenic offspring that simultaneously fail to express NOX2, whilst having whole-body or endothelium-specific insulin resistance respectively. For both colonies of mice, I intended to investigate the effect of NOX2 inhibition in the setting of insulin resistance in the following ways:

1. Phenotypic characterisation the double cross mice, with a comparison made to WT and insulin resistant (IRKO or ESMIRO) littermates.

2. Assessing whether the double cross mice display improved endothelial repair following vascular injury relative to insulin resistant littermates.

3. Assessing whether the double cross mice display improved ischaemic revascularisation following hind limb ischaemia relative to insulin resistant littermates.

4. Comparing the abundance of CPCs and EPCs across the genotypes.

5. Assessing the function of pulmonary-derived ECs across the genotypes.

2.2 HUVEC model of insulin resistance

A complementary model of insulin resistance was generated by using lentiviral transduction with appropriate shRNA to knock-down insulin receptor expression in HUVECs. These 'insulin resistant' HUVECs were treated with GP91ds-tat and then used in

functional and biochemical assays, which allowed an assessment to be made of the effects of pharmacological NOX2 inhibition on the function of insulin resistant ECs.

2.3 Hypotheses

1. Inhibition of NOX2 in the setting of insulin resistance can improve vascular repair and regeneration.

2. These improvements arise from a combination of increased progenitor cell-mediated vascular repair and improved resident EC function.

Chapter 3: **Materials**

Chapter 3 **Materials**

3.1 Animal Husbandry

Chow feed	B&K Universal Ltd

3.2 Genotyping

Sodium hydroxide	Fisher
Tris-hydrochloric acid	Fisher
Molecular grade H_2O	BD Biosciences
Biomix Red “Mastermix”	Bioline
Primers (see Methods)	Invitrogen
Tris base	Fisher
EDTA	Sigma-Aldrich
PCR reaction tubes/lids	Thermo Scientific
PTC-200 Thermal Cycler	MJ Research
Agarose	Bioline
Glacial acetic acid	Fisher
Ethidium bromide	Sigma-Aldrich
100 base pair ladder	Thermo Scientific
Syngene G-box imaging system	Syngene

3.3 Glucocompetence Testing

Accucheck glucometer/test strips	Aviva
D-glucose	Sigma
Actrapid insulin	Novo Nordisk
Dulbecco’s phosphate-buffered Saline (PBS)	Sigma

Veet hair removal cream	Reckitt-Benckiser
Vaseline® Paraffin-based ointment	Unilever
14G needle	Terumo
Microvette tubes (powdered lithium heparin)	Sarstedt
Microvette (EDTA-tripotassium)	Sarstedt
Liquid heparin sodium	Wockhardt
Ultrasensitive mouse insulin ELISA kit (90080)	Crystal Chem
Dynex MRX plate reader and Revelation v4.21	Dynex Technologies

3.4 Real-time quantitative PCR

Tissue Lyser	Qiagen
6mm cone balls (RS.22.455.0003C)	Retsch
RNAse Away spray	Molecular Bio Products
TRIzol® (Tri reagent)	Sigma
Phenol chloroform	Sigma
Isopropanol	Sigma
Ethanol	Fisher
RNAse free H2O	Life Technologies
NanoDrop® ND1000 Spectrophotometer	Thermo Scientific
ND-1000 v3.1 software	Thermo Scientific
High capacity cDNA reverse transcription kit	Applied Biosystems
96 well optical reaction plate	Applied Biosystems
ABI Prism 7900 HT PCR cycler	Applied Biosystems
SDS v2.2 software	Applied Biosystems
RT-PCR primers (SYBR green)	Invitrogen
Power SYBR® green PCR Mastermix	Applied Biosystems

Taqman® Gene Expression Mastermix	Applied Biosystems
RT-PCR primers (Taqman®)	Applied Biosystems
Molecular grade H_2O	BD Biosciences

3.5 Vascular Injury

Buprenorphine	Alsatoe Animal Health
Isoflurane	Abbott Logistics BV
Irripod (sterile 0.9% saline)	Unither
Lignol (1% lignocaine + adrenaline)	Arnolds
Dissecting microscope OPMI 1-FC	Zeiss
Veet hair removal cream	Reckitt-Benckiser
0.75% providone-iodine	Animal Care
Vicryl absorbable 8.0/6.0 suture	Ethicon
Iris Scissors and needle holder	World Precision Instruments
Dry sterilizer #500121	World Precision Instruments
Lubrital #31329	Dechra
Vannas spring scissors	Fine Science Tools
Dumont, atraumatic tipped forceps (11253-25)	Fine Science Tools
Round handled suture tying forceps	Fine Science Tools
Hitorque Cross-it 200XT guide wire	Abbott Vascular
Evans Blue (195550050)	Acros Organics
4% paraformaldehyde	Fisher
30% hydrogen peroxide	Sigma
Insulin syringe / 27Gx13mm needle	Terumo
Olympus Dissecting Stereo Microscope SZ61	Olympus
QiCam Olympus digital camera	Olympus

ImagePro Plus 7.2	Media Cybernetics
Micro-osmotic pump model 1002	Alzet
GP91-ds tat – RP21052	Genscript
GP91-ds tat scrambled peptide – RP21051	Genscript

3.6 Ischaemic revascularisation

Nikon SMZ1500 Stereo microscope	Nikon
Olympus SZ61 microscope	Olympus
Olympus QiCam digital camera	Olympus
Fluovac anaesthetising chamber	Harvard apparatus
Compact anaesthesia system AN001	Vet Tech solutions
Isofluorane key fill applicator AN003B	Vet Tech solutions
Heating plate	Vet Tech solutions
Thermal cage HE-011	Vet Tech solutions
Light source 1500 LCD	Schott KL
Guide wire 0.014” Hi-Torque Cross-IT	Abbott Vascular
Micro serrifine curved (18055-05)	Inter Focus
Forceps type clip applicator (18057-14)	Inter Focus
Needle holder (14109)	World Precision Instruments
Vannas scissors (501778)	World Precision Instruments
Vannas scissors (91501-09)	Inter Focus

Fine Iris scissors (14094-11)	Inter Focus
Tweezers Dumont #500339	World Precision Instruments
Insulin syringe 0.3ml with 29G x 13mm needle	Terumo
Insulin syringe 0.5ml with 27G x 13mm needle	Terumo
Insulin syringe 1ml with 29G x 13mm needle	Terumo
VICRYL absorbable surgical suture, 6-0	Ethicon, J&J
VICRYL absorbable surgical suture, 8-0	Ethicon, J&J
Microscope slide	Cell path
Microscope slide coverslip 22mm x 22mm	SLS
Veet hair removal cream	Reckitt-Benckiser
Isofluorane-vet	Merial Animal Health
Rodent No.1 maintenance diet	Specialist diet service
Buprenorphine	Alsatoe Animal Health
Laser Doppler analysis Moor LD12-HR	Moor systems

3.7 Enumeration of Circulating Progenitor Cells (CPCs)

Heparin 1000IU/mL	Wockhardt
Microvette (EDTA-tripotassium)	Sarstedt
Pharmlyse red cell lysis buffer	BD Biosciences
Syringe filter (0.2µm membrane)	Pall Life Science
Corning centrifuge tubes	Sigma

Foetal bovine serum (FBS)	Biosera
Bovine serum albumin (BSA)	Sigma
Fc block (CD16/CD32 rat anti-mouse 553142)	BD Biosciences
FITC (rat IgG2a Isotype Control 553929)	BD Biosciences
Sca1-FITC (rat IgG2a κ Ly6A/E 557405)	BD Biosciences
PE rat (IgG2a κ Isotype Control 553930)	BD Biosciences
Flk1-PE (Flk1 VEGFR2; 555308)	BD Biosciences
APC (rat IgG2b κ Isotype Control; 553991)	BD Biosciences
APC (rat anti-mouse CD117; 553356)	BD Biosciences
Fortessa Flow Cytometer	BD Biosciences

3.8 Isolation and Enumeration of Early Outgrowth EPCs

Insulin syringe / 29G x 13mm needle	Terumo
Sodium citrate from 4mL blood collection tubes	Greiner Bio-One
4mL EDTA blood tube	Greiner Bio-One
23G needle	Terumo
70µm nylon cell strainer	Greiner Bio-one
5cm Petri dish	BD Falcon
Histopaque-1083	Sigma
EGM-2 basal medium/bullet kit	Lonza
Foetal bovine serum	Biosera

Antibiotic/antimycotic supplement	Invitrogen
Trypan blue	Sigma
Neubauer Counting Chamber	Hawksley
24-well/6-well fibronectin coated cell culture plates	BD Biocoat
DiI-ac-LDL	Life Technologies
FITC-lectin	Sigma
CKX-41 fluorescent microscope	Olympus
Cell B software	Olympus
Image J v1.46r	National Institutes of Health

3.9 Isolation and Culture of Pulmonary Endothelial Cells (PECs)

Scalpel blades size 22	Swann-Morton
Dulbecco's Modified Eagle's Medium (31966-021)	Life Technologies
Hank's Balanced Salt Solution (H9269)	Sigma
Collagenase/Dispase (11097113001)	Roche
Bovine skin gelatin	Sigma
Bovine serum albumin 7.5%	Sigma
MACSmix™ tube rotator	Miltenyi Biotec
14G Cannula	BD Biosciences
10mL syringe	BD Biosciences
EC growth medium MV2 + supplements	PromoCell

Foetal bovine serum	Biosera
Antibiotic/antimycotic supplement	Invitrogen
CD146 (LSEC) microbeads, mouse	Miltenyi Biotec
T25 Corning® cell culture flask	Sigma
Trypsin-EDTA 0.25%	Sigma
OctoMACS manual separator	Miltenyi Biotec
MACS MS cell separation columns	Miltenyi Biotec
Dulbecco's phosphate-buffered Saline (PBS)	Sigma

3.10 Culture of human umbilical vein endothelial cells (HUVECs)

HUVECs cryopreserved (pooled)	Promo Cell
100mm TC- treated culture dish	Corning
Medium 199	Sigma Aldrich
Foetal bovine serum	Biosera
Antibiotic/antimycotic supplement	Invitrogen
Endothelial growth supplement (E2759-5X15MG)	Sigma Aldrich
Sodium pyruvate (P2256-25G)	Sigma Aldrich
Heparin 1000IU/mL	Wockhardt
HEPES 1M solution (15630-080)	Thermo Scientific
Dulbecco's phosphate-buffered Saline (PBS)	Sigma
MISSION® shRNA lentiviral particle 07101521MN	Sigma

GP91-ds tat – RP21052	Genscript
GP91-ds tat scrambled peptide – RP21051	Genscript

3.11 Endothelial cell functional assays

3.11.1 Endothelial cell proliferation assay

Click-iT® EdU Alexa Fluor 647 flow cytometry assay kit	Life technologies
Fortessa Flow Cytometer	BD Biosciences

3.11.2 Endothelial cell migration assay

ImageLock 96 well plate	Essen Biosciences
Woundmaker™ 96-pin tool	Essen Biosciences
Integrated Cell Migration Analysis Module	Essen Biosciences
IncuCyte™ Imaging System	Essen Biosciences
Alconox/Vircon cleaning solutions	Sigma

3.11.3 Superoxide assay

Clear 96 well cell culture plate	Thermo Scientific
Dihydroethidium D11347	Life Technologies
HEPES sodium salt	Sigma
Flex Station 3 Multi-mode microplate reader	Molecular Devices
SoftMax® Pro v5.4.5	Molecular Devices

3.12 Western blotting

Tris-HCl	Fisher

Glycerol	Sigma
EDTA	Sigma
Sodium dodecyl sulphate	Sigma
Phosphatase inhibitors 2&3	Sigma
Tween®-20	Sigma
Bovine serum albumin (BSA)	Sigma
Pierce® BCA protein assay kit	Thermo Scientific
96 well clear microplate	Greiner Bio-One
Micro-amp® optical adhesive film	Life Technologies
NuPAGE® LDS sample buffer	Invitrogen
NuPAGE® sample reducing agent	Invitrogen
NuPAGE® MES SDS running buffer	Invitrogen
NiPAGE® 4-12% Bis-Tris Gel	Invitrogen
XCell SureLock Electrophoresis cell	Thermo Scientific
Amersham Tracker Tape (#RPN2050)	GE Healthcare
Primary antibodies (see table 10)	Cell Signaling
Secondary antibodies (see table 10)	Dako
Immobilon Western Chemiluminescent HRP Substrate	Merck Millipore
Immobilon®-P transfer membrane	Merck Millipore
Syngene G-box imaging system	Syngene
Dynex MRX plate reader and Revelation v4.21	Dynex Technologies

Chapter 4: **Methods**

Chapter 4 **Methods**

4.1 Animal husbandry

4.1.1 Housing and experimental conditions

All experiments were performed under the Experimental Animals (Scientific Procedures) Act 1988. Mice were housed in the animal facility at the University of Leeds under standard laboratory conditions and were fed a standard chow diet and normal drinking water. In order to allow identification, the mice underwent ear notching at the age of 3-4 weeks, and the notched tissue was used for genotyping. Only male animals were used in order to exclude cardiovascular effects of cyclically varying oestrogen levels and lyonisation of the mutant NOX2 allele expressed on one of the X chromosomes.

4.1.2 ESMIRO mice

ESMIRO mice display endothelium-targeted over-expression of a dominant-negative mutant human insulin receptor (hIR). The IR is rendered less catalytically active in response to insulin binding due to an amino acid substitution in the kinase domain. To achieve this, a Thr^{1134} mutation was introduced into the cDNA encoding hIR by site-directed mutagenesis. In order to target the expression of the mutant hIR to the endothelium, a murine Tie2 promoter and intronic enhancer was used. The mutant hIR cDNA was cloned into a pHHNS plasmid following excision of the LacZ sequence with Sbf1 and Mlu1. The transgene Tie2-hIR was then microinjected into fertilised eggs from C57 black 6 (C57BL/6) x CBA mice, and the offspring backcrossed eight times onto a C57BL/6 background.

ESMIRO mice used for this project were obtained from established local colonies, having been originally generated by Duncan *et al* [56].

4.1.3 IRKO mice

IRKO mice, which are haploinsufficient for the IR, were originally developed at the National Institutes of Health (USA). Their generation was achieved by targeting the IR gene using a vector which incorporates a premature chain termination at exon 4, as well as a cassette encoding neomycin resistance. Using electroporation, this vector was used to transfect

embryonic stem cells, into which the gene could then be incorporated via homologous recombination. These embryonic stem cells were then grown in the presence of neomycin, allowing selection for the mutated allele. The surviving cells were expanded prior to being injected into murine embryos at day 3.5. These embryos were implanted into dark-coated female C57BL/6 mice, resulting in chimeric offspring identifiable by coat colour. The male offspring were bred with C57BL/6 females, and the resulting progeny used to establish colonies.

IRKO mice were purchased from Jackson laboratories and bred with female C57BL/6 mice for 12 generations in order to generate local colonies. The IRKO mice used in this project were obtained from these established local colonies, thus obviating the need for genetic manipulation at our site.

4.1.4 GP91phox $^{y/-}$ mice

GP91phox $^{y/-}$ mice display whole-body knockdown of the NOX2 enzyme, and the original generation of this model is described in detail by Pollock *et al* [207]. The gene for NOX2 is located on the X chromosome at a locus designated *Cybb.* A 4.8kb *Nco*I genomic fragment containing the second and third exons of the *Cybb* gene was used to construct a targeting vector by placing the expression cassette for neomycin-resistance into the third exon and attaching a flanking herpes thymidine kinase gene. Using electroporation, this vector was used to transfect embryonic stem cells which were then grown in the presence of neomycin, allowing selection for the mutated allele. A correctly targeted selected clone from the electroporated embryonic stem produced chimeric males, hemizygous for the disrupted gene. These were subsequently backcrossed to C57BL/6 in order to generate colonies.

The GP91phox $^{y/-}$ mice used in this project were obtained from established local colonies, having been originally purchased from the Jackson Laboratory.

4.1.5 ESMIROxGP91phox $^{y/-}$ mice

Male ESMIRO mice were bred with female GP91phox heterozygous mice, resulting in litter containing the ESMIRO x GP91phox $^{y/-}$ genotype. The other genotypes from this litter were

wild type (WT), ESMIRO and GP91phox $^{y/-}$. Experimental work was carried out on all genotypes except GP91phox $^{y/-}$.

4.1.6 IRKOxGP91phox $^{y/-}$ mice

Male IRKO mice were bred with female GP91phox heterozygous mice, resulting in litter containing the IRKO x GP91phox $^{y/-}$ genotype. The other genotypes from this litter were WT, IRKO and GP91phox $^{y/-}$. Experimental work was carried out on all genotypes except GP91phox $^{y/-}$.

4.1.5 Animal euthanasia

Animals were sacrificed in two ways depending on requirements. Prior to obtaining organs, mice were exposed to rising concentrations of carbon dioxide in a 12 minute cycle. After confirming death using cervical dislocation, the required tissue was dissected. For EPC isolation 1mL of blood was required, and since the 12 minute cycle resulted in intravascular thrombosis, these mice underwent terminal isoflurane anaesthesia. Following this, a caval bleed was performed and any other tissue was obtained by dissection.

4.2 Genotyping

4.2.1 DNA extraction

Ear notches were incubated in 100µL of 25mM NaOH/EDTA for 25 minutes at 95°C. Following this, 100µL of 40mM Tris-HCl was added and the sample vortexed thoroughly in order to disperse the DNA.

4.2.2 Polymerase chain reaction (PCR)

For each PCR reaction, a stock solution was prepared in a laminar flow hood. The stock solution comprised primers, distilled water and a commercially obtained pre-made 'Mastermix' which contained PCR buffer, magnesium chloride, deoxynucleotide triphosphate (dNTP) mixture and *Thermophilus aquaticus* (Taq)-derived DNA polymerase. The volume of each constituent within the stock solution per sample is listed in table 1.

	ESMIRO	IRKO	GP91$^{y/-}$
Mastermix (µL)	10	10	10
Primer 1 (µL)	0.5	0.5	0.5
Primer 2 (µL)	0.5	0.5	0.5
Primer 3 (µL)	N/A	0.5	1
Water (µL)	13	12.5	12

Table 1 Constituents of genotyping stock solution

Stocks of the primers were obtained commercially and reconstituted in TE buffer (10mM Tris, 1mM EDTA at pH 8) and then subsequently diluted 1:10 in distilled water.

All components were mixed and 24µL reaction volumes were measured into PCR tubes. 1µL of either DNA or controls were added to each tube and PCR was carried out by thermal cyclers with heated lids using a specific programme for the IRKO, ESMIRO and GP91phox$^{y/-}$ DNA.

4.2.3 ESMIRO PCR

Two primer sequences specific for the gene targeting cassette were used:

Forward – TGG CAG CTT TCC CCA ACA CT

Reverse – CCG TTC CTC AGG GGT GTCC

The PCR comprised the following cycles:

1. 94°C for 4 minutes
2. 94°C for 1 minute
3. 55°C for 1 minute
4. 72°C for 1 minute

   Repeat steps 2-4 for 32 cycles
5. 72°C for 15 minutes
6. 4°C on hold

On UV imaging following gel electrophoresis, WT DNA showed no bands whilst ESMIRO DNA displayed a band at 172bp.

4.2.4 IRKO PCR

Three primer sequences specific for the gene targeting cassette were used:

Forward - TTA AGG GCC AGC TCA TTC CTCC

Forward - AGC TGT GCA CTT CCC TGC TCAC

Reverse - TCT TTG CCT GTG CTC CAC TCT CA

The PCR comprised the following cycles:

1. 94°C for 4 minutes

2. 94°C for 1 minute

3. 62°C for 1 minute

4. 72°C for 1 minute

Repeat steps 2-4 for 31 cycles

5. 72°C for 4 minutes

On UV imaging following gel electrophoresis, WT DNA fluoresced as a single band at 232bp whilst IRKO DNA displayed a double band at 232bp and 255bp.

4.2.5 GP91phox PCR

Three primer sequences specific for the gene targeting cassette were used:

517 - AAG AGA AAC TCC TCT GCT GTG AA
518 – CGC ACT GGA ACC CCT GAG AAA GG
519 – GTT CTA ATT CCA TCA GAA GCT TAT CG

The PCR comprised the following cycles:

1. 94°C for 3 minutes
2. 94°C for 20 seconds
3. 64°C for 30 seconds
4. 72°C for 35 seconds

Repeat steps 2-4 for 12 cycles

5. 94°C for 20 seconds
6. 58°C for 30 seconds
7. 72°C for 35 seconds

Repeat steps 5-7 for 25 cycles

8. 72°C for 2 minutes

On UV imaging following gel electrophoresis, WT DNA fluoresced as a single band at 240bp. A single band at 195bp represented a DNA from a GP91phox$^{y/-}$ homozygote, whilst a double band at 195bp and 240bp represented DNA from a heterozygous female.

4.2.6 Gel electrophoresis

The products of the PCR were identified by electrophoresis on a 1.5% agarose gel containing 3µL of 10mg/ml ethidium bromide. Electrophoresis was performed at 110V for 60 minutes with a 1000bp reference ladder. Gels were imaged using Gene Sys V1.4.0.0 software and a Syngene Chemi XT4 imaging box.

4.3 Glucocompetence testing

4.3.1 Random capillary blood glucose measurements

Mice were gently coaxed head first into syringe-like restraining devices, leaving their tail freely accessible. Their baseline blood glucose level was assessed by obtaining a drop of blood from a superficial tail incision. The capillary blood glucose (CBG) level was analysed using Accu-Chek glucose testing strips and glucometer.

4.3.2 Glucose tolerance testing (GTT)

Prior to the GTT, mice were habituated to the syringe-like restraining device in order to minimise stress during the test. Once the mice were relatively comfortable with being restrained in this way, they were fasted overnight with unrestricted access to drinking water. The following morning they were weighed and their baseline CBG was assessed in the same way as described above. Following this, the mice received an intraperitoneal (IP) injection of 1mg glucose per gram of bodyweight. CBG was then measured at 30, 60, 90 and 120 minutes post injection using the same technique as for assessing baseline blood glucose. In between measurements, mice were placed back in their cage with free access to water but not chow.

4.3.3 Insulin tolerance testing (ITT)

As described above, mice were habituated to the restraining device prior to the test. Once relatively comfortable, mice were fasted for 4 hours with unrestricted access to drinking water. Following the fast, baseline CBG was measured as described above and the mice received an IP injection of insulin at a concentration of 0.75iu per kilogram of bodyweight.

Once again CBG was measured at 30, 60, 90 and 120 minutes and the mice had free access to water in between measurements.

4.3.4 Plasma insulin measurement

4.3.4.1 Blood collection

In order to obtain blood samples of sufficient quantity for plasma insulin measurement, saphenous vein puncture was required, and this was performed by my colleague Dr Anshuman Sengupta. Following an overnight fast, mice were coaxed into the restraining device as described above. The right hindlimb was gently pulled out of the open end of the tube, allowing a hair removal cream to be applied to the surface. The cream was allowed to take effect for approximately 30 seconds, after which the hair was wiped away using a tissue paper, thus allowing visualisation of the distal saphenous vein. Vaseline was applied to the skin surface and a puncture to the vein made using a 14G needle. The blood was collected using capillary tubes, and stored in heparin-lined Microvette tubes. The blood samples were transferred in ice with minimal delay and centrifuged at 6000 revolutions per minute (rpm) for six minutes, after which plasma was removed and stored at -80°C.

4.3.4.2 Enzyme linked immunosorbent assay (ELISA)

Ready-made ELISA kits for mouse insulin (Crystal Chem) were used according to manufacturer's instructions for a "low-range" assay (0.1-6.4ng/mL). This involved incubating 95µL of sample diluents with either duplicate serial dilutions of a mouse insulin standard (for a standard curve) or the plasma samples for two hours at 4°C in order to allow antibody binding. After five washes with 300µL of wash buffer, 100µL of an anti-insulin enzyme conjugate was added to each well and incubated at room temperature for 30 minutes. The wells were then washed seven times prior to adding 100µL of enzyme substrate solution. The plate was incubated in the dark for 40 minutes, following which the reaction was aborted by adding 100µL of a "stop" solution to each well. A Dynex MRX plate reader and Revelation v4.21 were used to perform colorimetric analysis at 450nm. The standard curve was appraised for linearity and correlation co-efficient (r^2), the latter accepted when >0.99. Sample insulin concentrations were inferred from the standard curve and accepted only at a co-efficient of variation (CV) of <10% between duplicates.

4.4 Real time quantitative PCR

This process was used to quantify the abundance of NOX2, human insulin receptor (hIR), murine insulin receptor (mIR), tumour necrosis factor α (TNFα), interleukin 1β (IL-1β) and vascular cell adhesion protein 1 (VCAM1) mRNA in the ESMIROxGP91phox mice. The experiment comprised three parts:

4.4.1 RNA extraction

The RNA was extracted from aortic and lung tissue. The organs were harvested from mice following euthanasia and transferred into individual 2ml micro-centrifuge tubes. These tubes were snap frozen in liquid nitrogen and then stored at -80°C. In order to proceed with RNA extraction the organs required homogenisation. This was achieved by adding a tissue lyser bead and 1ml of Trizol® to the micro-centrifuge tube, following which the samples were loaded into a tissue lyser machine and shaken in 3 cycles of 2 minutes at 30Hz. Once this process had completed, the solid material and lyser bead were discarded, leaving behind a supernatant.

The samples were centrifuged at 4°C at 10,000g and the supernatant transferred into fresh micro-centrifuge tubes. The samples were left to dissociate for 5 minutes at room temperature before 200µL of chloroform was added to each. The tubes were agitated for 15 seconds in order to ensure adequate mixing, and the samples left at room temperature for 3 minutes. Following this, the samples were centrifuged at 12,000g and 4°C for 15 minutes. Once again the supernatant was separated and 500µL of isopropanol added to each sample. Following gentle agitation the tubes were left at room temperature for 10 minutes and then centrifuged at 12,000g for 10 minutes at 4°C. On this occasion the supernatant was discarded and the pellet re-suspended in 1ml of 75% ethanol. The samples were then centrifuged at 7500g for 5 minutes at 4°C. Following this the ethanol was removed and the pellets left to air dry for 10 minutes at room temperature. The final step in the RNA extraction was to dissolve the pellet in 20µL of RNAase free water and allow the samples to cool on ice for 20 minutes.

The concentration of RNA in each sample was determined by placing a 2µL drop of the solution onto a NanoDrop® machine which would analyse the sample using ND-1000

V3.1.0 software to generate a concentration of RNA in ng/nL. This result was then divided into 2000 in order to give the volume of sample within which 2µg of RNA was contained. This volume of sample was then diluted with distilled water in order to create a total volume of 10µL, which could then be used for reverse transcription.

4.4.2 Reverse transcription of RNA

A mastermix was made using components within the High Capacity cDNA Reverse Transcription Kit in the quantities outlined in table 2.

Component	Volume (µL)
Water	4.2
Buffer	2
Random primers	2
Multiscribe® enzyme	1
dNTPs	0.8

Table 2 Constituents of the reverse transcription mastermix

dNTP: deoxynucleotide triphosphate

For each sample, 10µL of mastermix was added to 2µg of RNA in a PCR plate. The plate was then placed into a thermal cycler with a heated lid which then took the samples through the following cycle:

1. 25°C for 10 minutes

2.37°C for 2 hours

3. 85°C for 5 minutes

4. 4°C for 30 minutes

4.4.3 Quantitative Real-time PCR

Two different probes were used for this experiment, based on which samples were being assessed and which RNA was being quantified. The rationale for this was based upon prior work in our lab which had demonstrated that the two probes were differentially effective depending on what was being quantified. In all cases, beta actin was used as a housekeeping control. Table 3 outlines which probe was used for the different quantifications:

Transcript	Probe
hIR	SYBR green
NOX2	SYBR green
mIR	Taqman®
TNFα	Taqman®
IL-1β	Taqman®
VCAM1	Taqman®

Table 3 RT-qPCR probe selection

SYBR green: Synergy Brands (SYBR) Green probe; hIR: human insulin receptor; NOX2: NADPH oxidase 2; mIR: murine insulin receptor; TNFα: tumour necrosis factor α; IL-1β: interleukin 1β; VCAM1: vascular cell adhesion molecule 1.

The cDNA samples produced as a result of the reverse transcription were diluted 1:20 into TE buffer for use with the SYBR green probe, but used neat with the Taqman® probe. The sample was then added to a mastermix containing the probe, primers and double distilled

water. The constituents of the mastermix for the two probes are outlined in tables 4 and 5, whilst the sequences for each primer are listed in tables 6 and 7.

Component	Volume (µL)
Water	8.5
SYBR green	12.5
Forward primer	1.5
Reverse primer	1.5

Table 4 Constituents of SYBR green mastermix

Component	Volume (µL)
Water	8
Taqman® mastermix	10
Probe	1

Table 5 Constituents of Taqman® mastermix

Gene	Forward primer	Reverse primer
β actin	CGT GAA AAG ATG ACC CAG ATCA	TGG TAC GAC CAG AGG CAT ACAG
hIR	TGC CAC CAA CCC CTC TGT	CGG AGG GTG GTT TCC ACTT
NOX2	ACT CCT TGG GTC AGC ACT GG	GTT CCT GTC CAG TTG TCT TCG

Table 6 SYBR green primers

Gene	Assay number
β actin	Mm 00607939
mIR	Mm 01211875_m1
IL-1β	Mm00434228_m1
VCAM1	Mm01320970_m1
TNFα	Mm00607939_s1

Table 7 Taqman® primers

The PCR was performed by a thermal cycler with each sample being analysed in triplicate. This yielded three threshold (Ct) readings per sample, the mean of which was then calculated. The difference in Ct between the gene of interest and β actin (ΔCt) was then used to calculate the relative quantity using the following formula:

$$RQ = 2^{-\Delta Ct} \times 100.$$

4.5 Vascular repair

The surgery described in this section was performed by Dr Nadira Yuldasheva.

4.5.1 Arterial injury

Mice were operated on under conditions of general anaesthesia. Induction of anaesthesia was achieved by placing the mouse to be operated on in an anaesthetic chamber, into which 5% inhaled isoflurane was introduced. Once the mouse had lost consciousness, it was placed onto a warmed operating table in a supine position and anaesthesia maintained using 1-2% isoflurane delivered via facemask. Prior to the start of the operation, appropriate anaesthesia was confirmed by loss of withdrawal reflexes in the paw.

Veet® cream was used to remove hair from the hindlimb in order to allow clear visualisation of the skin surface. A small mid-thigh incision was made in order to gain access to the femoral canal, within which the femoral artery lies. Once identified, the femoral artery was separated from the neurovascular bundle and then loosely tied using an 8.0 suture and a proximal clamp. An arteriotomy was made in the profunda femoris, through which a 0.014 inch diameter angioplasty guide wire could be passed into the lumen of the femoral artery, aided by the application of 1% lignocaine in order to reduce vasospasm. The wire was advanced 2cm for three passes in order to achieve complete endothelial denudation. Following this, the wire was removed and the profunda femoris was ligated proximal to the arteriotomy via tightening of a suture. For control purposes, the contralateral artery underwent a sham procedure which did not involve the passage of a wire. Following surgery, the mice underwent a monitored recovery period during which they were checked daily until the end of the experiment.

4.5.2 Assessment of re-endothelialisation

Evans blue dye was used in order to identify areas of residual endothelial denudation, since it can only penetrate the subendothelial layer in these regions. As a result it stains areas of denudation blue, whilst leaving recovered areas unstained (see figure 7). The Evans blue dye (50µL of 5% in PBS) was injected into the mouse via the inferior vena cava under general anaesthesia four days after the vascular injury. Two minutes later, 4%

paraformaldehyde was injected into the left ventricle for the purposes of perfusion fixation. Once this had been achieved, as evidenced by muscle fasciculation, both femoral arteries were harvested and stored in 4% paraformaldehyde.

The vessel was opened longitudinally under microscopy and a 5mm segment of artery was identified at a distance of 5mm from the proximal end (the aortic bifurcation) of the vessel. The total segment area and the area of remaining denudation (i.e. the portion stained blue) were quantified using ImagePro Plus 6.2 software. Subtraction of the blue-stained area from the total segment area gave extent of endothelial regeneration, which could then be expressed as a percentage of recovery.

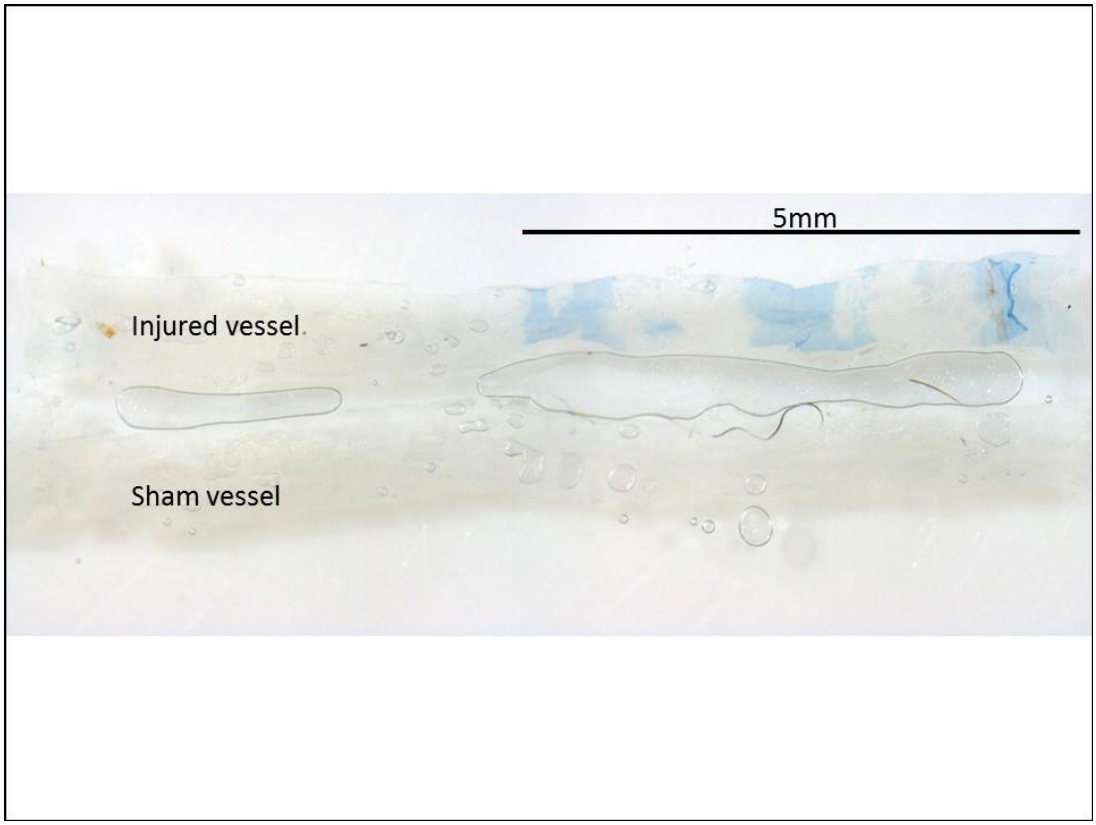

Figure 7 Vascular repair

The above image demonstrates 10mm segments of both femoral arteries taken from a mouse following vascular injury and staining with Evans blue dye. The bottom vessel is the contralateral femoral artery which was not injured, and therefore remains unstained. The top vessel is the femoral artery which underwent vascular injury, with the segment of interest (measuring 5mm in length) highlighted. The areas of blue within the 5mm portion represent regions where the endothelium has failed to regenerate, whilst the areas of white within the 5mm portion represent re-endothelialisation.

4.6.3 Micro-osmotic pump insertion

In order to investigate the effect of pharmacological NOX2 inhibition on vascular repair in the context of insulin resistance, experiments were performed whereby ESMIRO mice aged 18-19 weeks were chronically exposed to a specific NOX2 inhibitor named GP91-ds tat. This molecule is a commercially available chimeric peptide which inhibits $p47^{phox}$ association with $GP91^{phox}$, thereby preventing O_2^- production [72]. A scrambled ds-tat peptide was also administered to a cohort of equivalent-aged ESMIRO mice as a control. The GP91-ds tat or control scrambled peptide were delivered to the mice via a subcutaneously located micro-osmotic pump (Alzet, model 1002) which infused the drugs at a fixed rate over a 12 day period.

Prior to insertion, the pump was incubated in sterile saline at 37°C overnight. The pump was then filled with a solution of either GP91-ds tat or scrambled-ds tat control peptide. Both molecules were dissolved into solution (the diluent was made up from 100ml distilled water, 0.9g sodium chloride and 57.5µL acetic acid), and 100µL of this solution loaded into the micro-osmotic pump. The pump was pre-programmed to deliver the drugs at a rate of 0.25µL/hour, which equated to 10mg of GP91-ds tat or scrambled peptide per kg per day.

In order to insert the pump, the mouse was placed under general anaesthesia as described in section 4.5.1. Once anesthetised, the mouse was placed in the prone position and given an IP injection of 0.25mg/kg of buprenorphine. The hair covering the scruff of the mouse was removed using an electric shaver, and an 8mm vertical incision made between the scapulae. Using sterile artery forceps, a small pocket was formed by spreading the subcutaneous connective tissue apart. The pump was then inserted into the pocket and the incision closed using 6.0 Vicryl sutures.

Following insertion of the pumps, the mice were housed in normal conditions for one week, at which point they underwent arterial injury as described in section 4.5.1. The pump continued to infuse GP91-ds tat or scrambled peptide during the 5 day convalescence period, prior to the femoral artery being harvested and imaged as outlined in section 4.5.2.

4.6 Ischaemic revascularisation

The surgery described in this section was performed by Dr Nadira Yuldasheva.

4.6.1 Hindlimb ischaemia

Two to three days prior to surgery, mice underwent hair removal under general anaesthesia, which was induced and maintained in the same manner as detailed in section 4.5.1. An electric shaver and Veet® cream was used in order to remove hair from both hindlimbs and the lower abdominal wall. The mice were then allowed to recover for long enough to allow the cutaneous inflammation to resolve, as this would otherwise cause a background signal on laser Doppler imaging.

Surgery was carried out under general anaesthesia in the manner outlined above, but with the addition of an IP injection of buprenorphine (0.25mg/kg) for post-operative analgaesia. Once the subject was adequately anaesthetised and positioned, a mid-thigh incision was made in order to expose the femoral canal. Once the femoral artery had been identified and dissected, it was ligated proximally at the inguinal ligament and distally at the bifurcation of the saphenous and popliteal vessels. The intervening segment of artery was then excised and the skin closed. As with the vascular repair experiment, post-operatively the mice underwent a monitored recovery period where they were checked on a daily basis.

4.6.2 Laser Doppler assessment of reperfusion

Laser Doppler imaging was undertaken in order to confirm ischaemia 90 minutes post-operatively, and then at 7 day intervals for 28 days in order to assess reperfusion. The imaging was performed under general anaesthesia, which was induced in the same manner as described in section 4.5.1. Once anaesthetised, the mouse was laid supine on a non-reflective, light absorbing mat and the snout was placed into a facemask which allowed delivery of 1-2% isoflurane as maintenance anaesthesia. Both hindlimbs were extended and supinated, with the dorsal aspects of the paws stuck down to the mat using a 1mm strip of double-sided adhesive tape. Once the mouse was in position, a laser Doppler imager (Moor Systems LDI2-HIR) was used to scan both hindlimbs simultaneously. Analysis of the data was performed by MoorLDI V5.3 software, which produced an image

with a range of colours indicative of the relative perfusion within the limbs (see figure 8). A region of interest which incorporated the area below the ankle was chosen in each hindlimb, and the colour within this area analysed by the software to produce an overall index of perfusion. By dividing the perfusion index of the ischaemic limb by that of the non-ischaemic limb, a relative perfusion index (RPI) was generated. Following the scan, the mouse was awoken and allowed to recover.

As mentioned above, laser Doppler imaging was undertaken at 7-day intervals up until 28 days post-operation. Following the day 28 scan, the mice were sacrificed and 4% paraformaldehyde used for perfusion fixation in the same manner as described in section 4.5.2. The gastrocnemius muscle from the ischaemic and non-ischaemic limbs then were harvested and embedded in optimal cutting temperature compound (OCT), prior to being snap frozen in liquid nitrogen. These samples are currently being stored with a view to using them for capillary density quantification in future.

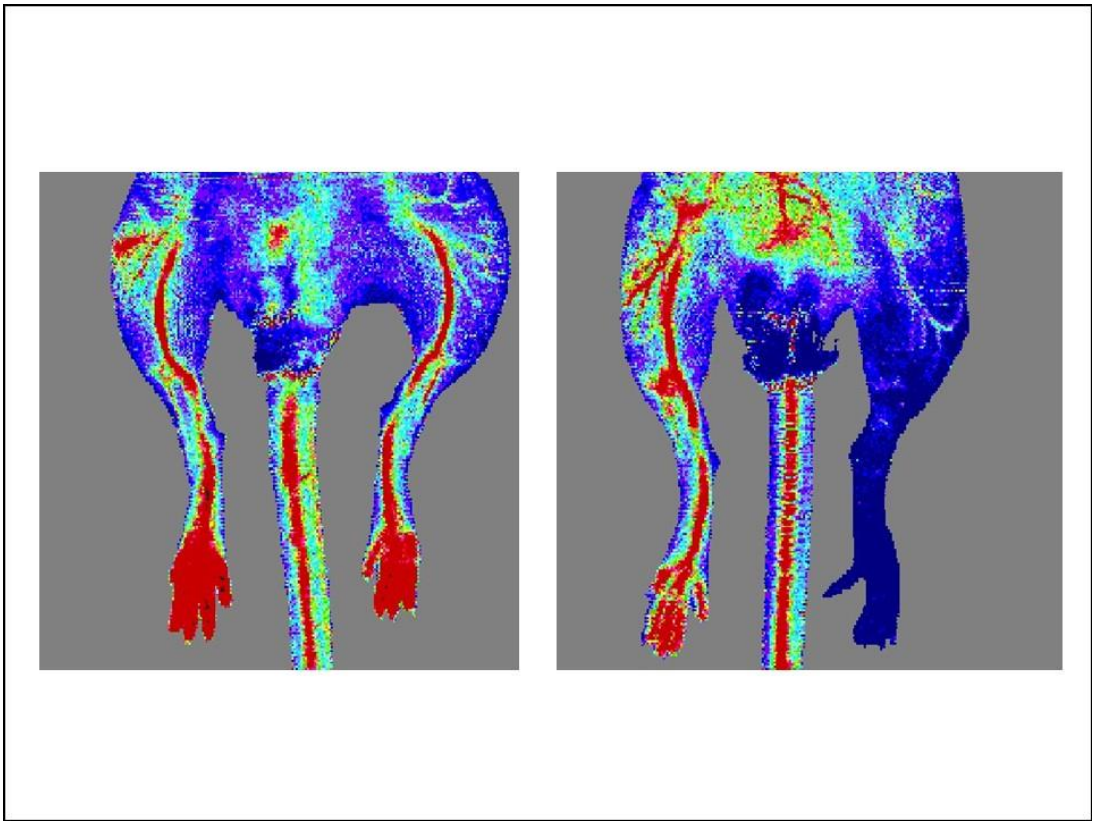

Figure 8 Hindlimb ischaemia

Laser Doppler images demonstrating blood flow in the hindlimbs before (left) and after (right) ligation and excision of the femoral artery.

4.7 Circulating progenitor cell (CPC) enumeration

4.7.1 Blood collection

Blood collection was carried out by Dr Anshuman Sengupta

150µL of blood was obtained following saphenous vein puncture in the same manner as described in section 4.3.4.1, and collected into Microvette tubes containing 50µL of heparin (1000 IU/mL). The blood samples were then transferred into 15ml centrifuge tubes containing 3mL of sterile 1:10 Pharmlyse™ red cell lysis buffer. The samples were transferred on ice from the animal facility to the laboratory, where thrombi were then removed using a 1ml pipette tip.

4.7.2 Incubation with antibodies

The samples were centrifuged at 300g and 18°C for 10 minutes, following which the supernatant was aspirated. The remaining pellet was then re-suspended in 1ml of FACS buffer and centrifuged at 300g for 10 minutes once again. The FACS buffer was made up of PBS with 0.5% (v/v) foetal calf serum (FCS) and 0.5% (m/v) bovine serum albumin (BSA). Once the supernatant had been discarded, the pellet was then re-suspended in 100µL of 1:10 Fc block and refrigerated in the dark for 10 minutes.

During this 10 minute incubation, two solutions were made up which contained 1:50 dilutions of either the three antibodies or their isotype controls, with FACS buffer being the diluent. The antibodies and their attached fluorochomes are listed below:

1. Stem cell antigen (Sca1)	Fluorescin isothiocyanate (FITC)
2. Kinase insert domain receptor (KDR)	R-phycoerythrin (PE)
3. C-kit/CD117	Allophycocyanin (APC)

Following this incubation, each sample was doubled in volume with the addition of 100µL of FACS buffer. The samples were then spilt into two halves, with one half receiving 10µL of antibody and the other half 10µL of isotype control. The mixtures were then refrigerated for 10 minutes to allow antibody binding. This was followed by a final

centrifugation step, after which the cell pellets were suspended in 500µL of fresh FACS buffer and transferred to the flow cytometer on ice.

4.7.3 Fluorescence Activated Cell Sorting (FACS)

A BD-LSR Fortessa flow cytometer was used for CPC enumeration. The lymphocyte gate was defined as shown in figure 9, and from this the number of $Sca1^+Flk1^+$ cells, $c\text{-}kit^+$ cells and $Sca1^+c\text{-}kit^+$ cells were quantified within the first 100,000 events. The results from the isotype control samples were subtracted from the corresponding antibody samples in order to negate the effect of non-specific fluorescence.

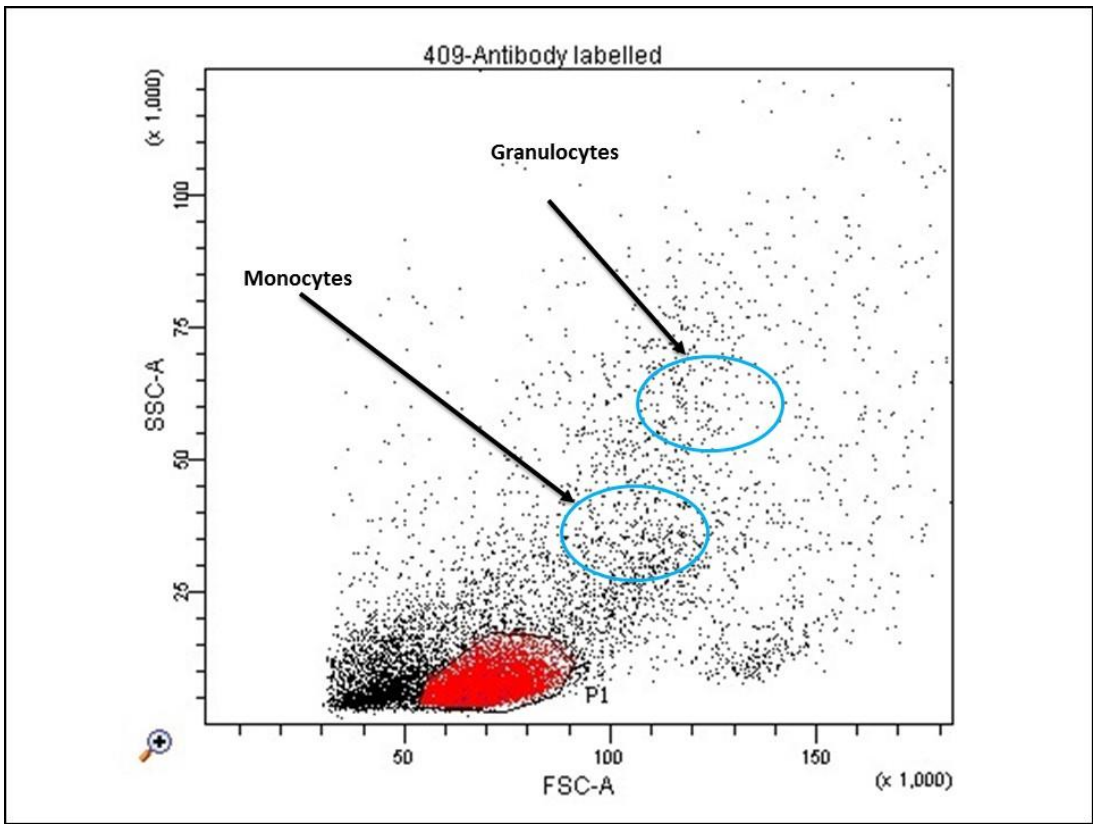

Figure 9 Definition of lymphocyte gate on flow cytometry

Red portion of the graph represents lymphocytes. Portions of the graph which represent monocytes and granulocytes are labelled.

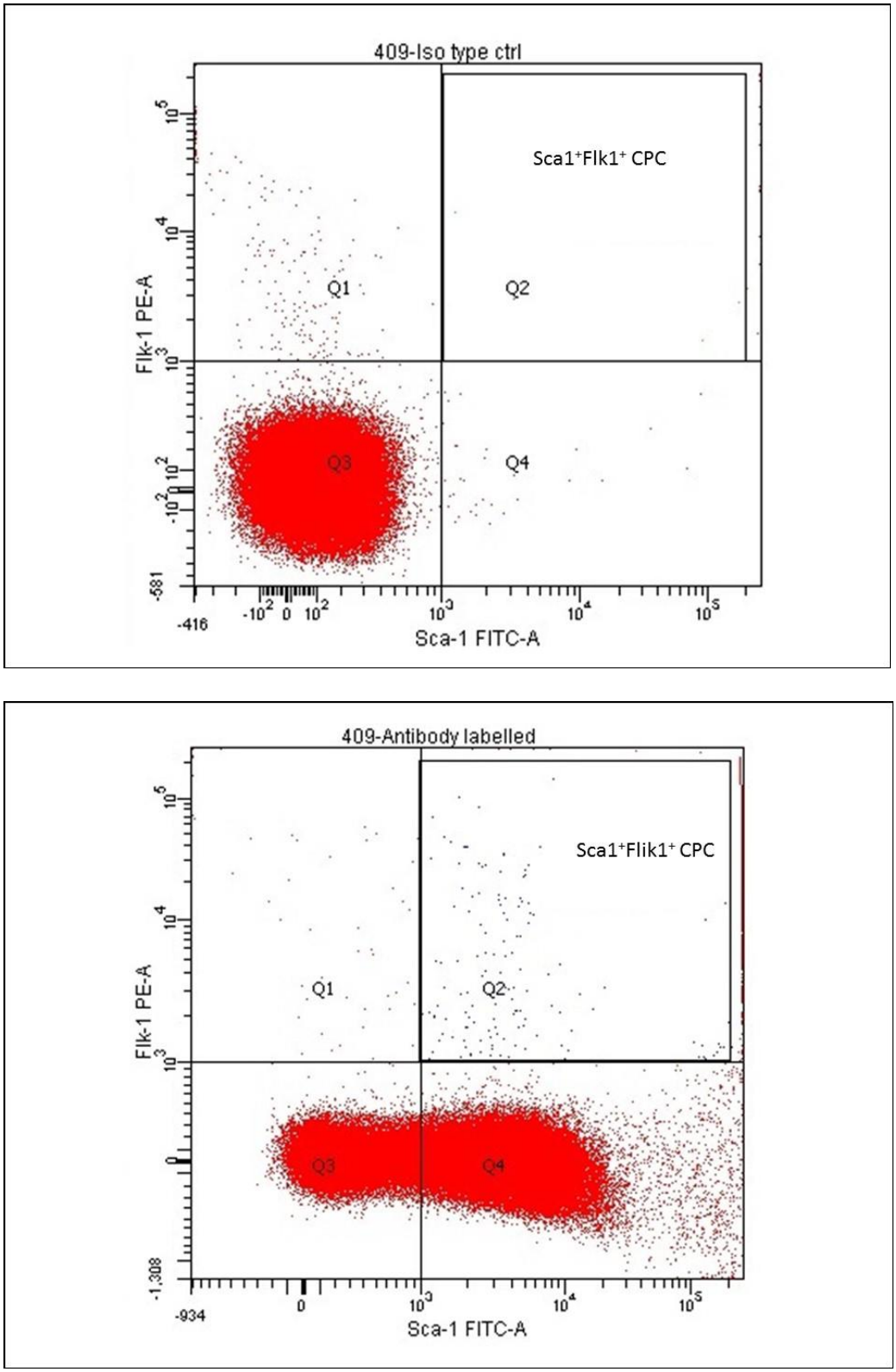

Figure 10 Definition of Sca^{+}Flk1^{+} circulating progenitor cells (CPCs)

Upper panel shows isotype control whilst lower panel shows antibody-labelled cells. Cells which co-express stem cell antigen 1 (Sca1) and foetal liver kinase 1 (Flk1) are seen in Q2.

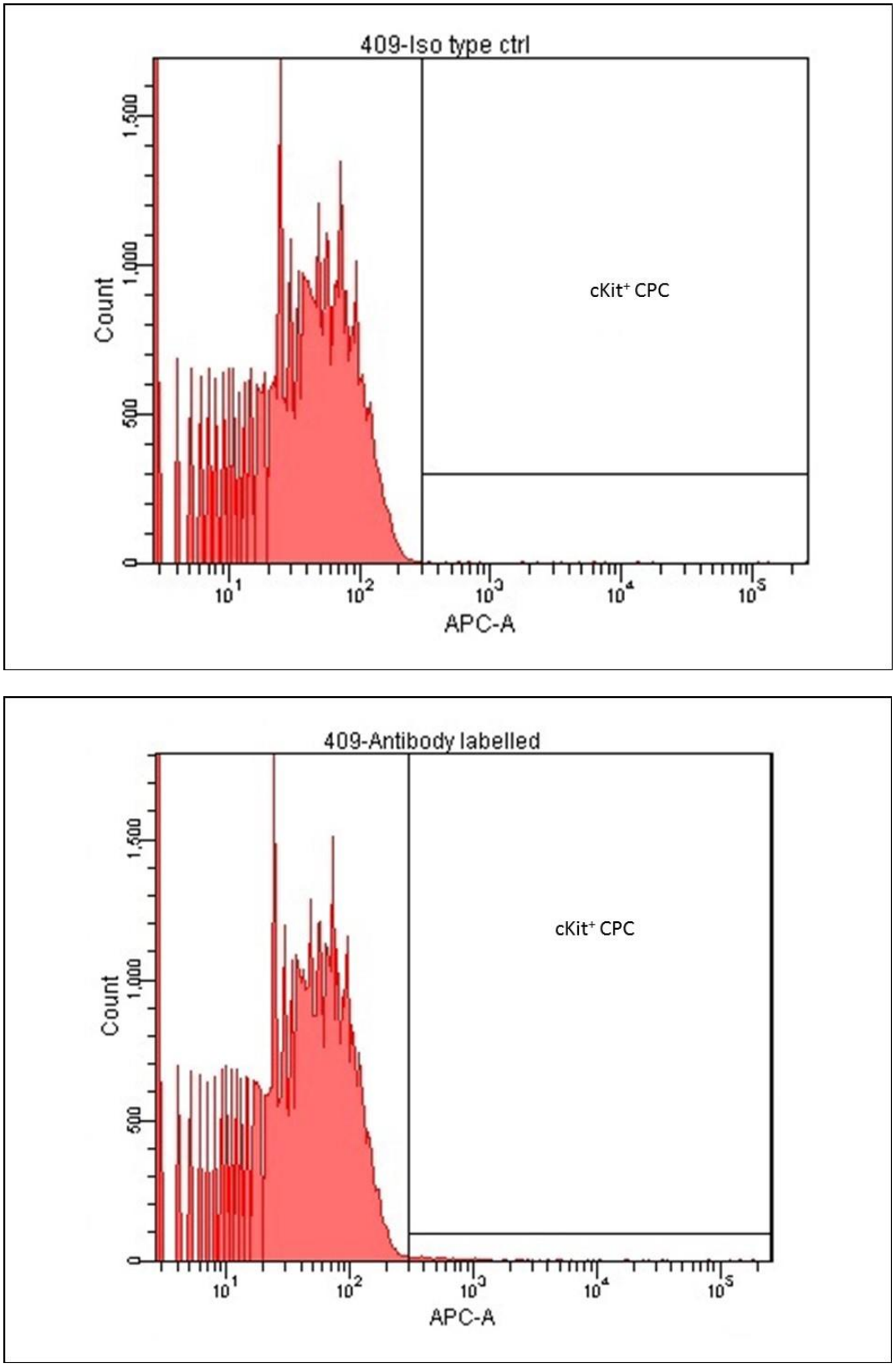

Figure 11 Definition of cKit$^+$ circulating progenitor cells (CPCs)

Upper panel shows isotype control whilst lower panel shows antibody-labelled sample. Cells expressing c-kit are in the labelled region.

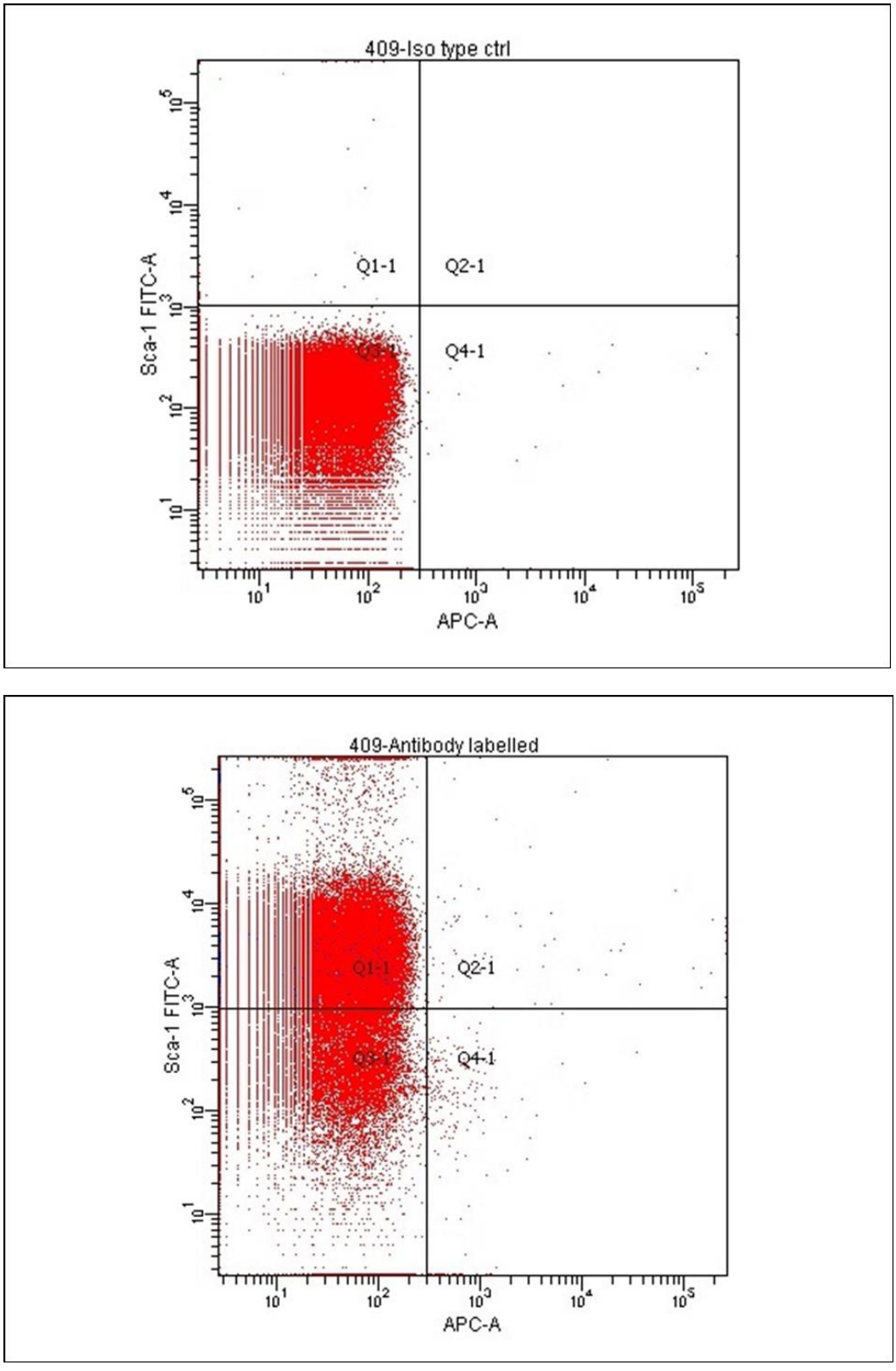

Figure 12 Definition of Sca1^{+}c-kit^{+} cells circulating progenitor cells (CPCs)

Upper panel shows isotype control whilst lower panel shows antibody-labelled sample. Cells co-expressing Sca1 and c-kit are in the quadrant labelled Q2-1.

4.8 Early outgrowth endothelial progenitor cell (EPC) culture

4.8.1 Tissue harvest

Blood, bone marrow and spleen tissue was harvested from each mouse under terminal general anaesthesia, induced and maintained in the same manner as described in section 4.5.1. Once adequate anaesthesia had been confirmed, a midline laparotomy incision was made which allowed visualisation of the IVC. A 1ml insulin syringe containing 50µL of sterile sodium citrate was used to puncture the IVC and extract the full circulating volume of blood (typically approximately 1ml), which was mixed into 4ml of sterile, ice cold PBS. Following this, the spleen was removed and also placed into ice cold sterile PBS. The final step involved extraction of bone marrow from the femurs and tibiae. Having extracted the bones, cuts were made at the metaphyses and a needle and syringe containing sterile PBS used to flush out the marrow tissue. All samples were stored on ice during transit back to the cell culture laboratory.

4.8.2 Mononuclear cell isolation

Diluted blood was filtered into a 50mL centrifuge tube through a 70µm cell strainer. Spleens were mechanically minced in 70µm cell strainers using syringe plungers into 3mL of fresh sterile PBS and the filtrate injected through the cell strainer into a 50mL tube. The marrow was also minced and filtered in similar fashion. Each suspension was washed with 2mL of PBS and the resulting cell suspensions were layered onto 5mL of Histopaque-1083, prior to density-mediated centrifugation at 400g for 30 minutes with a slow deceleration. Buffy layers were separated out and washed twice (for spleen and marrow) and three times (for blood) with 10mL of sterile PBS at 400g for 10 minutes.

4.8.3 Cell seeding and incubation

The cell pellets produced by the isolation steps were re-suspended in EPC growth medium, composed of EGM-2 basal medium supplemented with 20% FCS and an EGM-2 bullet kit. The pellets derived from blood and marrow tissue was re-suspended in 500µL media, whilst the spleen-derived pellet was re-suspended into 2ml. From each of these suspensions, 20µL was removed for cell counting purposes and mixed with an equal volume of trypan blue solution. The mixture was injected into a haemocytometer and the

number of cells counted under microscopy. Extrapolation of the count result estimated the cell concentration within solutions, which could then be seeded onto fibronectin-coated culture plates. The seeding densities varied depending on the cell origin; marrow samples were seeded at a density of $1x10^6$ cells/well, blood samples at $5x10^6$cells/well and spleen samples at $8x10^6$ cells/well. Cells from all three tissue sources were seeded onto 24 well cell culture plates. EPC media was added to each of the wells and the plates incubated at 37°C for 7 days. On day 4 the cells were washed twice with sterile PBS in order to remove non-adherent cells and fresh media was added.

4.8.4 EPC imaging

EPCs were identified based on their ability to import 1,1'-dioctadecy-3,3,3',3'-tetramethyllindocarbocyanine-labelled acetylated low-density lipoprotein (DiI-ac-LDL) and bind Ulex Europeaus lectin conjugated with fluorescein isothiocyanate (FITC). On day 7 the cells were washed twice with sterile PBS. DiI-ac-LDL was dissolved in EPC media and then added at a concentration of 10μg/mL. The cells were then incubated in the dark at room temperature for 3 hours. Following a further wash with sterile PBS, the cells were fixed using 4% paraformaldehyde. Ulex Eueopeaus lectin-FITC conjugate was then added, at a concentration of 10μg/mL in PBS, for one hour.

Imaging was performed using an Olympus CKX-41 fluorescent microscope at x100 magnification. Cell B software was used in order to take five images per well using phase contrast, red fluorescence (to identify DiI staining) and green fluorescence (to identify FITC staining). Image J software (v1.46r) was then used to create composite images in order to quantify the number of dual stained cells which represent EPCs [137] (see figure 13).

4.8.5 Conditioned media

In order to compare the functional effects of EPCs derived from mice of different genotypes, conditioned media was obtained following culture of these cells and used in assays of endothelial function (see section 4.11.2). In order to obtain conditioned media, spleen-derived EPCs were seeded onto a fibronectin-coated 6 well plate at a density of 30 million cells per well, and incubated at 37°C. On day 4, following a wash with PBS, the EPC growth media was replaced with 1ml of basal EPC media containing 1% FCS. The cells were

then re-incubated for 24 hours, at which point the basal media was removed and centrifuged at 6000rpm for 6 minutes. The resulting pellet was discarded, and the supernatant frozen at -80°C for later use in the scratch wound assay.

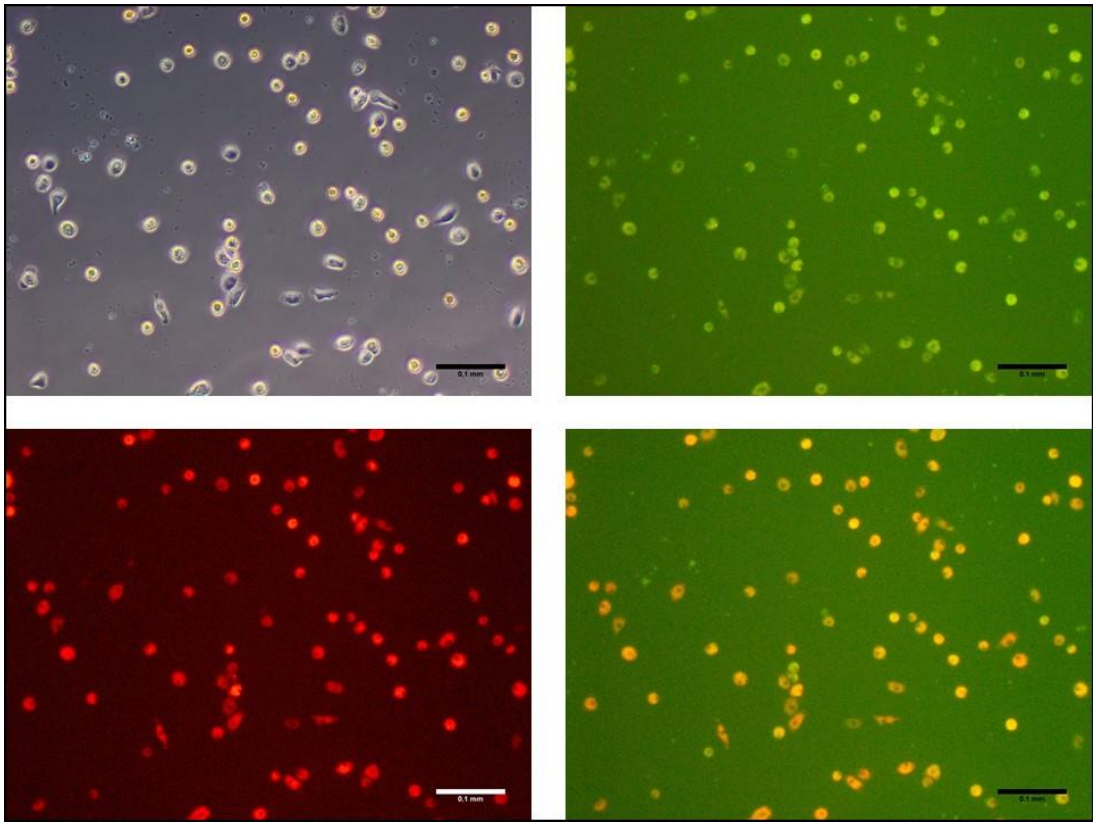

Figure 13 Imaging and quantification of EPCs

Representative images of EPCs derived from splenic tissue (x100 magnification). Top left = phase contrast image; top right = FITC-lectin; bottom left = DiI-acetylated-LDL; bottom right = composite image showing dual-staining cells. Scale bar represents 100µm.

4.9 Isolation and Culture of Pulmonary Endothelial Cells (PECs)

Murine pulmonary endothelial cells (PECs) were isolated and then used in functional and biochemical assays, including assessments of proliferation, migration and superoxide production. The method used to isolate and culture the cells was adapted from the technique described by Sobczak et al [208].

4.9.1 Lung harvest

Mice were euthanised between the ages of 3-6 weeks via exposure to rising concentrations of CO_2. Death was then confirmed using cervical dislocation. Following this, the lungs were carefully dissected out, stored in ice cold Hank's buffered salt solution (HBSS), and transferred back to the cell culture facility.

4.9.2 PEC isolation

The lungs were transferred into sterile $10cm^2$ petri dishes. Within a 15ml centrifuge tube, 10ml of a 1mg/ml solution of collagenase/dispase was made up, from which 100µL was added to the lungs. Two sterile scalpel blades were then used to mince the lung tissue, forming a homogenous mixture with the collagenase/dispase solution. The mixture was then added to the 10ml collagenase/dispase and the centrifuge tubes loaded onto a MACSmix™ rotator for 45 minutes at 37°C. Following this, the mixture was agitated gently using a 10ml syringe attached to a 14G cannula in order to create a single-cell suspension, and then injected through a 70µm cell strainer into a fresh 50ml centrifuge tube. In order to neutralise the collagenase/dispase, 5ml of PEC media (see section 4.9.5) was added. The resulting filtrate was centrifuged for 8 minutes at 400g, and the cell pellet then re-suspended in 200µL of 0.1% PBS/BSA in preparation for the magnetic bead separation.

4.9.3 Magnetic bead separation

In order to obtain a pure sample of PECs, cell separation was carried out using magnetic beads with conjugated CD146. Having been resuspended in 200µL of 0.1% PBS/BSA, the cells were transferred to a fresh 1.5ml micro-centrifuge tube and 20µL of commercially acquired magnetic beads with conjugated CD146 (Miltenyi Biotec) added. The micro-centrifuge tube was then loaded onto a MACSmix™ for 20 minutes and kept at 4°C.

Following this mixing step, 1ml of 0.1% PBS/BSA was added and the mixture centrifuged for 5 minutes at 400g. During this 5 minute period, the magnet used to separate the cells was set up, with a cell separation column placed above a 15ml centrifuge tube (see figure 14). The cell separation column was then flushed through with 500µL of 0.1% PBS/BSA.

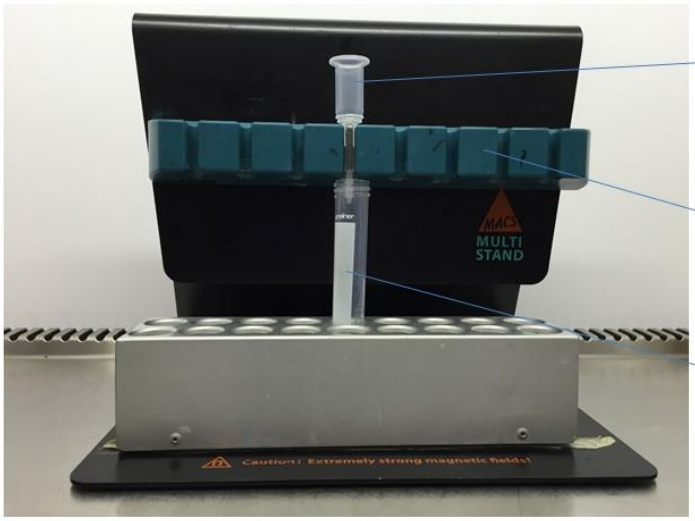

Figure 14 Apparatus used for magnetic bead separation of PECs

Once the sample had completed its 5 minute centrifugation, the cell pellet was carefully re-suspended in 500µL of 0.1% PBS/BSA, avoiding the formation of any bubbles. The suspension was then pipetted into the cell separation column. The suspension would pass through the magnet, allowing sequestration of the endothelial cells which had conjugated to the magnetic beads, whilst filtering out the supernatant into the centrifuge tube below. Once the suspension had completely filtered through, 3 washes were performed by adding 500µL of 0.1% PBS/BSA to the cell separation column. Following this, the cell separation column was removed from the magnet and placed on a fresh 15ml centrifuge tube, into which the contents of the column could be mechanically expelled. The tubes were then

centrifuged for 5 minutes at 400g in order pellet the cells, which were then re-suspended in 500µL of 0.1% PBS/BSA. The magnetic column separation was process was then carried out once more in order to maximise the purity of the sample.

Following the completion of the magnetic column separation, the remaining cells were then re-suspended in 500µL of PEC media and plated onto gelatin coated T25 flasks, and the total volume was then made up to 5ml with fresh PEC media. The cells were incubated at 37°C with 5% CO_2. The media was completely replaced 24 hours after isolation, following which the media was half changed on alternate days. The cells were allowed to grow until they reached confluence (see figure 15), at which point they were split into different plates for various assays (see section 4.11).

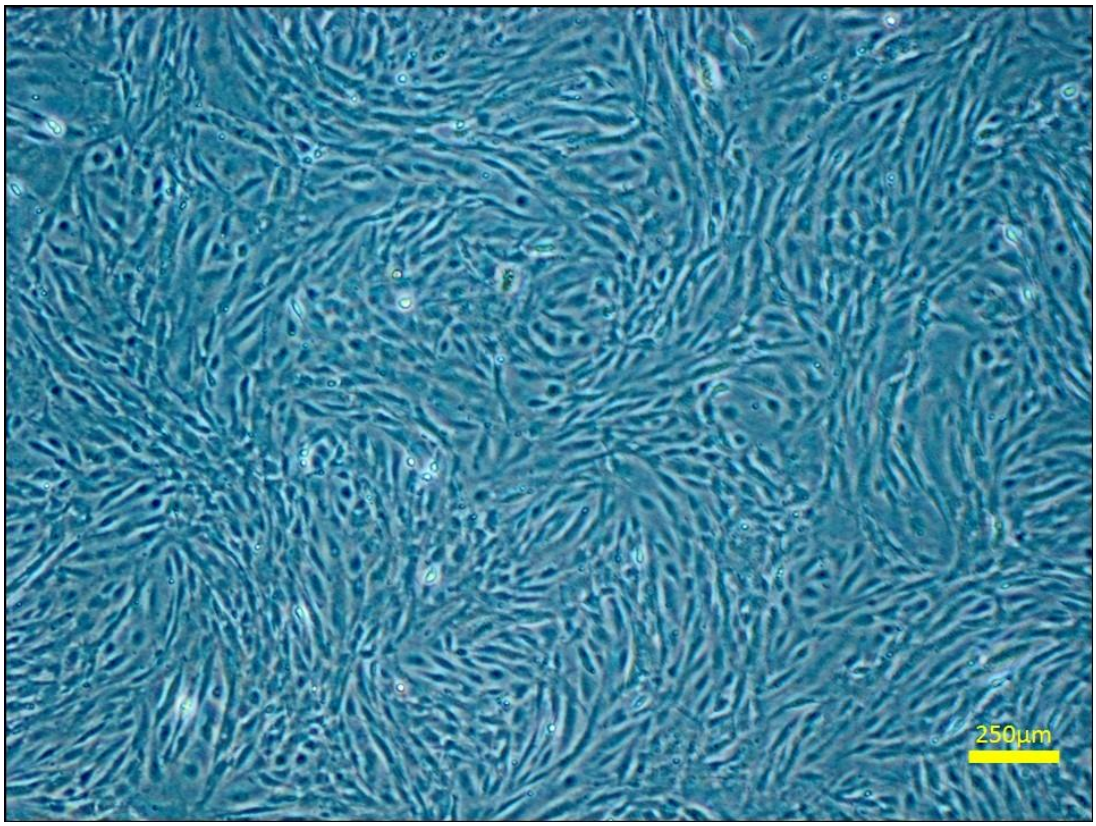

Figure 15 A representative image of PECs at confluence following magnetic bead separation (x40 magnification)

4.9.4 Determination of PEC purity

Previous work in our laboratory, carried out by Drs Richard Cubbon and Anshuman Sengupta, has been done to confirm endothelial lineage of cultured PECs.

Once the cells had become confluent, they were detached using 0.25% trypsin/EDTA (see section 4.10.3) and counted using trypan blue (see section 4.8.3). 15,000 cells were seeded onto 35mm imaging dishes and incubated at 37°C for 24 hours. Following 2 washes with sterile PBS, the cells were fixed by adding 1ml of 4% paraformaldehyde for 15 minutes. Following fixation, the cells were permebilised and blocked using a solution of 0.25% Triton X-100 and 1% BSA in PBS. They were then incubated for 2 hours at room temperature with 10µg/ml of isolectin B4-Alex Fluor® 488 conjugate. Three washes with PBS were then performed, followed by application of 5µg/mL Hoechst 33342 in PBS for ten minutes at room temperature. A final wash with PBS was performed, followed by imaging using an A Zeiss LSM700 confocal microscope.

4.9.5 PEC media

PEC media was made in advance of the culture process with the following components:

400ml of basal MV2 growth medium

20ml of endothelial growth supplement

50ml of foetal bovine serum

10ml of antibiotic-antimycotic solution

4.10 Culture and transduction of human umbilical vein endothelial cells (HUVECs)

Human umbilical vein endothelial cells were cultured and then transduced with an insulin receptor (or scrambled control) shRNA using commercially produced lentiviruses in order to knockdown the insulin receptor. This provided a complementary model of endothelial insulin resistance with which the effects of pharmacological NOX2 inhibition could be investigated.

4.10.1 HUVEC culture

Pooled donor samples of HUVECs were purchased commercially from PromoCell and stored as 1ml aliquots in liquid nitrogen. When required for experiments they were extracted from storage and transferred to the cell culture facility on ice, where they could then be defrosted rapidly in a water bath at 37°C.

Once the cells had defrosted they were re-suspended in 9ml of HUVEC media (see section 4.10.2), and the resulting 10ml split into halves and plated onto two 10cm^2 petri dishes pre-coated with 0.1% gelatin. The total volume within each petri dish was made up to 10ml with fresh HUVEC media and the cells then incubated at 37°C with 5% CO_2. The media was completely replaced 24 hours later and on alternate days thereafter. The cells were allowed to grow until 70% confluence prior to transduction.

4.10.2 HUVEC culture media

HUVEC media was made in advance of the culture process with the following components:

380ml of M199 basal media

100ml of fetal bovine serum

10ml of 1M HEPES buffer

5mls of antibiotic-antimycotic solution

10ml of sodium pyruvate solution

2500 units of heparin

2.5ml of endothelial cell growth supplement

4.10.3 Transduction of HUVECs with shRNA lentivirus

In order to examine insulin resistance in HUVECs, a commercially acquired shRNA lentivirus was used to knockdown expression of the insulin receptor. All work involving the lentivirus and the transduced cells was carried out in a designated 'Category 2' viral laboratory with appropriate precautions taken.

Based on results from pilot work done to assess the magnitude of IR knockdown with varying concentrations of the lentivirus (see section 5.3.1), a multiplicity of infection (MOI) of 15 was chosen for experimental work as this achieved approximately 50% knockdown of IR protein. The IR shRNA lentivirus virus was added to one dish of HUVECs, with the second dish of identical cells receiving a control lentivirus containing a scrambled shRNA at the same MOI. The cells were then incubated with the lentiviruses for 24 hours, at which point the 2 samples of cells were split into halves to form 4 cohorts of cells. The method used to split a sample of cells involved initially detaching them from their petri dishes using 0.25% trypsin/EDTA. Following aspiration of the media from the dish, the cells were washed with 10ml of warm, sterile PBS and 2ml of trypsin/EDTA was then added. The cells were incubated with the trypsin/EDTA at 37°C for 1 minute. Cell detachment was confirmed using light microscopy and the trypsin then neutralised with 3ml of HUVEC media. The resulting 5ml mixture was then split evenly into two fresh 10cm^2 petri dishes which had been pre-coated with 0.1% gelatin, and then topped up to a total volume of 10ml with the addition of 7.5ml of HUVEC media. Splitting the two dishes of HUVECs in this way produced 4 cohorts of cells, which allowed paired samples of virally-transduced (IR or control shRNA) to be treated with a NOX2 antagonist or control.

4.10.4 Pharmacological NOX2 inhibition

In order to study the effects of pharmacological NOX2 inhibition in the setting of insulin resistance, HUVECs were treated with a specific NOX2 inhibitor named GP91-ds tat (see section 4.6.3). *In vitro* work from the paper describing the original use of this molecule [72] demonstrated that GP91-ds tat at a concentration of 50µM could completely block

angiotensin II-induced O_2^- production in aortic rings from rats, and so the same concentration was used for experiments in this project. In order to create a 50µM solution, a 10mM stock solution was formed by dissolving 29mg of GP91-ds tat into a 1ml of a solution made up from 100ml distilled water, 0.9g sodium chloride and 57.5µL acetic acid. This stock solution could then be diluted to the desired concentration using HUVEC growth media. The GP91-ds tat was supplied with a scrambled-ds tat peptide which was used as a control. This molecule has the same molecular weight as GP91-ds tat and so was reconstituted into a 50µM experimental solution in the same way.

Once the 4 dishes of cells had become 70% confluent, GP91-ds tat was added to one dish of IR-knockdown cells and one dish of control lentivirus-treated cells, with the remaining dishes receiving the scrambled-ds tat control peptide. The resulting combinations of viral transduction and GP91-ds tat treatment is summarised in figure 16. The cells were incubated with the GP91-ds tat or scrambled control peptide for 24 hours, after which they were then used for the assays outlined in section 4.11. Lysates generated from the HUVECs were also used for Western Blotting in order to confirm effective IR knockdown (section 4.12).

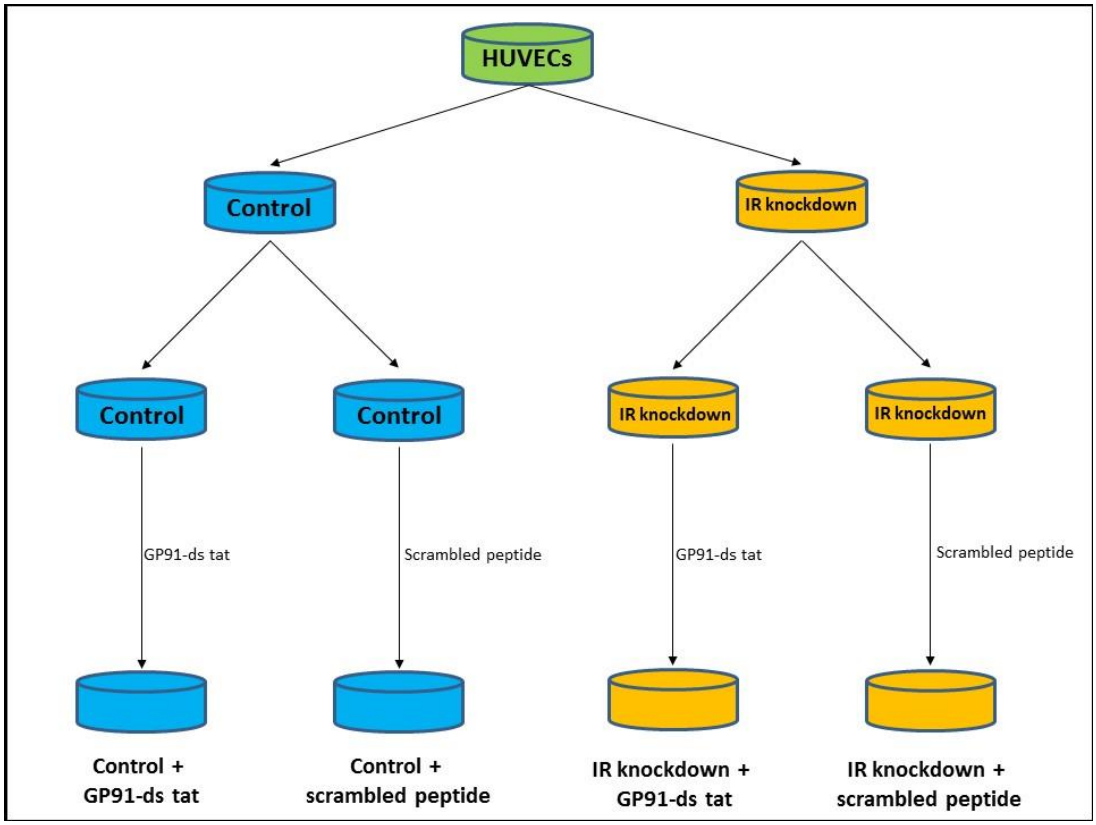

Figure 16. The four cohorts of HUVECs used to assess the effect of pharmacological NOX2 inhibition in insulin resistance

Control: HUVECs transfected with control shRNA lentivirus; IR knockdown: HUVECs transfected with IR shRNA lentivirus

4.11 Endothelial cell functional assays

Assays of cell proliferation, migration and superoxide quantification were carried out on PECs and lentiviral-transfected HUVECs in order to ascertain the effects of genetic and pharmacological NOX2 inhibition. The assays were carried out in an almost identical way for both types of cell, with the only difference pertaining to the number of cells seeded at the start of the experiment, and the concentration of gelatin used to coat the cell culture plates. These variations will be described in the relevant sections.

4.11.1 Endothelial cell proliferation assay

Proliferative capacity of PECs and HUVECs was assessed using 5-ethynyl-2'-deoxyuridine (EdU), a nucleoside analogue that incorporates into the DNA of replicating cells. The EdU was conjugated to an alkyne that can be detected with an Alexa Fluor® 647-conjugated azide, which allowed proliferating cells to be quantified by flow cytometry.

Prior to performing the assay, the cells were detached from their respective cell culture plates using 0.25% trypsin/EDTA (see section 4.10.3), counted using trypan blue (see section 4.8.3) and then seeded onto a well of a 6 well plate at a density of 100,000 cells per well. In the case of PECs, the well was pre-coated with 2% gelatin, whereas for HUVECs 0.1% gelatin was used. Fresh media was added to each well so that the volume totalled 2ml and the cells were then incubated at 37°C for 48 hours, with a full media change performed at 24 hours.

The assay was carried out using a commercially available Click-iT® kit (Life Technologies), and the constituents and required preparation of this kit is outlined in table 8. On the day of the assay, EdU diluted in growth media was added to each sample at a concentration of 10μM, and the cells then incubated at 37°C for 4 hours. Following this, the cells were washed with sterile PBS and then detached from the cell culture plate using 0.25% trypsin/EDTA. Following neutralisation of the trypsin with growth media, the samples were centrifuged for 1 minute at 400rcf in order to pellet the cells. The supernatant was discarded and the cells then washed with 3ml of 1% BSA dissolved in PBS. Following this, the cells were once again centrifuged for 1 minute at 400rcf and the supernatant discarded. The pellet was then resuspended in 100μL of 'Click-iT® fixative' and incubated for 15 minutes at room temperature, protected from light.

Reagent	Preparation
EdU	Reconstitute in DMSO
AlexaFluor® azide	Reconstitute in DMSO
DMSO	Used for reconstitution
Click-iT® fixative	Use neat
Click-iT® saponin based permebilisation and wash reagent	Diluted 1:10 in 1% BSA/PBS
Copper sulphate	Use neat
Click-iT® EdU buffer additive	Reconstitute in deionised water Dilute 1:10 for each use

Table 8 Components of Click-iT® EdU assay kit

EdU = 5-ethynyl-2'-deoxyuridine; DMSO = dimethyl sulfoxide; BSA = bovine serum albumin; PBS = phosphate buffered saline

Following this brief incubation, the cells were once again washed with 3ml of 1% BSA in PBS and centrifuged for 1 minute at 400rcf. Once the supernatant had been discarded, the pellet was resuspended in 100µL of 'Click-iT® saponin based permebilisation and wash reagent' and incubated in the dark for 15 minutes at room temperature. During this incubation period, a 'Click-iT® reaction cocktail' was prepared as outlined in table 9.

Component	Volume (µL)
PBS	438
Copper sulphate	10
AlexaFluor® azide	2.5
Click-iT® EdU buffer additive	50
Total	*500*

Table 9 Composition of 'Click-iT® reaction cocktail'. Volumes are given per well

Following the completion of the 15 minute incubation, 500µL of the 'reaction cocktail' was added to each sample and the cells then incubated for 30 minutes at room temperature, protected from light. The cells were then washed with 3ml of 'Click-iT® saponin based permebilisation and wash reagent' and centrifuged for 1 minute at 400rcf. The supernatant was discarded, the pellet resuspended in 500µL of 'Click-iT® saponin based permebilisation and wash reagent', and the samples transferred on ice to the flow cytometer.

Flow cytometry

A BD-LSR Fortessa flow cytometer was used in order to quantify the number of cells which had incorporated EdU, thereby providing a measure of the number of proliferative cells within the sample. In order to detect EdU with AlexaFluor 647, an excitation wavelength of 633/635nm with a red emission filter was used. The first 10,000 cells were used for quantification purposes and the results expressed as a proportion of proliferative cells. Representative images of the quantification process are shown in figure 17.

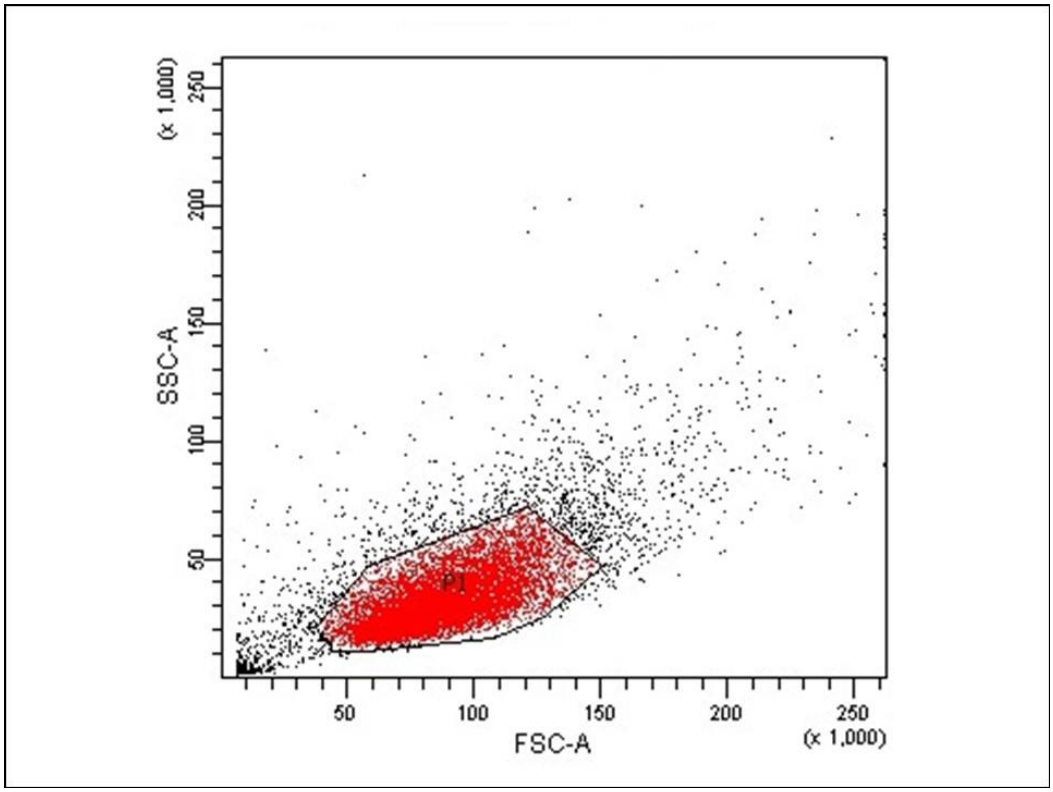
SSC-A
(x 1,000)
250
200
150
100
50
R1
50
100
150
200
250
FSC-A
(x 1,000)

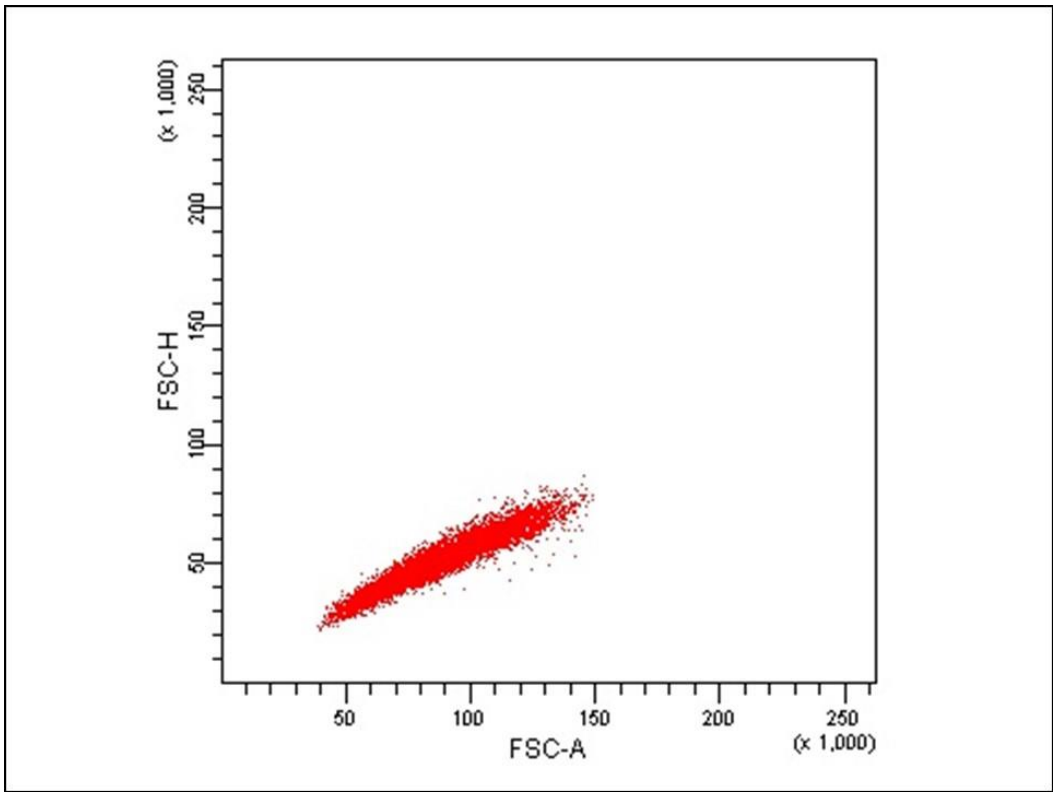
FSC-H
(x 1,000)
250
200
150
100
50
50
100
150
200
250
FSC-A
(x 1,000)

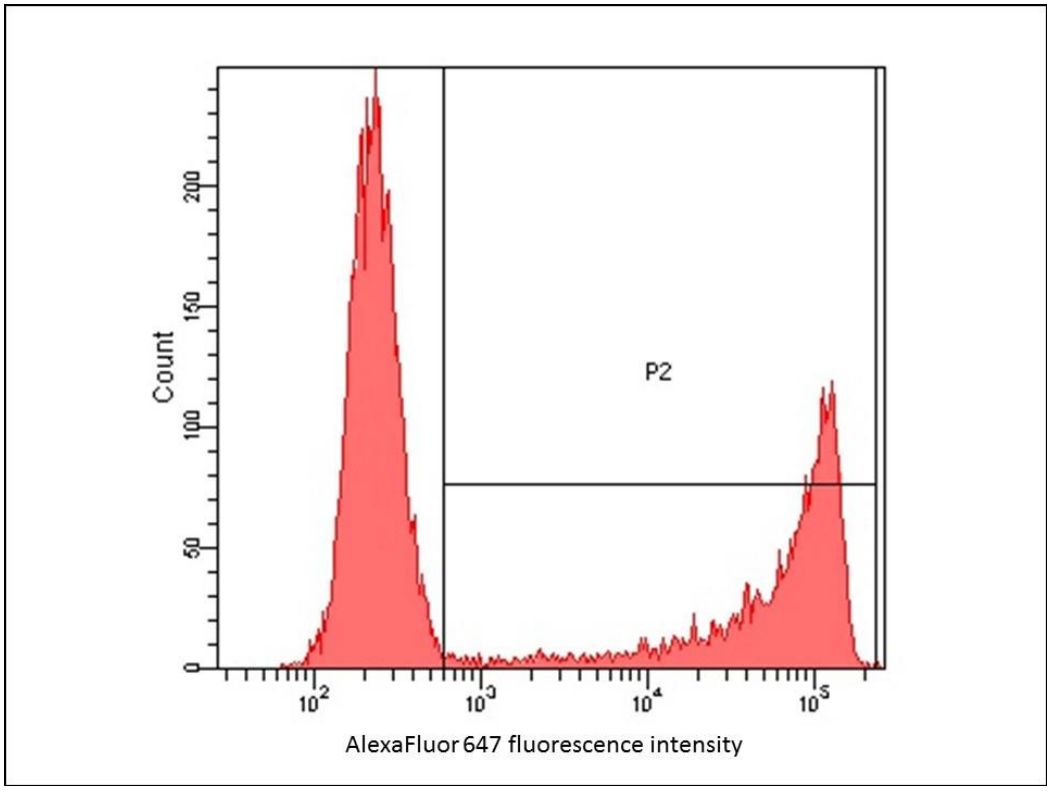

Figure 17 Flow cytometric quantification of proliferating cells based on uptake of EdU

The top panel shows which cells were used for quantification purposes, whilst the middle panel demonstrates the linear relationship between the height and width of the selected cells, indicating that these cells were individual as opposed to aggregated. The bottom panel shows the gating criteria used in order to quantify fluorescent (i.e. proliferating) cells, which are seen in the P2 segment.

4.11.2 Endothelial cell migration assay

The ability of PECs and HUVECs to migrate was studied using an assay of scratch wound closure.

Creation of a scratch wound

The initial step involved detaching the cells from their respective cell culture plates using 0.25% trypsin/EDTA, and counting them using trypan blue as described previosuly. The cells were then seeded onto wells in an Essen imagelock 96 well plate. For PECs, 50,000 cells were seeded onto each well of a plate that had been pre-coated with 2% gelatin, whilst for HUVECs 30,000 cells were seeded into each well of a plate that had been pre-coated with 0.1% gelatin. This difference in cell seeding density resulted from prior optimisation experiments, and reflected the fact that HUVECs reach confluence quicker than PECs. In both cases 5 wells were used per sample, and growth media added so that each well contained a total of 300µL. The cells were then incubated at 37°C for 48 hours to allow them to reach confluence, with a full media change performed at 24 hours.

Following the 48 hour incubation, the cells were washed with sterile PBS and then incubated for 4 hours with reduced-serum media. For PECs, serum-free media was used, whilst for HUVECs media with 1% serum was used. After the 4 hours had elapsed, 100µL of PBS was added to the empty wells of the plate and the cells then mechanically scratched using the Woundmaker^{TM} 96-pin tool. This created a longitudinal scratch across the middle of each well. The cells were then gently washed with sterile PBS to remove any debris and 100µL of full growth media then added.

Analysis of scratch closure

In order to assess the extent of wound closure, the cells were imaged straight after the scratch had been performed (t0), and once again following an 18 hour incubation at 37°C (t18). In both cases the imaging was done using an Olympus CKX-41 microscope with an attached camera. The Essen imagelock plates have a vertical marking line drawn onto the base of each well which perpendicularly bisected the scratch wound. Two images at x40 magnification were taken per well, either side of this marking line. Olympus Cell F software was used to capture and store images which were then analysed using Image J. The area of

the wound at t0 and t18 was measured, and a ratio of these was used to calculate the extent of wound closure (see fig 18).

Endothelial progenitor cell function

The scratch wound assay was also used to compare the functional effects of murine EPCs derived from mice of different genotypes. For this experiment, untreated HUVECs were plated into the wells of a 96 well plate in the same way as described above. Following the creation of a wound, the cells were incubated in conditioned media obtained from EPCs (see section 4.8.5) rather than usual growth media, and then imaged 18 hours later as per the usual protocol.

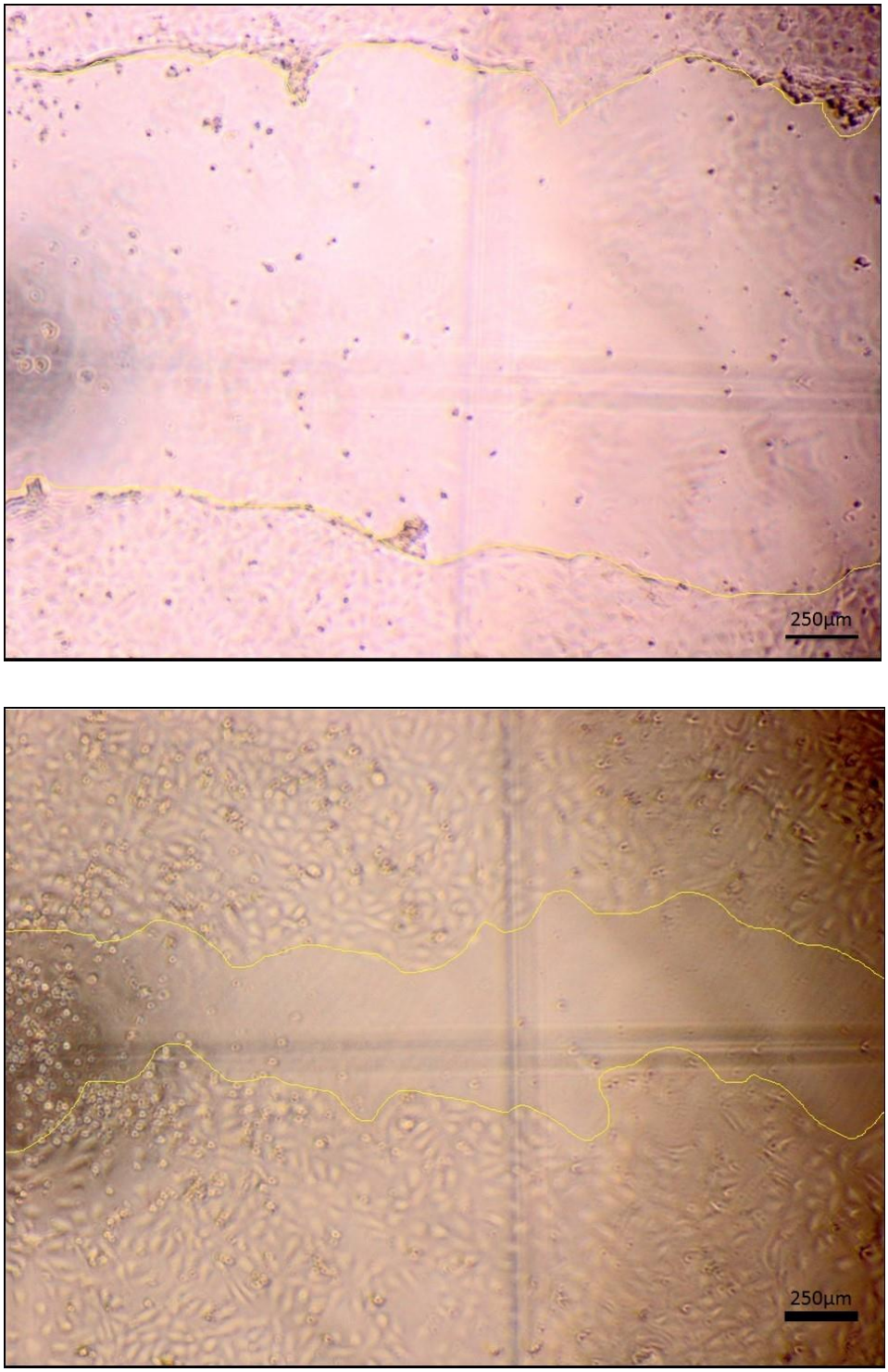

Figure 18 Scratch wound analysis

The upper panel shows HUVECs immediately after scratch, whilst the lower panel shows the same cells following an 18 hour incubation (x40 magnification). A ratio of the respective wound areas was used in order to calculate closure.

4.11.3 Superoxide quantification assay

In order to assess the effect of genetic and pharmacological NOX2 inhibition on superoxide production, the cultured PECs and HUVECs were incubated with the compound dihydroethidium (DHE). In the presence of superoxide, DHE is oxidised to 2-hydroxyethidium, which fluoresces red. Quantification of this fluorescence using a microplate plate reader allows indirect quantification of superoxide production.

To carry out this assay, PECs and HUVECs were detached from their respective cells culture plates and counted, as described previously. In both cases the cells were plated onto uncoated wells of a 96 well plate, but the number of cells varied, with 50,000 cells/well of PECs and 30,000 cells/well of HUVECs. As with the scratch wound assay, this difference was a corollary of the fact that HUVECs tended to grow and reach confluence more rapidly than PECs. Four wells were used per sample and growth media added to each so that the volume in each well totalled 300µL. The cells were then incubated at 37°C for 48 hours with a full media change performed at 24 hours

Following this incubation, the cells were washed twice with sterile PBS. For each sample, DHE was added to two of the four wells, whilst the remaining two were used as controls. DHE was dissolved into Krebs-HEPES buffer at a concentration of 25µM, and 100µL of this solution added to the relevant wells. The remaining control wells received 100µL of Krebs-HEPES alone, and the cells were then incubated at 37°C for 20 minutes. Following this, the cells were washed twice with sterile PBS and 100µL of fresh Krebs-HEPES buffer then added to all wells. Upon completion of this step, the plate was protected from light and transferred to the microplate reader for measurement of fluorescence.

Once the plate had been inserted into the microplate reader, SoftMax® Pro (v5.4.5; Molecular Devices) software was used to detect and quantify fluorescence at excitation and emission wavelengths of 500nm and 600nm respectively, at 10 second intervals for 3 minutes. A mean of the fluorescence readings was then calculated and the measurement for the control cells subtracted from the DHE-labelled cells in order to give the final results.

4.12 Western blotting

Western blotting was performed on lysates from transduced HUVECs in order to confirm effective IR knockdown. All western blots were performed in conjunction with Dr Romana Mughal.

4.12.1 Sample preparation

In order to produce lysates that could be used for Western Blotting, cells from each of the four cohorts of HUVECs (see figure 16) were seeded onto wells of a 6 well cell culture plate that had been pre-coated with 0.1% gelatin. These cells were then incubated at 37°C until they reached confluence (typically 4 days), with half media changes on alternate days.

Once confluent, the cells were washed twice with ice-cold PBS to ensure arrest of cellular processes. The cells were then lysed via addition of 100µL of lysis buffer, composed of radio-immunoprecipitation assay (RIPA) buffer with added phosphatase 2&3 inhibitors. The lysis buffer was kept on the cells for 5 minutes, and the cells then harvested using cell scrapers. The samples were immediately stored at -80°C from where they could be used by Dr Mughal for protein quantification and Western Blotting.

4.12.2 Protein quantification

Cell lysates were gradually defrosted over a 30 minute period on ice and then centrifuged at 15,000g and 4°C for 10 minutes. The resulting pellets were discarded, and the supernatants transferred into fresh microcentrifuge tubes where they could then be used in a bicinchoninic acid (BCA) assay for protein quantification.

BCA assay

An 8µL sample from each lysate was added to 56µL of distilled water to create a 1:8 dilution. From these diluted samples, 25µL was added in duplicate to the wells of a 96 well plate, whilst nine standards of bovine serum albumin (BSA) of known concentrations were also added in duplicate to neighbouring wells in the same plate. The next step involved combining the two colorimetry reagents A (sodium carbonate, bicinchoninic acid and sodium tartrate in 0.1M sodium hydroxide) and B (4% cupric sulphate) from the BCA assay

kit in a 50:1 ratio, and then adding 200µL of the resulting mixture to each well. The plate was then covered and incubated at 37°C for 30 minutes.

Following this incubation, colorimetric analysis was performed using a Dynex MRX TC microplate reader and Revelation software (version 4.21) at a wavelength of 562nm. A standard curve was constructed using the colorimetric measurements from the BSA standards, and this curve was appraised to ensure linearity and a correlation coefficient (r^2)>0.99. Provided the standard curve was satisfactory, the protein concentrations of the samples could be inferred from their colorimetry results and, following a correction for the 1:8 dilution, the protein concentration of the original lysates could be ascertained.

4.12.3 Gel electrophoresis

Using the calculated protein concentrations, a volume of each lysate containing 20µg of protein was added to 4µL of reducing agent and 10µL of sample buffer. Distilled water was then added to each sample so that the volume totalled 40µL. These samples were heated at 95°C for 5 minutes, and this time was used to fill a Criterion Cell tank (Bio-Rad) with 500ml of running buffer, composed of 25mL of 2-(N-morpholino) ethanesulfonic acid/sodium dodecyl sulphate (MES SDS) running buffer and 475mL of de-ionised water. Following the completion of the 5 minute heating step, the samples were loaded into a pre-cast, commercially purchased 4-12% polyacrylamide gel along with 6µL of a protein reference ladder. The gel was subsequently placed into the Criterion Cell tank where electrophoresis could be performed at 100V for two hours.

4.12.4 Transfer

Following completion of the electrophoresis, the gels were removed and washed with deionised water. Two pieces of filter paper and a polyvinylidene fluoride (PDVF) membrane were then cut to match the size of the gel and the membrane soaked in methanol for 15 seconds, water for 5 minutes and finally 1:10 transfer buffer (composed of 6.06g tris, 28.84 glycine, 400ml methanol and 1600ml distilled water) for 2 minutes. Simultaneously, the 2 pieces of filter paper as well as 2 sponges were also soaked in 1:10 transfer buffer. Once all of the components had been appropriately soaked, a ‘transfer sandwich’ was then made with the gel and membrane in the middle, flanked on each side by filter paper, which themselves were flanked by the sponges. This ‘transfer sandwich’ was loaded into a plastic

cassette which could then be placed into an electrophoresis tank containing 1:10 transfer buffer. Electrophoresis was then performed at 100V for 1 hour.

4.12.5 Immunostaining

Following the protein transfer, the membrane was separated from the 'transfer sandwich' and washed in a blocking solution containing 5% BSA in tris-buffered saline with Tween (TBST; 0.1%) for five minutes. A clean scalpel was then used to cut the membrane at the level corresponding to 75kDa from the reference ladder, thus allowing simultaneous immunostaining for the insulin receptor and β actin as a control. The two membranes were then incubated at room temperature for 1 hour in 15ml of TBST in order to block non-specific binding.

During this one hour period, the primary antibody was prepared in a BSA-TBST solution at a dilution outlined in table 10. Following removal of the 15ml of TBST, the membranes were then incubated with their respective primary antibody solutions overnight at 4°C. The following morning, the membranes were washed three times for five minutes each in TBST. At this stage, the secondary antibody was then prepared (see table 10) in 5% BSA-TBST and the membrane then incubated in this solution for one hour at room temperature.

Antibody type	Targeted protein	Dilution	Manufacturer
Primary	Insulin receptor	1:1000	Cell signalling
Primary	β Actin	1:20,000	Cell signalling
HRP-conjugated secondary	Polyclonal goat anti-rabbit	1:1000	Dako

Table 10 Antibodies used in Western Blotting.

HRP = horseradish peroxidase

Following this incubation, the membranes were once again washed in TBST three times for 15 minutes each.

4.12.6 Imaging

Each membrane was placed onto cling film and uniformly covered with 1ml of Immobilon Western Chemiluminescent HRP Substrate (500uL peroxide solution, 500uL enhancer solution), before being imaged using the Syngene G imaging system.

4.13 Statistical analysis

All continuous data sets are expressed as mean with standard error of mean (SEM) unless otherwise stated. Graphs and statistical analyses were performed using GraphPad Prism v6 (2012). For the majority of analyses, two-tailed unpaired or paired Student's t-tests were performed as appropriate. For analysis of body weights, GTT, ITT and ischaemic revascularisation data, area under the curve (AUC) was calculated. In all analyses, a p value of <0.05 was deemed statistically significant.

Chapter 5**: Results**

Chapter 5 **Results**

5.1 IRKOxGP91phox$^{y/-}$

5.1.1 Genotyping

Example PCR gels for identifying IRKO and GP91 genotypes are displayed in figures 19 and 20 respectively, with a 1000 base pair ladder on the left for reference.

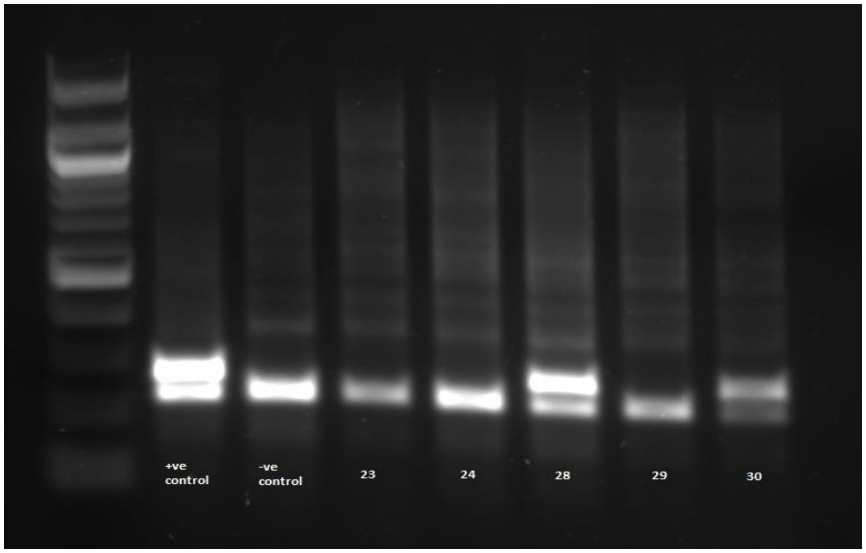

Figure 19. IRKO PCR

IRKO gene cassette is denoted by a double band at 235 and 255 base pairs (e.g. 28), with a single band at 235 base pairs for wild-types (e.g. 23).

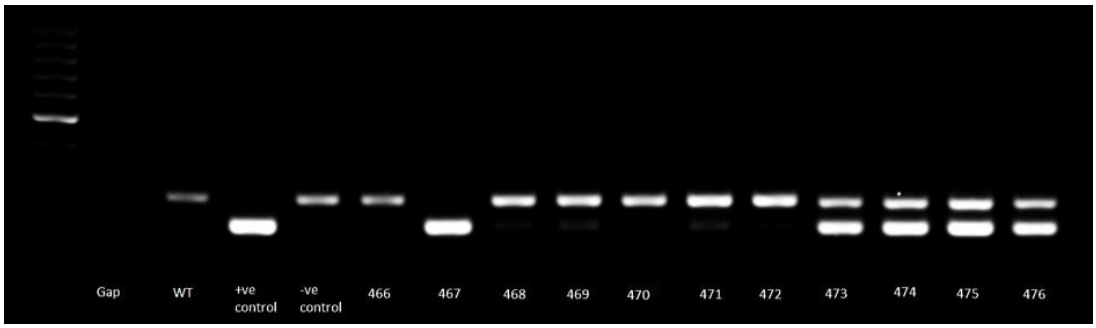

Figure 20. GP91phox PCR

WT mice are identified by the presence of an upper single band at 240 base pairs (e.g. 466), whilst GP91phox$^{y/-}$ homozygote mice display a lower single band at 195 base pairs for (e.g. 467). Double bands represent heterozygote females (e.g. 473).

5.1.2 Body weights

No differences in bodyweight were identified between mice of WT, IRKO or IRKOxGP91phox$^{y/-}$ genotypes (see figure 21).

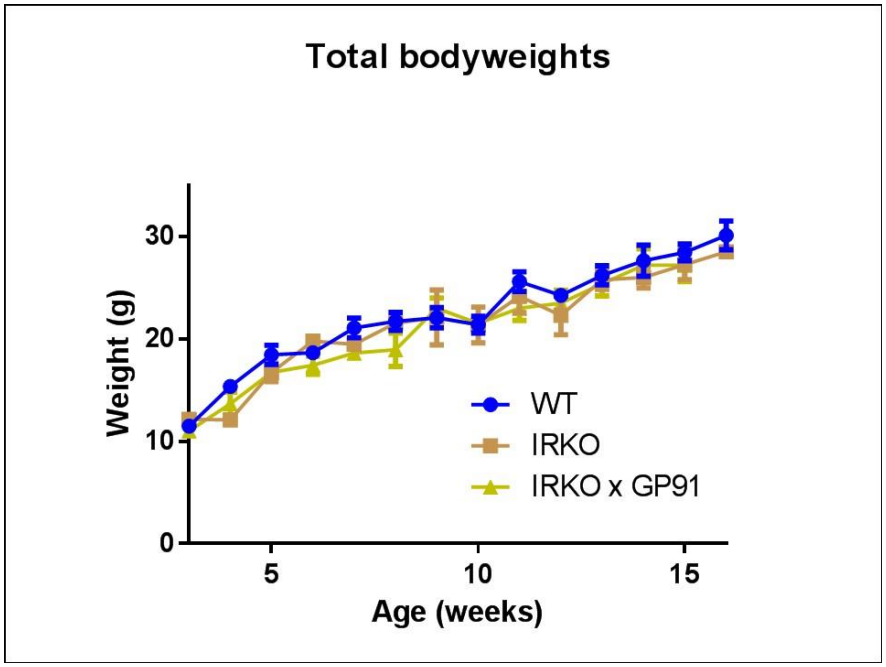

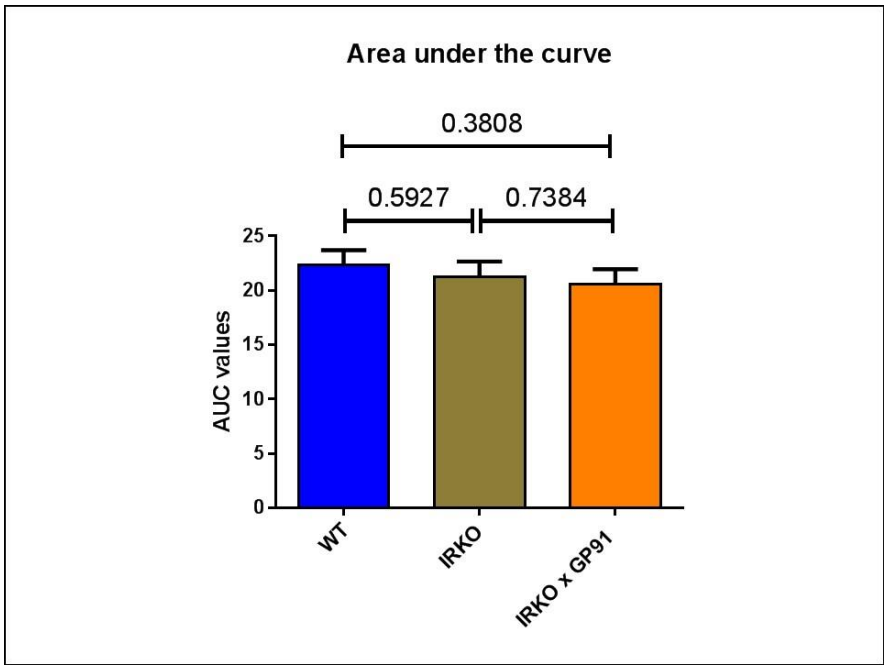

Figure 21 Total bodyweight

Upper panel: Body weight at various time points; Lower panel: Area under curve analysis (N=5, 5, 3)

5.1.3 Glucocompetence testing

Previously published data demonstrate that IRKO mice display no significant difference to WT littermates with respect to glucocompetence [120]. Data from the current study recapitulated these findings, with no differences seen in non-fasting blood glucose concentration (figure 22), glucose tolerance testing (figure 23) or insulin tolerance testing (figure 24). The same tests also demonstrated no significant difference between these mice and IRKOxGP91phox$^{y/-}$ littermates, although a trend towards a reduced non-fasting blood glucose concentration was seen in the double cross mice.

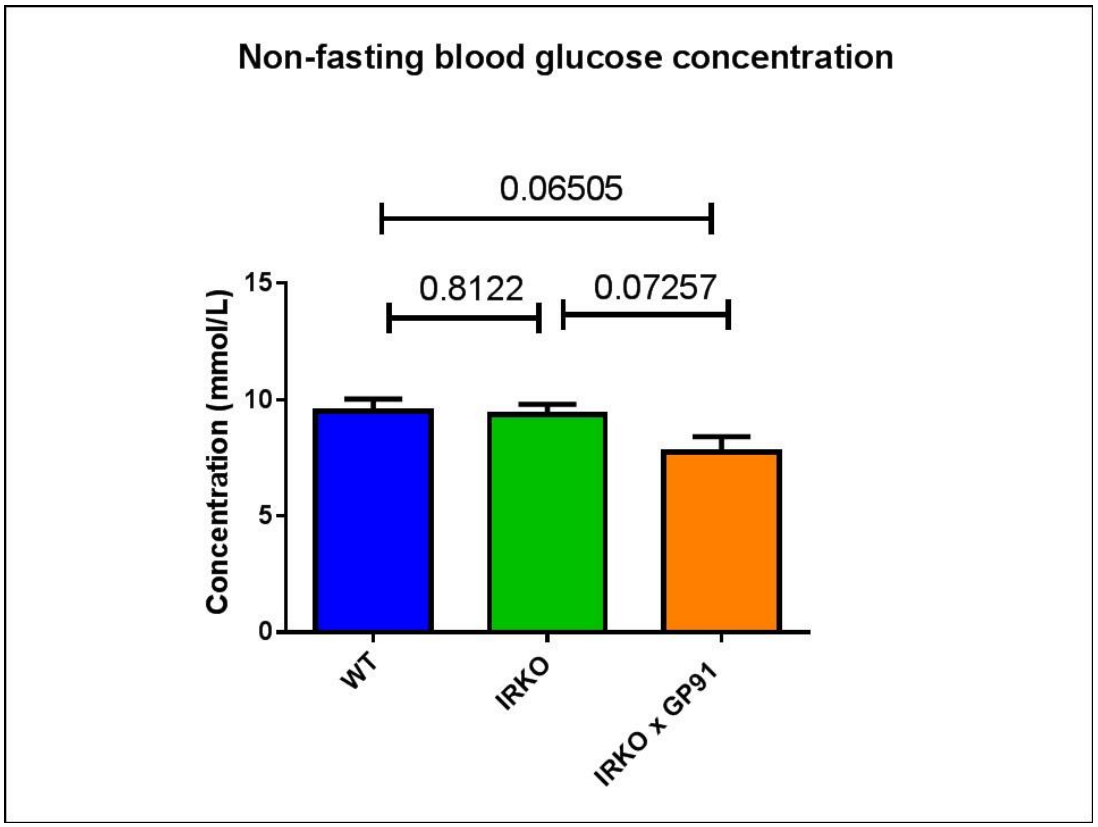

Figure 22 Non-fasting blood glucose concentration

(N=6, 6, 4)

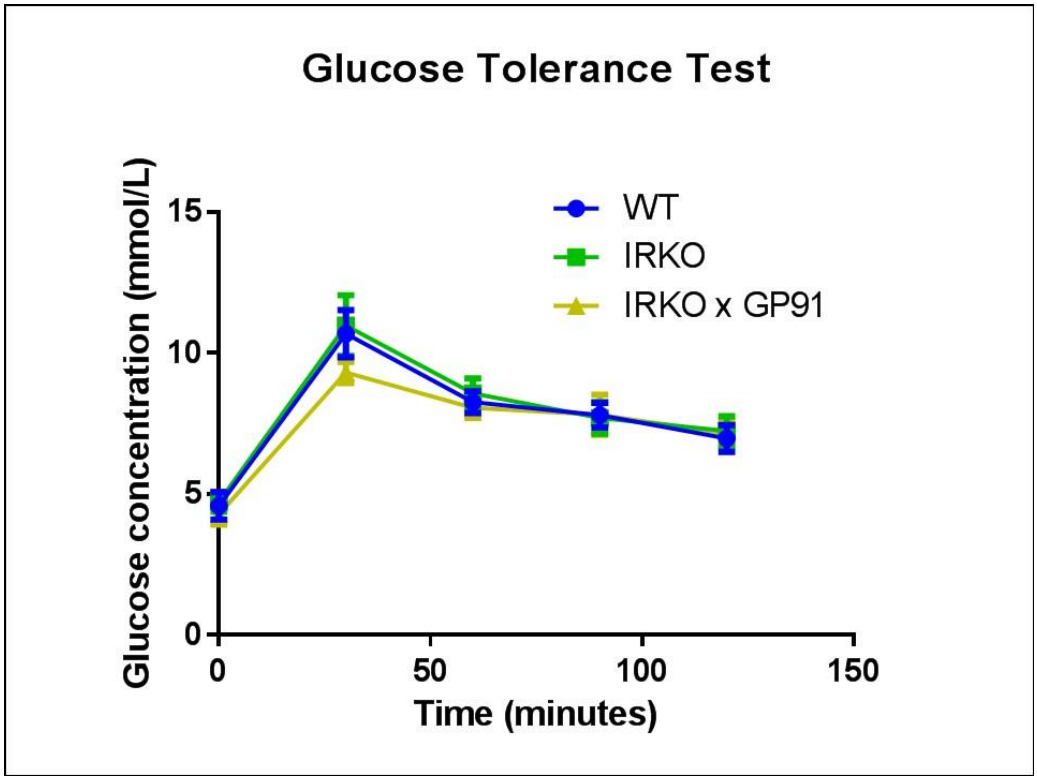

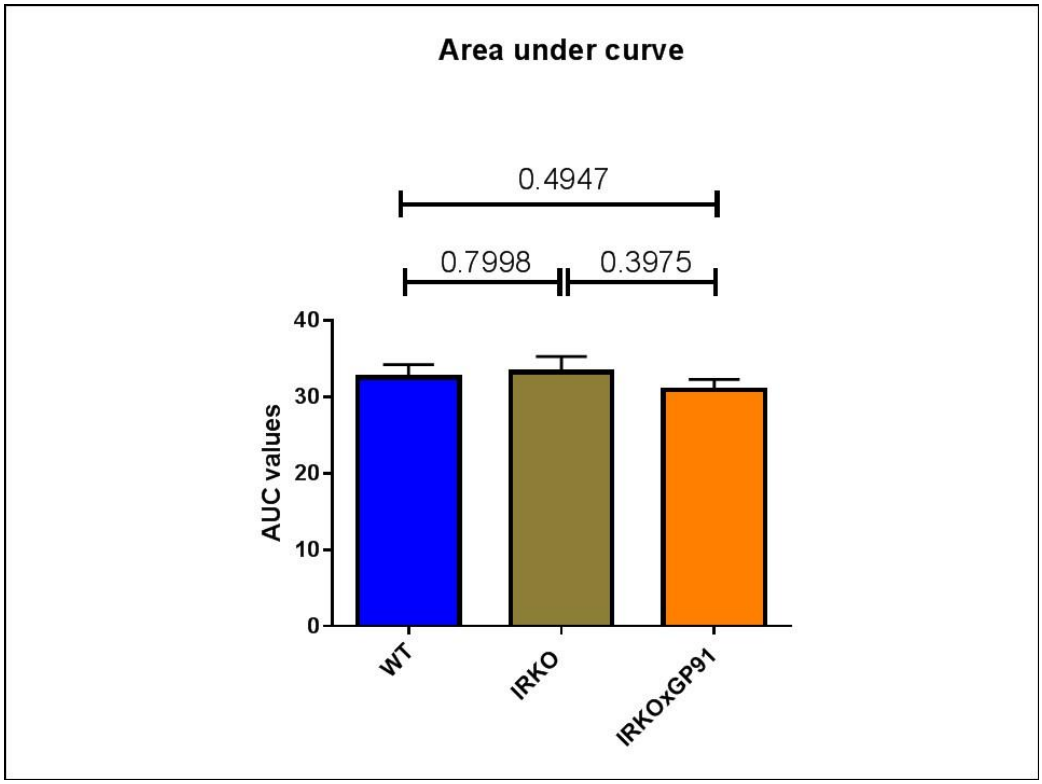

Figure 23 Glucose tolerance testing

Upper panel: Blood glucose concentration following IP glucose injection. Lower panel: Area under curve analysis. (N=7, 6, 5)

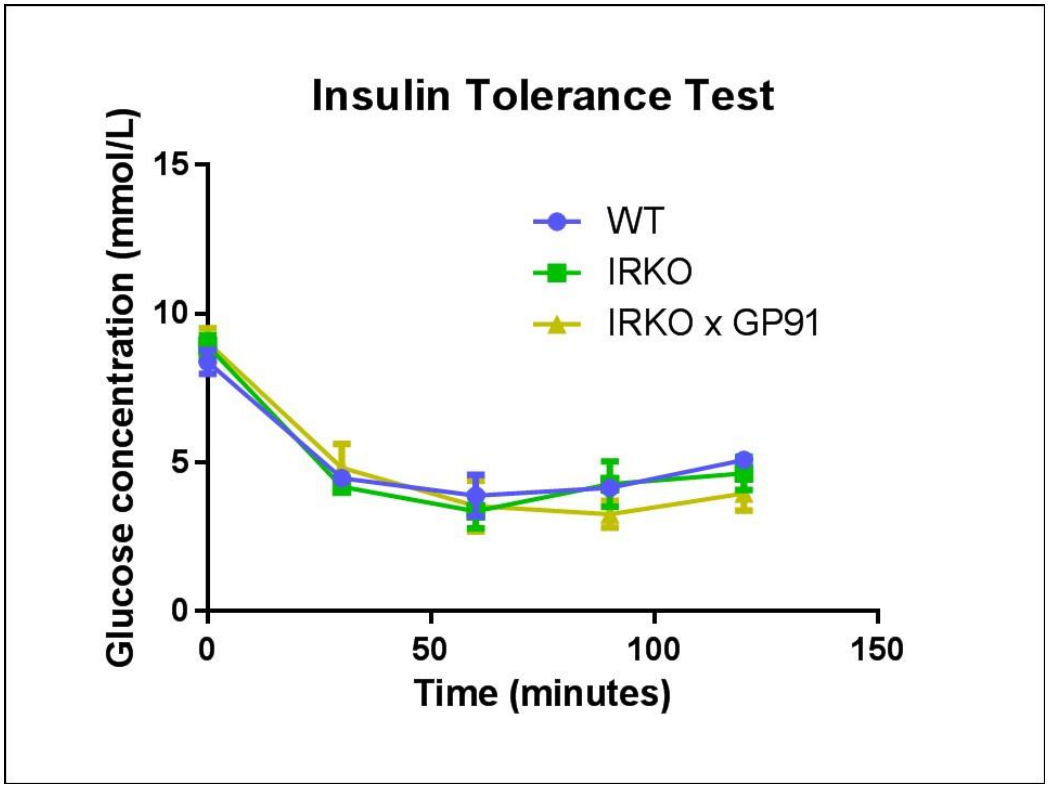

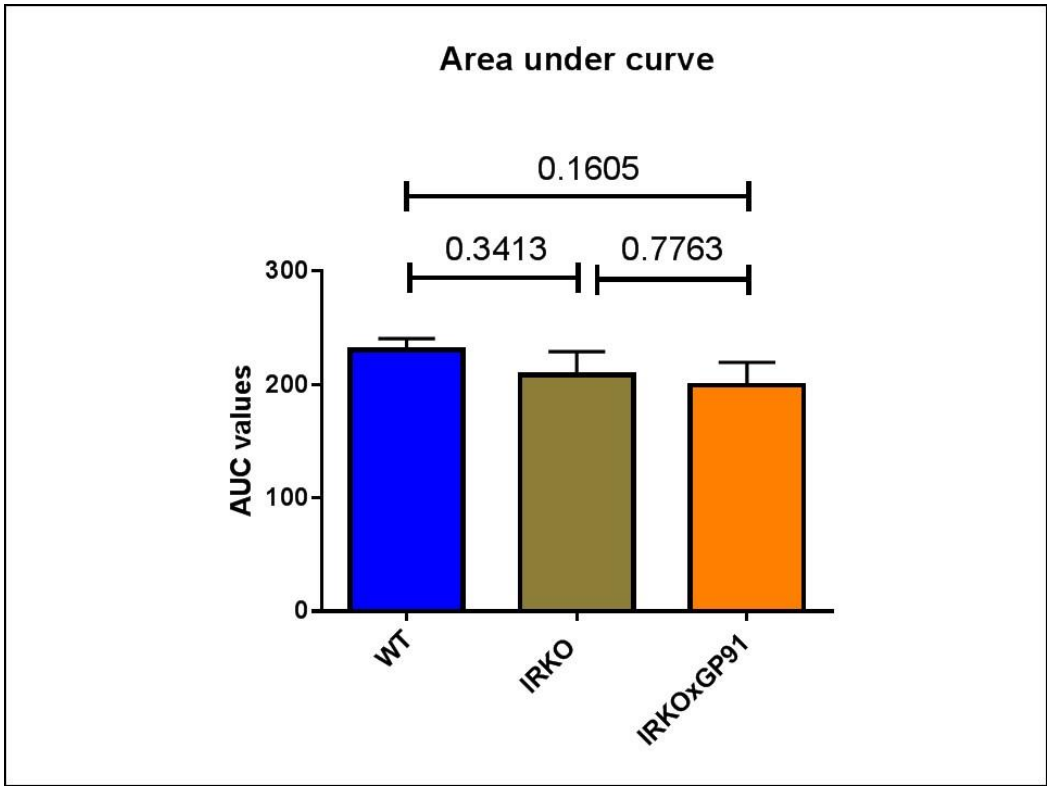

Figure 24 Insulin tolerance testing

Upper panel: Blood glucose concentration following IP insulin injection. Lower panel: Area under curve analysis. (N=7, 6, 4)

5.1.4 Vascular repair

Assessment of vascular repair following endothelial denudation demonstrated no significant difference between WT, IRKO and IRKOxGP91phox$^{y/-}$ mice.

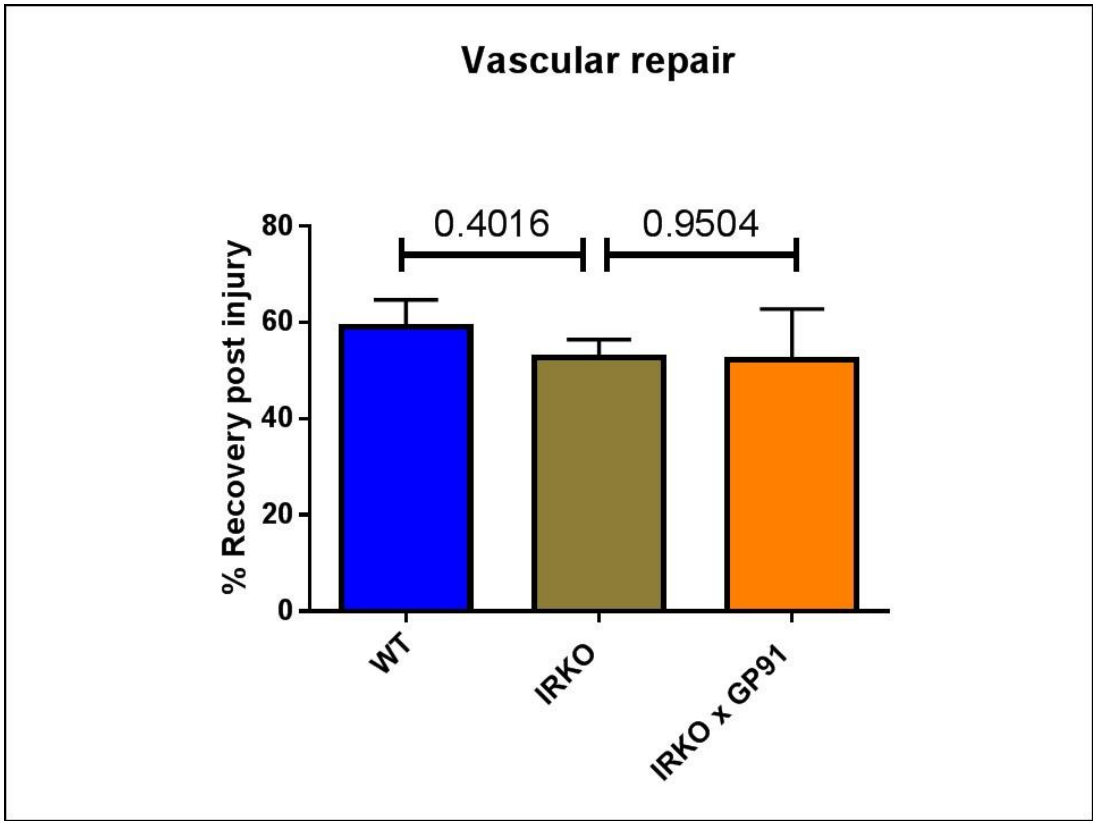

Figure 25 Vascular repair

Endothelial regeneration following vascular injury (N=7, 5, 2)

Experiments assessing vascular repair were halted prematurely after it was noted that IRKOxGP91phox$^{y/-}$ mice were failing to recover optimally post-operatively. Further observation of mice from this colony revealed that the double cross mice were failing to thrive following invasive interventions, and on occasion developing granulomas (discussed in detail in section 6.1.4). In view of these concerns, it was decided to curtail experiments on this colony and focus investigation on the ESMIROxGP91phox$^{y/-}$ colony.

5.2 ESMIROxGP91phox$^{y/-}$

5.2.1 Genotyping

An example PCR gel for identifying mice with the ESMIRO genotype is displayed in figure 26, with a 1000 base pair ladder on the left for reference. For an example of a PCR gel for used to identify the GP91phox genotype, see figure 20.

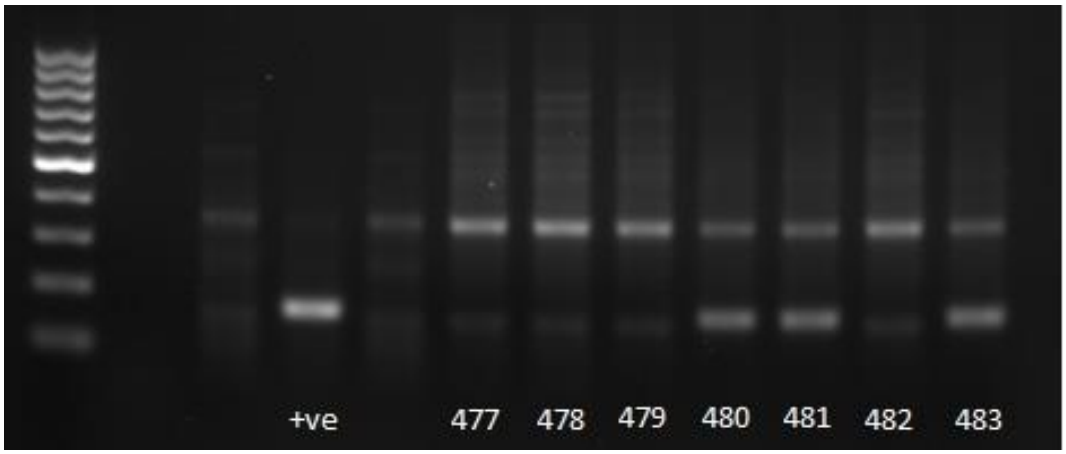

Figure 26 ESMIRO PCR

ESMIRO genotype is denoted by an extra band at 172bp (e.g. 480), whilst WT mice display only one band at approximately 350bp (e.g. 482).

5.2.2 Body weights

No significant differences in bodyweight were identified between mice of WT, ESMIRO or ESMIROxGP91phox$^{y/-}$ genotypes (see figure 27).

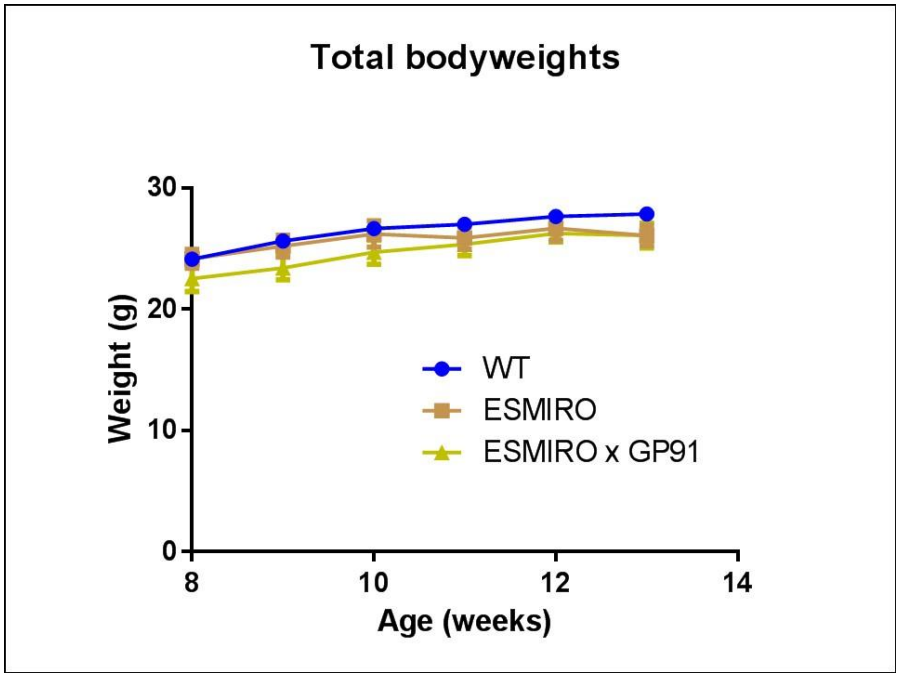

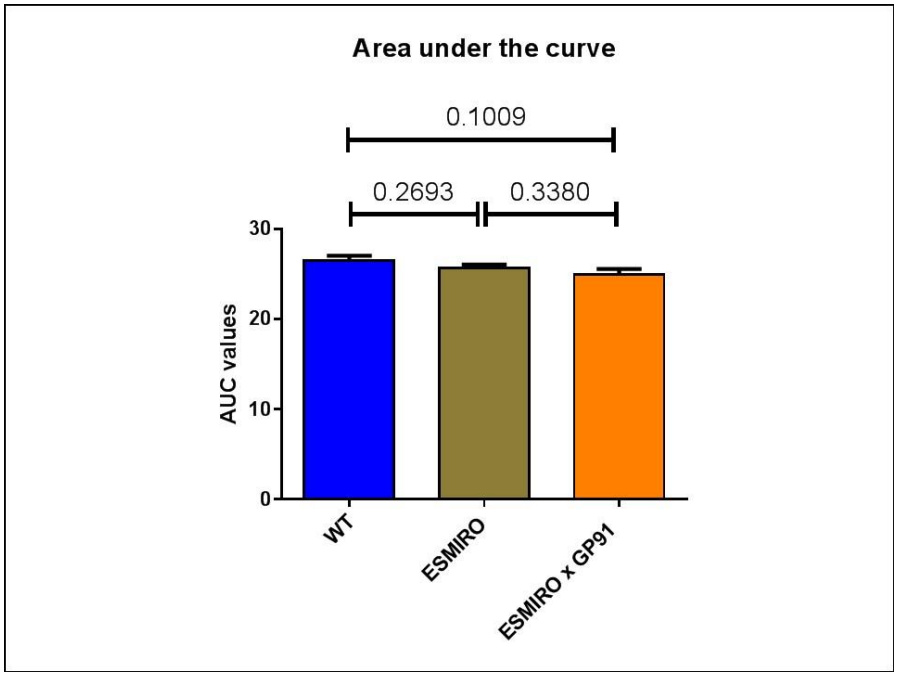

Figure 27 Total body weight

Upper panel: Body weight at between weaning & adulthood; Lower panel: Area under curve analysis (N=4, 4, 4)

5.2.3 Glucocompetence testing

Previously published data demonstrate that there are no significant differences in glucocompetence between WT and ESMIRO mice [56], nor between ESMIRO and ESMIROxGP91phox$^{y/-}$ littermates [123]. The current study recapitulated these findings, with no significant differences seen in non-fasting blood glucose (figure 28), glucose tolerance testing (figure 29), insulin tolerance testing (figure 30), or plasma insulin concentration (figure 31).

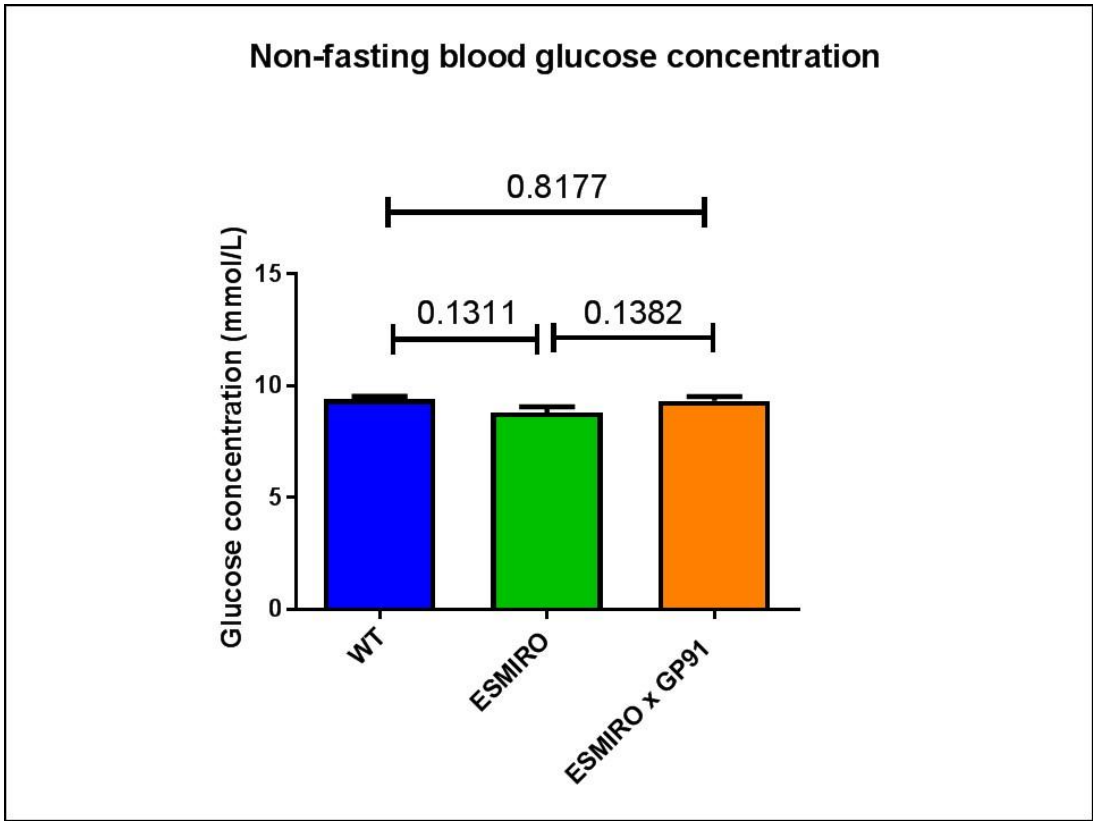

Figure 28 Non-fasting glucose concentration

(N=4, 7, 7)

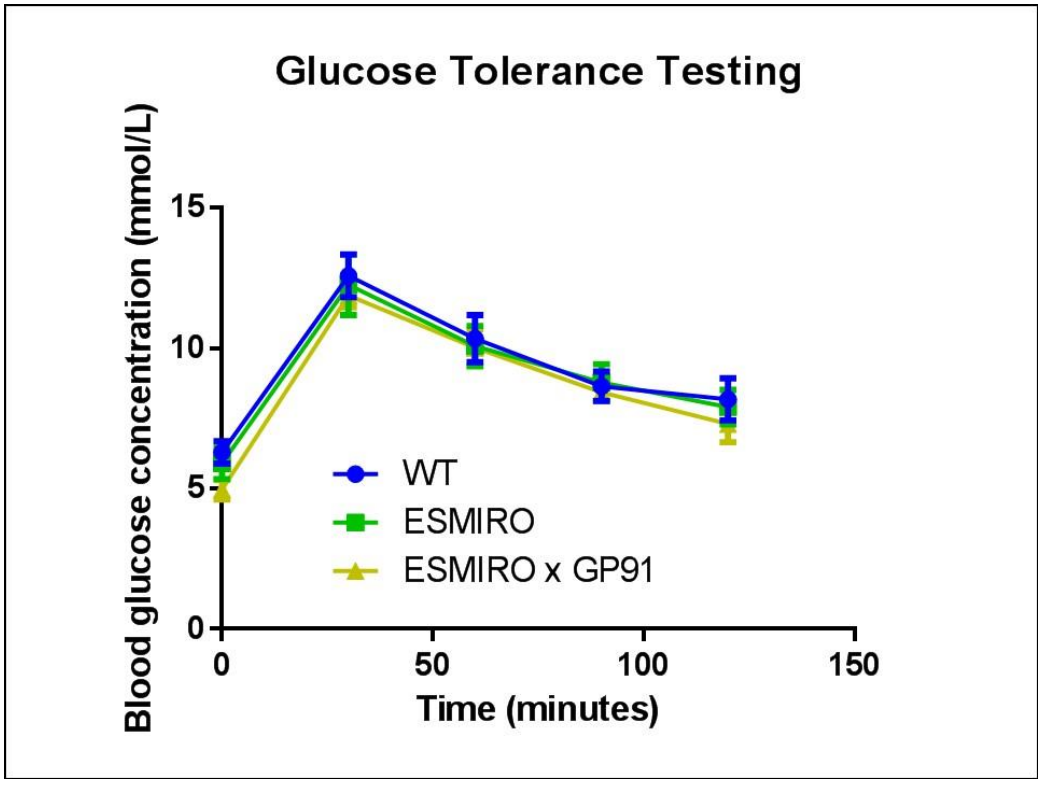

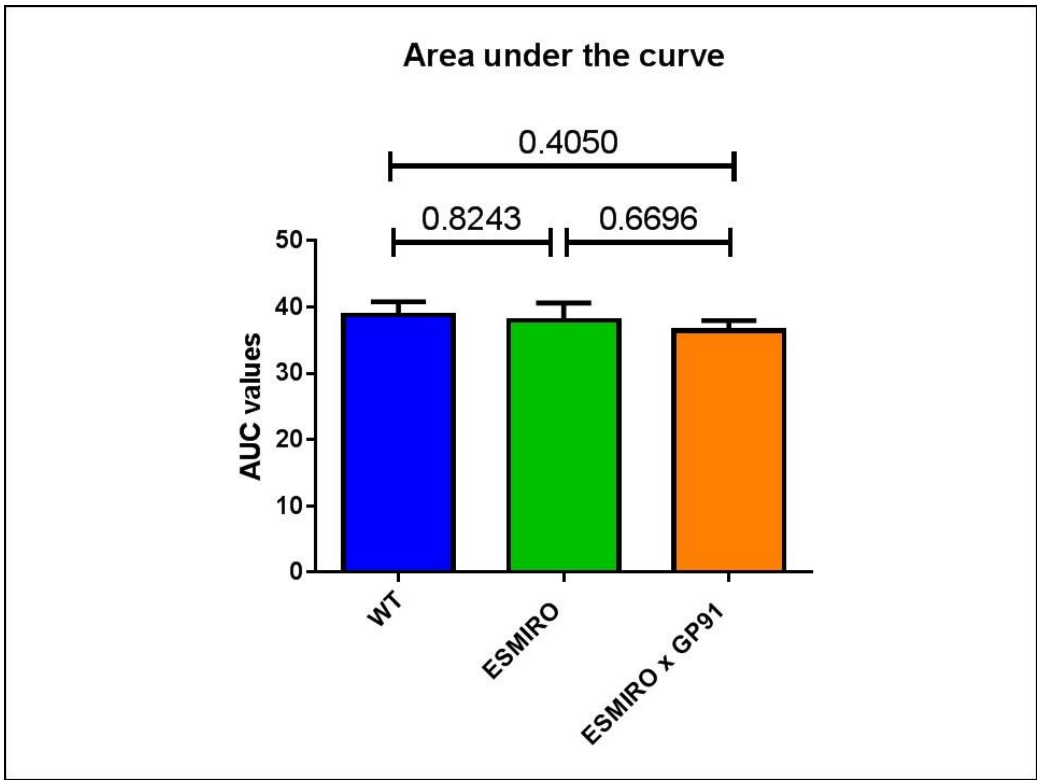

Figure 29 Glucose tolerance testing

Upper panel: Blood glucose concentration following IP glucose injection. Lower panel: Area under curve analysis. (N=5, 6, 4)

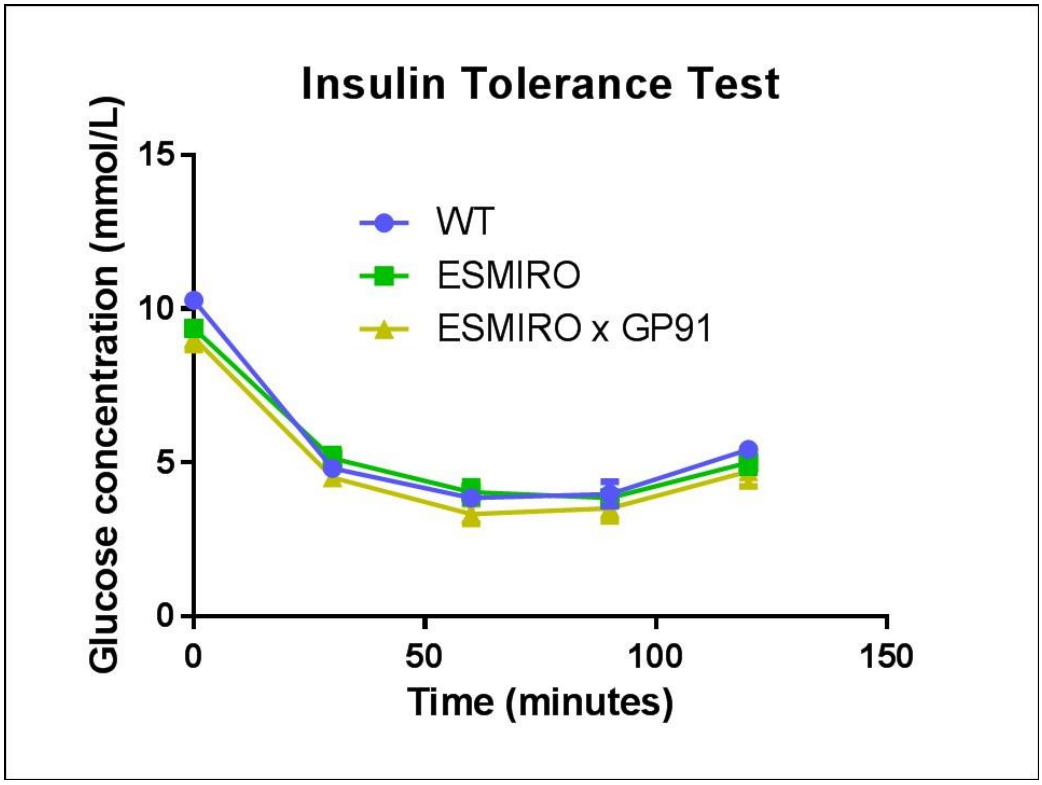

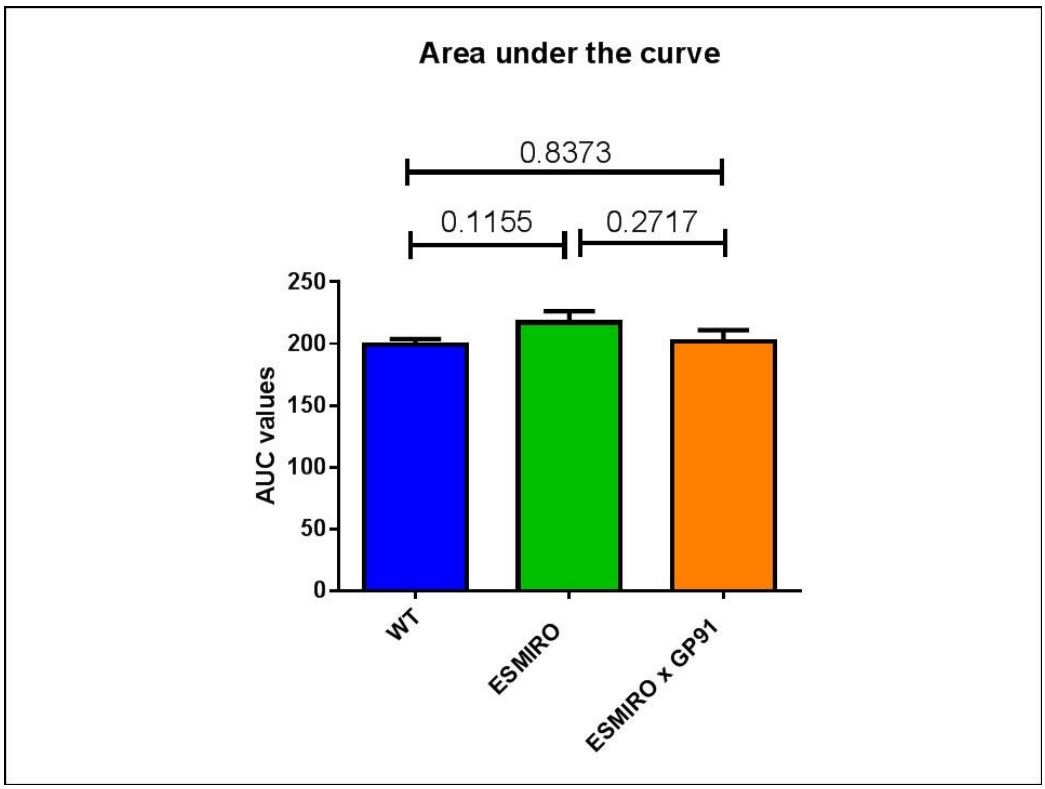

Figure 30 Insulin tolerance testing

Upper panel: Blood glucose concentration following IP insulin injection. Lower panel: Area under curve analysis. (N=6, 6, 6)

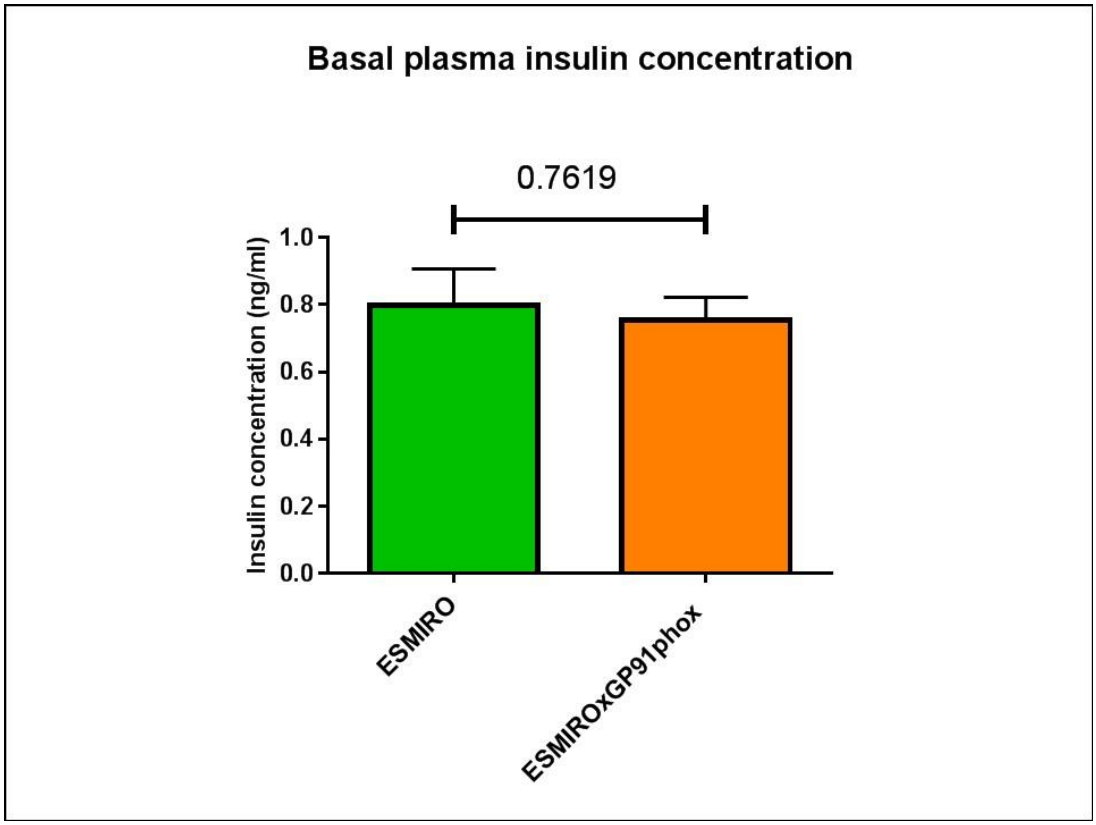

Figure 31 Fasting plasma insulin concentration

(N=9, 7)

5.2.4 Real-time quantitative PCR

Real-time quantitative PCR (RT-qPCR) was performed on aortic and lung tissue in order to validate the expression of human insulin receptor (hIR) in ESMIRO and ESMIROxGP91phox$^{y/-}$ mice, as well as to confirm successful knockdown of NOX2 in ESMIROxGP91phox$^{y/-}$ mice. No manipulation to the native murine insulin receptor (mIR) was carried out, and expression was checked to ensure that there were no significant variations between genotypes. In view of previously published work suggesting that NOX2 knockdown results in alterations in expression of pro-inflammatory cytokines (see section 1.8), further RT-qPCR analyses were carried out to ascertain the expression of IL-1β, VCAM1 and TNFα.

5.2.4.1 Validation of the genetic model

As figure 32 illustrates, hIR was demonstrable in aortic and lung tissue from ESMIRO and ESMIROxGP91phox$^{y/-}$ mice with no significant difference in expression, whilst being undetectable in WT littermates.

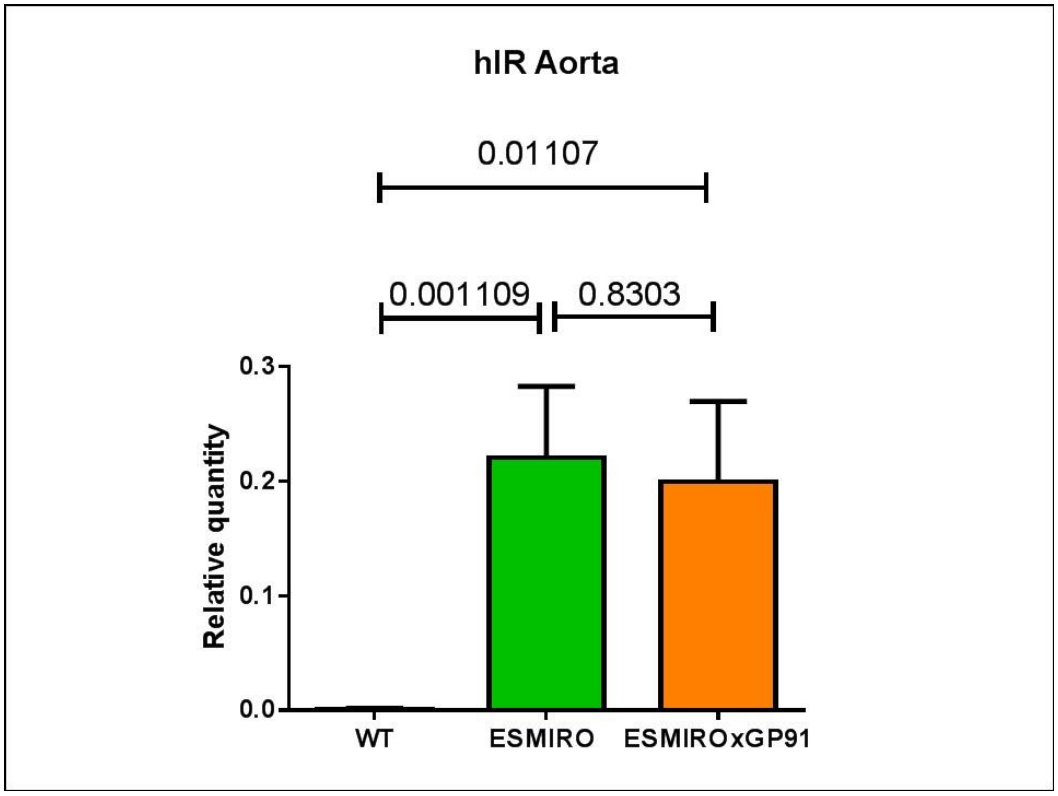

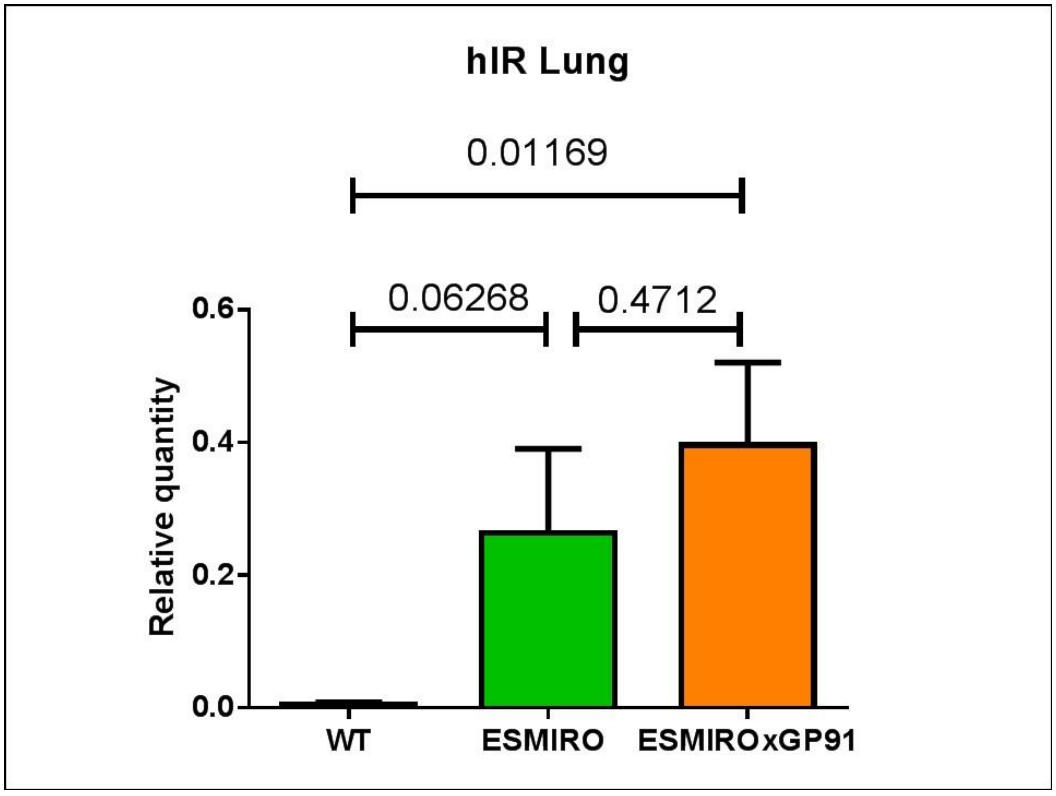

Figure 32 Expression of human insulin receptor (hIR)

Quantified as a ratio relative to β actin expression. Top panel: hIR expression in aortic tissue (N= 10, 8, 10); bottom panel: hIR expression in lung tissue (N=7, 7, 8).

The absence of detectable NOX2 mRNA from aortic or lung tissue in ESMIROxGP91phox$^{y/-}$ mice confirmed successful enzymatic knockdown (see figure 33). No significant difference was seen between WT and ESMIRO littermates with respect to NOX2 expression.

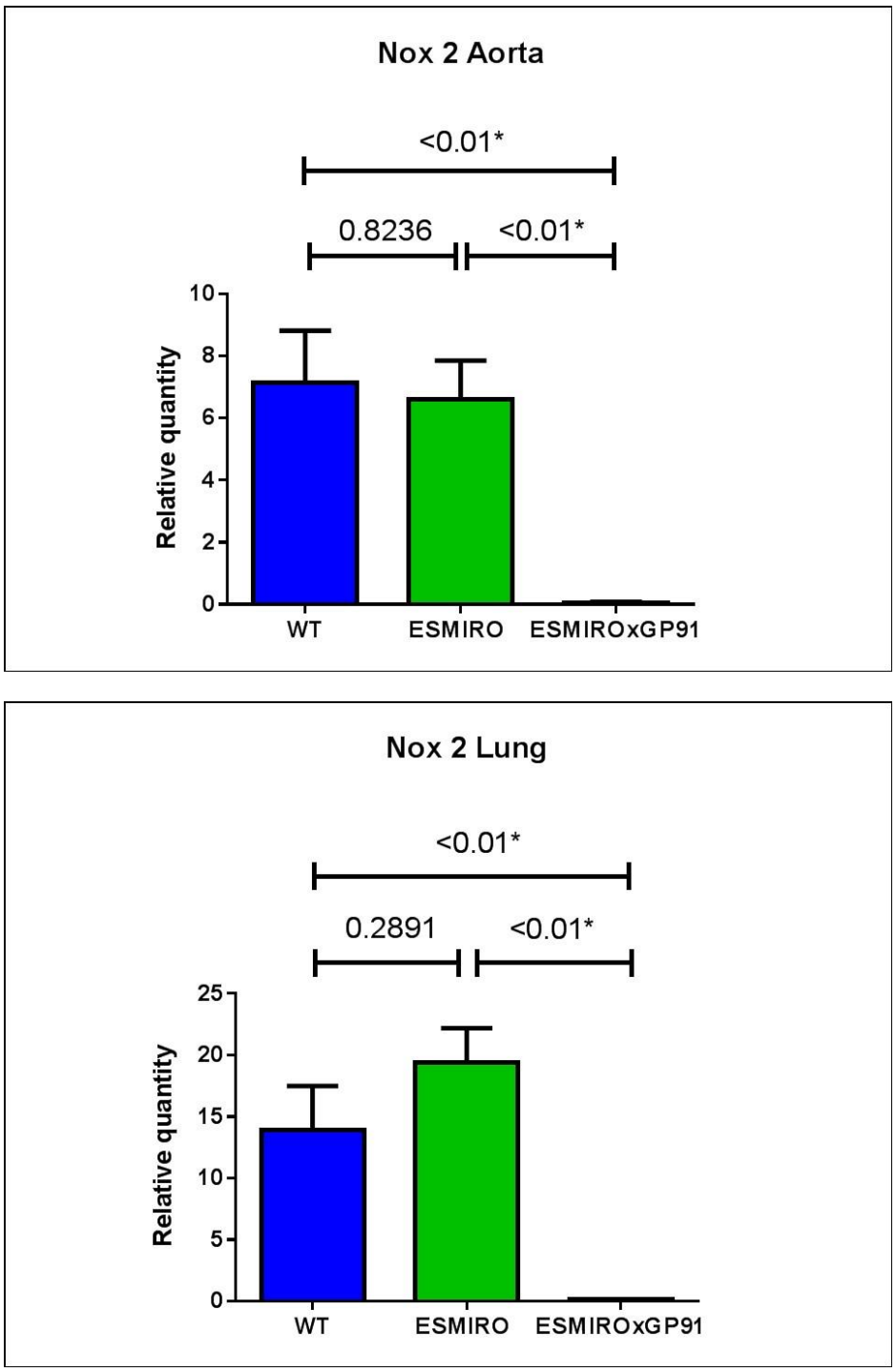

Figure 33 Expression of NOX2

Quantified as a ratio relative to β actin expression. Top panel: NOX2 expression in aortic tissue (N= 11, 7, 9); bottom panel: NOX2 expression in lung tissue (N=7, 5, 8).

No significant differences were seen with respect to aortic expression of mIR in the three genotypes of mice, as shown in figure 34.

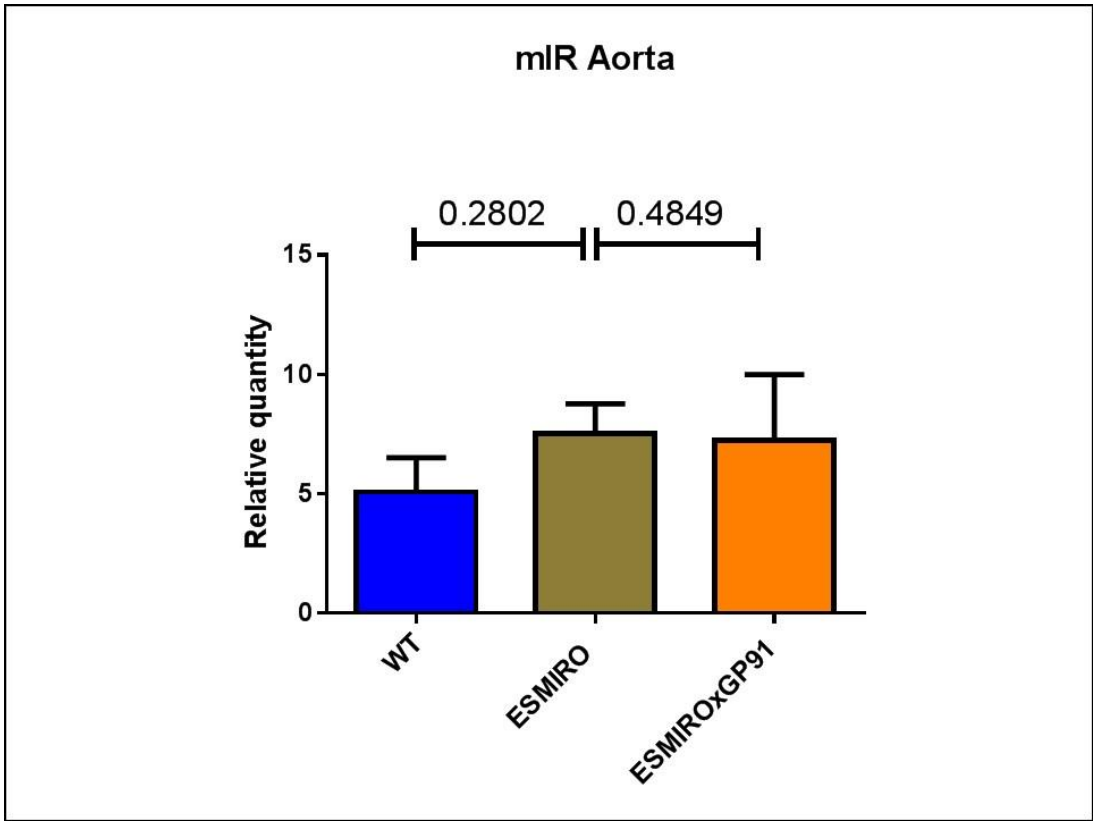

Figure 34 Expression of murine insulin receptor (mIR) in aortic tissue

Quantified as a ratio relative to β actin expression (N= 4, 3, 3).

5.4.2.2 Assessing expression of pro-inflammatory cytokines

A trend toward increased IL-1β expression in double cross mice when compared to WT and ESMIRO counterparts was demonstrated (0.0251 [0.0137] vs. 0.0164 [0.0102] vs. 0.0155 [0.0075]), although this did not reach statistical significance (p=0.17 and 0.10 respectively; see figure 35).

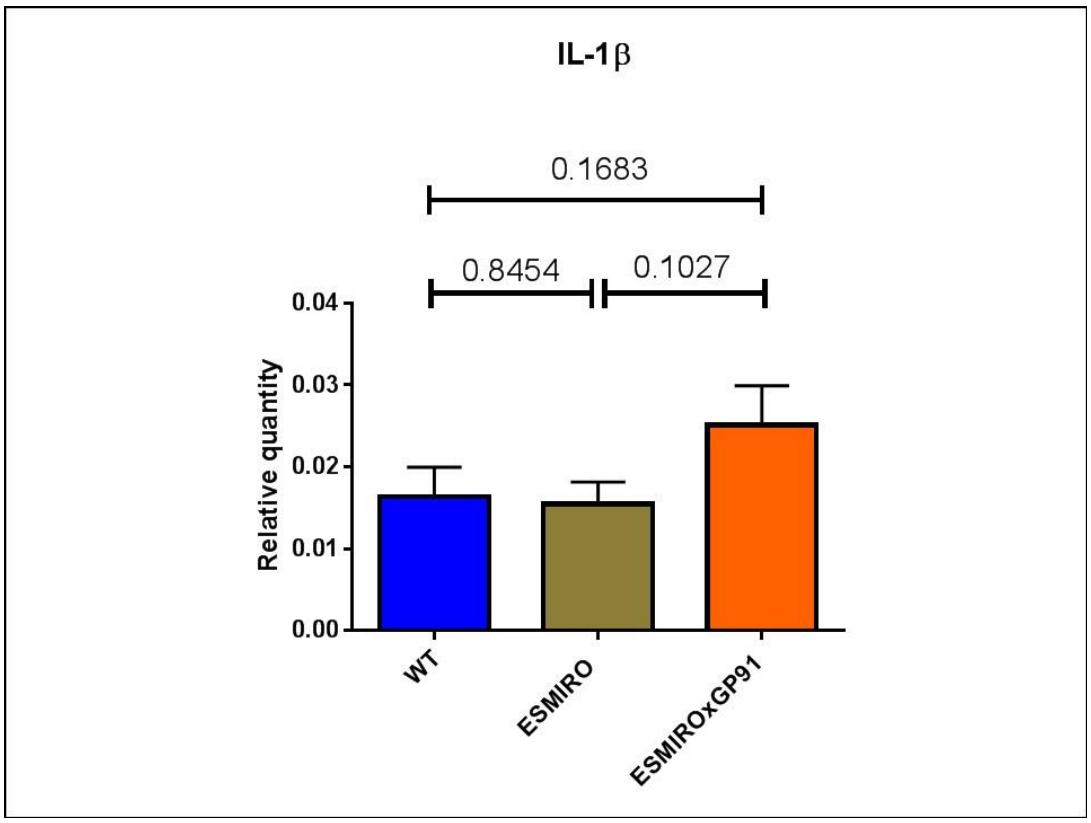

Figure 35 Expression of interleukin 1β (IL-1β) in aortic tissue

Quantified as a ratio relative to β actin expression (N= 8).

No significant differences were demonstrated with regard to expression of TNF-α between the three genotypes of mice (figure 36).

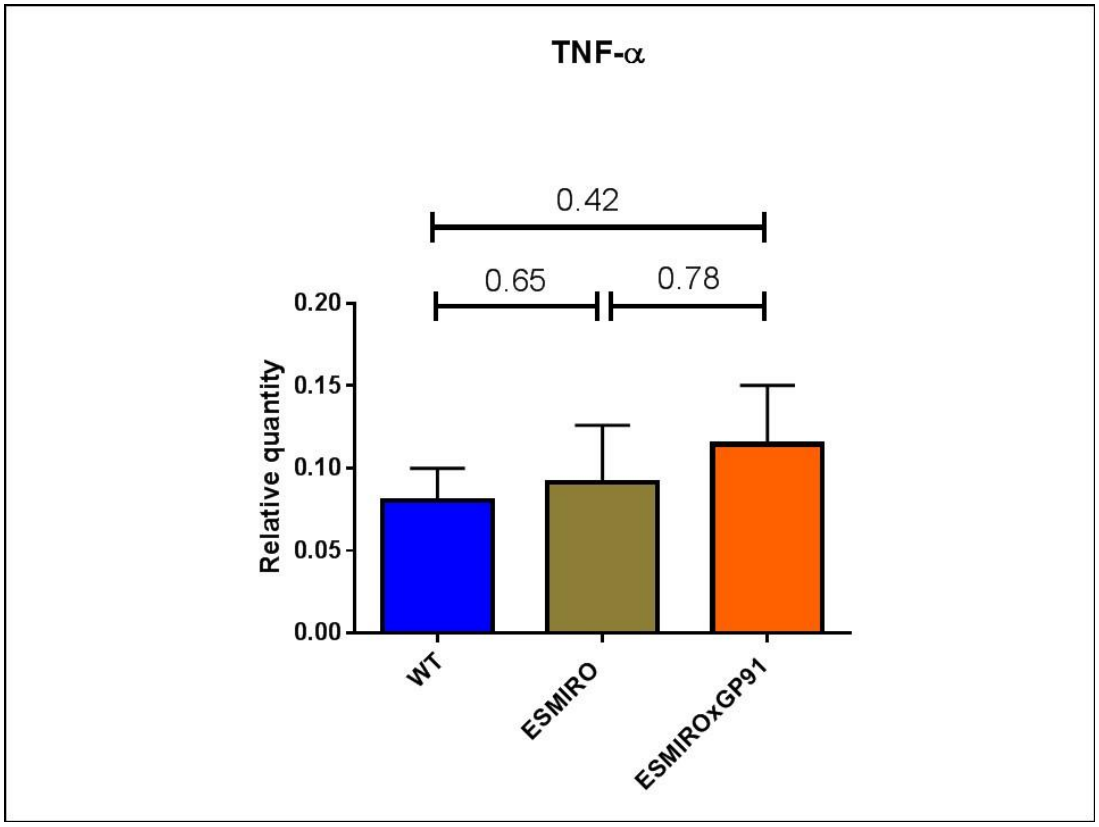

Figure 36 Expression of tumour necrosis factor α (TNF-α) in aortic tissue

Quantified as a ratio relative to β actin expression (N= 8).

Similarly, no significant differences were demonstrated with regard to expression of VCAM1 between the 3 genotypes, although a trend towards reduced expression in ESMIRO mice was noted (figure 37).

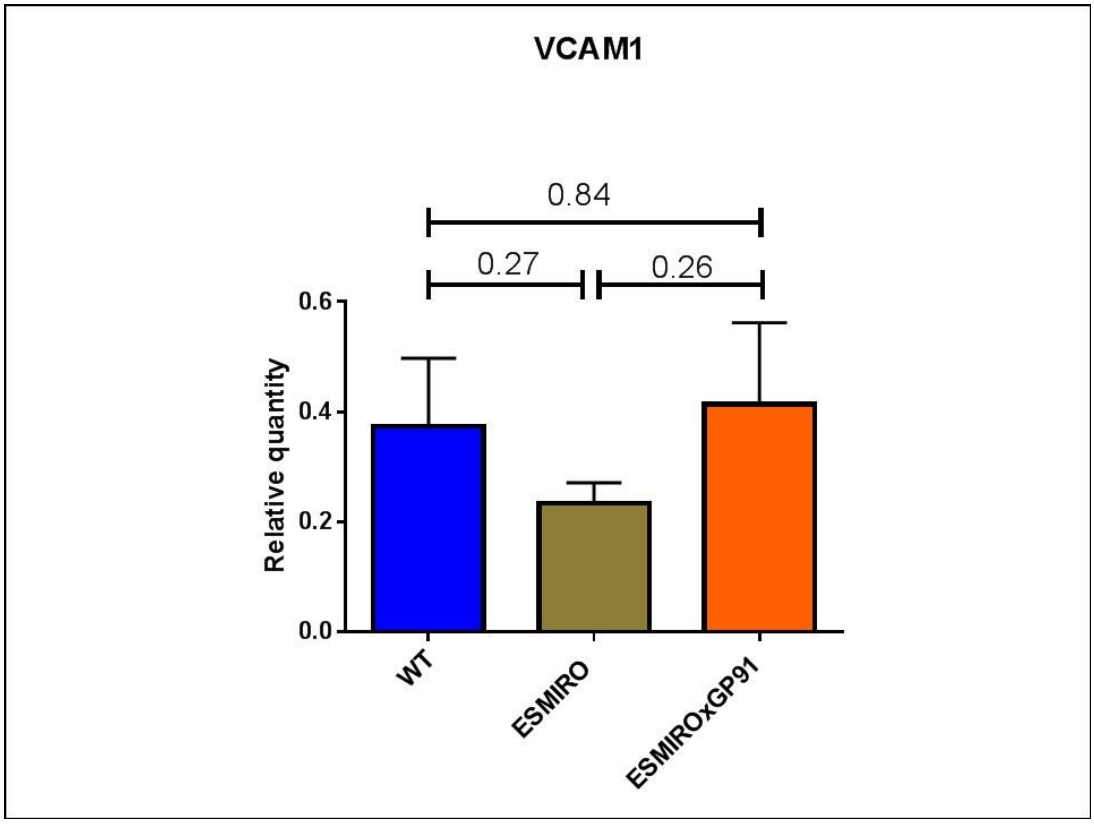

Figure 37 Expression of vascular cell adhesion molecule 1 (VCAM1) in aortic tissue

Quantified as a ratio relative to β actin expression (N= 8, 8, 7).

5.2.4.3 Preliminary data assessing expression of NOX4

In view of the findings regarding the effect of NOX2 knockdown on endothelial cell migration (see section 5.2.10.2), preliminary work was undertaken in order to ascertain the effect the of NOX2 knockdown on the expression of NOX4. As illustrated in figure 38, no significant difference was seen in NOX4 expression when comparing aortic samples from ESMIRO and ESMIROxGP91phox mice (0.328 [0.09] vs. 0.243 [0.06]; p=0.45). It must be borne in mind that, given the preliminary nature of these data, the sample sizes are small and thus these results are not conclusive. Potential avenues for further investigation into the concept of compensatory NOX4 expression following NOX2 knockdown are discussed in section 6.3.4.

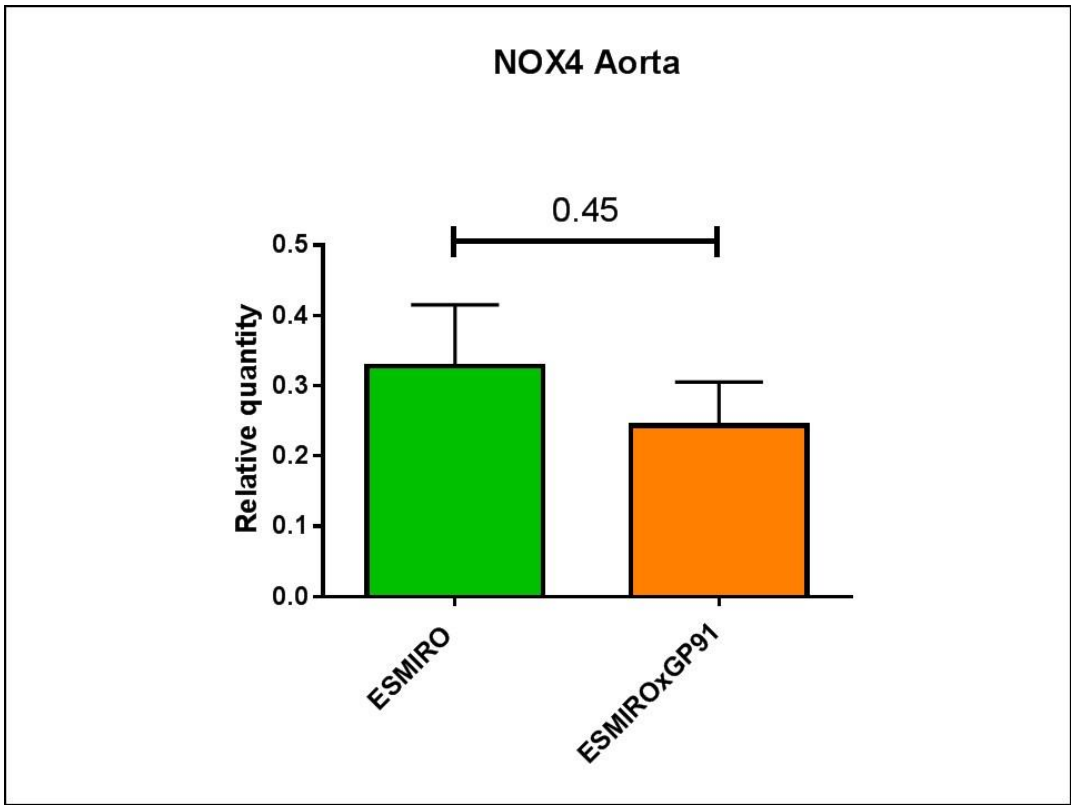

Figure 38 Expression of NOX4 in aortic tissue

Quantified as a ratio relative to β actin expression (N= 3, 4).

5.2.5 Vascular repair

As outlined in section 4.5, two sets of vascular injury experiments were carried out in order to investigate the effects of NOX2 inhibition in the context of insulin resistance; firstly, double-cross transgenic mice were compared to ESMIRO and WT littermates in order to assess the effect of genetic NOX2 knockdown. Subsequently, the effect of pharmacological NOX2 inhibition was investigated via implantation micro-osmotic pumps containing either GP91-ds tat or scrambled peptide into ESMIRO mice.

Investigating the effect of genetic NOX2 knockdown

Assessment of vascular repair following endothelial denudation demonstrated that ESMIROxGP91phox$^{y/-}$ mice display significantly improved recovery compared to ESMIRO littermates (62% [4%] vs. 46% [3%]; p<0.01. See figure 39). Surprisingly, the WT mice from this colony displayed poorer recovery than expected based on historical comparisons or when compared to WT mice from the IRKOxGP91phox colony (43% [4%]).

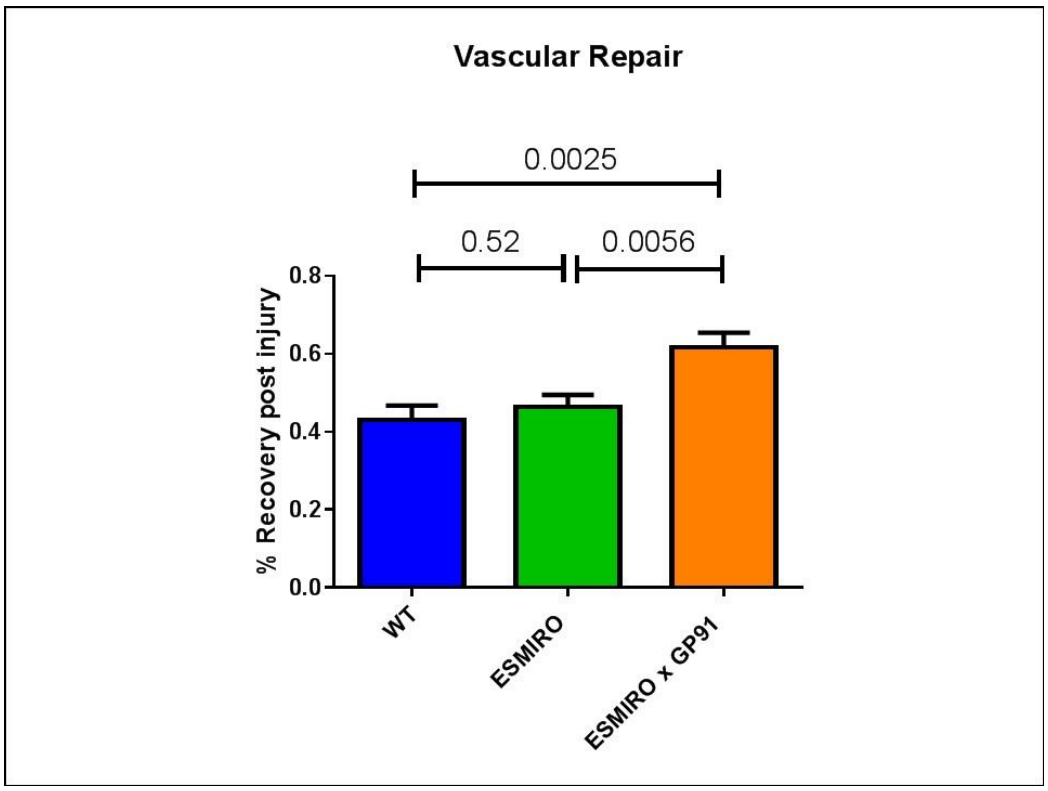

Figure 39 Vascular repair

Endothelial regeneration following vascular injury (N=13, 9, 9)

Investigating the effect of pharmacological NOX2 inhibition

Whereas genetic NOX2 inhibition in ESMIRO mice achieved a significant improvement in vascular repair, these findings were not recapitulated with pharmacological inhibition, which was shown to confer no significant improvement when compared to scrambled peptide (55.7 [6.1] vs 52.8 [4.8]; p=0.7. See figure 40).

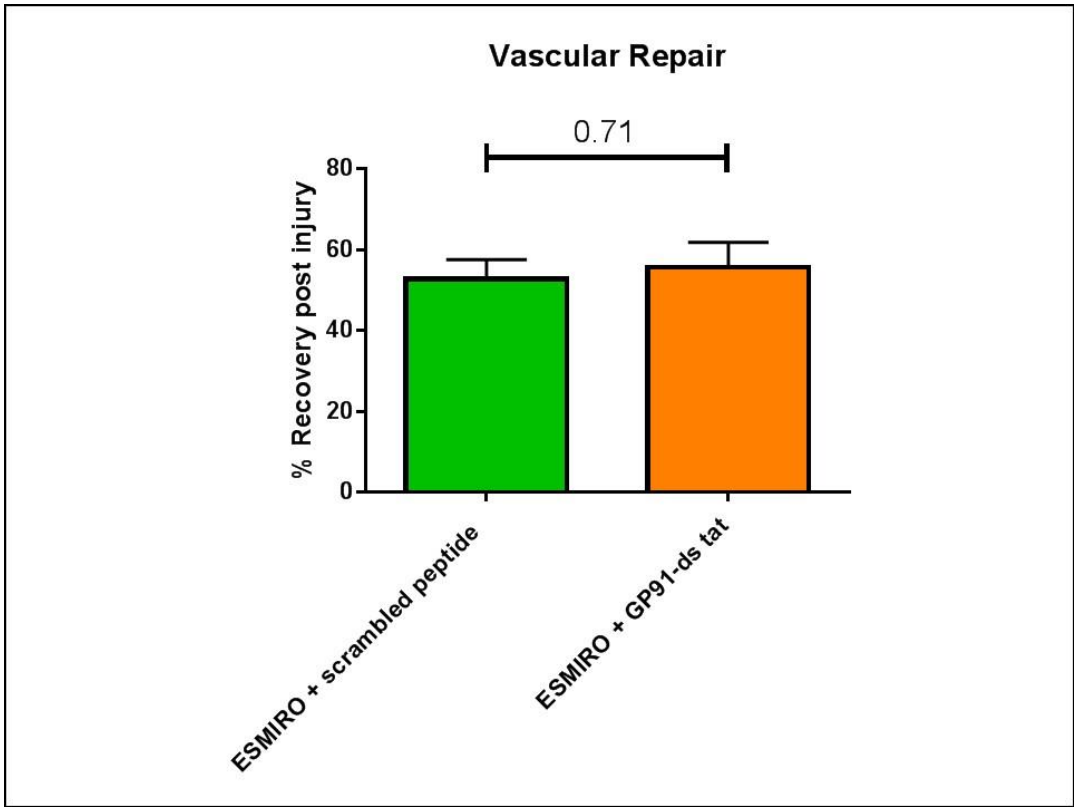

Figure 40 Vascular repair following pharmacological NOX2 inhibition

Endothelial regeneration following vascular injury (N=5).

5.2.6 Ischaemic revascularisation

In order to assess the effect of NOX2 inhibition on ischaemic revascularisation, the protocol of hindlimb ischaemia and laser Doppler imaging outlined in section 4.6 was carried out in WT, ESMIRO and ESMIROxGP91phox mice. Limb perfusion was assessed via Doppler imaging on days 0, 7, 14, 21 and 28. As figure 41 illustrates, no significant differences were seen between the three genotypes at any of these time points, or over the entire 28 day period (AUC analysis: WT 1.52 [0.18] vs. ESMIRO 1.59 [0.17] vs. ESMIROxGP91phox$^{y/-}$ 1.38 [0.12]).

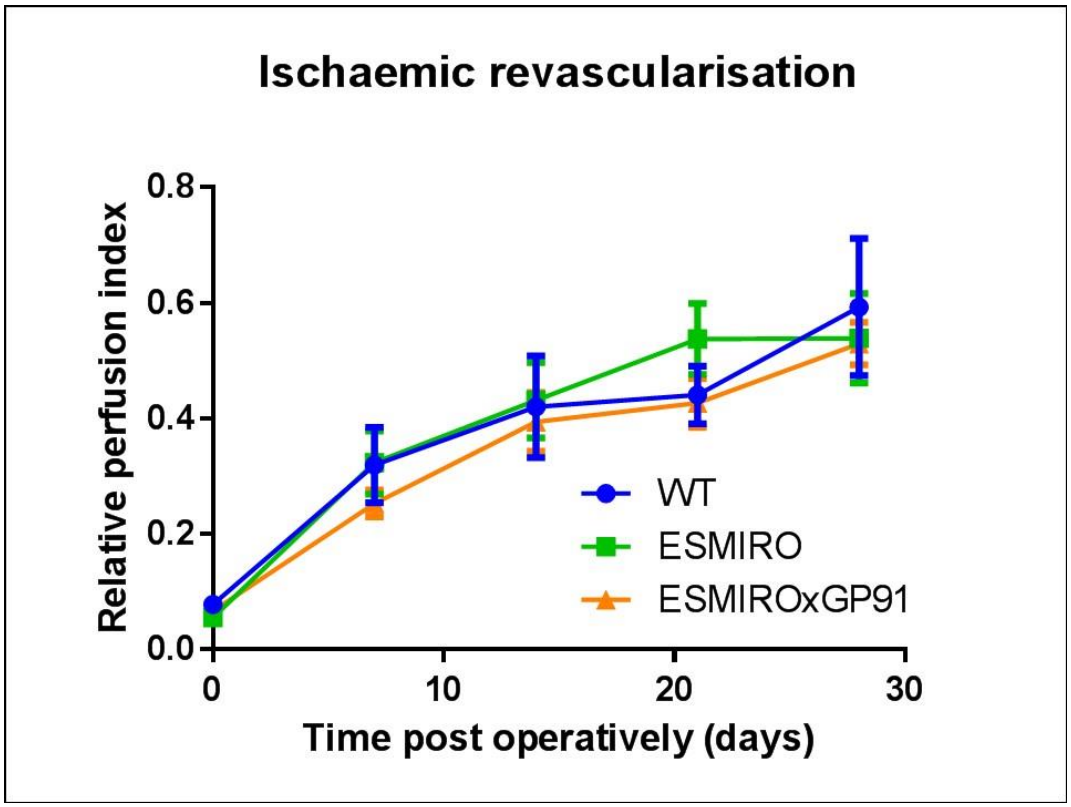

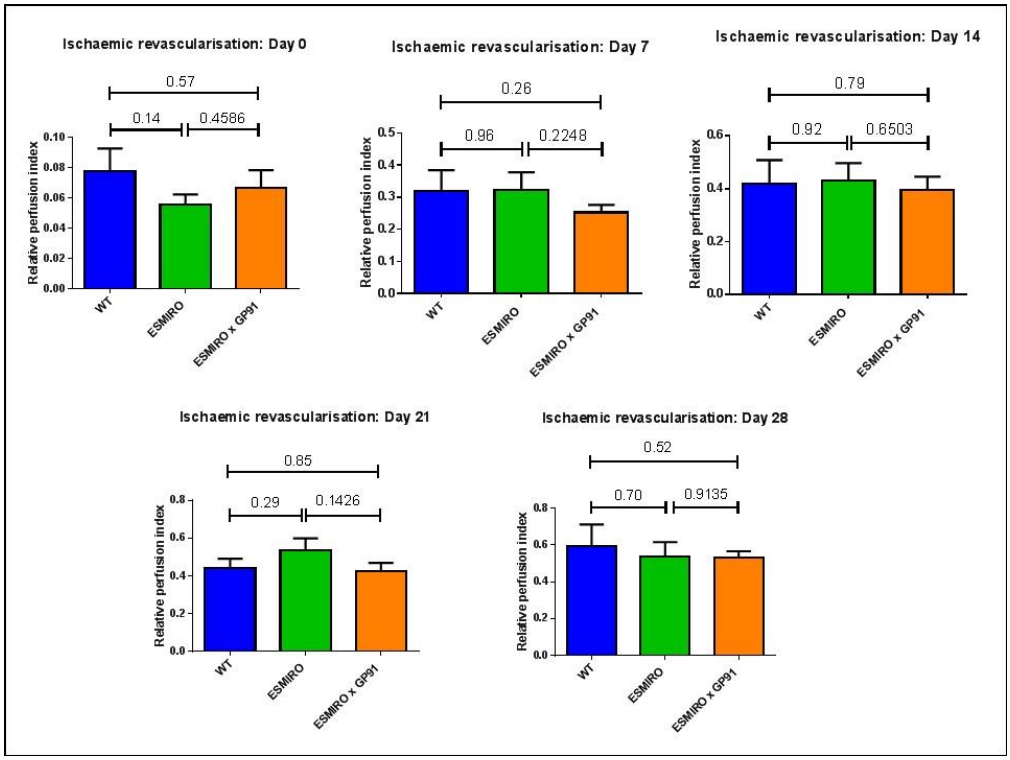

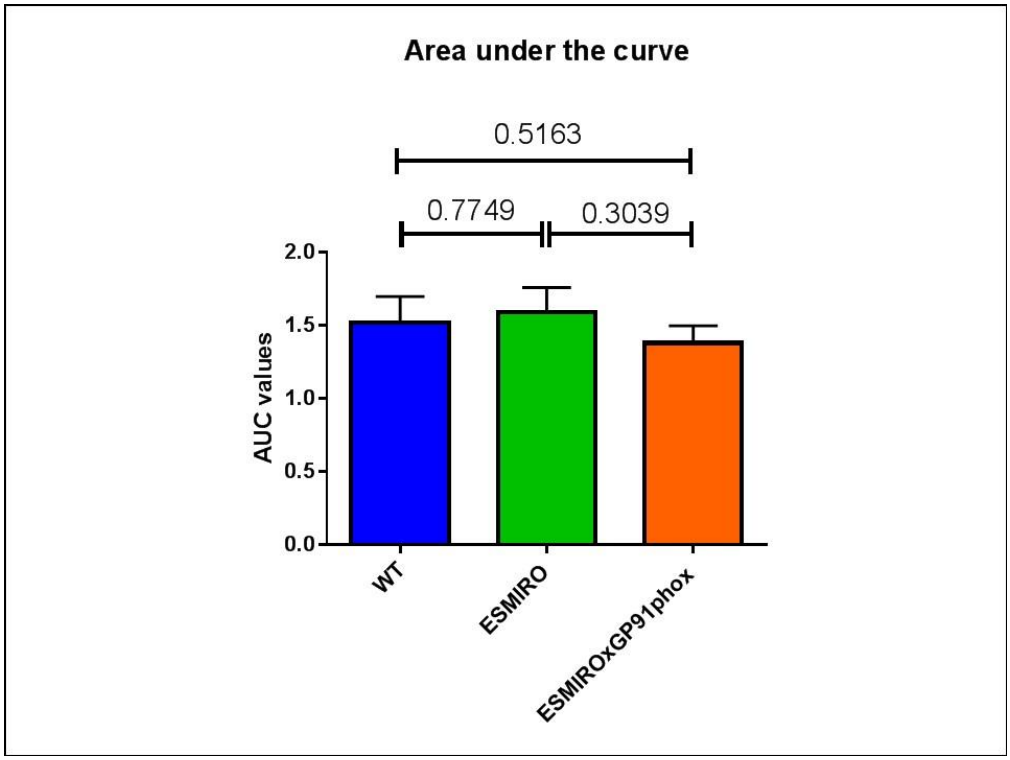

Figure 41 Ischaemic revascularisation

Top panel: Time course of recovery following hindlimb ischaemia. Middle panel: Comparisons of relative perfusion index at each time point. Bottom panel: Area under the curve analysis (N= 6, 10, 12)

5.2.7 Circulating progenitor cell (CPC) enumeration

Having observed a significant difference in vascular repair between ESMIROxGP91phox$^{y/-}$ and ESMIRO mice, the focus of the project shifted to explore the potential mechanisms underpinning this finding. One of the postulated mechanisms for vascular repair is via release of bone marrow derived CPCs, which home to the site of injury and assist with repair either by direct incorporation, or by secreting paracrine factor to stimulate native ECs. To assess whether a differential CPC abundance might contribute to the differences observed in vascular repair, experiments of CPC enumeration using flow cytometry were carried out. For the current study, CPCs were denoted by co-expression of either Stem cell antigen 1 (Sca1) with Foetal liver kinase 1 (Flk1), or cKit with Sca1.

As figure 42 illustrates, a significantly higher number of Sca1/Flk1 expressing CPCs were observed in blood from ESMIROxGP91phox$^{y/-}$ mice compared to ESMIRO littermates (202.6 [20.3] per 100,000 lymphocytes vs. 134.3[10.6]; $p<0.01$). In contrast, there was no significant difference with respect to ckit/Sca1 expressing CPCs (73.1 [9.9] vs. 49.1 [7.5]; $p=0.08$). No significant differences were observed between WT and ESMIRO littermates with respect to either type of CPC.

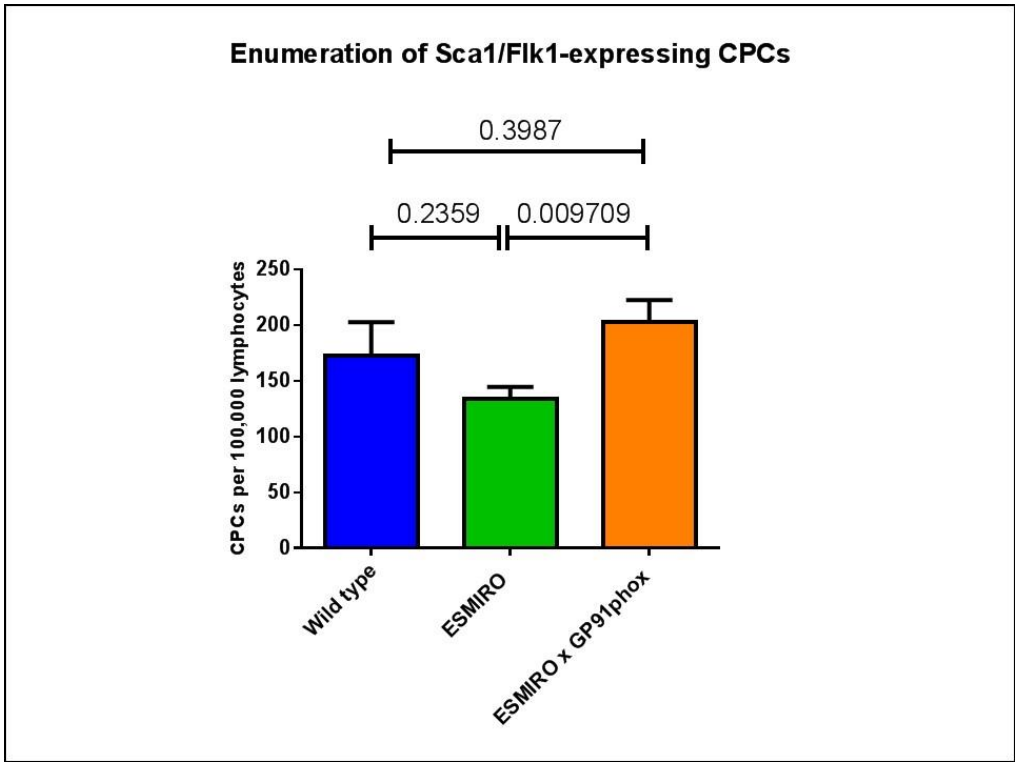

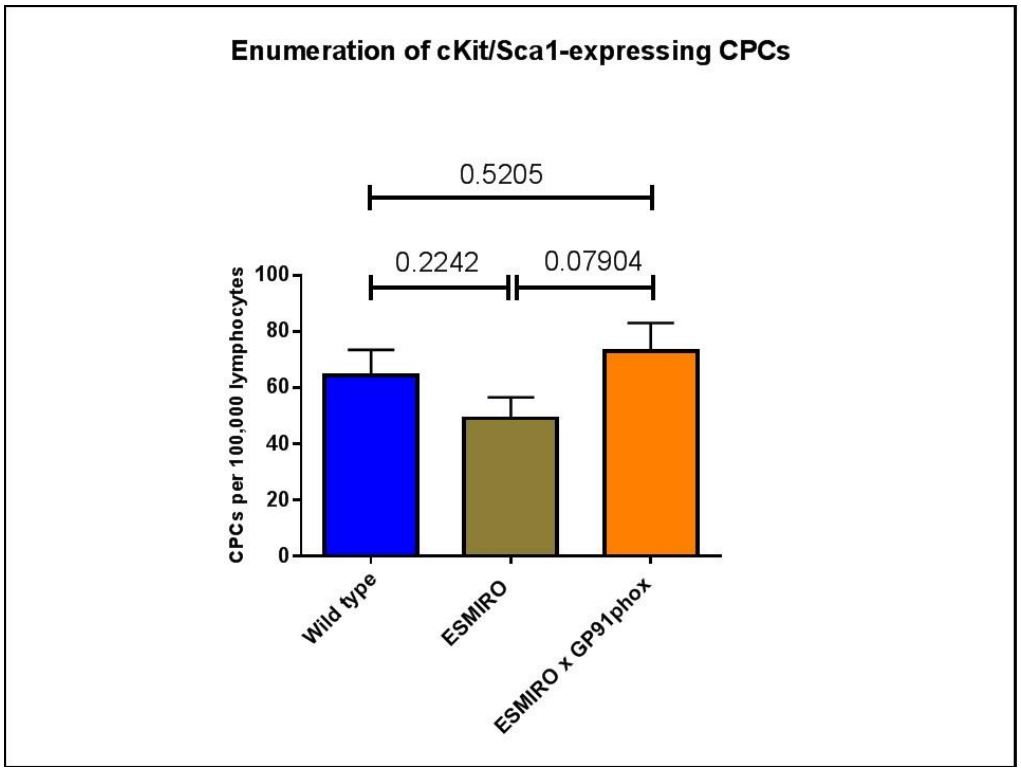

Figure 42 Enumeration of CPCs

Top panel: Enumeration of Sca1/Flk1-expressing CPCs (N= 13, 16, 12); Bottom panel: Enumeration of cKit/Sca1-expressing CPCs (N= 12, 10, 14).

5.2.8 Early outgrowth endothelial progenitor cell (EPC) enumeration

To complement the flow cytometry based method of progenitor cell quantification, early outgrowth endothelial cells (EPCs) were also cultured and quantified from blood, bone marrow and splenic tissue. As outlined in section 4.8.4, EPCs were identified by their ability to import DiI-ac-LDL and bind lectin-FITC.

Blood-derived EPCs

Blood-derived EPCs from transgenic mice were sparse, and no significant difference in their abundance was demonstrated between the two genotypes (ESMIRO 0.2 [0.1] EPCs/high powered field vs. ESMIROxGP91phox$^{y/-}$ 0.04 [0.04] EPCs/HPF). However, a significantly higher number of blood-derived EPCs were observed from WT littermates (2.3 [0.8] EPCs/HPF); $p<0.05$ for both comparisons (see figure 43).

Bone marrow-derived EPCs

Bone marrow-derived EPCs were much more abundant than their blood-derived counterparts, and no significant differences were demonstrated between the three genotypes with regard to number (figure 44).

Spleen-derived EPCs

Of the three tissue sources, splenic tissue produced the highest number of EPCs for all genotypes. Interestingly, ESMIROxGP91phox mice demonstrated a significantly higher number of spleen-derived EPCs than WT littermates (85.7 [13.6] vs. 41.8 [6.6]; $p=0.02$), and a trend toward a higher number than ESMIRO littermates (85.7 [13.6] vs. 58.4 [6.9]; $p=0.09$. See figure 45).

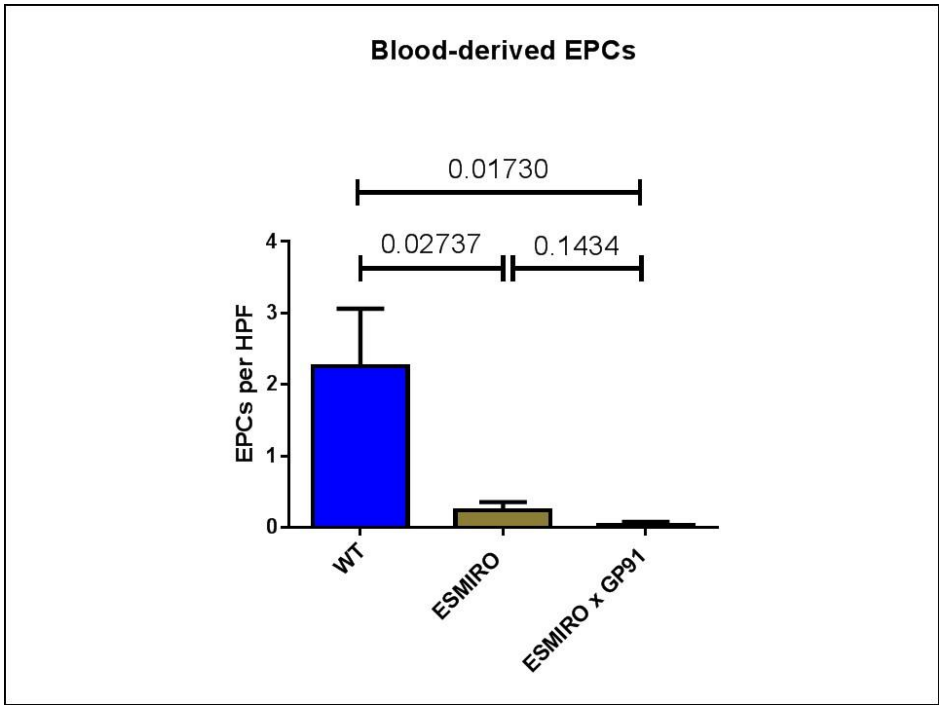

Figure 43 Quantification of blood-derived EPCs

HPF=High powered field; (N= 4, 5, 5)

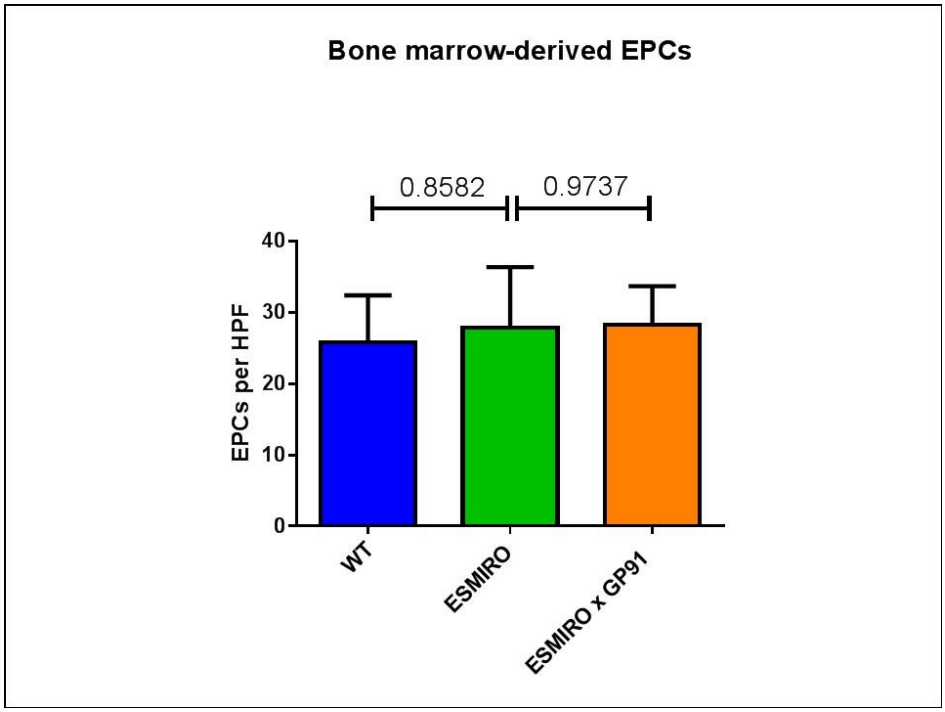

Figure 44 Quantification of bone marrow-derived EPCs

HPF=High powered field; (N= 5, 7, 6)

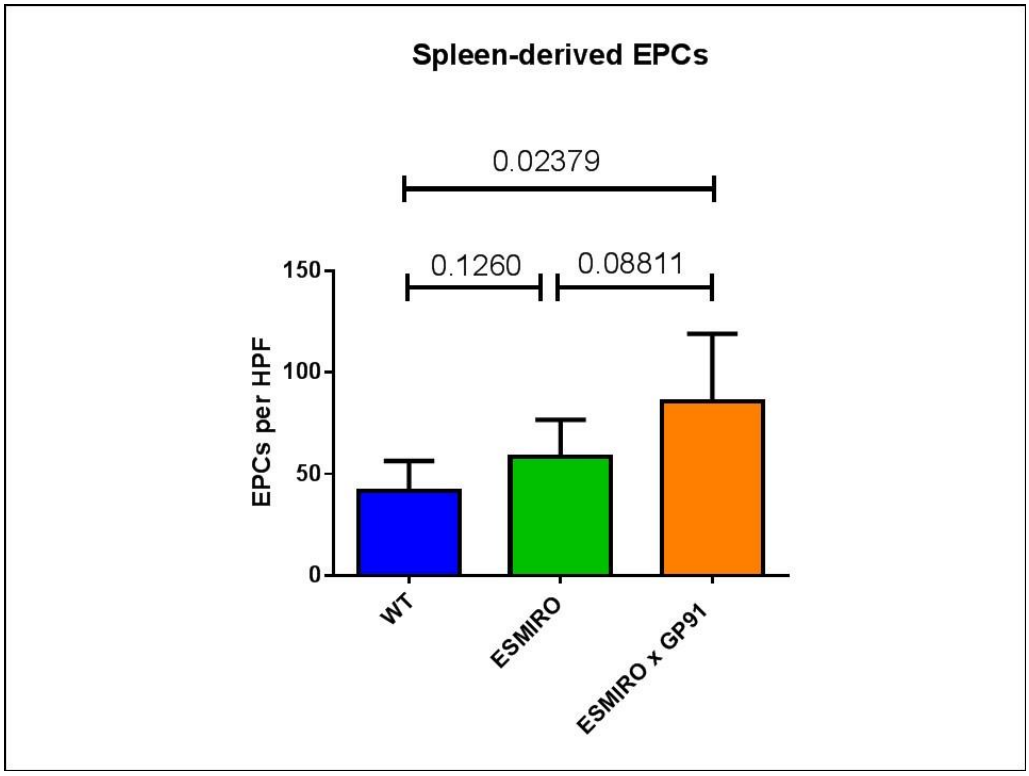

Figure 45 Spleen-derived EPCs

HPF=High powered field; (N= 5, 7, 6)

5.2.9 Early outgrowth endothelial progenitor cell function

Function of EPCs was assessed via use of conditioned media in a HUVEC scratch wound assay. As figure 46 illustrates, no significant differences were demonstrated with respect to extent of wound closure when comparing conditioned media from the three genotypes of mice.

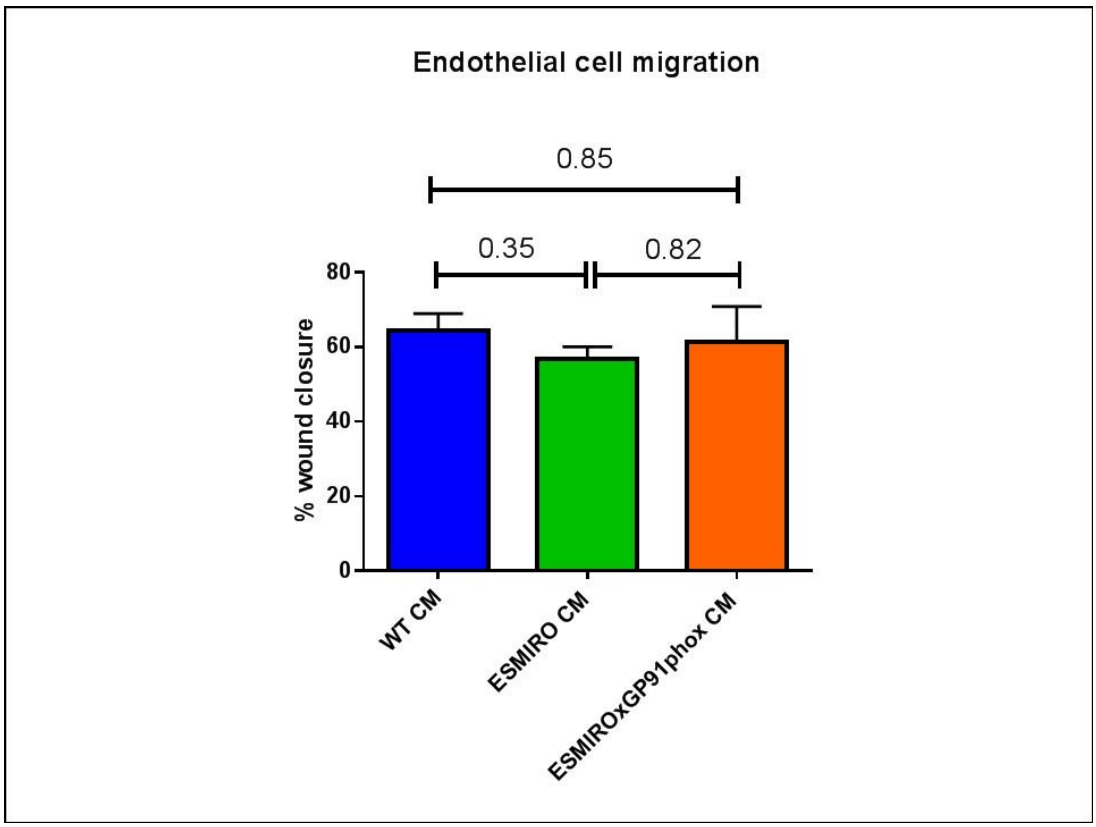

Figure 46 HUVEC migration with EPC conditioned media

CM = conditioned media; (N = 3, 2, 3).

5.2.10 Pulmonary endothelial cell functional assays

The finding of a higher number of CPCs in ESMIROxGP91phox than ESMIRO mice (section 5.2.7) provides a potential explanation for their notable difference in vascular repair (section 5.2.5). However, as outlined in section 1.5.3, there remains significant debate regarding the role and extent of contribution of CPCs to the process of re-endothelialisation. In view of this, the current study also went on to assess for differences in EC function, as a means of identifying additional explanations for the *in vivo* findings.

In order to ascertain the effects of genetic NOX2 inhibition on ECs in the context of insulin resistance, a number of assays were carried out on murine PECs.

5.2.10.1 Endothelial cell proliferation

Increased EC proliferative capacity resulting from NOX2 inhibition was one of the postulated mechanisms for improved vascular repair. Proliferating cells were identified based upon their ability to incorporate EdU, and then quantified using flow cytometry. No significant differences were demonstrated between the three genotypes with respect to PEC proliferation (figure 47).

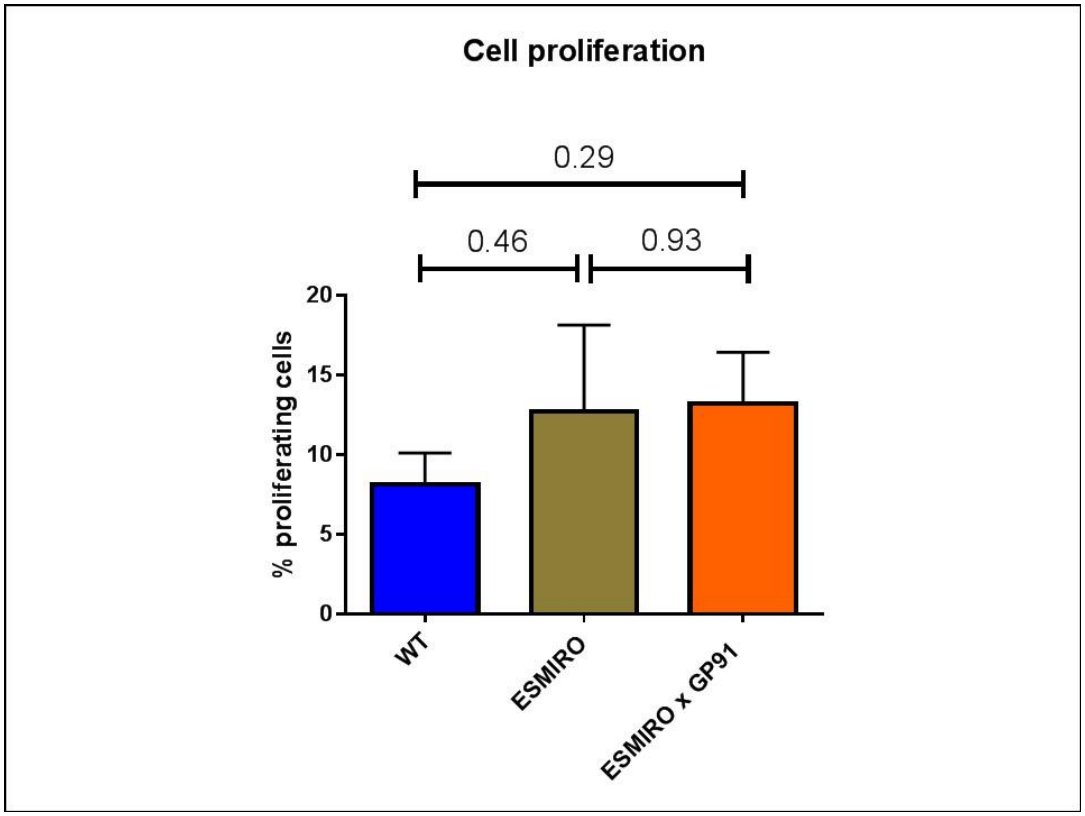

Figure 47 PEC proliferation

(N = 4, 4, 7)

5.2.10.2 Endothelial cell migration

An alternative mechanism to explain the improved vascular repair noted following NOX2 inhibition is via enhanced EC migration. The ability of ECs to migrate was assessed using a scratch wound assay, with a measurement made for the extent of wound closure in an 18 hour time period.

As illustrated in figure 48, PECs derived from ESMIRO mice displayed significantly reduced migration relative to WT PECs (28.1 [3.6] vs. 45.1 [3.8]; p=0.02). Genetic NOX2 knockdown rescued this impairment, with PECs derived from ESMIROxGP91 mice displaying significantly improved migration compared to ESMIRO (45.1 [5.1] vs. 28.1 [3.6]; p=0.04), thereby returning migratory capacity back to WT levels.

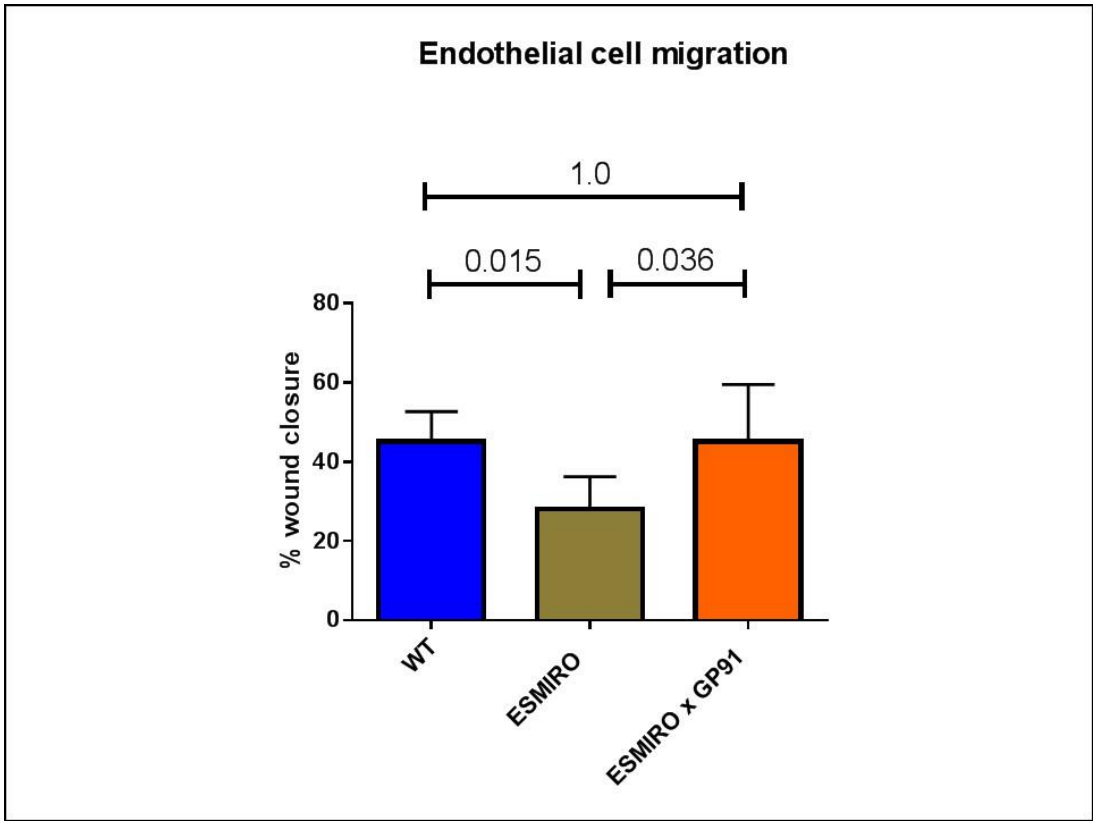

Figure 48 PEC migration

(N= 4, 5, 8)

5.2.10.3 Superoxide quantification

Quantification of superoxide concentration was carried out on PECs and in order to assess the effect of genetic NOX2 inhibition on ROS production. Superoxide concentration was measured via a fluorescence-based assay using DHE.

PECs derived from ESMIRO mice displayed a significantly higher concentration of superoxide than those derived from WT littermates (2.30 [0.26] vs. 1.32 [0.22]; p=0.02). Genetic knockdown of NOX2 resulted in a significantly lower superoxide concentration (1.38 [0.17] vs. 2.30 [0.26]; p<0.01), thereby normalising the level back to that of WT PECs (figure 49). These results recapitulate the findings from previous work published work by our laboratory group [123].

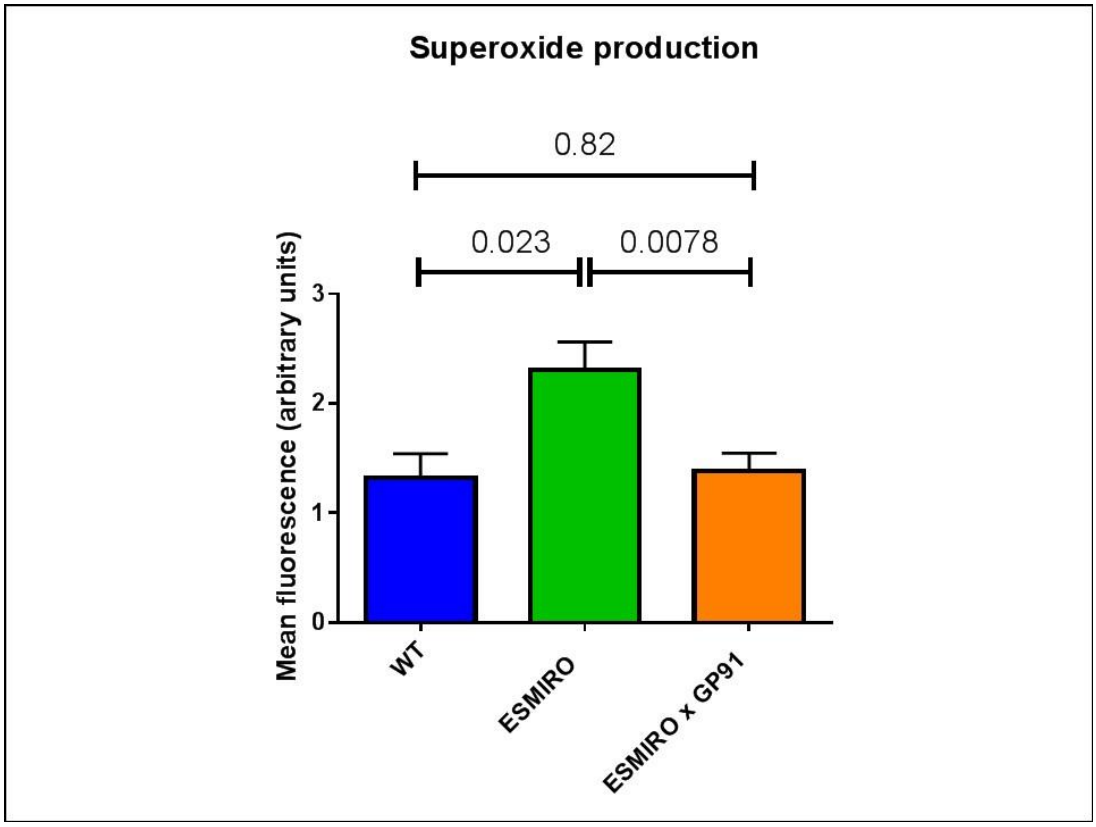

Figure 49 PEC superoxide concentration

(N= 5, 8, 9)

5.3 Virally-transduced HUVECs

In addition to examining the effect of genetic NOX2 inhibition in the context of insulin resistance using murine PECs, the current study also assessed the effect of pharmacological NOX2 inhibition using virally-transduced HUVECs and the NOX2 inhibitor GP91-ds tat. Prior to carrying out these experiments, pilot work was undertaken to optimise the concentration of the shRNA lentivirus to be used in order to achieve an approximate 50% knockdown of the IR.

5.3.1 Optimisation experiments

In order to identify the optimal dose of the shRNA lentivirus to apply to the HUVECs, dose-response experiments were carried out using 5, 10 and 20 MOI. Western blotting using these doses demonstrated 20 MOI to generate approximately a 50% reduction in IR expression compared to control (see figure 50).

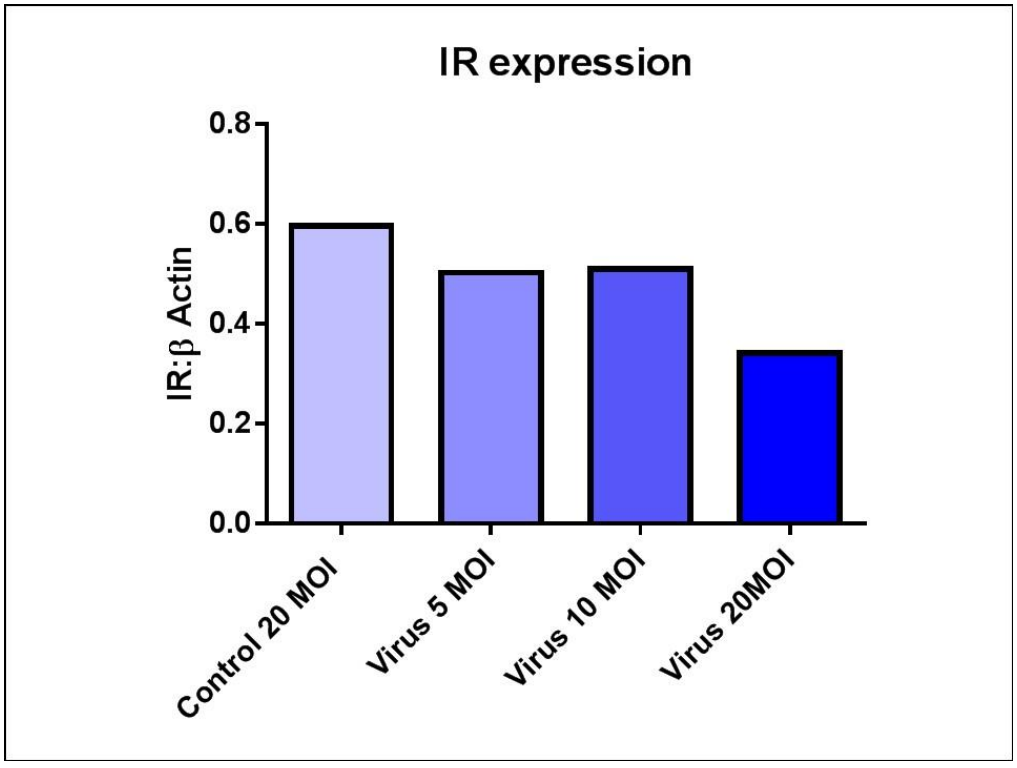

Figure 50 Dose response curve illustrating differential insulin receptor expression with increasing concentrations of shRNA lentivirus

MOI = multiplicity of infection. Expressed as a ratio of β actin (N=1).

In addition to assessing IR knockdown via western blotting, superoxide production was also assessed as a marker of insulin resistance following viral transduction. As figure 51 illustrates, increasing doses of the shRNA lentivirus resulted in higher concentrations of superoxide, suggesting increasing levels of insulin resistance.

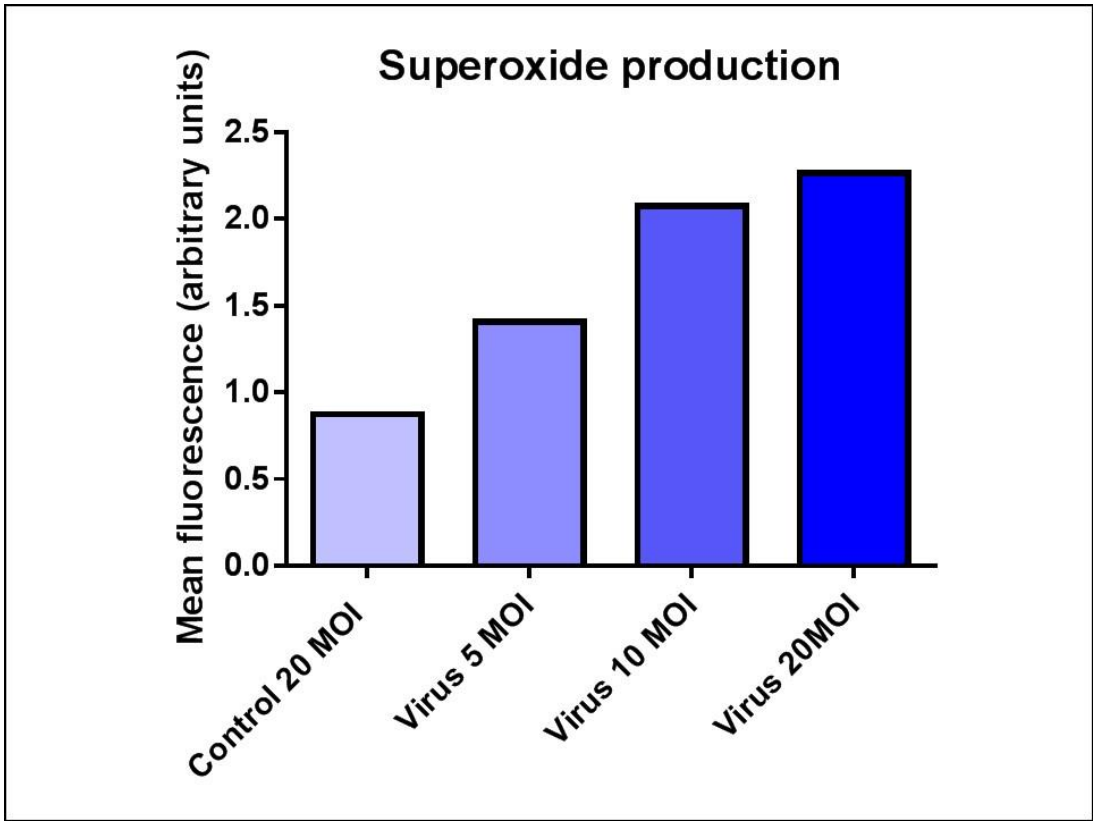

Figure 51 Dose response curve illustrating differential superoxide concentration with increasing concentrations of shRNA lentivirus

MOI = multiplicity of infection. Expressed as a ration of β actin (N=1).

During these optimisation experiments, it was noted that HUVECs treated with either shRNA lentivirus at a concentration of 20 MOI seemed to grow poorly relative to the other cell samples. Therefore, as a compromise between effective IR knockdown and viral toxicity, an MOI of 15 was chosen for subsequent experiments.

5.3.2 Human umbilical vein endothelial cell functional assays

5.3.2.1 Endothelial cell proliferation

As illustrated in figure 52, no significant differences were seen between control and insulin resistant HUVECs with regard to proliferative capacity (37.2 [3.4] vs. 37.2 [2.4]; p=0.98). Furthermore, addition of the NOX2 inhibitor GP91-ds tat to either of these groups of HUVECs made no significant difference to proliferation.

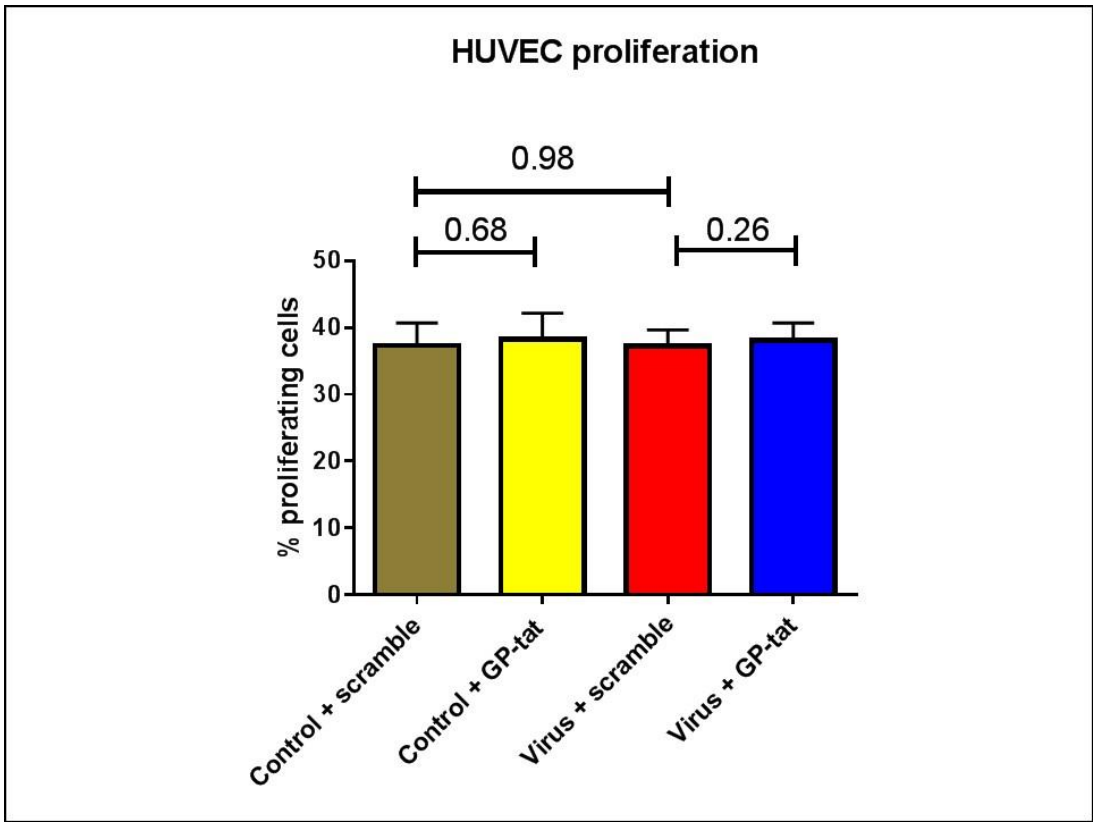

Figure 52 HUVEC proliferation in the setting of insulin resistance with or without NOX2 inhibition

Control = HUVECs treated with scrambled shRNA; GP-tat = GP91-ds tat; Virus = HUVECs treated with IR shRNA lentivirus; (N=5).

5.3.2.2 Endothelial cell migration

Insulin resistance conferred a significant impairment to the migratory capability of ECs, as demonstrated by comparing control and virally-transduced HUVECs (extent of wound closure 84.7% [4.7%] vs. 74.0% [3.7%]; p=0.02. See figure 53). Interestingly, this impairment was ameliorated by addition of GP91ds-tat to the insulin resistant HUVECs (83.5% [3.8%] vs. 74.0% [3.7%]; p=0.02), returning migration back to the level of control-HUVECs.

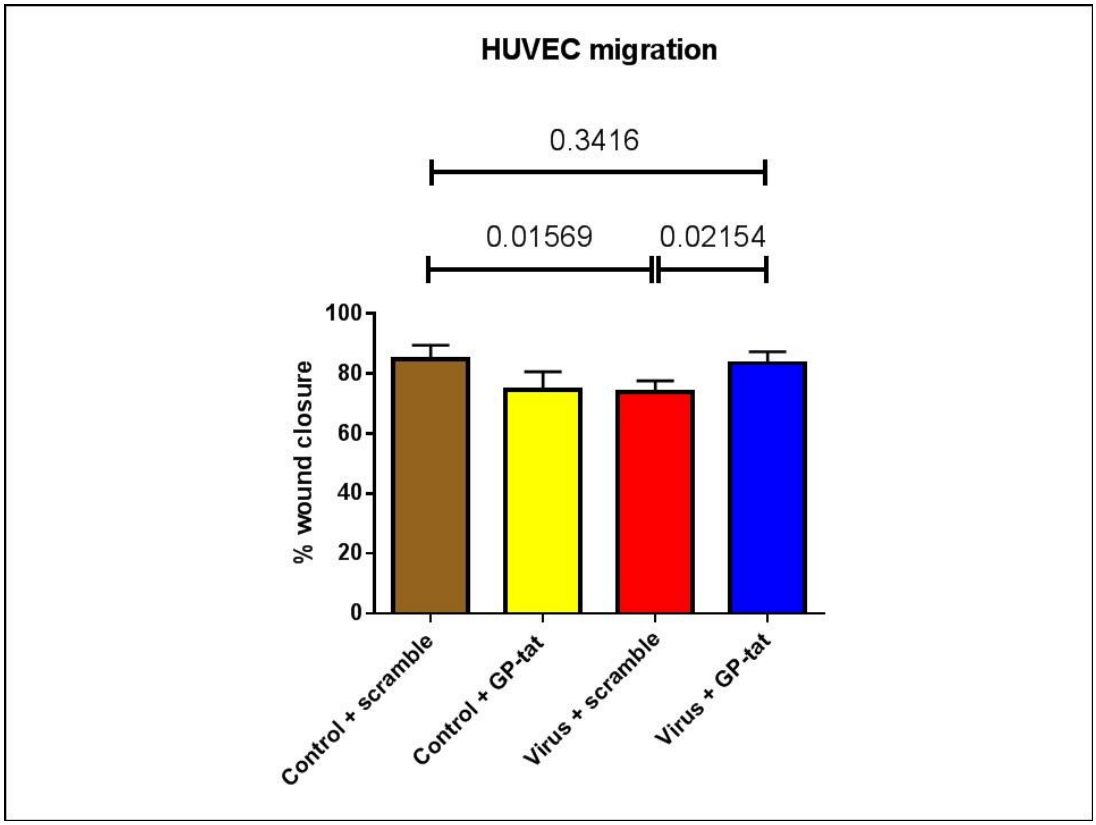

Figure 53 HUVEC migration in the setting of insulin resistance with or without NOX2 inhibition

Control = HUVECs treated with scrambled shRNA; GP-tat = GP91-ds tat; Virus = HUVECs treated with IR shRNA lentivirus; (N=4).

5.3.2.3 Superoxide production

Virally-transduced HUVECs demonstrated a significantly higher concentration of superoxide than their control counterparts (1.6 [0.3] vs. 1.3 [0.3]; p=0.03. See figure 54), in keeping with our understanding that insulin resistance is associated with oxidative stress (see section 1.2.4). Previously published work has demonstrated GP91-ds tat to be effective at suppressing superoxide production in insulin resistant cultured endothelial cells [123], and this finding was recapitulated in the current study. Treatment of the virally-transduced HUVECs with GP91-ds tat was shown to significantly lower concentration of superoxide (1.6 [0.3] vs. 1.1 [0.2]; p=0.01), back to the level of the control cells. Interestingly, this experiment also showed that GP91-ds tat has no significant effect on superoxide concentration in the absence of insulin resistance (1.3 [0.3] vs. 1.0 [0.3]; p=0.2).

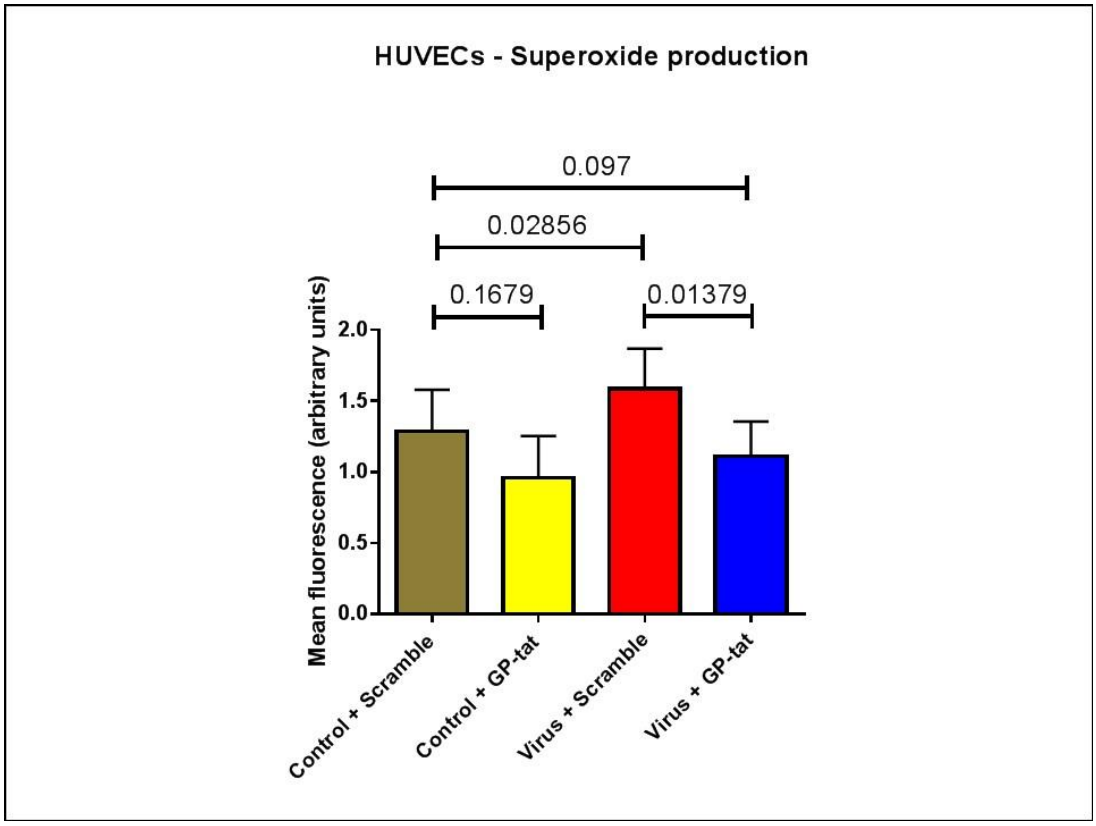

Figure 54 HUVEC superoxide concentration in the setting of insulin resistance with or without NOX2 inhibition

Control = HUVECs treated with scrambled shRNA; GP-tat = GP91-ds tat; Virus = HUVECs treated with IR shRNA lentivirus; (N=5).

5.3.3 Western blotting

Western blotting was carried out on transduced HUVECs in order to confirm successful shRNA lentiviral-mediated knockdown of the IR. A representative blot is shown in figure 55, whilst a quantified analysis of IR expression is shown in figure 56. Taken together, these highlight a significant reduction in IR expression for the virally-transduced cells when compared to control samples (1.0 [0.1] vs. 0.5[0.1]; p=0.01). Importantly, the representative blot also demonstrates that GP91-ds tat has no significant effect on IR expression.

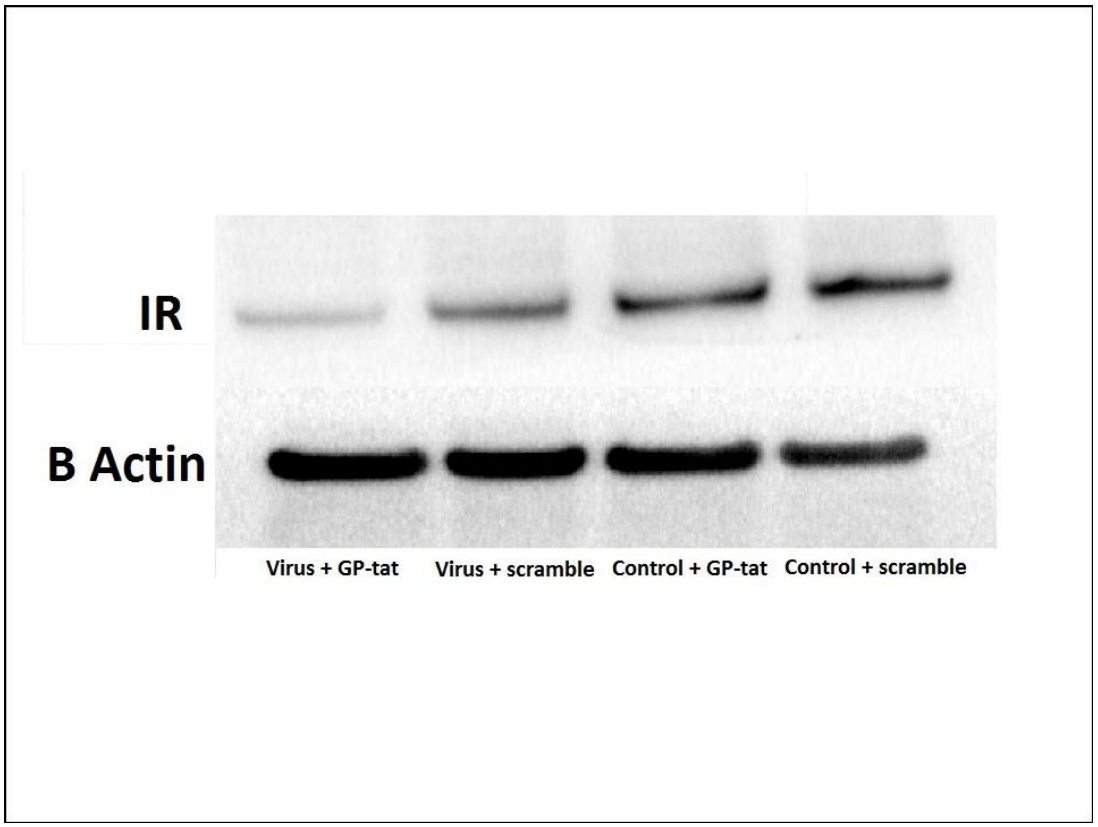

Figure 55 A representative Western blot showing expression of the insulin receptor in HUVECs

Control = HUVECs treated with scrambled shRNA; GP-tat = GP91-ds tat; Virus = HUVECs treated with IR shRNA lentivirus.

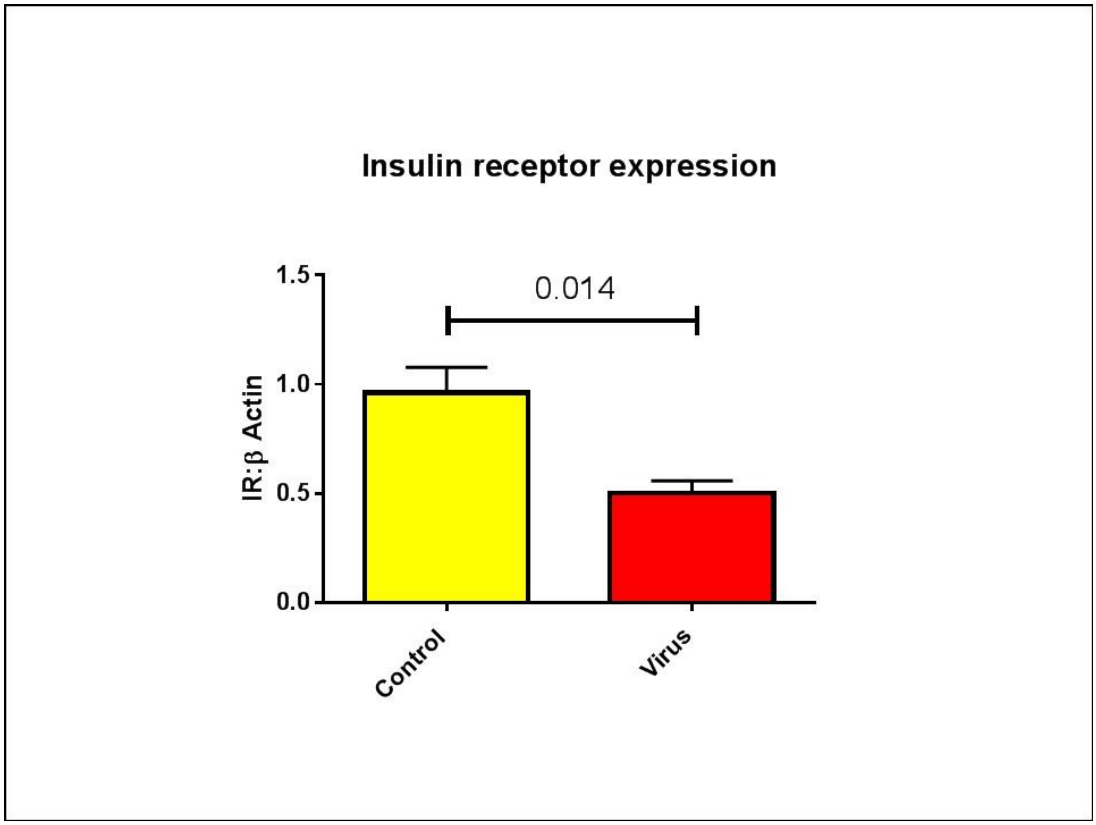

Figure 56 Insulin receptor expression in HUVECs

Control = HUVECs treated with scrambled shRNA; Virus = HUVECs treated with IR shRNA lentivirus (N=4).

Chapter 6**: Discussion**

Chapter 6 **Discussion**

In recent years, it has become accepted that insulin resistance is independently linked to cardiovascular disease [54]. One of the key, and most widely studied, aspects of this relationship is the way in which insulin resistance contributes to the initiation of atherosclerosis via endothelial dysfunction. However, equally importantly, it is thought that insulin resistance also interferes with repair mechanisms which would otherwise serve to mitigate against the progression and sequelae of cardiovascular disease. Key among these are the processes of vascular repair and angiogenesis; following injury to a blood vessel, appropriate vascular repair is essential in order to mediate endothelial healing, as a failure to do so leaves the damaged portion of vessel potentially more vulnerable to atherosclerotic plaque or local thrombus formation. Meanwhile, angiogenesis is the process of generating new blood vessels in adulthood, and is thus crucial for reperfusing tissues following an ischaemic vascular occlusion. A study published by our own laboratory group has demonstrated that IRKO mice, with haploinsufficiency of the IR at a whole-body level but unperturbed glucose homeostasis, display delayed vascular repair following denuding endothelial injury [12]. Furthermore, additional work from our laboratory has gone on to show that IRKO mice also have impaired ischaemic revascularisation following hindlimb ischaemia [130]. Taken together, these findings corroborate the theory that insulin resistance independently interferes with vascular repair and regeneration.

A number of avenues have been explored with the aim of improving the diminished vascular repair and regeneration associated with insulin resistance. One of the areas which shows promise is via modulation of ROS. There is evidence in the literature to demonstrate that inhibiting production of NOX2-derived ROS can improve angiogenesis in the context of diabetes [170]. Furthermore, a study published by Sorrentino *et al* [209] demonstrated that the impaired reparative capacity of EPCs derived from individuals with T2DM can be reversed via siRNA silencing of the p47phox subunit of NOX2, suggesting that inhibition of ROS production by NOX2 can improve vascular repair in diabetes. However, whilst these papers suggest NOX2 inhibition may be a promising translational target to improve reparative processes in diabetes, the prospect of this strategy conferring the same benefits in insulin resistance *per se* remains untested. To this end, the current project aimed to

explore the effects of NOX2 inhibition on angiogenesis and vascular repair in murine models of whole-body and endothelial-specific insulin resistance.

A number of interesting findings were generated as a result of this work. Firstly, genetic NOX2 knockdown was demonstrated to have no significant effect on post ischaemic re-perfusion in the setting of endothelial-specific insulin resistance. However, in contrast, the knockdown of NOX2 was associated with a significant improvement in vascular repair following femoral artery wire injury in ESMIRO mice, and subsequent *in vitro* work provided two potential explanations: improved EC migration, and an increased abundance of CPCs.

Interestingly, pharmacological NOX2 inhibition could not fully recapitulate these findings. Whilst treatment of insulin resistant HUVECs with the NOX2 inhibitor GP91-ds tat was associated with an improvement in cell migration, when the same inhibitor was used *in vivo* on ESMIRO mice*,* there was no significant improvement in vascular repair.

Finally, whilst genetic NOX2 knockdown proved to be a viable, and in some ways beneficial, strategy in the context of endothelial-specific insulin resistance, the converse was true in the setting of whole-body insulin resistance. Double cross IRKOxGP91phox$^{y/-}$ mice displayed a failure to thrive following invasive procedures that led to the premature cessation of experiments, and post mortem examination revealed the presence of presumed granulomas suggesting a possible immunodeficient state.

Each of these findings will be explored in more detail in the following section.

6.1 Summary of key findings

6.1.1 The effects of genetic NOX2 knockdown on angiogenesis in the context of endothelial-specific insulin resistance

In vivo experiments carried out on the ESMIROxGP91phox$^{y/-}$ colony of mice as part of the current project demonstrated that, in the context of endothelial-specific insulin resistance, NOX2 inhibition has no significant effect upon ischaemic revascularisation following hindlimb ischaemia. In fact, all three tested genotypes of mice displayed similar levels of perfusion within the ischaemic limb at all time points within the 28 day experimental protocol. When comparing the results obtained from ESMIRO and WT mice it is interesting to note that, when limited to the endothelium, this model of insulin resistance does not seem to confer any detriment to ischaemic revascularisation. This data contrasts with the aforementioned findings from IRKO mice, in which whole-body insulin resistance does indeed impair angiogenesis based upon use of the same *in vivo* assay. Combining the findings from the current study with previous work from our laboratory group, it seems that whilst the phenotypic aberration seen in ESMIRO mice is sufficient to impair endothelial function [123], unlike IRKO counterparts it is not significant enough to significantly affect reperfusion. This divergence between ESMIRO and IRKO mice has a precedent, as discussed earlier in section 1.1.2. Whilst the ESMIRO and IRKO murine models share a number of characteristics such as endothelial dysfunction and normal glucose homeostasis, it is notable that the ESMIRO mice display a milder phenotype as evidenced by their lack of hypertension.

The initial hypothesis of ESMIROxGP91phox$^{y/-}$ mice displaying enhanced post-ischaemic reperfusion relative to ESMIRO counterparts was predicated upon endothelial-specific insulin resistance having a detrimental effect on vascular regeneration following hindlimb ischaemia. Given that our findings in fact suggest no significant perturbation of ischaemic reperfusion in ESMIRO mice, and in the context of previously published work which demonstrates NOX2 knockdown to be detrimental in the absence of pathology [153, 167], it would perhaps be intuitive to expect ESMIROxGP91phox$^{y/-}$ mice to suffer with diminished post-ischaemic reperfusion. However, as mentioned, analysis of our results show that ESMIROxGP91phox$^{y/-}$ mice demonstrate no significant difference with regard to

ischaemic reperfusion compared to either WT or ESMIRO counterparts. Whilst it would appear that our findings are contradictory to those from the aforementioned papers, it is important to bear in mind that although ESMIRO mice do not have a significant aberration in post-ischaemic revascularisation, in contrast to the controls used in those studies they are not healthy mice, as illustrated by the presence of oxidative stress and endothelial dysfunction [56]. Referring back to the 'redox window hypothesis' (section 1.9), it is possible that whilst endothelial-specific insulin resistance is associated with oxidative stress, the ROS level remains within 'redox window' required for effective post-ischaemic reperfusion, resulting in an impairment which is too subtle to be detected by use of the hindlimb ischaemia experiment. Knockdown of NOX2 in ESMIRO mice may result in reduced ROS, but once again this may remain within the 'redox window', meaning that any adverse effect on post-ischaemic reperfusion is non-significant.

An alternative explanation for the lack of differences demonstrated between the genotypes pertains to the method used for quantification. Laser Doppler analysis provides a functional assessment of reperfusion, but does not provide conclusive evidence regarding angiogenesis *per se,* for which capillary density is a better measure. In view of the equivocal results obtained with regard to ischaemic revascularisation, a decision was taken to prioritise pursuing other *in vivo* findings that were deemed to be of higher translational potential. As a result, an analysis of capillary density in the harvested ischaemic muscles has not been undertaken as part of this project, and it is possible that variations between the genotypes are more readily apparent when using this method of analysis.

6.1.2 The effects of genetic NOX2 knockdown on vascular repair in the context of endothelial-specific insulin resistance

Whilst genetic NOX2 knockdown had no significant effect on post-ischaemic reperfusion in the setting of endothelial-specific insulin resistance, a significant improvement was demonstrated in vascular repair following endothelial denuding arterial injury. This was perhaps the key finding from the current project, and as a result a significant proportion of the *in vitro* assays were conducted in order to understand this observation.

As discussed in section 1.5.2, our current understanding of vascular repair following endothelial injury is founded upon two mechanisms: proliferation and migration of ECs adjacent to the injured vessel segment which replace lost and damaged cells; and/or the recruitment of bone marrow derived progenitor cells which home to the site of injury and assist in repair, by either direct incorporation or paracrine stimulation of resident ECs. The findings from *in vitro* experiments investigating these mechanisms are expanded upon in the following sections.

6.1.2.1 Endothelial cell migration

In addition to being pivotal to vascular repair, the ability of ECs to migrate is also thought to be essential to other physiological and pathological processes, including angiogenesis and vascular graft healing [210]. Previous studies have employed a number of assays to investigate EC motility, including the use of a Boyden chamber which assesses the migration of quiescent ECs along a chemotactic gradient, traditionally generated with use of a specific chemoattractant [211, 212]. Whilst this assay is undoubtedly valuable in studying EC migration, it arguably models only one aspect of a three-step process; as well as chemotaxis to a gradient of pro-migratory mediators, EC migration is also thought to involve the steps of haptotaxis, which describes directional migration toward a gradient of immobilised ligands, and mechanotaxis which is the term given to directional migration generated by mechanical forces as a result of actin cytoskeletal reorganisation [164]. In view of this limitation of the Boyden chamber assay, the scratch wound assay was used to investigate the EC migration component of vascular repair in the current study, as we believe it may provide a more accurate representation of the process that occurs *in vivo* following an endothelial denudation injury.

The data obtained from PECs using the scratch wound assay appears to demonstrate insulin resistance diminishing EC migration, as attested to by the comparison between WT and ESMIRO mice. Interestingly, this apparent impairment is entirely abrogated by genetic NOX2 knockdown, since PECs from ESMIROxGP91phox$^{y/-}$ mice display significantly enhanced migration when compared to their ESMIRO counterparts, returning migratory capacity back to WT levels. The concept that insulin resistance may impair EC migration has been mooted previously, and indeed insulin has been demonstrated to stimulate human microvascular endothelial cell migration via interaction with its receptor and increased Akt phosphorylation [213]. The cited paper also found that the observed enhancement in migration could be abrogated with use of a PI3K inhibitor, thereby implicating this specific signalling pathway. Interestingly, this paper made no direct reference to ROS as a potential mechanism to explain the migratory impairment associated with insulin resistance. Nonetheless, there exists a great deal of evidence highlighting the key role played by ROS in EC migration. As alluded to earlier, actin remodelling is an important component of the EC migratory process since it modulates cell shape and motility, as well as cell–cell contacts and cell contact with adhesion molecules [165]. ROS have emerged as a key regulator of actin remodelling, leading to the observation that NADPH oxidase activation and the ensuing superoxide production could modulate cell migration. Previous studies have demonstrated that migrating cells at wound margins produce increased quantities of ROS. Building on these observations, siRNA knockdown of NOX2 has been demonstrated to impair EC migration [214]. Furthermore, either NADPH oxidase inhibition or superoxide scavenging by an SOD mimetic can reduce both the speed and directionality of EC migration into a wound [215]. Interestingly, as well as ROS having the ability to modulate actin, there is also evidence in the literature to support the existence of a reciprocal relationship whereby actin can itself directly interact with components of NADPH oxidase such as p47phox to stabilise the enzyme, thus promoting ROS production [216].

The precise mechanisms by which ROS control actin reorganisation are complex, and incompletely understood. However, it is accepted that the actin cytoskeleton is affected profoundly by the prevailing redox environment [165], and based on this it would be intuitive to expect oxidative stress to be detrimental to actin remodelling, and thus by extension, EC migration. This concept has been corroborated in a study published by van

Aalst *et al,* the hypothesis for which was that the ability of oxidised low-density lipoproteins (oxLDL) to impair EC migration is secondary to increased ROS production [210]. The paper stated that oxidative stress diminished EC migration through excessive cytoskeletal disruption, suggested by the rounded appearance of the endothelial cells after exposure to inhibitory concentrations of oxLDL. Furthermore, SOD was shown to decrease oxLDL-induced reactive oxygen species production by ECs, which had the effect of preserving EC migration in the presence of oxLDL concentrations which alone would be inhibitory. Whilst the mechanism by which oxidative stress results in cytoskeletal disruption was not explored in this paper, the authors postulated that increased superoxide production may lead to formation of high levels of peroxynitrite, which has been reported to inhibit actin polymerization and impair neutrophil chemotaxis and fibroblast migration [217, 218]. The concept of oxidative stress inhibiting actin polymerisation had been discussed in a prior paper which examined the effect of ROS on glutathionylation of various proteins in T lymphocytes [219]. A variety of cytoskeletal proteins, including actin, were observed to be glutathionylated in the setting of oxidative stress. Importantly, glutathionylation has been demonstrated to reversibly inhibit actin polymerisation [220], thus linking oxidative stress, via disruption of mechanotaxis, to impaired EC motility.

Accordingly, our observation that NOX2 knockdown rescues the diminished EC migration associated with endothelial-specific insulin resistance is in keeping with prior findings. It is possible that in the setting of endothelial-specific insulin resistance, downregulation of the PI3K signalling pathway combines with dysfunctional actin cytoskeletal remodelling secondary to oxidative stress to impair EC migration, and that inhibition of ROS production via NOX2 knockdown rescues this deficit by restoring the redox environment to physiological levels.

6.1.2.2 Endothelial cell proliferation

The findings from the experiments exploring EC migration provide a potential mechanism for the improved vascular repair seen in ESMIROxGP91phox$^{y/-}$ mice relative to their ESMIRO counterparts. Another putative mechanism which warranted investigation was whether increased EC proliferation was a contributory factor, and this was assessed using an *in vitro* assay of EdU uptake. The experiment is based upon the principle that replicating

cells will incorporate EdU into their DNA, and if this is conjugated to a fluorophore, the proportion of replicating cells can be quantified using flow cytometry. The data obtained from the current study shows no significant differences between the PECs derived from the three genotypes of mice tested with respect to proliferation. In contrast to the assay of EC migration, insulin resistance did not appear to confer any functional deficit, with the proliferative capacity of ESMIRO PECs not differing significantly from WT PECs. Previous studies provide an insight into this finding, as it has been shown that exogenous insulin has no significant effect on the proliferation of human microvascular ECs [213]. Extrapolation of this observation suggests that insulin resistance may not influence EC proliferation. The role of NOX2-derived ROS in cell proliferation is not certain, but there are papers which suggest that, unlike NOX4-derived hydrogen peroxide which is pro-proliferative, superoxide generated by NOX2 instead prevents apoptosis and promotes survival [163]. With this in mind, our observation that NOX2 knockdown has no significant effect on endothelial cell proliferation is perhaps unsurprising.

6.1.2.3 Circulating progenitor cells

The concept of native ECs contributing to the process of re-endothelialisation via proliferation and migration is well accepted. In contrast, the hypothesis that bone marrow-derived progenitor cells assist in repair via differentiation into ECs is more controversial, although the possibility of paracrine effects on local ECs remains more widely accepted [141]. In a paper published by our own laboratory group, impaired mobilisation of CPCs from the bone marrow was postulated as a mechanism underpinning the diminished vascular repair observed in IRKO mice relative to WT littermates [12]. This hypothesis was substantiated by the finding that transfusion of $cKit^+$ CPCs from WT mice normalised the vascular repair of IRKO mice, whilst transfusion of $cKit^+$ CPCs from other IRKO mice achieved partial restoration of re-endothelialisation. As a counterview, another group has published work which appears to demonstrate that vascular repair following carotid artery wire injury is solely mediated by the migration of ECs from adjacent healthy endothelium, with no demonstrable role for direct incorporation of CPCs [141]. Whilst the evidence provided in this paper is compelling and apparently contradictory to the mechanism postulated by Khan *et al*, it must be borne in mind that the mice used in this study were healthy and therefore presumably had a normally functioning endothelium. This contrasts

with the IRKO mice used by Khan *et al,* which have been demonstrated to display endothelial dysfunction [54]. Moreover, the conclusions of these studies are not mutually exclusive, since paracrine effects of CPCs were not excluded by Hagensen *et al*, and direct incorporation of infused cKit$^+$ cells was not tested by Kahn *et al*. With this in mind, we felt it important to investigate the potential contribution of CPC abundance and function to the differences observed in vascular repair between ESMIRO and ESMIROxGP91phox$^{y/-}$ mice.

Quantification of CPCs was performed using flow cytometric detection of both Sca1$^+$/ Flk1$^+$ and cKit$^+$/Sca1$^+$ populations. When considering either population, although no statistically significant difference in CPC abundance is demonstrated between WT and ESMIRO mice, a trend toward reduced CPCs in ESMIRO mice is visible. Previously published data suggests that CPC mobilisation is dependent upon NO [159], and as discussed in section 1.6.4, as well as sequestering NO, an excess of ROS can lead to the uncoupling of eNOS, resulting in production of yet more superoxide at the expense of NO. Based on this, it is therefore possible that the oxidative stress associated with endothelial-specific insulin resistance compromises CPC mobilisation to some degree, resulting in fewer CPCs within the bloodstream. Knockdown of NOX2 in ESMIRO mice resulted in a significant increase in Sca1$^+$/Flk1$^+$ CPCs. These data suggests that by correcting the oxidative stress associated with endothelial-specific insulin resistance, NOX2 deletion overturns the deficit of CPCs in ESMIRO mice. Enhanced bioavailability of NO offers one potential explanation for this, although further studies would be required to test this hypothesis. The fact that there was no significant difference in the abundance of cKit$^+$/Sca1$^+$ expressing CPCs between ESMIRO and ESMIROxGP91phox mice may be a reflection of the fact that this population of cells differs from Sca1$^+$/Flk1$^+$ CPCs.

An alternative explanation for the increased quantity of Sca1$^+$/Flk1$^+$ CPCs in the ESMIROxGP91phox$^{y/-}$ mice, as well as the link between this and the improved re-endothelialisation observed in this cohort of mice, pertains to the concept of vascular repair being an inflammatory process [221]. Recruited inflammatory cells play a critical role in the reparative process following vessel injury, and inflammatory reactions can influence proliferation and migration of ECs and smooth muscle cells (SMCs). As discussed in section 1.8, NOX2 deletion has been previously associated with increased macrophage secretion of pro-inflammatory cytokines, such as IL-1β and TNF-α. Interestingly, the results of the

current study also demonstrate a trend toward increased IL-1β expression in the aortic tissue of ESMIROxGP91phox$^{y/-}$, and it is notable that this trend is seen in comparison to WT as well as ESMIRO counterparts. Given the uncertainty surrounding the identification and role of CPCs (section 1.5.3), it is possible that the increased quantity of Sca1^{+}/Flk1^{+} we observed in the ESMIROxGP91phox$^{y/-}$ mice actually represent inflammatory cells which can themselves augment vascular repair by stimulating resident ECs and SMCs [221]. Further weight behind this hypothesis comes from the observation of a significantly higher number of spleen-derived EPCs in ESMIROxGP91phox$^{y/-}$ mice compared to WT counterparts, and a trend toward a higher number compared to ESMIRO. Whilst for the purposes of this project (based upon accepted definitions [137]), the uptake of DiI-ac-LDL and lectin-FITC denoted these cells as EPCs, it is known that these are in fact macrophage lineage cells, which could clearly influence tissue repair via paracrine mechanisms. This potentially correlates with the observation from previous studies of increased macrophage-derived inflammatory cytokines in mice with NOX2 knockdown [193].

Extrapolating the theory that the increased abundance of progenitor cells in ESMIROxGP91phox$^{y/-}$ mice is a manifestation of increased inflammation leads to the possibility that the observed improvement in vascular repair in fact represents a prelude to increased atherosclerosis. The same inflammatory processes which augment vascular repair are known to be key to the development of stenotic lesions [221], and in a paper assessing the influence of NOX2 on abdominal aortic aneurysm progression, a trend toward increased atherosclerosis associated with NOX2 knockdown was visible in a small sample of mice [194]. Since this is an area which is incompletely understood, it would be instructive to further investigate the relationship between NOX2 inhibition, inflammation and atherosclerosis. Possible avenues for exploration are discussed in section 6.3.

6.1.3 Pharmacological NOX2 inhibition does not fully recapitulate the effects of genetic enzymatic knockdown

The findings from experiments on ESMIROxGP91phox$^{y/-}$ mice, which demonstrated that genetic knockdown of NOX2 can improve vascular repair and EC migration in the setting of endothelial-specific insulin resistance, were translationally encouraging. However, part of

the aim of this project was to appraise the potential applicability of NOX2 inhibition in a clinical setting. In this context, whilst genetic knockdown of NOX2 provides important insight as a proof of concept, in order to assess the translational potential of this strategy it was important to investigate whether we could recapitulate the positive findings using pharmacological NOX2 inhibition. As before, *in vitro* and *in vivo* experiments were carried out with the aim of acquiring both observational and mechanistic data. The drug GP91-ds tat was chosen as the pharmacotherapy for the current study since, unlike other ROS-reducing agents, it is relatively specific to NOX2. Furthermore, previously published work by our laboratory group has demonstrated its efficacy in reversing oxidative stress-associated endothelial dysfunction both *in vitro* and *in vivo* [123].

The *in vitro* work in this thesis was undertaken using HUVECs which had an approximate 50% knockdown of the IR using lentivirus-introduced shRNA (or scrambled control). Reflecting the work undertaken on the PECs, assays of cell migration, proliferation and superoxide production were carried out on the transduced HUVECs following treatment with either GP91-ds tat or a scrambled peptide. Since the ischaemic revascularisation experiment in the ESMIROxGP91phox$^{y/-}$ mice demonstrated no improvement following NOX2 knockdown, we elected to focus our *in vivo* work for this part of the project exclusively on vascular repair. Micro-osmotic pumps containing either GP91-ds tat or a scrambled peptide were subcutaneously inserted into ESMIRO mice, which then underwent the vascular repair experiment as described previously.

6.1.3.1 In vitro findings

The DHE assay for superoxide quantification demonstrated that HUVECs with knockdown of the IR produced a significantly higher concentration of superoxide than control specimens, in keeping with our understanding that insulin resistance is associated with oxidative stress [87]. Reassuringly, GP91-ds tat fully reversed the observed oxidative stress, returning superoxide concentration of insulin resistant HUVECs to control levels. The results from the scratch wound assay showed that this reversal of oxidative stress translated to an improvement in EC migration, as the functional deficit experienced by insulin resistant HUVECs was fully overturned via treatment with GP91-ds tat. Paralleling our findings from the PECs, no significant differences were observed with respect to proliferation. This finding suggests firstly, that the extent of insulin resistance associated

with a 50% knockdown of the IR is insufficient to alter the proliferative ability of ECs, and secondly, that NOX2 inhibition has no significant effect on EC proliferation.

To summarise the *in vitro* findings, we demonstrated that insulin resistance is associated with oxidative stress and diminished EC migration. Treatment of the insulin resistant ECs with a NOX2 inhibitor can ameliorate the oxidative stress, which translates into improved migration. As with genetic knockdown of NOX2, the mechanism by which pharmacological NOX2 inhibition improves EC migration in the context of insulin resistance is presumed to be via modulation of actin remodelling, as discussed in section 6.1.2.1.

6.1.3.2 In vivo findings

Whilst the *in vitro* findings following pharmacological NOX2 inhibition correlate well with the *in vitro* results obtained following genetic NOX2 knockdown, the *in vivo* vascular repair results were conflicting. The data illustrate that in the setting of endothelial-specific insulin resistance, pharmacological NOX2 inhibition has no significant effect on vascular repair. The disparity between the *in vitro* and *in vivo* effects of GP91-ds tat, whereby improved EC migration is not translated into a corresponding improvement in vascular repair, is difficult to reconcile. This is particularly true in view of the fact that the aforementioned study by our laboratory group demonstrated that chronic infusion of GP91-ds tat can reverse the endothelial dysfunction observed in ESMIRO mice [123]. One possible explanation relates to the dose of the drug reaching the relevant tissues in the *in vivo* model. The *in vitro* experiments were conducted using GP91-ds tat at a concentration of 50μM. To this author's knowledge, there are no published data that confirm the concentration of GP91-ds tat achieved in the murine bloodstream following infusion via micro-osmotic pump, but it is highly likely that the concentration of the drug reaching the tissues is significantly lower. Based on our previous findings, it would appear that whilst the *in vivo* concentration being achieved is sufficient to improve vasomotor function of ESMIRO mice, it is insufficient to impact upon vascular repair.

The inability of GP91-ds tat to improve vascular repair may also relate to the concept of the reparative process being driven by inflammation. It is plausible that pharmacological NOX2 inhibition fails to illicit the same pro-inflammatory effect as total genetic NOX2 knockdown. Indeed, whilst there is evidence to show that IL-1β production is increased

following genetic NOX2 knockdown (discussed in section 6.1.2.3), a paper studying the role of NADPH Oxidase during hyperhomocysteinemia demonstrated that treatment of mice with GP91-ds tat actually reduced IL-1β production [222]. Thus, if the improved vascular repair in ESMIRO mice following genetic NOX2 knockdown is a consequence of a pro-inflammatory state, it is perhaps understandable that pharmacological NOX2 inhibition, which appears incapable of generating such a reaction, fails to reproduce the same phenotype.

6.1.4 Viability of the IRKOxGP91phox$^{y/-}$ murine model

The IRKO murine model, with haploinsufficiency of the IR at a whole-body level but without dysglycaemia, is one which has been extensively studied by our laboratory group. Previously published work demonstrates that aortic rings and ECs from IRKO mice display endothelial dysfunction, and that this dysfunction can be corrected via use of a SOD mimetic, implicating a role for oxidative stress in the pathological process [120]. Subsequent work has gone on to show that the endothelial dysfunction of IRKO mice is associated with delayed vascular repair following denuding endothelial injury [12]. As discussed at the beginning of this chapter, there is a body of evidence which supports the concept of NOX2 inhibition as a potential approach to rescue the impaired vascular repair associated with insulin resistance. In order to investigate this, we created a novel double transgenic murine model which combines haploinsufficiency of the IR with genetic knockdown of NOX2.

Initial experiments comprised phenotypic characterisation of this new colony and demonstrated that the double cross (IRKOxGP91phox$^{y/-}$) mice grew appropriately, whilst not differing significantly from WT or IRKO counterparts with respect to glucose homeostasis. Following this, the focus shifted to *in vivo* studies to assess whether NOX2 deletion could reverse the impaired vascular repair observed in IRKO mice. During these experiments, it became apparent that the double cross mice were failing to thrive following invasive procedures. Their recovery period tended to be longer than that of age-matched mice of differing genotypes, and on occasion double cross mice would die following an ostensibly complication-free procedure. Whilst post-mortem examination of these mice did not reveal a direct cause for the unexpectedly high mortality rates, a notable finding was the frequent presence of presumed granulomas. All experiments on

this colony of mice were halted prematurely in view of these observations, meaning that it was not possible to fully elucidate the effect NOX2 knockdown on vascular repair in the setting of whole-body insulin resistance. Furthermore, the planned experiment to investigate ischaemic revascularisation following hindlimb ischaemia was never started. Whilst the premature cessation of experiments mean that we have only limited data on this colony, the limited stress resistance of the double cross genotype is interesting, and the potential reasons underpinning it warrant further discussion.

Historically, one of the concerns associated with inhibition of the action of NOX2 is the potentially detrimental effect on the innate immune system. As mentioned in section 1.2.2, NOX2 was first discovered in phagocytes where it plays an important role in host defence mechanisms by producing a 'respiratory burst' of ROS in order to kill internalised bacteria. It is therefore intuitive to assume that a global NOX2 knockdown would leave the recipient vulnerable to invading pathogens, and indeed there is a recognised analogue of this in human disease, in the form of chronic granulomatous disease (CGD). Patients suffering with this primary immunodeficient condition are characterised by a significantly increased susceptibility to severe bacterial or fungal infections as a result of a mutation in one of four genes encoding the subunits of phagocytic NOX2 [223]. As the name implies, the condition is also associated with granulomatous complications secondary to excessive inflammation.

Whilst genetic inhibition of NOX2 in mice with endothelial-specific insulin resistance seemed to be well tolerated, translating that into the setting of whole-body insulin resistance appeared to result in a phenotype which more closely mimics CGD. The fact that ESMIRO mice countenance NOX2 inhibition better than IRKO counterparts is interesting, and may reflect the milder phenotypic derangement associated with resistance to insulin in limited tissues, as opposed to global resistance. This distinction may be of importance with regard to application of NOX2 inhibition in clinical practice, since the IRKO murine model presumably provides a more accurate representation of patients with insulin resistance than does ESMIRO. Our observations from IRKOxGP91phox$^{y/-}$ mice raise the possibility that complete NOX2 inhibition in insulin resistant patients may adversely affect the immune system to a degree that would negate any theoretical benefit derived from improved vascular repair. Nevertheless, it is worth bearing in mind that these detrimental

effects were only seen following genetic knockdown of NOX2 which, as discussed in the preceding section, appears to provide a more potent enzymatic inhibition than pharmacological blockade. It might therefore be interesting to observe whether IRKO mice tolerate chronic treatment with GP91-ds tat without adverse immunological consequences in the same way as their ESMIRO counterparts. Provided no concerns arose following chronic pharmacological NOX2 inhibition, an assessment could then be made of whether this is associated with improved vascular repair, with the caveat that no alteration was seen following GP91-ds tat treatment in ESMIRO mice.

6.1.3 Summary of mechanisms

Pulling together the findings from the *in vitro* and *in vivo* experiments conducted as part of this project, we can surmise that pharmacological NOX2 inhibition can reverse the impaired EC migration associated with endothelial-specific insulin resistance *in vitro*, but is unable to augment vascular repair. Total NOX2 knockdown via genetic means can also reverse the impaired EC migration associated with endothelial-specific insulin resistance, with the additional benefit of improving vascular repair following a denuding wire injury.

Based on our understanding from the existing literature, the improvement in EC migration following either pharmacological or genetic NOX2 inhibition most likely reflects modulation of the actin cytoskeleton, whereby the reduction in ROS corrects the oxidative stress associated with insulin resistance and results in a redox environment more conducive to effective actin remodelling.

This observation is both interesting and encouraging. However, the findings from the current study hint at the complexity and highly nuanced nature of role of NOX2 in vascular biology, thus highlighting the need for circumspection when attempting to modulate it. The fact that the improved EC migration observed *in vitro* following pharmacological NOX2 inhibition did not translate into a corresponding improvement in *in vivo* vascular repair is an indication that improved EC function may not be the sole mechanism underpinning the augmented re-endothelialisation demonstrated following NOX2 knockdown in ESMIRO mice. It is accepted that the inflammation which ensues following vascular injury is a critical factor in directing the subsequent reparative processes, and involves interaction between multiple cell types including ECs and SMCs [224]. Previously published work has demonstrated deletion of NOX2 to be associated with a pro-inflammatory state, and a number of observations from the present study serve to substantiate this. In particular, the trend towards increased IL-1β expression and the demonstration of increased CPC and splenic EPC abundance in ESMIROxGP91phox$^{y/-}$ mice are potentially consistent with increased inflammation. Taken together, the augmented vascular repair observed in ESMIROxGP91phox$^{y/-}$ mice may therefore be a corollary of a pro-inflammatory state facilitating improved re-endothelialisation following injury.

Whilst the identification of a mechanism to augment vascular repair in the setting of endothelial-specific insulin resistance is promising, it is important to note that the post-injury inflammation which initially benefits re-endothelialisation may ultimately also stimulate atherosclerosis and vessel stenosis [224]. As a result, the hypothesis that an improvement in re-endothelialisation following NOX2 deletion is mediated via an inflammatory response portends a potentially significant hurdle to the translation of NOX2 inhibition from bench to bedside. The contrasting effects of pharmacological and genetic NOX2 inhibition on ESMIRO mice *in vivo* suggests that a significant blockade of NOX2 function is required in order to augment vascular repair. However, the concept that improved vascular repair may be a harbinger of a pro-atherosclerotic state means that significant caution will need to be exercised in recreating the level of NOX2 inhibition seen following genetic knockdown with a pharmacological agent.

Accentuating these concerns are the insights gleaned from experiments in the IRKOxGP91phox$^{y/-}$ colony of mice, which highlight the potential of complete NOX2 knockdown in the setting of whole-body insulin resistance to compromise immune function, leading to phenotype analogous to the immunodeficient condition CGD.

It is clear that more work needs to be undertaken before NOX2 modulation can be considered a viable therapeutic intervention, and a few suggestions that arose from work in the current project are discussed in section 6.3.

6.2 General limitations

Whilst the methods and techniques employed during this project have been honed and refined by previous studies, as well as optimised for the current study, there are inherent limitations which need to be borne in mind when appraising data and drawing conclusions.

6.2.1 Fidelity of animal insulin resistance models to the human disease state

As research into the area of human insulin resistance grows, it becomes ever more apparent that it is a complex, multi-level pathological state. Rather than dysfunction of a single component in a signalling axis, insulin resistance is likely acquired as a result of modification of signalling pathways at various levels due to myriad co-existing pathological factors including, but not confined to, inflammation, lipotoxicity and hyperglycaemia. The IRKO and ESMIRO murine models used in this project attempt to model insulin resistance via haploinsufficiency of the IR, or overexpression of a mutated form of the IR in the endothelium, respectively. These comparatively blunt measures cannot fully recapitulate the nuances of the human disease process. Furthermore the ESMIRO mouse, with its endothelial-specific insulin resistance, has no true correlate in human pathology. Accordingly, some caution needs to be exercised when extrapolating findings from these models to clinical settings. Nevertheless, whilst conceding that these murine models cannot truly recreate human insulin resistance, the following points provide justification for the reliance on them during this project. Firstly, both IRKO and ESMIRO mice have been demonstrated to faithfully mimic aspects of the vascular dysfunction observed in insulin resistant humans [54, 56]. Secondly, the experiments carried out using virally transduced HUVECs recapitulated the key findings from the PEC assays, lending credence to the robustness of the transgenic model. Thirdly, the inclusion of transgenic mice, as opposed to exclusively using human cells, allowed *in vivo* work to be carried out alongside *in vitro* experimentation, granting a better understanding of the therapeutic effects of NOX2 inhibition. And finally, the *in vivo* experiments carried out in the current study clearly could not be performed in humans, whilst use of larger mammals would introduce additional logistical hurdles such as longer breeding cycles and increased time taken to reach maturation.

6.2.2 Models of vascular disease

Accepting that the models of insulin resistance utilised in this project are a simplification of the human disease process, in a similar vein it must be also be appreciated that the *in vivo* experiments used to model vascular diseases are approximations rather than true representations of clinical pathology. The hindlimb ischaemia model is widely used to assess ischaemic revascularisation, and when combined with laser Doppler imaging it allows for functional data to be collected at varied times from the same mouse, thus obviating the need to sacrifice mice at different time points to allow analysis. However, whereas human peripheral vascular disease usually progresses chronically, allowing for the development of collateral vessels prior to possible arterial occlusion, in this model the ischaemia is truly acute in a way that is rarely seen in clinical practice.

The vascular repair experiment, which provided pivotal data for the current study, also bears similar limitations. The assay provides an insight into the process of re-endothelialisation which occurs following arterial injury, caused either by vascular disease or stent deployment. In order to allow reproducibility the injury to the endothelium is linear and discrete in nature, which may not reflect diverse range of insults that the endothelial lining in a diseased human artery may be subject to. Furthermore, the fact that the extent of repair is analysed four days following the injury does not allow for any assessment of longer-term recovery.

6.2.3 Choice of endothelial cells for *in vitro* assays

As discussed in section 6.1, the observation that genetic NOX2 knockdown improves vascular repair in the context of endothelial-specific insulin resistance was one of the most exciting of the current project, and a large proportion of the subsequent in *vitro work* was performed in order to understand the mechanisms underpinning this finding. Assays exploring EC function were pivotal in providing mechanistic insight, and so the selection of ECs used bears further scrutiny.

The *in vivo* finding of improved vascular repair was based upon experiments using the femoral artery, which forms part of the macrovascular circulation. Ideally, the *in vitro* work that followed wound focus on ECs derived from other macrovascular arterial vessels, such as the aorta. For the current project, the ECs used were PECs and HUVECs; cells

predominantly from the microvascular and venous circulations respectively. It could be argued that this is a significant disparity, since these circulatory systems are exposed to differing haemodynamic pressures. As a result, the ECs are likely to display a cellular and molecular heterogeneity which may influence vascular function and repair [225]. However, whilst accepting the caveat that the ECs used are not fully representative of the endothelium used in the vascular repair experiment, we feel that the selected cohorts of cells share enough overlap to provide mechanistic insight. Our laboratory has extensive experience culturing PECs, and previous unpublished work has shown that this subset of cells tend to reflect aberrations in macrovascular endothelial dysfunction. Meanwhile, HUVECs are widely used by many groups and are thought to provide a robust model of endothelial cell function [226, 227].

As well as the need to use suitable surrogates for macrovascular arterial ECs, pragmatic considerations also influenced our selection of cells for *in vitro* experimentation. It is not feasible to obtain a sufficient quantity of ECs from aortic tissue alone for all of the assays performed in this project. Whilst an option could have been to pool together the aortae from multiple mice for each experimental sample, this would have necessitated the use of a prohibitive number of animals and we deemed the benefit of using macrovascular ECs as insufficient justification for such use of resources.

6.2.4 Sample size

One of the limitations inherent in the current study is the relatively small sample sizes used for a number of the experiments. Whilst statistical power calculations were used to determine the minimum sample sizes for the key measures of vascular repair and ischaemic revascularisation, additional ethical considerations were taken into account when deciding on the sample size for experiments such as PEC assays or progenitor cell quantification, since these represent hypothesis-generating mechanistic work. As is necessary when conducting animal research, during this project we made a concerted effort to balance the need for a representative sample size with the desire to minimise animal usage. Whilst it would be ideal to use large cohorts in each experimental group in order to provide more conclusive data, a pragmatic approach is required when deciding how many replicates are needed in order to answer an exploratory scientific question. This

represents a different approach to clinical trials, where sample size for all experiments are traditionally determined by use of statistical power calculations.

In addition to ethical issues, resource considerations also had a role in shaping experimental planning, since funds and time available for this project were finite and the development and optimisation of assays undertaken prior to data acquisition required significant investment.

Overall, a number of the mechanistic experiments undertaken in this project were designed to be exploratory, rather than to provide definitive conclusions. When viewed in that context, and taking into account the ethical and resource considerations outlined above, we feel that the sample sizes used represent a satisfactory compromise which allows the generation of data which can form the basis for future work.

6.2.5 Mechanistic insight

The current project has highlighted a number of interesting findings which warrant further exploration in future studies. Whilst great effort has been made during this project to elucidate the mechanisms underpinning the changes observed following NOX2 inhibition in insulin resistance, it is important to recognise that there remain a number of important unanswered questions. Part of this is attributable to time constraints that are inevitably associated with fixed-term research posts. This has necessarily meant that certain experiments have been prioritised based on our current understanding, whilst other avenues which may have proven more fruitful have been left unexplored. In recognition of this, the following section outlines additional experiments which may aid in developing a deeper mechanistic insight into the observations discussed in this thesis.

An additional limiting factor which needs to be recognised is our currently limited knowledge on the function of NOX2, and its interaction with other NOX isoforms. A more intimate understanding of the workings of these enzymes would facilitate a more nuanced modulation of ROS production. In lieu of this, we have had to employ the relatively crude approaches of total genetic knockdown or single dose pharmacological inhibition. For the purposes of examining downstream and compensatory effects, it would be useful to be able to make more subtle alterations to NOX2 function.

6.3 Future directions

As discussed in section 6.1, the current project has identified a number of interesting findings which could potentially lead on to clinically useful developments. However, further work is required in order to fully understand our own observations, as well as the nature and extent of the effects of NOX2 inhibition in the context of insulin resistance in general. In this section, we outline a number of potential directions for future studies to build upon the work described in this thesis.

6.3.1 Endothelial cell migration and actin remodelling

The current study demonstrates that endothelium-specific insulin resistance significantly diminishes EC migration, and that this impairment can be fully reversed via either genetic or pharmacological NOX2 inhibition. Based on existing literature, we postulate that these findings are a corollary of changes in the redox environment affecting actin cytoskeletal remodelling, and further experiments would be useful to explore this theory in more detail. As an initial step, fluorescently labelled phalloidin could be used to provide an insight into actin filament arrangement, allowing comparisons to be made between ECs with differing levels of oxidative stress. By carrying out this assay in the PECs and HUVECs used elsewhere in this project, the effects of insulin resistance and NOX2 inhibition on EC migration could be examined.

Whilst staining actin with fluorescently labelled phalloidin provides useful information into gross filament arrangement, the technique is limited by the fact that direct fluorescent labelling of actin inhibits its function and dynamics. As a result, an alternative approach such as use of a novel live cell-compatible probe is required for studying the dynamics of actin within living cells [228]. Such a technique could potentially be used in an *in vivo* model, and could ultimately provide a detailed understanding into the effects of NOX2 inhibition on EC migration following vascular injury.

6.3.2 NOX2 inhibition, inflammation and vascular repair

Whilst enhanced EC migration may provide a mechanism for the improved vascular repair noted in ESMIROxGP91phox$^{y/-}$ mice compared to ESMIRO counterparts, results from experiments studying IL-1β expression and CPC quantity suggest that increased

inflammation following NOX2 knockdown may also be a contributory factor. It is important to recognise that our RT-qPCR experiments assessing the expression of pro-inflammatory cytokines were incomplete due to time constraints, and so completion of these would be the next step. Based upon the trend visible from the experiment in the current study, as well as previously published work [193], we feel that it is highly probable that tissues from ESMIROxGP91phox$^{y/-}$ mice will display significantly higher quantities of IL-1β than either WT or ESMIRO littermates.

As already alluded to, one of the key questions to arise from this project is the relative contribution of increased inflammation to the improved vascular repair observed in ESMIROxGP91phox$^{y/-}$ mice. An interesting way to dissect this out would be to combine vascular repair experiments in ESMIROxGP91phox$^{y/-}$ mice with administration of the drug canakinumab, a monoclonal antibody targeted at IL-1β [229]. The use of canakinumab would isolate and remove the effect of IL-1β in the reparative process, thus providing evidence of the role of inflammation in re-endothelialisation following NOX2 inhibition.

6.3.3 The effect of NOX2 inhibition on atherosclerosis

One of the concerns identified from work in the present study is that the increased inflammation associated with NOX2 knockdown may ultimately lead to a corresponding increase in atherosclerosis. Indeed, it is possible that the improved vascular repair seen in the ESMIROxGP91phox$^{y/-}$ mice is actually a prequel to a pro-atherosclerotic state. Clearly, before pharmacological NOX2 inhibition can be used as a therapeutic intervention, more work is required to confirm or refute this hypothesis since a pro-atherosclerotic tendency would severely limit the applicability of this strategy in clinical practice. One way to investigate this would be to cross ESMIROxGP91phox$^{y/-}$ with ApoE$^{-/-}$ mice to create triple-cross progeny. A comparison could then be made between ESMIROxApoE$^{-/-}$ and ESMIROxGP91phox$^{y/-}$xApoE$^{-/-}$ mice with regard to atherosclerotic burden via *en face* analysis of different portions of the aorta, as published by Gage *et al* [13].

6.3.4 The effect of NOX2 inhibition on other NOX isoforms

One aspect of NOX2 inhibition that hasn't been fully addressed in the present study is the effect on other NOX isoforms, and in particular NOX4. Previously published work has demonstrated that NOX4 expression is increased in response to NOX2 knockdown [214],

and this may have a significant bearing on the findings from this project. As discussed in section 1.2.2, NOX4 differs from NOX2 in both structure and product, with hydrogen peroxide being the predominant ROS generated by this isoform of NADPH oxidase. Further differentiating NOX4 from other isoforms is the possibility that NOX4-derived ROS have a protective effect within the vasculature. A recently published paper demonstrated that $NOX4^{-/-}$ diabetic $ApoE^{-/-}$ mice suffered with increased atherosclerosis compared to diabetic $ApoE^{-/-}$ counterparts, and that NOX4 overexpression in human aortic ECs results in reduced expression of profibrotic markers [230]. Extrapolating from these findings, it is plausible that the benefit seen following NOX2 knockdown with regard to EC migration and/or vascular repair are influenced to some extent by an increase in the expression of NOX4, and therefore the abundance of hydrogen peroxide. Whilst preliminary data comparing NOX4 expression in ESMIRO and ESMIROxGP91phox mice was obtained (see section 5.2.4.3), the sample sizes were small and the results therefore not conclusive. Therefore, in order to investigate the hypothesis of NOX2 knockdown leading to compensatory NOX4 overexpression, the first step would be to undertake further RT-qPCR, followed by an assessment of hydrogen peroxide production as a marker of activity. Whilst not demonstrated in our preliminary data, based on the aforementioned papers, we would perhaps expect increased NOX4 expression following genetic NOX2 knockdown. It would be particularly interesting to examine whether this is also true following pharmacological NOX2 inhibition, which could be achieved by analysis of lysates obtained from the experiments on transduced HUVECs.

If increased NOX4 mRNA is associated with both genetic knockdown and pharmacological inhibition of NOX2, the next step would be an assessment of the contribution of elevated hydrogen peroxide levels to EC migration and ultimately *in vivo* vascular repair. A potential strategy to enable this would be the creation of murine model which combined endothelial-specific insulin resistance with genetic knockdown of both NOX2 and NOX4.

6.3.5 Pharmacological NOX2 inhibition in whole-body insulin resistance

As discussed in section 6.1.4, when combining genetic NOX2 knockdown with whole-body insulin resistance, the resulting mice had a phenotype which mimicked the immunodeficient condition CGD. Since the IRKO mouse represents arguably a more accurate representation of human insulin resistance than its ESMIRO counterpart, this

observation is concerning as it suggests that NOX2 inhibition in insulin resistant patients may result in compromised immune function. However, this apprehension needs to be balanced against the knowledge that genetic NOX2 knockdown appears to provide a significantly more potent enzymatic inhibition than can be achieved by pharmacological means. Therefore, it would be instructive to implant micro-osmotic pumps containing GP91-ds tat into IRKO mice in order to observe the effect of chronic pharmacological NOX2 inhibition in the context of whole-body insulin resistance, with a particular focus on immunodeficient sequelae. Provided the mice proved healthy and viable, vascular repair experiments could then be performed to investigate whether pharmacological NOX2 inhibition can rescue the impaired re-endothelialisation associated with the IRKO genotype [12].

6.3.6 The extent of superoxide production suppression achieved by pharmacological NOX2 inhibition

One of the reasons postulated for the beneficial effect of pharmacological NOX2 inhibition on EC cell migration *in vitro* failing to translate into improved vascular repair is a failure to reach the required dose of GP91-ds tat *in vivo*. As discussed in section 6.1.2, it is unlikely that the concentration of GP91ds-tat reaching the relevant tissues in the vascular repair experiment reached the 50μM used in the *in vitro* assays. The ideal way to address this uncertainty in future would be to accurately assess the extent of superoxide production being achieved *in vivo,* and then adjust the dose of GP91-ds tat accordingly to ensure sufficient enzymatic inhibition. One possible method to achieve this is to harvest aortae from mice following chronic *in vivo* exposure to different doses of GP91-ds tat, and then perform a DHE assay on the explanted tissue. However, whilst the DHE assay used in the current study is a useful and widely used tool for superoxide quantification, it must be recognised that all existing techniques for identification of oxidative stress have limitations. The main limitation of the DHE assay is the fact that DHE oxidation yields at least two fluorescent products, which have varying specificities for superoxide. In order to improve the accuracy of the assay, high performance liquid chromatography (HPLC) could be used to isolate the fluorescent product of interest, allowing a more representative assessment of the level of NOX2 inhibition being achieved.

6.5 Concluding remarks

Whilst great advances have been made regarding the prevention and treatment of cardiovascular disease (CVD) amongst the general population, the incidence and mortality rate of CVD among patients with diabetes mellitus remain concerningly high [4]. Our lack of effective treatments for the insulin resistant syndrome which underpins diabetes mellitus, as opposed to simply the hyperglycaemia which results from it, is accepted as one of the likely contributory factors to this observation. As such, there is an impetus to explore new avenues through which novel therapeutic agents to treat insulin resistance-associated vascular disease can be developed. One area that has provided promising results is the modulation of ROS in order to improve vascular repair and regeneration, processes which have been demonstrated to be impaired in the setting of insulin resistance. At the outset of this project, the aim was to study the effect of inhibiting the production of NOX2-derived ROS on angiogenesis and vascular repair in models of insulin resistance, with the ultimate goal of assisting with the translation of a potentially promising concept into clinical utility.

A number of the findings from the present study are encouraging and, whilst being novel, also correlate with insights and hypotheses borne of previous work. Key among these are the observations that, firstly, in the setting of endothelial insulin resistance, a normalisation of the redox state via NOX2 inhibition significantly improves EC migration, and secondly, that this translates into augmented vascular repair provided that NOX2 inhibition is complete. These beneficial effects provide hope that NOX2 inhibition may potentially become a useful tool in the treatment of insulin resistant patients; however this project has also served to highlight pitfalls that need to be investigated before this potential can be harnessed and utilised. Our findings corroborate existing concerns relating to NOX2 inhibition and compromised immune function, as well as supporting to some extent the notion that inhibition of NOX2 runs the risk of inciting a pro-inflammatory state.

Based upon our findings, and those in the existing literature, NOX2 remains a potentially suitable target for therapeutic intervention. However, what is required is an ability to carefully modulate its activity to a degree which augments endothelial function, whilst not curtailing immune responses or promoting inflammation. In order to achieve this,

regulation of NOX2 function would ideally be controlled both spatially and temporally, whereby the inhibition of ROS production is specific to the vasculature at the exclusion of immune cells, and would be of a sufficient duration to improve vascular repair but not so prolonged as to generate a sustained inflammatory response. Such nuanced manipulation of NOX2 is not currently possible and in order to expedite it, a greater understanding of the roles and interactions of NOX2 is required. It is hoped that the work carried out in this project can be built upon in order to facilitate that understanding and ultimately generate therapeutic agents which can benefit many patients in future.

References

1. Laakso, M. and J. Kuusisto, *Insulin resistance and hyperglycaemia in cardiovascular disease development.* Nat Rev Endocrinol, 2014. **10**(5): p. 293-302.

2. Gu, K., C.C. Cowie, and M.I. Harris, *Mortality in adults with and without diabetes in a national cohort of the U.S. population, 1971-1993.* Diabetes Care, 1998. **21**(7): p. 1138-45.

3. Kannel, W.B. and D.L. McGee, *Diabetes and cardiovascular disease. The Framingham study.* Jama, 1979. **241**(19): p. 2035-8.

4. Cubbon, R.M., et al., *Temporal trends in mortality of patients with diabetes mellitus suffering acute myocardial infarction: a comparison of over 3000 patients between 1995 and 2003.* Eur Heart J, 2007. **28**(5): p. 540-5.

5. Almdal, T., et al., *The independent effect of type 2 diabetes mellitus on ischemic heart disease, stroke, and death: a population-based study of 13,000 men and women with 20 years of follow-up.* Arch Intern Med, 2004. **164**(13): p. 1422-6.

6. Booth, G.L., et al., *Relation between age and cardiovascular disease in men and women with diabetes compared with non-diabetic people: a population-based retrospective cohort study.* Lancet, 2006. **368**(9529): p. 29-36.

7. Haffner, S.M., et al., *Cardiovascular risk factors in confirmed prediabetic individuals. Does the clock for coronary heart disease start ticking before the onset of clinical diabetes?* Jama, 1990. **263**(21): p. 2893-8.

8. *Is the current definition for diabetes relevant to mortality risk from all causes and cardiovascular and noncardiovascular diseases?* Diabetes Care, 2003. **26**(3): p. 688-96.

9. Anogeianaki, A., et al., *Atherosclerosis: a classic inflammatory disease.* Int J Immunopathol Pharmacol, 2011. **24**(4): p. 817-25.

10. Ross, R., *Atherosclerosis--an inflammatory disease.* N Engl J Med, 1999. **340**(2): p. 115-26.

11. Kim, J.A., et al., *Reciprocal relationships between insulin resistance and endothelial dysfunction: molecular and pathophysiological mechanisms.* Circulation, 2006. **113**(15): p. 1888-904.

12. Kahn, M.B., et al., *Insulin resistance impairs circulating angiogenic progenitor cell function and delays endothelial regeneration.* Diabetes, 2011. **60**(4): p. 1295-303.

13. Gage, M.C., et al., *Endothelium-specific insulin resistance leads to accelerated atherosclerosis in areas with disturbed flow patterns: a role for reactive oxygen species.* Atherosclerosis, 2013. **230**(1): p. 131-9.

14. Ceriello, A. and E. Motz, *Is oxidative stress the pathogenic mechanism underlying insulin resistance, diabetes, and cardiovascular disease? The common soil hypothesis revisited.* Arterioscler Thromb Vasc Biol, 2004. **24**(5): p. 816-23.

15. Dworakowski, R., S.P. Alom-Ruiz, and A.M. Shah, *NADPH oxidase-derived reactive oxygen species in the regulation of endothelial phenotype.* Pharmacol Rep, 2008. **60**(1): p. 21-8.

16. Schroder, K., et al., *NADPH oxidase Nox2 is required for hypoxia-induced mobilization of endothelial progenitor cells.* Circ Res, 2009. **105**(6): p. 537-44.

17. Wilcox, G., *Insulin and insulin resistance.* Clin Biochem Rev, 2005. **26**(2): p. 19-39.

18. Soria, B., et al., *Novel players in pancreatic islet signaling: from membrane receptors to nuclear channels.* Diabetes, 2004. **53 Suppl 1**: p. S86-91.

19. Kido, Y., J. Nakae, and D. Accili, *Clinical review 125: The insulin receptor and its cellular targets.* J Clin Endocrinol Metab, 2001. **86**(3): p. 972-9.

20. Hubbard, S.R., *Crystal structure of the activated insulin receptor tyrosine kinase in complex with peptide substrate and ATP analog.* Embo j, 1997. **16**(18): p. 5572-81.

21. Cubbon, R.M., et al., *Importance of insulin resistance to vascular repair and regeneration.* Free Radic Biol Med, 2013. **60**: p. 246-63.

22. Neumann-Haefelin, E., et al., *SHC-1/p52Shc targets the insulin/IGF-1 and JNK signaling pathways to modulate life span and stress response in C. elegans.* Genes Dev, 2008. **22**(19): p. 2721-35.

23. Hsueh, W.A., C.J. Lyon, and M.J. Quinones, *Insulin resistance and the endothelium.* Am J Med, 2004. **117**(2): p. 109-17.

24. Lee, K.K., et al., *Insulin resistance independently predicts the progression of coronary artery calcification.* Am Heart J, 2009. **157**(5): p. 939-45.

25. Pyorala, M., et al., *Insulin resistance syndrome predicts the risk of coronary heart disease and stroke in healthy middle-aged men: the 22-year follow-up results of the Helsinki Policemen Study.* Arterioscler Thromb Vasc Biol, 2000. **20**(2): p. 538-44.

26. Virkamaki, A., K. Ueki, and C.R. Kahn, *Protein-protein interaction in insulin signaling and the molecular mechanisms of insulin resistance.* J Clin Invest, 1999. **103**(7): p. 931-43.

27. Almind, K., et al., *Aminoacid polymorphisms of insulin receptor substrate-1 in non-insulin-dependent diabetes mellitus.* Lancet, 1993. **342**(8875): p. 828-32.

28. Laakso, M., et al., *Insulin receptor substrate-1 variants in non-insulin-dependent diabetes.* J Clin Invest, 1994. **94**(3): p. 1141-6.

29. Almind, K., et al., *A common amino acid polymorphism in insulin receptor substrate-1 causes impaired insulin signaling. Evidence from transfection studies.* J Clin Invest, 1996. **97**(11): p. 2569-75.

30. Hansen, T., et al., *Identification of a common amino acid polymorphism in the p85alpha regulatory subunit of phosphatidylinositol 3-kinase: effects on glucose disappearance constant, glucose effectiveness, and the insulin sensitivity index.* Diabetes, 1997. **46**(3): p. 494-501.

31. Yki-Jarvinen, H., I. Puhakainen, and V.A. Koivisto, *Effect of free fatty acids on glucose uptake and nonoxidative glycolysis across human forearm tissues in the basal state and during insulin stimulation.* J Clin Endocrinol Metab, 1991. **72**(6): p. 1268-77.

32. Samuel, V.T. and G.I. Shulman, *Mechanisms for insulin resistance: common threads and missing links.* Cell, 2012. **148**(5): p. 852-71.

33. Haring, H., et al., *Tumor-promoting phorbol esters increase the Km of the ATP-binding site of the insulin receptor kinase from rat adipocytes.* J Biol Chem, 1986. **261**(8): p. 3869-75.

34. Jacobs, S., et al., *Phorbol esters stimulate the phosphorylation of receptors for insulin and somatomedin C.* Proc Natl Acad Sci U S A, 1983. **80**(20): p. 6211-3.

35. Yu, C., et al., *Mechanism by which fatty acids inhibit insulin activation of insulin receptor substrate-1 (IRS-1)-associated phosphatidylinositol 3-kinase activity in muscle.* J Biol Chem, 2002. **277**(52): p. 50230-6.

36. Li, Y., et al., *Protein kinase C Theta inhibits insulin signaling by phosphorylating IRS1 at Ser(1101).* J Biol Chem, 2004. **279**(44): p. 45304-7.

37. Wang, B., I.S. Wood, and P. Trayhurn, *Dysregulation of the expression and secretion of inflammation-related adipokines by hypoxia in human adipocytes.* Pflugers Arch, 2007. **455**(3): p. 479-92.

38. Hosogai, N., et al., *Adipose tissue hypoxia in obesity and its impact on adipocytokine dysregulation.* Diabetes, 2007. **56**(4): p. 901-11.

39. Aguirre, V., et al., *Phosphorylation of Ser307 in insulin receptor substrate-1 blocks interactions with the insulin receptor and inhibits insulin action.* J Biol Chem, 2002. **277**(2): p. 1531-7.

40. Hotamisligil, G.S., et al., *IRS-1-mediated inhibition of insulin receptor tyrosine kinase activity in TNF-alpha- and obesity-induced insulin resistance.* Science, 1996. **271**(5249): p. 665-8.

41. Ye, J., et al., *Hypoxia is a potential risk factor for chronic inflammation and adiponectin reduction in adipose tissue of ob/ob and dietary obese mice.* Am J Physiol Endocrinol Metab, 2007. **293**(4): p. E1118-28.

42. Goodpaster, B.H., F.L. Thaete, and D.E. Kelley, *Thigh adipose tissue distribution is associated with insulin resistance in obesity and in type 2 diabetes mellitus.* Am J Clin Nutr, 2000. **71**(4): p. 885-92.

43. Feldstein, A.E., et al., *Free fatty acids promote hepatic lipotoxicity by stimulating TNF-alpha expression via a lysosomal pathway.* Hepatology, 2004. **40**(1): p. 185-94.

44. Ueno, M., et al., *Regulation of insulin signalling by hyperinsulinaemia: role of IRS-1/2 serine phosphorylation and the mTOR/p70 S6K pathway.* Diabetologia, 2005. **48**(3): p. 506-18.

45. Fiorentino, T.V., et al., *Hyperglycemia-induced oxidative stress and its role in diabetes mellitus related cardiovascular diseases.* Curr Pharm Des, 2013. **19**(32): p. 5695-703.

46. Nishikawa, T., et al., *Normalizing mitochondrial superoxide production blocks three pathways of hyperglycaemic damage.* Nature, 2000. **404**(6779): p. 787-90.

47. Furukawa, S., et al., *Increased oxidative stress in obesity and its impact on metabolic syndrome.* J Clin Invest, 2004. **114**(12): p. 1752-61.

48. Gao, Z., et al., *Serine phosphorylation of insulin receptor substrate 1 by inhibitor kappa B kinase complex.* J Biol Chem, 2002. **277**(50): p. 48115-21.

49. Miele, C., et al., *Human glycated albumin affects glucose metabolism in L6 skeletal muscle cells by impairing insulin-induced insulin receptor substrate (IRS) signaling through a protein kinase C alpha-mediated mechanism.* J Biol Chem, 2003. **278**(48): p. 47376-87.

50. Cusi, K., et al., *Insulin resistance differentially affects the PI 3-kinase- and MAP kinase-mediated signaling in human muscle.* J Clin Invest, 2000. **105**(3): p. 311-20.

51. Jiang, Z.Y., et al., *Characterization of selective resistance to insulin signaling in the vasculature of obese Zucker (fa/fa) rats.* J Clin Invest, 1999. **104**(4): p. 447-57.

52. Accili, D., et al., *Early neonatal death in mice homozygous for a null allele of the insulin receptor gene.* Nat Genet, 1996. **12**(1): p. 106-9.

53. Joshi, R.L., et al., *Targeted disruption of the insulin receptor gene in the mouse results in neonatal lethality.* Embo j, 1996. **15**(7): p. 1542-7.

54. Wheatcroft, S.B., et al., *Preserved glucoregulation but attenuation of the vascular actions of insulin in mice heterozygous for knockout of the insulin receptor.* Diabetes, 2004. **53**(10): p. 2645-52.

55. Vicent, D., et al., *The role of endothelial insulin signaling in the regulation of vascular tone and insulin resistance.* J Clin Invest, 2003. **111**(9): p. 1373-80.

56. Duncan, E.R., et al., *Effect of endothelium-specific insulin resistance on endothelial function in vivo.* Diabetes, 2008. **57**(12): p. 3307-14.

57. Harman, D., *Aging: a theory based on free radical and radiation chemistry.* J Gerontol, 1956. **11**(3): p. 298-300.

58. Taniyama, Y. and K.K. Griendling, *Reactive oxygen species in the vasculature: molecular and cellular mechanisms.* Hypertension, 2003. **42**(6): p. 1075-81.

59. Zhou, Y., et al., *Reactive oxygen species in vascular formation and development.* Oxid Med Cell Longev, 2013. **2013**: p. 374963.

60. Liou, G.Y. and P. Storz, *Reactive oxygen species in cancer.* Free Radic Res, 2010. **44**(5): p. 479-96.

61. Guzik, T.J., et al., *Mechanisms of increased vascular superoxide production in human diabetes mellitus: role of NAD(P)H oxidase and endothelial nitric oxide synthase.* Circulation, 2002. **105**(14): p. 1656-62.

62. Fortuno, A., et al., *Phagocytic NADPH oxidase overactivity underlies oxidative stress in metabolic syndrome.* Diabetes, 2006. **55**(1): p. 209-15.

63. Silver, A.E., et al., *Overweight and obese humans demonstrate increased vascular endothelial NAD(P)H oxidase-p47(phox) expression and evidence of endothelial oxidative stress.* Circulation, 2007. **115**(5): p. 627-37.

64. Kleikers, P.W., et al., *NADPH oxidases as a source of oxidative stress and molecular target in ischemia/reperfusion injury.* J Mol Med (Berl), 2012. **90**(12): p. 1391-406.

65. Ushio-Fukai, M. and N. Urao, *Novel role of NADPH oxidase in angiogenesis and stem/progenitor cell function.* Antioxid Redox Signal, 2009. **11**(10): p. 2517-33.

66. Konior, A., et al., *NADPH oxidases in vascular pathology.* Antioxid Redox Signal, 2014. **20**(17): p. 2794-814.

67. Sumimoto, H., *Structure, regulation and evolution of Nox-family NADPH oxidases that produce reactive oxygen species.* Febs j, 2008. **275**(13): p. 3249-77.

68. Lassegue, B., A. San Martin, and K.K. Griendling, *Biochemistry, physiology, and pathophysiology of NADPH oxidases in the cardiovascular system.* Circ Res, 2012. **110**(10): p. 1364-90.

69. Schroder, K., et al., *Nox4 is a protective reactive oxygen species generating vascular NADPH oxidase.* Circ Res, 2012. **110**(9): p. 1217-25.

70. Craige, S.M., et al., *NADPH oxidase 4 promotes endothelial angiogenesis through endothelial nitric oxide synthase activation.* Circulation, 2011. **124**(6): p. 731-40.

71. Takac, I., et al., *The E-loop is involved in hydrogen peroxide formation by the NADPH oxidase Nox4.* J Biol Chem, 2011. **286**(15): p. 13304-13.

72. Rey, F.E., et al., *Novel competitive inhibitor of NAD(P)H oxidase assembly attenuates vascular O(2)(-) and systolic blood pressure in mice.* Circ Res, 2001. **89**(5): p. 408-14.

73. Ali, N., M.T. Kearney, and R.M. Cubbon, *The role of reactive oxygen species in insulin resistance–associated cardiovascular disease.* Diabetes Management, 2015. **5**(3): p. 203-213.

74. Bartosz, G., *Reactive oxygen species: destroyers or messengers?* Biochem Pharmacol, 2009. **77**(8): p. 1303-15.

75. Brieger, K., et al., *Reactive oxygen species: from health to disease.* Swiss Med Wkly, 2012. **17**(142): p. 13659.

76. Ostman, A., et al., *Regulation of protein tyrosine phosphatases by reversible oxidation.* J Biochem, 2011. **150**(4): p. 345-56.

77. Guo, D.Q., et al., *Tumor necrosis factor employs a protein-tyrosine phosphatase to inhibit activation of KDR and vascular endothelial cell*

growth factor-induced endothelial cell proliferation. J Biol Chem, 2000. **275**(15): p. 11216-21.

78. Huang, L., et al., *HCPTPA, a protein tyrosine phosphatase that regulates vascular endothelial growth factor receptor-mediated signal transduction and biological activity.* J Biol Chem, 1999. **274**(53): p. 38183-8.

79. Kroll, J. and J. Waltenberger, *The vascular endothelial growth factor receptor KDR activates multiple signal transduction pathways in porcine aortic endothelial cells.* J Biol Chem, 1997. **272**(51): p. 32521-7.

80. Nakagami, H., et al., *Tumor necrosis factor-alpha inhibits growth factor-mediated cell proliferation through SHP-1 activation in endothelial cells.* Arterioscler Thromb Vasc Biol, 2002. **22**(2): p. 238-42.

81. Mitola, S., et al., *Type I collagen limits VEGFR-2 signaling by a SHP2 protein-tyrosine phosphatase-dependent mechanism 1.* Circ Res, 2006. **98**(1): p. 45-54.

82. Giannoni, E., M.L. Taddei, and P. Chiarugi, *Src redox regulation: again in the front line.* Free Radic Biol Med, 2010. **49**(4): p. 516-27.

83. Kemble, D.J. and G. Sun, *Direct and specific inactivation of protein tyrosine kinases in the Src and FGFR families by reversible cysteine oxidation.* Proc Natl Acad Sci U S A, 2009. **106**(13): p. 5070-5.

84. Nakashima, I., et al., *Redox-linked signal transduction pathways for protein tyrosine kinase activation.* Antioxid Redox Signal, 2002. **4**(3): p. 517-31.

85. Corcoran, A. and T.G. Cotter, *Redox regulation of protein kinases.* Febs J, 2013. **280**(9): p. 1944-65.

86. Greene, E.L., et al., *5-HT(2A) receptors stimulate mitogen-activated protein kinase via H(2)O(2) generation in rat renal mesangial cells.* Am J Physiol Renal Physiol, 2000. **278**(4): p. F650-8.

87. Houstis, N., E.D. Rosen, and E.S. Lander, *Reactive oxygen species have a causal role in multiple forms of insulin resistance.* Nature, 2006. **440**(7086): p. 944-8.

88. Tiganis, T., *Reactive oxygen species and insulin resistance: the good, the bad and the ugly.* Trends Pharmacol Sci, 2011. **32**(2): p. 82-9.

89. Shoelson, S.E., J. Lee, and A.B. Goldfine, *Inflammation and insulin resistance.* J Clin Invest, 2006. **116**(7): p. 1793-801.

90. Gual, P., Y. Le Marchand-Brustel, and J.F. Tanti, *Positive and negative regulation of insulin signaling through IRS-1 phosphorylation.* Biochimie, 2005. **87**(1): p. 99-109.

91. Rotter, V., I. Nagaev, and U. Smith, *Interleukin-6 (IL-6) induces insulin resistance in 3T3-L1 adipocytes and is, like IL-8 and tumor necrosis factor-alpha, overexpressed in human fat cells from insulin-resistant subjects.* J Biol Chem, 2003. **278**(46): p. 45777-84.

92. Hoehn, K.L., et al., *Insulin resistance is a cellular antioxidant defense mechanism.* Proc Natl Acad Sci U S A, 2009. **106**(42): p. 17787-92.

93. Esper, R.J., et al., *Endothelial dysfunction: a comprehensive appraisal.* Cardiovasc Diabetol, 2006. **5**: p. 4.

94. Loscalzo, J. and G. Welch, *Nitric oxide and its role in the cardiovascular system.* Prog Cardiovasc Dis, 1995. **38**(2): p. 87-104.

95. Andrew, P.J. and B. Mayer, *Enzymatic function of nitric oxide synthases.* Cardiovasc Res, 1999. **43**(3): p. 521-31.

96. Stuehr, D., S. Pou, and G.M. Rosen, *Oxygen reduction by nitric-oxide synthases.* J Biol Chem, 2001. **276**(18): p. 14533-6.

97. Yetik-Anacak, G. and J.D. Catravas, *Nitric oxide and the endothelium: history and impact on cardiovascular disease.* Vascul Pharmacol, 2006. **45**(5): p. 268-76.

98. Davis, M.E., et al., *Shear stress regulates endothelial nitric oxide synthase expression through c-Src by divergent signaling pathways.* Circ Res, 2001. **89**(11): p. 1073-80.

99. Forstermann, U. and W.C. Sessa, *Nitric oxide synthases: regulation and function.* Eur Heart J, 2012. **33**(7): p. 829-37, 837a-837d.

100. Rees, D.D., R.M. Palmer, and S. Moncada, *Role of endothelium-derived nitric oxide in the regulation of blood pressure.* Proc Natl Acad Sci U S A, 1989. **86**(9): p. 3375-8.

101. Vallance, P., J. Collier, and S. Moncada, *Effects of endothelium-derived nitric oxide on peripheral arteriolar tone in man.* Lancet, 1989. **2**(8670): p. 997-1000.

102. Arnold, W.P., et al., *Nitric oxide activates guanylate cyclase and increases guanosine 3':5'-cyclic monophosphate levels in various tissue preparations.* Proc Natl Acad Sci U S A, 1977. **74**(8): p. 3203-7.

103. Garg, U.C. and A. Hassid, *Nitric oxide-generating vasodilators and 8-bromo-cyclic guanosine monophosphate inhibit mitogenesis and proliferation of cultured rat vascular smooth muscle cells.* J Clin Invest, 1989. **83**(5): p. 1774-7.

104. Tsihlis, N.D., et al., *Nitric oxide inhibits vascular smooth muscle cell proliferation and neointimal hyperplasia by increasing the ubiquitination and degradation of UbcH10.* Cell Biochem Biophys, 2011. **60**(1-2): p. 89-97.

105. Naseem, K.M., *The role of nitric oxide in cardiovascular diseases.* Mol Aspects Med, 2005. **26**(1-2): p. 33-65.

106. Kubes, P., M. Suzuki, and D.N. Granger, *Nitric oxide: an endogenous modulator of leukocyte adhesion.* Proc Natl Acad Sci U S A, 1991. **88**(11): p. 4651-5.

107. Radomski, M.W., R.M. Palmer, and S. Moncada, *An L-arginine/nitric oxide pathway present in human platelets regulates aggregation.* Proc Natl Acad Sci U S A, 1990. **87**(13): p. 5193-7.

108. Bhardwaj, R. and P.K. Moore, *Endothelium-derived relaxing factor and the effects of acetylcholine and histamine on resistance blood vessels.* Br J Pharmacol, 1988. **95**(3): p. 835-43.

109. Radomski, M.W., R.M. Palmer, and S. Moncada, *The role of nitric oxide and cGMP in platelet adhesion to vascular endothelium.* Biochem Biophys Res Commun, 1987. **148**(3): p. 1482-9.

110. Deanfield, J., et al., *Endothelial function and dysfunction. Part I: Methodological issues for assessment in the different vascular beds: a statement by the Working Group on Endothelin and Endothelial Factors of the European Society of Hypertension.* J Hypertens, 2005. **23**(1): p. 7-17.

111. Luscher, T.F. and M. Barton, *Biology of the endothelium.* Clin Cardiol, 1997. **20**(11 Suppl 2): p. Ii-3-10.

112. Anderson, T.J., et al., *Systemic nature of endothelial dysfunction in atherosclerosis.* Am J Cardiol, 1995. **75**(6): p. 71b-74b.

113. Ludmer, P.L., et al., *Paradoxical vasoconstriction induced by acetylcholine in atherosclerotic coronary arteries.* N Engl J Med, 1986. **315**(17): p. 1046-51.

114. Schachinger, V., M.B. Britten, and A.M. Zeiher, *Prognostic impact of coronary vasodilator dysfunction on adverse long-term outcome of coronary heart disease.* Circulation, 2000. **101**(16): p. 1899-906.

115. Thomas, S.R., K. Chen, and J.F. Keaney, Jr., *Hydrogen peroxide activates endothelial nitric-oxide synthase through coordinated phosphorylation and dephosphorylation via a phosphoinositide 3-kinase-dependent signaling pathway.* J Biol Chem, 2002. **277**(8): p. 6017-24.

116. Higashi, Y., et al., *Endothelial function and oxidative stress in cardiovascular diseases.* Circ J, 2009. **73**(3): p. 411-8.

117. Lusis, A.J., *Atherosclerosis.* Nature, 2000. **407**(6801): p. 233-41.

118. Mayerl, C., et al., *Atherosclerosis research from past to present--on the track of two pathologists with opposing views, Carl von Rokitansky and Rudolf Virchow.* Virchows Arch, 2006. **449**(1): p. 96-103.

119. Mondy, J.S., et al., *Platelet-derived growth factor ligand and receptor expression in response to altered blood flow in vivo.* Circ Res, 1997. **81**(3): p. 320-7.

120. Duncan, E.R., et al., *Accelerated endothelial dysfunction in mild prediabetic insulin resistance: the early role of reactive oxygen species.* Am J Physiol Endocrinol Metab, 2007. **293**(5): p. 21.

121. Du, J., et al., *Crucial roles of Nox2-derived oxidative stress in deteriorating the function of insulin receptors and endothelium in dietary obesity of middle-aged mice.* Br J Pharmacol, 2013. **170**(5): p. 1064-77.

122. Rask-Madsen, C., et al., *Loss of insulin signaling in vascular endothelial cells accelerates atherosclerosis in apolipoprotein E null mice.* Cell Metab, 2010. **11**(5): p. 379-89.

123. Sukumar, P., et al., *Nox2 NADPH oxidase has a critical role in insulin resistance-related endothelial cell dysfunction.* Diabetes, 2013. **62**(6): p. 2130-4.

124. Simons, M., *Angiogenesis: where do we stand now?* Circulation, 2005. **111**(12): p. 1556-66.

125. Silvestre, J.S., D.M. Smadja, and B.I. Levy, *Postischemic revascularization: from cellular and molecular mechanisms to clinical applications.* Physiol Rev, 2013. **93**(4): p. 1743-802.

126. Potente, M., H. Gerhardt, and P. Carmeliet, *Basic and therapeutic aspects of angiogenesis.* Cell, 2011. **146**(6): p. 873-87.

127. Duh, E. and L.P. Aiello, *Vascular endothelial growth factor and diabetes: the agonist versus antagonist paradox.* Diabetes, 1999. **48**(10): p. 1899-906.

128. Rivard, A., et al., *Rescue of diabetes-related impairment of angiogenesis by intramuscular gene therapy with adeno-VEGF.* Am J Pathol, 1999. **154**(2): p. 355-63.

129. Chen, Y.L., et al., *Impact of obesity control on circulating level of endothelial progenitor cells and angiogenesis in response to ischemic stimulation.* J Transl Med, 2012. **10**: p. 86.

130. Cubbon, R.M., et al., *Vascular regeneration is impaired in the setting of systemic insulin resistance*, in *Heart*. 2014. p. A1-138.

131. Altabas, V., *Diabetes, Endothelial Dysfunction, and Vascular Repair: What Should a Diabetologist Keep His Eye on?* Int J Endocrinol, 2015. **2015**: p. 848272.

132. Ishigami, K., et al., *Long-term follow-up of neointimal coverage of sirolimus-eluting stents--evaluation with optical coherence tomography.* Circ J, 2009. **73**(12): p. 2300-7.

133. Asahara, T., et al., *Isolation of putative progenitor endothelial cells for angiogenesis.* Science, 1997. **275**(5302): p. 964-7.

134. Peichev, M., et al., *Expression of VEGFR-2 and AC133 by circulating human CD34(+) cells identifies a population of functional endothelial precursors.* Blood, 2000. **95**(3): p. 952-8.

135. Vasa, M., et al., *Increase in circulating endothelial progenitor cells by statin therapy in patients with stable coronary artery disease.* Circulation, 2001. **103**(24): p. 2885-90.

136. Werner, N., et al., *Circulating endothelial progenitor cells and cardiovascular outcomes.* N Engl J Med, 2005. **353**(10): p. 999-1007.

137. Hirschi, K.K., D.A. Ingram, and M.C. Yoder, *Assessing identity, phenotype, and fate of endothelial progenitor cells.* Arterioscler Thromb Vasc Biol, 2008. **28**(9): p. 1584-95.

138. Hur, J., et al., *Characterization of two types of endothelial progenitor cells and their different contributions to neovasculogenesis.* Arterioscler Thromb Vasc Biol, 2004. **24**(2): p. 288-93.

139. Urao, N., et al., *Erythropoietin-mobilized endothelial progenitors enhance reendothelialization via Akt-endothelial nitric oxide synthase activation and prevent neointimal hyperplasia.* Circ Res, 2006. **98**(11): p. 1405-13.

140. Martin-Ramirez, J., et al., *Establishment of outgrowth endothelial cells from peripheral blood.* Nat Protoc, 2012. **7**(9): p. 1709-15.

141. Hagensen, M.K., et al., *Circulating endothelial progenitor cells do not contribute to regeneration of endothelium after murine arterial injury.* Cardiovasc Res, 2012. **93**(2): p. 223-31.

142. Cross, M.J., et al., *VEGF-receptor signal transduction.* Trends Biochem Sci, 2003. **28**(9): p. 488-94.

143. Zhou, Y., et al., *Reactive oxygen species in vascular formation and development.* Oxid Med Cell Longev, 2013. **374963**(10): p. 22.

144. Matsumoto, T. and L. Claesson-Welsh, *VEGF receptor signal transduction.* Sci STKE, 2001. **11**(112).

145. Okuno, Y., et al., *Pathological neoangiogenesis depends on oxidative stress regulation by ATM.* Nat Med, 2012. **18**(8): p. 1208-16.

146. Bonello, S., et al., *Reactive oxygen species activate the HIF-1alpha promoter via a functional NFkappaB site.* Arterioscler Thromb Vasc Biol, 2007. **27**(4): p. 755-61.

147. Block, K., et al., *NAD(P)H oxidases regulate HIF-2alpha protein expression.* J Biol Chem, 2007. **282**(11): p. 8019-26.

148. Aicher, A., A.M. Zeiher, and S. Dimmeler, *Mobilizing endothelial progenitor cells.* Hypertension, 2005. **45**(3): p. 321-5.

149. Lapidot, T. and I. Petit, *Current understanding of stem cell mobilization: the roles of chemokines, proteolytic enzymes, adhesion molecules, cytokines, and stromal cells.* Exp Hematol, 2002. **30**(9): p. 973-81.

150. Chavakis, E., C. Urbich, and S. Dimmeler, *Homing and engraftment of progenitor cells: a prerequisite for cell therapy.* J Mol Cell Cardiol, 2008. **45**(4): p. 514-22.

151. De Falco, E., et al., *SDF-1 involvement in endothelial phenotype and ischemia-induced recruitment of bone marrow progenitor cells.* Blood, 2004. **104**(12): p. 3472-82.

152. Yamaguchi, J., et al., *Stromal cell-derived factor-1 effects on ex vivo expanded endothelial progenitor cell recruitment for ischemic neovascularization.* Circulation, 2003. **107**(9): p. 1322-8.

153. Urao, N., et al., *Role of nox2-based NADPH oxidase in bone marrow and progenitor cell function involved in neovascularization induced by hindlimb ischemia.* Circ Res, 2008. **103**(2): p. 212-20.

154. Higai, K., A. Shimamura, and K. Matsumoto, *Amadori-modified glycated albumin predominantly induces E-selectin expression on human umbilical*

vein endothelial cells through NADPH oxidase activation. Clin Chim Acta, 2006. **367**(1-2): p. 137-43.

155. Ishikawa, M., et al., *Cerebral microvascular responses to hypercholesterolemia: roles of NADPH oxidase and P-selectin.* Circ Res, 2004. **94**(2): p. 239-44.

156. Akgur, F.M., et al., *Role of superoxide in hemorrhagic shock-induced P-selectin expression.* Am J Physiol Heart Circ Physiol, 2000. **279**(2): p. H791-7.

157. Min, J.K., et al., *TNF-related activation-induced cytokine enhances leukocyte adhesiveness: induction of ICAM-1 and VCAM-1 via TNF receptor-associated factor and protein kinase C-dependent NF-kappaB activation in endothelial cells.* J Immunol, 2005. **175**(1): p. 531-40.

158. Napoli, C., et al., *Effects of nitric oxide on cell proliferation: novel insights.* J Am Coll Cardiol, 2013. **62**(2): p. 89-95.

159. Cubbon, R.M., et al., *Human exercise-induced circulating progenitor cell mobilization is nitric oxide-dependent and is blunted in South Asian men.* Arterioscler Thromb Vasc Biol, 2010. **30**(4): p. 878-84.

160. Aicher, A., et al., *Essential role of endothelial nitric oxide synthase for mobilization of stem and progenitor cells.* Nat Med, 2003. **9**(11): p. 1370-6.

161. Ballinger, S.W., et al., *Hydrogen peroxide- and peroxynitrite-induced mitochondrial DNA damage and dysfunction in vascular endothelial and smooth muscle cells.* Circ Res, 2000. **86**(9): p. 960-6.

162. Guzik, T.J., et al., *Nitric oxide modulates superoxide release and peroxynitrite formation in human blood vessels.* Hypertension, 2002. **39**(6): p. 1088-94.

163. Peshavariya, H., et al., *NADPH oxidase isoform selective regulation of endothelial cell proliferation and survival.* Naunyn Schmiedebergs Arch Pharmacol, 2009. **380**(2): p. 193-204.

164. Lamalice, L., F. Le Boeuf, and J. Huot, *Endothelial cell migration during angiogenesis.* Circ Res, 2007. **100**(6): p. 782-94.

165. Moldovan, L., et al., *Reactive oxygen species in vascular endothelial cell motility. Roles of NAD(P)H oxidase and Rac1.* Cardiovasc Res, 2006. **71**(2): p. 236-46.

166. Ushio-Fukai, M., *Localizing NADPH oxidase-derived ROS.* Sci STKE, 2006. **22**(349).

167. Tojo, T., et al., *Role of gp91phox (Nox2)-containing NAD(P)H oxidase in angiogenesis in response to hindlimb ischemia.* Circulation, 2005. **111**(18): p. 2347-55.

168. Urao, N., et al., *Critical role of endothelial hydrogen peroxide in post-ischemic neovascularization.* PLoS One, 2013. **8**(3): p. 5.

169. Zhang, M., et al., *NADPH oxidase-4 mediates protection against chronic load-induced stress in mouse hearts by enhancing angiogenesis.* Proc Natl Acad Sci U S A, 2010. **107**(42): p. 18121-6.

170. Ebrahimian, T.G., et al., *NADPH oxidase-derived overproduction of reactive oxygen species impairs postischemic neovascularization in mice with type 1 diabetes.* Am J Pathol, 2006. **169**(2): p. 719-28.

171. Haddad, P., et al., *Nox2-containing NADPH oxidase deficiency confers protection from hindlimb ischemia in conditions of increased oxidative stress.* Arterioscler Thromb Vasc Biol, 2009. **29**(10): p. 1522-8.

172. Haddad, P., et al., *Nox2-derived reactive oxygen species contribute to hypercholesterolemia-induced inhibition of neovascularization: effects on endothelial progenitor cells and mature endothelial cells.* Atherosclerosis, 2011. **217**(2): p. 340-9.

173. Hanahan, D. and R.A. Weinberg, *The hallmarks of cancer.* Cell, 2000. **100**(1): p. 57-70.

174. Arbiser, J.L., et al., *Reactive oxygen generated by Nox1 triggers the angiogenic switch.* Proc Natl Acad Sci U S A, 2002. **99**(2): p. 715-20.

175. Garrido-Urbani, S., et al., *Targeting vascular NADPH oxidase 1 blocks tumor angiogenesis through a PPARalpha mediated mechanism.* PLoS One, 2011. **6**(2): p. 0014665.

176. Zheng, L. and T.S. Kern, *Role of nitric oxide, superoxide, peroxynitrite and PARP in diabetic retinopathy.* Front Biosci, 2009. **14**: p. 3974-87.

177. Al-Shabrawey, M., et al., *Role of NADPH oxidase in retinal vascular inflammation.* Invest Ophthalmol Vis Sci, 2008. **49**(7): p. 3239-44.

178. Saito, Y., et al., *Activated NAD(P)H oxidase from supplemental oxygen induces neovascularization independent of VEGF in retinopathy of prematurity model.* Invest Ophthalmol Vis Sci, 2008. **49**(4): p. 1591-8.

179. Lee, M.Y., et al., *Mechanisms of vascular smooth muscle NADPH oxidase 1 (Nox1) contribution to injury-induced neointimal formation.* Arterioscler Thromb Vasc Biol, 2009. **29**(4): p. 480-7.

180. Roberts, C.K. and K.K. Sindhu, *Oxidative stress and metabolic syndrome.* Life Sci, 2009. **84**(21-22): p. 705-12.

181. Virdis, A., et al., *Role of NAD(P)H oxidase on vascular alterations in angiotensin II-infused mice.* J Hypertens, 2004. **22**(3): p. 535-42.

182. Murdoch, C.E., et al., *Role of endothelial Nox2 NADPH oxidase in angiotensin II-induced hypertension and vasomotor dysfunction.* Basic Res Cardiol, 2011. **106**(4): p. 527-38.

183. Touyz, R.M., et al., *Angiotensin II-dependent chronic hypertension and cardiac hypertrophy are unaffected by gp91phox-containing NADPH oxidase.* Hypertension, 2005. **45**(4): p. 530-7.

184. Elmarakby, A.A., et al., *NADPH oxidase inhibition attenuates oxidative stress but not hypertension produced by chronic ET-1.* Hypertension, 2005. **45**(2): p. 283-7.

185. Ray, R., et al., *Endothelial Nox4 NADPH oxidase enhances vasodilatation and reduces blood pressure in vivo.* Arterioscler Thromb Vasc Biol, 2011. **31**(6): p. 1368-76.

186. Vincent, H.K., et al., *Effects of antioxidant supplementation on insulin sensitivity, endothelial adhesion molecules, and oxidative stress in normal-weight and overweight young adults.* Metabolism, 2009. **58**(2): p. 254-62.

187. Judkins, C.P., et al., *Direct evidence of a role for Nox2 in superoxide production, reduced nitric oxide bioavailability, and early atherosclerotic plaque formation in ApoE-/- mice.* Am J Physiol Heart Circ Physiol, 2010. **298**(1): p. H24-32.

188. Sibley, C.T., et al., *Assessment of atherosclerosis in chronic granulomatous disease.* Circulation, 2014. **130**(23): p. 2031-9.

189. Gray, S.P., et al., *NADPH oxidase 1 plays a key role in diabetes mellitus-accelerated atherosclerosis.* Circulation, 2013. **127**(18): p. 1888-902.

190. Marumo, T., et al., *Platelet-derived growth factor-stimulated superoxide anion production modulates activation of transcription factor NF-kappaB and expression of monocyte chemoattractant protein 1 in human aortic smooth muscle cells.* Circulation, 1997. **96**(7): p. 2361-7.

191. Cybulsky, M.I., et al., *A major role for VCAM-1, but not ICAM-1, in early atherosclerosis.* J Clin Invest, 2001. **107**(10): p. 1255-62.

192. Mach, F., et al., *Differential expression of three T lymphocyte-activating CXC chemokines by human atheroma-associated cells.* J Clin Invest, 1999. **104**(8): p. 1041-50.

193. Deffert, C., et al., *Hyperinflammation of chronic granulomatous disease is abolished by NOX2 reconstitution in macrophages and dendritic cells.* J Pathol, 2012. **228**(3): p. 341-50.

194. Kigawa, Y., et al., *NADPH oxidase deficiency exacerbates angiotensin II-induced abdominal aortic aneurysms in mice.* Arterioscler Thromb Vasc Biol, 2014. **34**(11): p. 2413-20.

195. Chouchani, E.T., et al., *Ischaemic accumulation of succinate controls reperfusion injury through mitochondrial ROS.* Nature, 2014. **515**(7527): p. 431-5.

196. Yun, J., et al., *Redox-dependent mechanisms in coronary collateral growth: the "redox window" hypothesis.* Antioxid Redox Signal, 2009. **11**(8): p. 1961-74.

197. Ali, Z.A., et al., *Oxido-reductive regulation of vascular remodeling by receptor tyrosine kinase ROS1.* J Clin Invest, 2014. **124**(12): p. 5159-74.

198. McCord, J.M., *Therapeutic control of free radicals*. Drug Discov Today. 2004 Sep 15;9(18):781-2.

199. Stephens, N.G., et al., *Randomised controlled trial of vitamin E in patients with coronary disease: Cambridge Heart Antioxidant Study (CHAOS).* Lancet, 1996. **347**(9004): p. 781-6.

200. Virtamo, J., et al., *Effect of vitamin E and beta carotene on the incidence of primary nonfatal myocardial infarction and fatal coronary heart disease.* Arch Intern Med, 1998. **158**(6): p. 668-75.

201. Jialal, I. and S. Devaraj, *Vitamin E supplementation and cardiovascular events in high-risk patients*. N Engl J Med. 2000 Jun 22;342(25):1917-8.

202. *MRC/BHF Heart Protection Study of antioxidant vitamin supplementation in 20,536 high-risk individuals: a randomised placebo-controlled trial.* Lancet, 2002. **360**(9326): p. 23-33.

203. *Dietary supplementation with n-3 polyunsaturated fatty acids and vitamin E after myocardial infarction: results of the GISSI-Prevenzione trial. Gruppo Italiano per lo Studio della Sopravvivenza nell'Infarto miocardico.* Lancet, 1999. **354**(9177): p. 447-55.

204. Lonn, E., et al., *Effects of long-term vitamin E supplementation on cardiovascular events and cancer: a randomized controlled trial.* Jama, 2005. **293**(11): p. 1338-47.

205. Guzik, T.J. and D.G. Harrison, *Vascular NADPH oxidases as drug targets for novel antioxidant strategies.* Drug Discov Today, 2006. **11**(11-12): p. 524-33.

206. Drummond, G.R., et al., *Combating oxidative stress in vascular disease: NADPH oxidases as therapeutic targets.* Nat Rev Drug Discov, 2011. **10**(6): p. 453-71.

207. Pollock, J.D., et al., *Mouse model of X-linked chronic granulomatous disease, an inherited defect in phagocyte superoxide production.* Nat Genet, 1995. **9**(2): p. 202-9.

208. Sobczak, M., J. Dargatz, and M. Chrzanowska-Wodnicka, *Isolation and culture of pulmonary endothelial cells from neonatal mice.* J Vis Exp, 2010(46).

209. Sorrentino, S.A., et al., *Oxidant stress impairs in vivo reendothelialization capacity of endothelial progenitor cells from patients with type 2 diabetes mellitus: restoration by the peroxisome proliferator-activated receptor-gamma agonist rosiglitazone.* Circulation, 2007. **116**(2): p. 163-73.

210. van Aalst, J.A., et al., *Role of reactive oxygen species in inhibition of endothelial cell migration by oxidized low-density lipoprotein.* J Vasc Surg, 2004. **40**(6): p. 1208-15.

211. Steinritz, D., et al., *Assessment of Endothelial Cell Migration After Exposure to Toxic Chemicals.* J Vis Exp, 2015(101): p. e52768.

212. Ramer, R., et al., *Cannabinoids inhibit angiogenic capacities of endothelial cells via release of tissue inhibitor of matrix metalloproteinases-1 from lung cancer cells.* Biochem Pharmacol, 2014. **91**(2): p. 202-16.

213. Liu, Y., M. Petreaca, and M. Martins-Green, *Cell and molecular mechanisms of insulin-induced angiogenesis.* J Cell Mol Med, 2009. **13**(11-12): p. 4492-504.

214. Pendyala, S., et al., *Role of Nox4 and Nox2 in hyperoxia-induced reactive oxygen species generation and migration of human lung endothelial cells.* Antioxid Redox Signal, 2009. **11**(4): p. 747-64.

215. Moldovan, L., et al., *Redox changes of cultured endothelial cells and actin dynamics.* Circ Res, 2000. **86**(5): p. 549-57.

216. Tamura, M., et al., *Direct interaction of actin with p47(phox) of neutrophil NADPH oxidase.* Biochem Biophys Res Commun, 2000. **276**(3): p. 1186-90.

217. Clements, M.K., et al., *Inhibition of actin polymerization by peroxynitrite modulates neutrophil functional responses.* J Leukoc Biol, 2003. **73**(3): p. 344-55.

218. Sato, E., et al., *Reactive oxygen and nitrogen metabolites modulate fibronectin-induced fibroblast migration in vitro.* Free Radic Biol Med, 2001. **30**(1): p. 22-9.

219. Fratelli, M., et al., *Identification by redox proteomics of glutathionylated proteins in oxidatively stressed human T lymphocytes.* Proc Natl Acad Sci U S A, 2002. **99**(6): p. 3505-10.

220. Johansson, M. and M. Lundberg, *Glutathionylation of beta-actin via a cysteinyl sulfenic acid intermediary.* BMC Biochem, 2007. **8**: p. 26.

221. Davis, C., et al., *The role of inflammation in vascular injury and repair.* J Thromb Haemost, 2003. **1**(8): p. 1699-709.

222. Abais, J.M., et al., *NADPH oxidase-mediated triggering of inflammasome activation in mouse podocytes and glomeruli during hyperhomocysteinemia.* Antioxid Redox Signal, 2013. **18**(13): p. 1537-48.

223. Heyworth, P.G., A.R. Cross, and J.T. Curnutte, *Chronic granulomatous disease.* Curr Opin Immunol, 2003. **15**(5): p. 578-84.

224. Inoue, T., et al., *Vascular inflammation and repair: implications for re-endothelialization, restenosis, and stent thrombosis.* JACC Cardiovasc Interv, 2011. **4**(10): p. 1057-66.

225. Aird, W.C., *Phenotypic heterogeneity of the endothelium: I. Structure, function, and mechanisms.* Circ Res, 2007. **100**(2): p. 158-73.

226. Shi, M.Q., et al., *Cilostazol suppresses angiotensin IIinduced apoptosis in endothelial cells.* Mol Med Rep, 2016.

227. Burgazli, K.M., et al., *The impact of statins on FGF-2-stimulated human umbilical vein endothelial cells.* Postgrad Med, 2014. **126**(1): p. 118-28.

228. McKayed, K.K. and J.C. Simpson, *Actin in action: imaging approaches to study cytoskeleton structure and function.* Cells, 2013. **2**(4): p. 715-31.

229. Hoy, S.M., *Canakinumab: a review of its use in the management of systemic juvenile idiopathic arthritis.* BioDrugs, 2015. **29**(2): p. 133-42.

230. Gray, S.P., et al., *Reactive Oxygen Species Can Provide Atheroprotection via NOX4-Dependent Inhibition of Inflammation and Vascular Remodeling.* Arterioscler Thromb Vasc Biol, 2016. **36**(2): p. 295-307.